Development of the Medical Workflow and Gating Tools for Ventricular Tachycardia Ablation With High-energy Ion Beams at MedAustron

DIPLOMARBEIT

zur Erlangung des akademischen Grades

Diplom-Ingenieurin

im Rahmen des Studiums

Biomedical Engineering - Medical Physics and Imaging

eingereicht von

Ariadna Cherit Hernández, BSc
Matrikelnummer 12030155

an der Fakultät für Physik

der Technischen Universität Wien

Betreuung: Assistant Prof. Dipl.-Ing. Dr.techn. Albert Hirtl
Mitwirkung: Dipl.-Ing. Dr. Claus-Stefan Schmitzer
Univ.-Prof. PD Dipl.-Ing. Dr. Markus Stock

Wien, 12. Dezember 2023

Ariadna Cherit Hernández | Albert Hirtl

Technische Universität Wien
A-1040 Wien ▪ Karlsplatz 13 ▪ Tel. +43-1-58801-0 ▪ www.tuwien.at

Erklärung zur Verfassung der Arbeit

Ariadna Cherit Hernández, BSc

Hiermit erkläre ich, dass ich diese Arbeit selbständig verfasst habe, dass ich die verwendeten Quellen und Hilfsmittel vollständig angegeben habe und dass ich die Stellen der Arbeit – einschließlich Tabellen, Karten und Abbildungen –, die anderen Werken oder dem Internet im Wortlaut oder dem Sinn nach entnommen sind, auf jeden Fall unter Angabe der Quelle als Entlehnung kenntlich gemacht habe.

Wien, 12. Dezember 2023

Ariadna Cherit Hernández

Danksagung

Diese Arbeit wäre ohne meinen Betreuer Dr. Claus Schmitzer nicht möglich gewesen, der mich vom ersten Tag an fachlich und theoretisch angeleitet und beraten hat wie einen "Padawan". Darüber hinaus möchte ich ihm für seine Rolle als Leiter der Gruppe AVID danken, da er mir die Möglichkeit gegeben hat, bei der EBG MedAustron GmbH für die Zeit meiner Diplomarbeit angestellt zu sein. Ich danke meinem Team hier bei MedAustron AVID dafür, dass sie mich von Anfang an willkommen geheißen und während des gesamten Projekts stets unterstützt haben. Ich möchte auch Dr. Markus Stock meinen tiefsten Dank dafür aussprechen, dass er mir die Möglichkeit gegeben hat, mit ihm und der Abteilung für medizinische Physik bei MedAustron zusammenzuarbeiten. Sein Fachwissen und seine Geduld waren für mich von unschätzbarem Wert und haben eine entscheidende Rolle für den Erfolg dieser Arbeit gespielt. Ich danke ganz besonders auch Dipl.-Ing., Msc.Svetlana Marić, Dr. Martina Fuß und MSc. Jingyang Xie für ihre Freundlichkeit, ihre Zeit und ihre enge Zusammenarbeit.

Ich möchte Dr. Lukas Fiedler für seinen Enthusiasmus und sein fundiertes klinisches Fachwissen in der Kardiologie danken, so wie Dr. Oliver Blanck und Dr. Melanie Grehn für die Bereitstellung von CT-Datensätzen und die Zeit, welche sie sich genommen haben mir Empfehlungen zu geben und mich anzuleiten. Ihr Beitrag als Experten des STOPSTORM Konsortiums und ihre Erfahrungen aus der RAVENTA-Studie haben den Horizont meiner Arbeit erweitert. Ganz besonders schätzte ich das aufmerksame Feedback und die Unterstützung durch meinen akademischen Betreuer Dr. Albert Hirtl. Ich danke Dr. Elisabeth Renner, die mir bei allen Fragen, die ich über Beschleunigerphysik hatte, immer zur Seite gestanden ist und meine Tage als beste Bürokollegin und Freundin verschönert hat. Darüber hinaus danke ich Dr. Adriano Garona für die kardialen Gating-Tools und die Beschleuniger-Instrumentierung. Schließlich möchte ich mich bei meiner Familie und meinen Freunden für ihre ständige Unterstützung bedanken, insbesondere bei Dipl.-Ing. Anna Shilo, Dipl.-Ing. Hanna-Helene Steiner und Christian Ramsl für das Korrekturlesen meiner Diplomarbeit. Meinem Vater Adib Cherit danke ich von ganzem Herzen dafür, dass er als erster an mein Potenzial geglaubt hat und meiner Großmutter Concepción Cardoso dafür, dass sie mich gelehrt hat, niemals aufzugeben. Nicht zuletzt möchte ich der IAEA dafür danken, dass sie meinen Masterstudiengang über ihr Marie Skłodowska-Curie-Stipendienprogramm unterstützt hat.

Acknowledgements

This endeavor would not have been possible without my supervisor Dr. Claus Schmitzer who provided me with technical guidance, theoretical direction, and counselling like a "Padawan" since day one. Furthermore, I want to thank him for his role as lead of the AVID group as he gave me the possibility to be employed at EBG MedAustron GmbH for the time it took to execute the required work constituting this diploma thesis. In addition, I would like to acknowledge my team here at MedAustron AVID, for making me feel welcome since the beginning, and for their constant support throughout the entire development of this project. I would also like to express my deepest gratitude to Dr. Markus Stock, for providing me with the opportunity to collaborate with him and the Medical Physics Department at MedAustron. His expertise and patience have been invaluable to me and have played a crucial role in the success of this thesis. I would also like to thank Dipl.-Ing., Msc. Svetlana Marić and Dr.Martina Fuß, MSc. Jingyang Xie for their kindness, time, and close collaboration.

I want to thank Dr. Lukas Fiedler for his enthusiasm, and his deep clinical expertise in cardiology. I would also like to thank Dr. Oliver Blanck and Dr. Melanie Grehn for providing CT datasets and for always finding the time to provide me guidance, and recommendations, that were key for the resolution of this work. Their input as experts form the STOPSTORM Consortium and their experience from the RAVENTA study in Germany broadened the horizon of my work. Moreover, I deeply appreciate the thoughtful feedback and support provided by my academic supervisor Dr. Albert Hirtl. From the academic side, I also want to thank Dr. Elisabeth Renner, she was always there to support me with any doubts I had regarding accelerator physics, and she made my on-site days better by being the best office colleague and friend. Furthermore, I would like to express my gratitude towards Dr. Adriano Garona from EBAMed, regarding the cardiac gating tools and accelerator instrumentation aspects. Finally, I would like to thank my family and friends for their continuous support. Particularly from Dipl.-Ing. Anna Shilo, Dipl.-Ing. Hanna-Helene Steiner and Christian Ramsl for correcting and proofreading this diploma thesis. I would like to wholeheartedly thank my father Adib Cherit Cardoso for being the first one to ever believe in my potential and my grandma Concepción Cardoso Martínez for teaching me to never give up. Last but not least, I would like to thank the International Atomic Energy Agency for supporting my master's in full via their IAEA Marie Skłodowska-Curie Fellowship Programme.

Kurzfassung

Ventrikuläre Tachykardie ist ein lebensbedrohlicher Zustand, der die Wahrscheinlichkeit eines plötzlichen Herzversagens erhöht. Stereotaktische ablative Strahlentherapie wurde als wirksame lebensrettende Behandlung für refraktäre (resistent gegen medikamentöse und interventionelle Behandlung) Patienten durchgeführt. Die Ionenstrahltherapie ist in der Lage, gezielt Energie in einer bestimmten Tiefe zu deponieren. Dies ermöglicht eine höhere Konformität der Dosisverteilung und eine bessere Schonung des gesunden Gewebes und von Risikoorganen. Diese Art externer Strahlentherapie benötigt Neuentwicklungen im Bereich von Gating-Tools, Synchronisations- und Oberflächenüberwachungstechnologien, welche bewegliche Irradiationsvolumnia und Atmungsdynamik berücksichtigen, um die Behandlungsgenauigkeit zu erhöhen.

Im Rahmen dieser Arbeit wurde ein Konzept für einen neuen medizinischen Arbeitsablauf entwickelt, welcher eine Behandlung von Ventrikulärer Tachykardie mittels hochenergetischer Teilchenstrahlen am MedAustron (Wiener Neustadt, Österreich) Therapie- und Forschungszentrum ermöglichen könnte. Die Kompatibilität zwischen dem Kontrollsystem des Teilchenbeschleunigers und externen Timings sowie Instrumenten, welche für diese spezielle Behandlung notwendig wären, wurde analysiert. Basierend darauf wurden fehlende Werkzeugen und Interoperabilitätsmängel ermittelt und Lösungen vorgeschlagen. Zusätzlich wurden drei Fallstudien durchgeführt, um geeignete Behandlungsdosen, Risikoorgane, klinische Ziele und Dosisgrenzen darzulegen. Darüber hinaus wurde die plattformübergreifende Kompatibilität der medizinischen Bilder mit den lokal verfügbaren Tools auf der Grundlage der Erfahrungen mit der stereotaktischen Photonentherapie untersucht. Optionen für die Extraktion von elektroanatomischen Daten, ihre Verarbeitung und Migration, -verarbeitung und -migration wurden skizziert und auf der Grundlage des aktuellen Stands der Literatur und von Expertenkonsultationen mit einem Benchmarking versehen. Zukünftige Entwicklungen umfassen die Simulation, das Testen und die Optimierung des gesamten medizinischen Arbeitsablaufs unter Berücksichtigung von Beam Gating, Atmungsdynamik und plattformübergreifender Bildkompatibilität sowie die Evaluierung der Auswirkungen einer neuartigen kardialen Gating-Sonde mit einem anthropomorphen 4D-Phantom. Darüber hinaus soll die Erforschung biologischer Effekte (z. B. Stenose, Depolarisierung oder Proteinaktivierung) bei unterschiedlichen Dosen in Herzgewebezellen untersucht werden.

Abstract

Ventricular tachycardia is a life-threatening condition that increases the probability of sudden cardiac failure. Stereotactic ablative radiotherapy has been performed as an effective life-saving treatment for refractory (resistant to pharmaceutical and interventional treatment) patients. Ion beam radiotherapy can deposit targeted energy at a specified depth. Allowing for higher conformity of the dose distribution and improved organs at risk sparing. For this type of external beam radiation therapy novel gating tools, synchronization, and surface monitoring devices that account for moving targets like the heart, and respiration dynamics are being explored to further favour treatment accuracy.

This work provides a prospective medical workflow to potentially accomplish life-saving ventricular tachycardia treatments with high-energy particle beams at the therapy and research centre MedAustron (Wiener Neustadt,Austria). In-house accelerator gating technology, external triggering signals and devices that could aid this specific treatment indication were assessed. As a result, the missing tools, possible bottlenecks and interoperability shortcomings were identified and solutions recommended. Additionally, three treatment planning case studies were performed to propose a suitable treatment dose, organs at risk, clinical goals and constraints. Furthermore, cross-platform medical image compatibility with the locally available tools based on the stereotactic photon therapy experience was investigated. Electroanatomical mapping data extraction, processing and target migration options were outlined and benchmarked based on state-of-the-art literature and expert consultations. Future developments encompass simulating, testing and streamlining the entire medical workflow considering beam gating, respiration dynamics, cross-platform image compatibility and evaluating the impact of a novel cardiac gating ultrasound probe with an anthropomorphic 4D phantom. In addition. the exploration of biological effects (e.g. stenosis, depolarization or protein activation) at different doses in cardiac tissue cells is to be investigated.

Contents

CHAPTER 1

Introduction

Radiofrequency catheter ablation (RFCA) is the current treatment approach for Ventricular Tachycardia (VT), but throughout the years it has been observed that this type of therapy has several limitations [1–4]. It is a very lengthy fluoroscopic guided catheter intervention that may take between 2–10 hours; it heavily relies on the experience of the cardiologist, the electrophysiologist, and the rest of the team (technicians, nurses, etc.), making it prone to failure and repetition (re-treatment). Furthermore, suppose the arrhythmogenic substrate in the heart is located closer to the septum. In that case, it is practically impossible to treat with this technique, primarily because the amount of energy required to reach this area and cause a scar is not attainable with radiofrequency.

Although stereotactic arrhythmia radioablation (STAR) has demonstrated clinical potential to overcome most of these drawbacks, radiotherapy with photons deposits higher doses to critical surrounding normal tissue when compared to ion beam therapy [5]. Ions possess a physical and biological advantage over photons, due to the targeted energy and dose deposition (Bragg Peak) at a certain depth. However, dose sparing, signal gating/triggering for moving targets, being able to cope with the interplay effect, and overall standardization remain a big challenge for ion beam radiotherapy. Considering that ion beam therapy is now well established for certain oncological indications, the opportunities to explore other treatments and techniques such as VT ablation are now possible. MedAustron [6] is an ion beam therapy centre and research facility focusing on radiation therapy, radiobiology, and acceleration physics. Making it a unique place for top-notch clinical and technological development in Austria and the European Union. Furthermore, it is one of the few centres worldwide to offer proton and carbon clinically and soon helium particles (currently being commissioned and only available for research purposes). Hence, new technologies are to be explored, validated, tested, and eventually implemented in the future.

Since VT radiotherapy ablation with ions is still experimental, it requires new technological developments, proper documentation, consistency, and evaluation of possible workflows to follow before becoming a clinical procedure. Making it the perfect occasion for MedAustron and the Landesklinikum Wiener Neustadt to collaborate and together develop the integral workflow for VT ablation utilizing high-energy ion beams (protons).

Furthermore, in 2020, the European Union's Horizon research and innovation program provided a grant (No 945119) to the Standardized Treatment and Outcome Platform for Stereotactic Therapy Of Re-entrant Tachycardia by a Multidisciplinary (STOPSTORM) consortium to benchmark, consolidate, and standardize all efforts across the European Union related to VT radiation treatments, presenting a very favourable situation to learn from more experienced centres and experts within the consortium.

In parallel, the interoperability of gating, synchronization, and monitoring devices will be evaluated in terms of the available technological resources on-site. Since the chest cavity has several dynamic structures (heart, lungs, and the diaphragm) that are governed by the respiration cycle, surface scanning is essential for delivering the desired dose at the target volume with the highest degree of precision and accuracy.

1.1 Objectives and Aims

Aim: Conceive the required workflow from beamline extraction up to in-room treatment delivery with its respective technical specifications and constraints. Taking into account in-house interfaces, clinical and technological availability.

Objective sequence:

- Study novel treatment methods using particle therapy with potential application in ventricular tachycardia treatments.
- Study interfaces of the MedAustron particle therapy facility and evaluate the technical compatibility with new tracking devices based on ultrasound diagnostics and benchmark (if available) other triggering technologies.
- Once technical compatibility is ensured, conceive, study, and analyze the potential data acquisition workflow to identify existing bottlenecks and shortcomings.
- Propose a treatment plan with reasonable constraints, dose and target coverage with potential clinical application.
- Explore the compatibility of medical and physiological imaging and its optimal visualization for treatment planning.
- As a final step, the potential medical workflow from cardiac diagnostics, treatment planning, target tracking, gating application, and delivery will be outlined.

CHAPTER 2

Theoretical Background and Related Work

2.1 Clinical Cardiology - Ventricular Tachycardia

The burden of morbidity and mortality in patients with heart failure is heavily influenced by ventricular tachycardia (VT) [7]. A VT is a tachycardia originating from the ventricles, resulting in a heart rate of more than 100 beats per minute resulting in an abnormal heart rhythm [8]. These abnormal heartbeat signals occur due to an electrical conductivity disarray where the impulse starts at the ventricles and not at the sinoatrial (SA) node. Consequently, the heart is no longer able to adequately supply oxygenated blood with the optimal flow and pressure throughout the body. This condition is life-threatening and increases the probability of death due to sudden cardiac failure [9]. The main cause of VT is damage to the cardiomyocytes (heart muscle cells) after ischemic [1] heart disease resulting in cardiac electrical conduction impairment.

2.1.1 Etiology of Ventricular Tachycardia (VT)

There are two classifications for tachycardia, normal or unsustained and sustained. The first one occurs when people undergo mental or physical stress which leads to an elevated heart rate condition, originating at the sinoatrial node (SA) located in the right atrium of the heart. This type of tachycardia is regulated within a few seconds and has no adverse effects on hemodynamic stability [10]. Whereas sustained tachycardia refers to an abnormal condition that arises at the ventricular septum, and manifests as a prevalent heart rate increase for more than 30 s due to premature ventricular contraction (PVC).

Inducing critical hemodynamic compromise, where it is no longer possible to adequately supply oxygenated blood with the optimal flow, and pressure throughout the body; especially to peripheral organs due to the reduced ejection fraction [11]. Additionally, hereditary or genetic conditions like Brugada syndrome or long QT [2] syndrome might contribute to the development of VT.

[1] Debilitated heart muscle due to reduced blood flow over time.
[2] Interval between ventricular depolarisation (activation) and repolarisation (recovery) of the heart, see figure 2.1 in the section below

Other risk factors include abnormal heart valves, cardiomyopathy, and preexisting heart failure. The electrocardiogram (ECG) is the primary diagnostic tool and a basal treatment planning component for VT therapy. With it, the cardiac cycles are analyzed in terms of their rhythm, localization, and electrical activity [12]:

- **P wave:** atrial depolarization. The sinus node, also known as the sinoatrial node, creates an action potential that depolarizes the atria.
- **QRS complex:** represents the depolarization and therefore the contraction of ventricular muscle fibers of the heart:
  - Normal duration: 0.08 and 0.10 s,
  - Intermediate duration: 0.10 and 0.12 s,
  - Abnormal duration: + 0.12 s.
- **T wave:** repolarization of the ventricles.

The PR interval, QT interval, and ST segment are other ECG characteristics that provide more details on the timing and length of electrical activity in the heart (see figure 2.1).

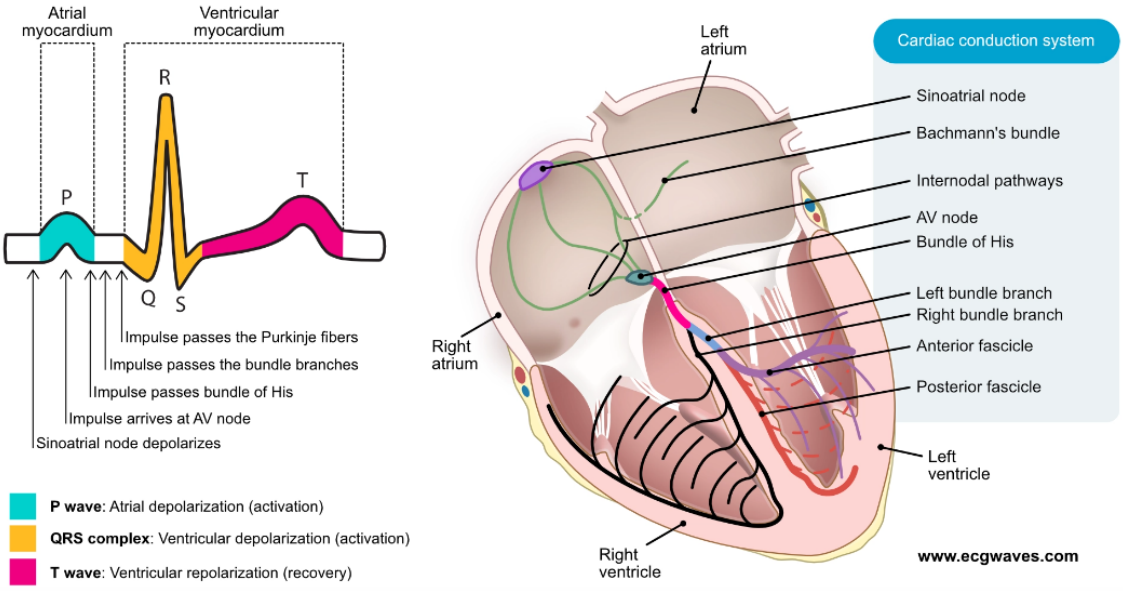

Figure 2.1: The action potential released by sinoatrial node cells initiates the cardiac cycle by sending an electrical impulse from the atria through the atrioventricular node and into the ventricles. A contraction reaction is triggered by the moving impulses, which generate the ECG signal. The P-wave represents atria activation (aquamarine highlight), the QRS complex represents ventricular activity (yellow highlight), and the T-wave shows depolarization recovery (magenta highlight) [13].

Understanding the origin of ventricular tachycardia is crucial for the management of VT and the avoidance of sudden cardiac death. VT can be monomorphic (MVT) and polymorphic (PVT), which refers to single or multiple areas of the heart that have abnormal rates, clinically denominated as arrhythmogenic substrates.

MVT occurs when the origin of the arrhythmogenic substrate occurs within the ventricle, and the ECG records identical QRS complexes. The most typical form of monomorphic ventricular tachycardia is seen in patients with underlying structural heart disease with pulsations around 220 beats per minute. In this form of ventricular tachycardia, there is a predominant zone of sluggish conduction caused by scarring or fibrillar disarray. Whereas for PVT arrhythmogenic substrates originate from various locations within the ventricles. As a result, it induces a continually changing and asymmetrical morphology of the QRS complex. In this case, pulsations may vary between 150 to 250 beats per minute, which leads to heavily compromised haemodynamics [14].

If the patient is symptomatic and unstable (which means that there are signs of inadequate perfusion or negligible cardiac output), an immediate shock cardioversion should be performed. Non-life-threatening cases are evaluated by the cardiologist to decide upon the most suitable treatment [15].

2.1.2 Patient Selection: Symptoms, Indications, and Treatment Eligibility Criteria

Cardiovascular diseases account for 45% of the major causes of death in Europe [16]. Sudden cardiac death is significantly influenced by ventricular tachycardia (VT) and ventricular fibrillation. Therefore, it is of utmost importance to characterise the VT, its etiology and identify all the symptoms in order to be able to adequately manage the patient's condition. Depending on individual circumstances and particular features of the patient's VT, the precise requirements and eligibility for certain treatments may change. However, the following conditions, often suggest that a patient is a suitable candidate for VT ablation [17]:

1. **Acute Symptomatic:** repeated bouts of monomorphic VT that cause palpitations, light-headedness, fainting, chest discomfort, or shortness of breath.

2. **Haemodynamically unstable:** low blood pressure or reduced cardiac output, these patients require prompt intervention and care.

3. **Medication intolerance or insufficient response:** delayed or bad response to antiarrhythmic drugs or who are unable to tolerate their adverse effects.

4. **Structural heart disease:** previous heart attacks (myocardial infarction), cardiomyopathy, or scar tissue in the heart.

5. **Electrical storm:** numerous and recurring bouts of VT ($>$ 3 VTs requiring ICD (implantable cardioverter defibrillator) therapy (antitachycardia pacing or shocks) or external defibrillation in 24 hours).

A medical doctor and the electrophysiologist make the final judgment for treatment eligibility on an individual basis. Only after carefully evaluating the patient's medical history, metabolism, symptoms, electrocardiographic features, imaging data, and comorbidities a decision is made.

2.1.3 Surgical Methods

During the 50s and late 60s, the only approach to cure VT maladies was to perform open heart surgery, in which ventricular arrhythmias were eliminated after excising ventricular aneurysms (aneurysmectomy) [18–20] or bypassing the coronary artery for revascularization [21, 22]. Years later, between the 80s and early 90s with the introduction of minimally invasive surgery (electrode catheter interventions) [23, 24] and the implementation of cardiac electrophysiology [11, 25], the approach changed radically worldwide. Additionally, electrophysiological mapping (EAM) [26, 27] and fluoroscopy became the standard to plan and manoeuvre inside the patient's heart chambers and circulatory system [28]. With time, radiofrequency ablation became the standard to treat VT. Today, patients are prescribed beta-blocker antiarrhythmic medication (adrenaline inhibitors to reduce the heartbeat) [29], ICDs as first-line solutions before undergoing interventional radiofrequency catheter ablation (RFCA). Any of these approaches aim to control cardiac electrical signals to reduce the rapid heart rate and reset the heart rhythm to a normal pace[30].

However, for some patients, these techniques turn out to be futile and impose additional risk, due to their critical or complex condition. Catheter interventions, typically need to be repeated because of recurrent arrhythmia. The reachability of the appropriate VT area poses another obstacle to ablation. Effective ablation is hampered by deep intramural or subepicardial sites, particularly those close to structures like coronary arteries, and as a result, 20–50% of patients experience recurrent VT following catheter ablation [31, 32]. Furthermore, catheter ablation interventions are time-consuming (between 4 to 10 hours) and have an inherent risk of adverse effects making them poorly effective and even impossible to perform in some cases.

Additionally, these interventions are highly dependent on the experience of the surgeons and require the constant use of fluoroscopy with doses around 15 mSv [33]. Radiofrequency catheter ablation has another major drawback, high energies and pressure are required to penetrate the arrhythmogenic tissue.

This means that VT locations at the catheter distal pathways, primarily within the septum are practically impossible to treat with this technique. Because the amount of energy required to do so is out of range for radiofrequency.

2.2 Radiation Therapy Treatment for Ventricular Tachycardia

For patients with refractory (resistant against treatment) VT, stereotactic arrhythmia radiotherapy (STAR), also known as cardiac radioablation with photons or high-energy ion beams has emerged as an innovative and promising therapeutic option. Both are non-invasive procedures that accurately "ablate" the identified arrhythmogenic substrate by inducing fibrosis at the ventricles using ionising radiation. In the upcoming subsections, both will be presented historically and addressed in terms of the current state-of-the-art, advantages and disadvantages.

2.2.1 Cardiac stereotactic arrhythmia radio-ablation

Cardiac stereotactic arrhythmia radio-ablation (STAR) is an image-guided catheter-free photon radiotherapy treatment for VT. The first preclinical studies date back to 2010 [34], and the first clinically approved treatments were performed in 2012 [2, 35] and 2014 [36]. Ever since, this treatment has shown promising results, especially over the last 5 years for persistent/recurrent VT or risk of an electrical storm [4, 37–39]. STAR therapy is an intricated multidisciplinary procedure that involves several professionals and components that are highly specialized. The team must involve cardiology, radiation oncology, medical and potentially accelerator physics, engineering, and instrumentation professionals. This therapy may enhance the patient's quality of life, and lessen and even eliminate the uncomfortable and potentially deathly effects of VT [40].

In 2015, Loo et al. presented the first STAR case report, using a 4DCT-based internal target volume (ITV) to account for cardiac and respiratory motion. Cuculich et al. reported the first series of patients (5 in total) treated with a C-arm LINAC with 25 Gy in a single fraction. Four weeks post-treatment, a 99% reduction of VT episodes was observed. In terms of dose, fast delivery of 25 Gy has proven to be effective. Nonetheless, overall functional impact on the scar with potentially higher doses over 30 Gy to the main VT substrate and potentially lower doses to 20 Gy in the direction of close OARs seems to be clinically effective, safe, and attainable [41]. Likewise, Neuwirth et al. reported on 10 patients who received cyberknife treatments between 2014 and 2017. Cardiac dynamics were compensated by delineating an ITV and conveniently utilizing the implantable cardioverter defibrillator (ICD) lead as a fiducial marker. After receiving a single dose of 25 Gy, the VT load diminished by 87.5% [42]. Thereafter, publications addressed different treatment planning approaches and workflows for STAR treatments. The typical workflow overview [43] can be seen in figure 2.2:

1. **Diagnostics and Pre-Planning:** the cardiologist and electrophysiologist define the VT arrhythmogenic substrate. This is obtained through electroanatomical mapping (EAM) which can be derived from previous invasive procedures (e.g., radiofrequency ablation), and/or a non-invasive approach (e.g., superficial electrodes).

2. **Treatment Planning and Imaging:** the patient undergoes a 4DCT scan with the aid of some fixation/immobilization devices. Subsequently, the resulting imaging study and any other anatomical data from other modalities like contrasted CT, magnetic resonance imaging (MRI), and/or positron emission tomography (PET), or scintigraphy imaging are revised and registered if needed [44–47].

3. **Treatment Planning Design:** the VT target locations are transferred to the planning CT form the EAM. At this stage, organs at risk (OARs) with their respective dose constraints are defined and the dose prescription to the target is defined. These factors are considered in the treatment planning software (TPS) for the dose distribution optimization (Monte Carlo dose engine). Ideally, the full prescription dose is given to the entire target volume and OARs are maximally spared [5].

4. **Treatment Delivery:** at first, the plan is transferred to the medical frontend and the patient-specific-quality assurance (PSQA) of the treatment plan is performed with a water phantom and dosimetric equipment instead of the patient.

As soon as the comparison of the calculated dose distribution shows good results with the measured dose distribution, the patient can come for treatment. Once the patient arrives, she or she must be carefully positioned with the aid of some fixation devices to replicate the same geometry, set-up and configuration as the imaging planning stage.

In some cases, repositioning might be required after target volume localization. Typically a single dose of 25 Gy (photons) is given to the patient and the beam is gated to respiration (via surface scanning) [46]. In some cases, breathing techniques and forced respiration are used to reduce one dynamic degree of freedom and reduce overall uncertainty [48].

5. **Treatment Evaluation and Follow-up:** the cardiologist together with the radiation oncologist evaluates the patient's treatment response, outcomes, and toxicity over time. If all of the patient's symptoms have vanished (there has been no recurrence) and no new ones have appeared, the treatment is deemed successful. Instant relief from VT symptoms has been reported in patients hours after the treatment delivery. Some others were VT free for 6-12 months after treatment was received and a particular case is known where a patient has been 4 years VT free and asymptomatic [42, 49, 50].

The acute and long-term effects of STAR irradiation on the whole heart (animal models only [51]) or in certain substructures are being investigated. Additionally, the precise radiobiological processes in both healthy and diseased cardiac tissue are still not fully explored, despite recent data suggesting that STAR at lower doses (20-25 Gy) may quickly induce reprogramming of cardiac conduction and radio ablation at higher doses > 30 Gy up to 55 Gy may induce scar formation [52–55]. Accurate suggestions for the prescription dose, ideal dose inhomogeneity, and maximum dose are difficult to address because it is a relatively novel technique. Initial clinical data revealed encouraging outcomes, with a significantly decreased or even suppressed VT load following therapy [1, 3, 41, 56, 57]. Robinson et al.'s initial prospective clinical study (NCT02919618) assessed the safety and effectiveness of STAR. Limited initial toxicities were observed, and the 1-year survival rate was equivalent to that of patients who had been treated with antiarrhythmic medications or RFCA. Furthermore, significant improvement of their QOL was observed[56].

Due to its complexity in terms of substrate identification by EAM, target volume delineation, assessment of cardiac and respiratory movements, and application of high-dose single-STAR remains a multidisciplinary challenge. Even though there are multiple clinical studies for STAR that are presently recruiting in Europe (such as NCT03867747 [58],23,04642963 [59], and NCT04066517[60]), further multi-centre assessment and standardization of this innovative method in terms of substrate mapping, target delineation, dosimetry and other aspects is urgently required [58, 61].

At the moment there is an initiative called the "STOPSTORM Consortium" led by Dr. Martin Fast and coordinated by his team at the University Medical Centre Utrecht in the Netherlands. Constituted by 31 members, 22 radiation oncology departments and 24 electrophysiology departments throughout eight European nations.

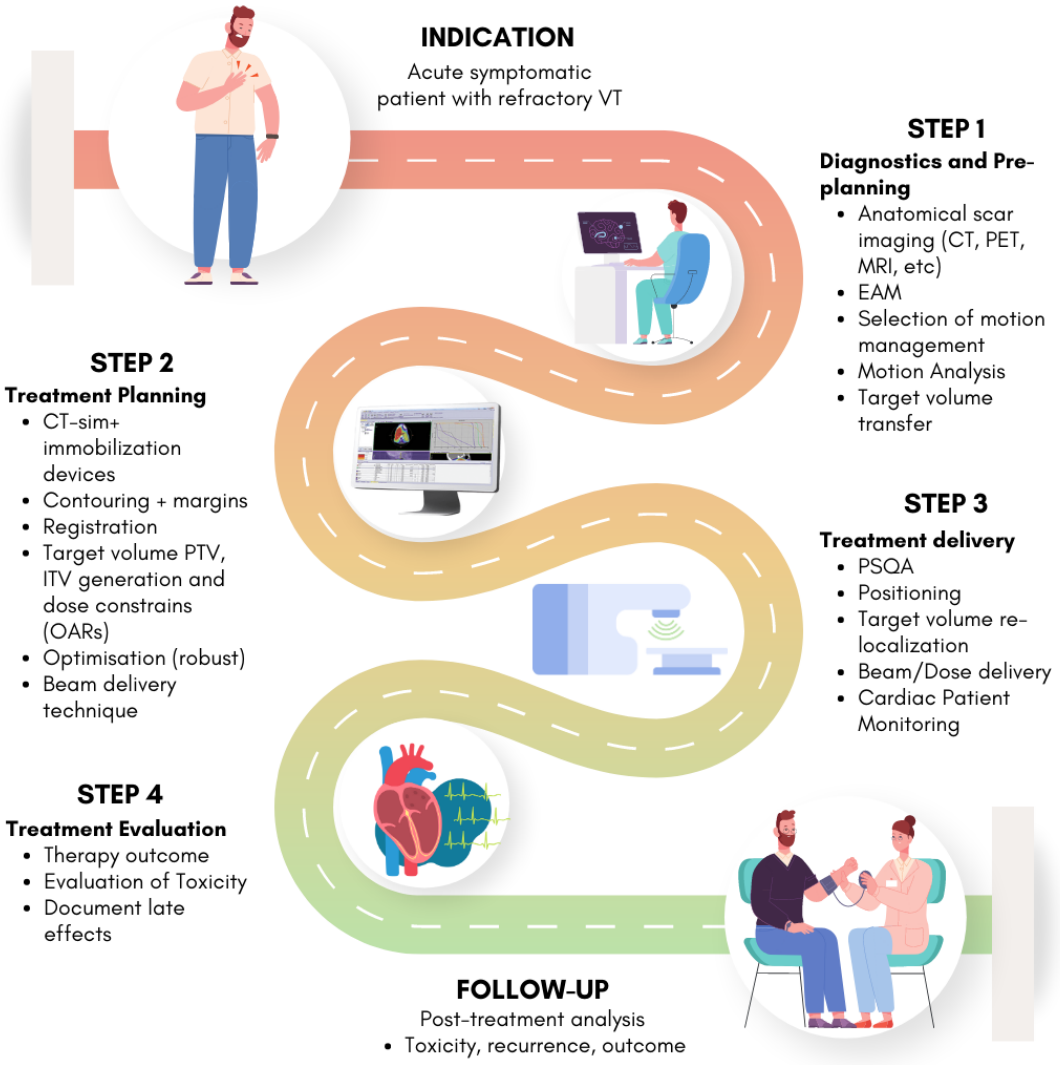

Figure 2.2: Workflow for Noninvasive Cardiac Radioablation via Electrophysiological Mapping (EAM). Applicable to STAR (Created with Canva).

This group brings together clinical and technological competence in catheter ablation, and/or STAR therapy. All members are eager to collaborate on a European level to implement radioablation for VT in clinical practice [62]. To this date, their major contributions to the field are reflected in a comprehensive survey in which they evaluated the outcomes and current clinical practice of STAR in Europe [63]. Dr. Oliver Blanck and Dr. Melanie Grehn are leading and coordinating the biggest benchmark study on Radiosurgery for ventricular tachycardia (RAVENTA). As a result, they have suggested dose constraints for OAR, cardiac substructures and treatment goals [64].

2.2.2 Cardiac Ablation with Ion Beams

Ion beam therapy is well established for certain indications in oncology and it has demonstrated enhanced physical and biological advantages over conventional therapy with photons or electrons [65].

Particle beams release the vast majority of their energy at the Bragg Peak, which is located at the most distal part of their kinetic trajectory. Whereas photon and electron beams have the highest energy deposition close to the patient surface as one has to consider the build-up effect [66]. Therefore, ion beam therapy has the advantage of reducing the overall integral dose and selectively sparing the most sensitive structures [67]. Hence, high-energy beams of proton and carbon-ions have been investigated to treat VT (see figure 2.4). One of the most influential in-vivo studies regarding ion beam cardiac treatment was performed back in 2006 at HIMAC (Heavy Ion Medical Accelerator in Chiba) in Japan. The coronary arteries of 24 rabbits were injected with microspheres to induce non-transmural myocardial infarction (MI). As controls, 24 rabbits without MI were kept in a separate group.

Two weeks after inducing MI, an accelerator was used to administer targeted external heavy ion beam irradiation (THIR; 15 Gy). It was then concluded that rabbits with MI, after heavy-ion radiotherapy presented elevated connexin-43 (Cx43) expression (gap junction protein of the cardiac tissue that is responsible for intercellular communication) in the ventricle, which enhances conductivity, lessens repolarization's spatial heterogeneity, and lessens VT/VF susceptibility [68]. To this date, there are only few studies that have been published about the effects of ion beam therapy on the overexpression of potentially helpful proteins for improved cardiac conductivity pathways in humans [52, 69] and in animal models [68, 70–73].

The next major contributions to the field were the first ECG-4D treatment planning method, and dose reconstruction algorithms for cardiac ablation with scanned C-12 particles also in a porcine model [74]. In addition to the first design of immobilization techniques and devices to handle cardiac dynamics (porcine model), as well as robust RT planning methods [75]. A couple of years later, in 2018, a comprehensive overview of the VT radiotherapy state-of-the-art at that time was performed, in parallel to the first feasibility study of intensity-modulated proton therapy. The Helmholtz Centre for Heavy Ion Research (GSI) in Darmstadt Germany; the Mayo Clinic Rochester in USA, and the Heidelberg University Clinic in Germany also participated in this project. As a result, they emitted some recommendations on how to overcome the most common workflow challenges and guidelines on how to perform the transition from porcine to human models for clinical trials [76]. Based on this series of recommendations, in 2018 the Washington School of Medicine performed its study on treating patients with VT using intensity-modulated proton therapy. Their suggestions call for further investigations regarding delivery errors caused by target motion due to interplay effects [77]. A year later in 2019, a group at the Mayo Clinic proposed proton dose levels for scar formation in VT patients. Pre-clinical investigations determined that myocardial tissue subjected to a dose of at least 25 Gy is more likely to develop lesions than tissue exposed to a dose of less than 10 Gy.

Overall, the association between external proton beam therapy dose and the development of cardiac lesions was quantified in this study, which is significant for setting the correct dose levels in the treatment of VT with ions for the future [78]. The same year, a method to evaluate proton VT treatment success in a porcine model by quantifying the left ventricular ejection fraction (LVEF) was published. However, the doses investigated were between 40 Gy and 30 Gy which are significantly higher than the doses employed and reported by other groups at different centres [71].

By 2020, the proton research group from Azienda Provinciale per i Servizi Sanitari APSS in Trento Italy led by Lamberto Widesott, compared for the first time photon vs. proton radiation therapy for VT. Breath-holding and ECG-gated robust optimisation treatment planning techniques were also evaluated for these two modalities. They concluded that for both modalities robust optimization techniques resulted in a significant dose sparing, this was even higher for ions. Additionally, respiration and cardiac dynamics were mentioned as the most critical challenges to deal with; due to the consequences of the interplay effect and the treatment aims to improve precision [5].

A few months later in 2021, the National Center of Oncological Hadrontherapy (CNAO) in Pavia Italy, performed the first-in-man case of non-invasive proton radiotherapy for refractory ventricular tachycardia in advanced heart failure. The dose prescription and fractionation scheme were based on Japanese ion therapy techniques [52] and other dose prescription experiences by Molinelli et al. and Fossati et al. [79, 80]. The treatment was tolerated by the patient, safe and suppressed almost immediately the VT episodes. Nevertheless, they pointed out that doses above 25 Gy are more likely to induce transmural scar formation, and that this effect is directly proportional to the dose applied to the tissue. Early endothelial cell vacuolization and oedema, along with up-regulation of connexin-43 expression in cardiomyocytes are other effects observed at this dose threshold (25-30 Gy) [49]. This protein expression increases conduction velocity and decreases repolarization heterogeneity, hence they have been proposed as transient mechanisms for acute VT suppression while the scar formation process induced by a certain dose is still unknown [81].

Apart from the dynamic challenges imposed by this type of therapy, another point of interest is to build consistent clinical evidence and Relative Biological Effectiveness (RBE) [3] confidence. Making networks between accelerator facilities, hospitals, and academic institutions is crucial to accomplish standardization [82, 83]. Moreover, patients with recurrent VT, do not form a uniform population. However, with only one reported case it is too early to know if ions will have the same effect with protein upregulation as photons do, as studies in this regard are lacking or simply not reported in scientific literature. It is also important to highlight that in general cardiac toxicities in humans remain poorly studied when compared to the toxicities reported and studied for oncology [84, 85]. The adequate dose prescription is relevant because it determines the effect that can be inflicted on biological cells like critical DNA damage, induced fibrosis, or loss of polarization, these ultimately result in impaired or lost conductivity (especially relevant for myocardial tissue) [86].

The biggest challenge relies on the fact that each facility has its inclusion standards, imaging protocols, and/or target definitions. Present studies and facilities don't have the power to prepare for late-stage phase III trials or clinically verify the most suitable treatment strategy or dose levels to address high-energy ion VT treatment. For this reason, the STOPSTORM consortium includes this treatment modality under its scope to aim for clinical safety and consistency hereafter. This will be achieved by collecting and analyzing all data in a validation cohort study, standardizing pre-treatment and follow-up protocols, and coordinating all European efforts to clinically validate radiation therapy for VT.

[3] For more information on RBE see section 2.7.

At the time being, pre-existing protocols and recommendations are revised and improved in terms of volumes of interest, specify and model the ideal target region and target dose in relation to surrounding healthy tissues (OAR), and ascertain which patient population and underlying cardiopathies that best respond to any VT ablation modality: STAR or high-energy ion RT [62]. Additionally in 2022, the AAPM (American Association of Physicists in Medicine) published task group report 290. They emitted a series of recommendations that aim to standardize respiratory motion assessment and SOPs for particle therapy [87], because, the dose uncertainty induced by respiratory motion and moving target dynamics (heart) remains a major clinical concern in this area. To this end, the best motion-mitigation and beam gating/triggering approaches are being investigated in various clinics and research centres in terms of the local capabilities and resources. Ensuingly, further follow-up and development of standard operating procedures (SOPs) will be necessary [86, 88, 89].

EBAMed [90] (Geneva, Switzerland) is a startup company that designs gating instrumentation for cardiac arrhythmia non-invasive EBRT with protons. In 2022, there was a collaboration between EBAMed and MedAustron's AVID department to quantify accelerator beam losses via BLM sensor probes. With the aim to determine which detector (gamma or neutron) had the best in-room sensitivity performance at different configurations, when a signal was used as a trigger to open or close the accelerator chopper ([4]). BLMs are conventionally used in the accelerator ring for beam diagnostics and safety purposes [91], but in this case, they were used as in-room measurement devices for gating latency determination. In order to measure in-room beam delays, the beam only gets "unblocked" by the chopper at the StartChopper timing event signal, in it is expected that there is a delay of several hundred ms from StartExtraction (triggered command) to the first detection of beam in the room. The results of these measurements were then used as a reference for testing a potential medical device of their design to gate the accelerator chopper at a specific trigger signal.

Two of the biggest obstacles that ion beam radioablation must overcome are controlling the target cardio-respiratory movements and minimizing positioning-related uncertainty. To tackle these issues, an ultrasound probe assisted with artificial intelligence (AI) algorithm has been developed by EBAMed to create a system prototype that can automatically capture and analyse ECG data to determine cardiac displacement in real-time. This is performed by matching the LINAC coordinate system to the reference CT data via optical tracking of IR-markers attached to the ultrasound probe[92].

In addition, a case study was conducted to demonstrate the feasibility of transthoracic ultrasound guidance in cardiac particle therapy to monitor heart motion, particularly in proton therapy due to its strong dose gradient [93]. The knowledge gained from the BLM measurements and these case-study findings were used as groundwork for further investigations regarding the functionality and compatibility of this novel gating technology into the medical workflow.

[4]For more information see section 2.9.1 Synchroton Acceleration Technology for more information.

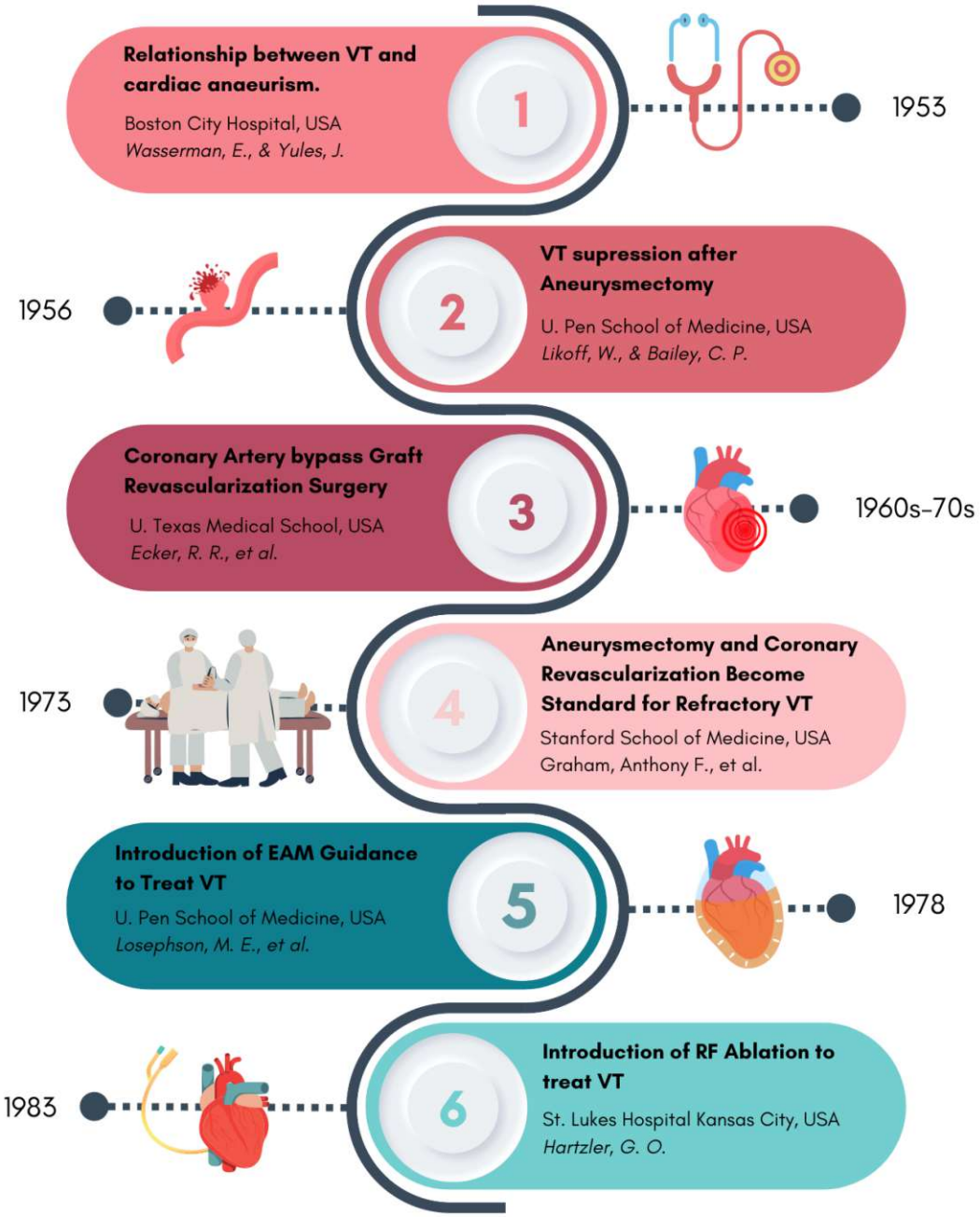

Figure 2.3: Milestones through the history of VT ablation (Part 1: Surgical Methods). From open heart surgery, through minimally invasive catheter interventions (created with Canva).

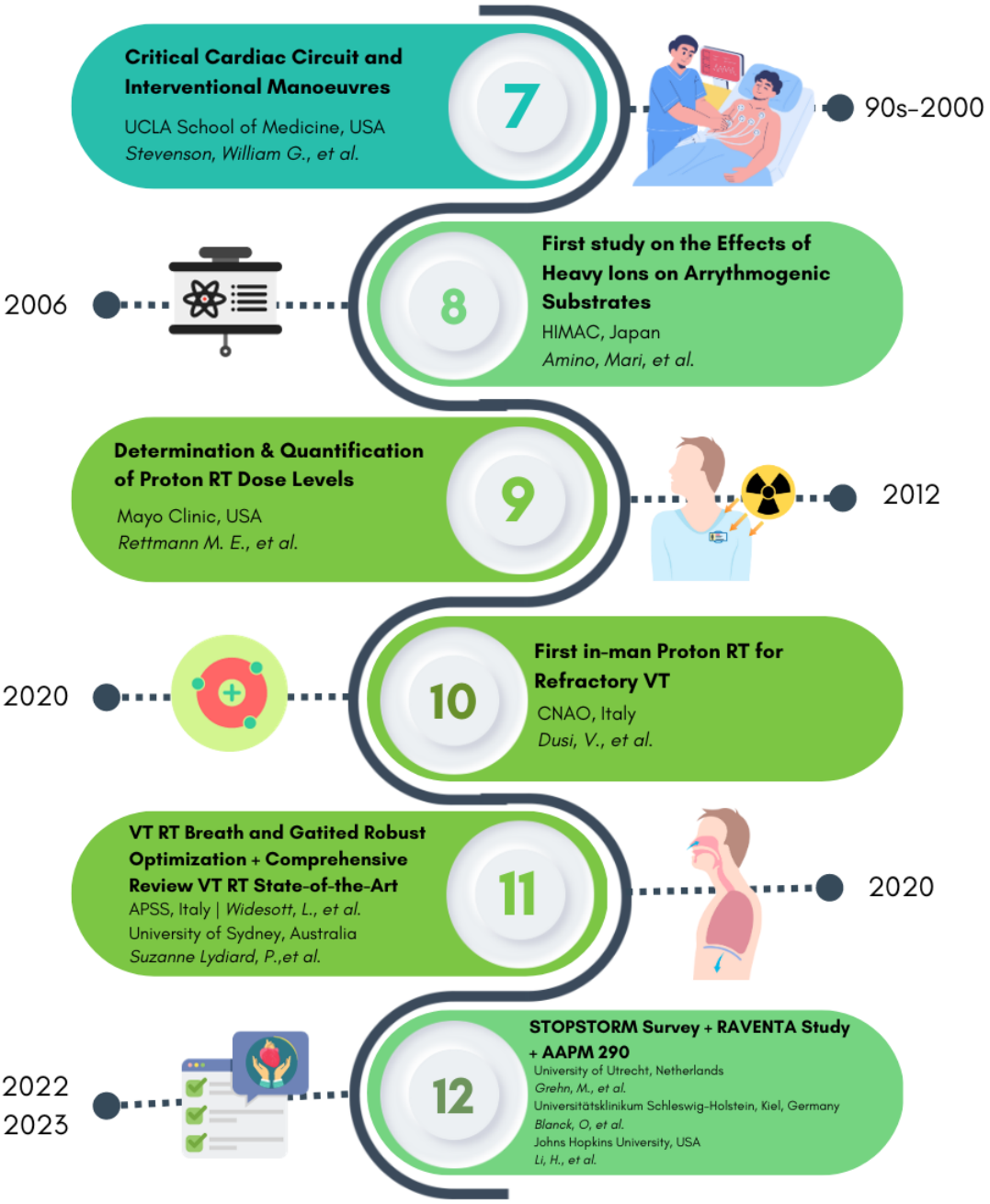

Figure 2.4: Milestones through the history of VT ablation (Part 2: Radiation Therapy). From cardiac circuit interventional manoeuvres to photon and high-energy ion beam therapy (created with Canva).

2.3 Basic Principles of Ion Beam Therapy

Ion beam therapy has physical and biological advantages when compared to photon or electron beam therapy, which are associated with how ions lose energy in matter and the so-called "Bragg Peak". This allows precise dose and energy deposition at a specific depth with no or very low exit dose [5]. In comparison, photon beams deposit the maximum dose after the build-up region (near the proximal surface) and have an infinite range. As a result, some of their energy is deposited into the healthy tissue situated behind the tumour. Thus, to achieve a conformal dose distribution the amount of rays used and their respective angles must be increased. Potentially raising the risk for secondary tumours and other side effects [94, 95]. In figure 2.5, the depth dose profiles of electron, photon [6], and proton beams are shown for energy deposition comparison.

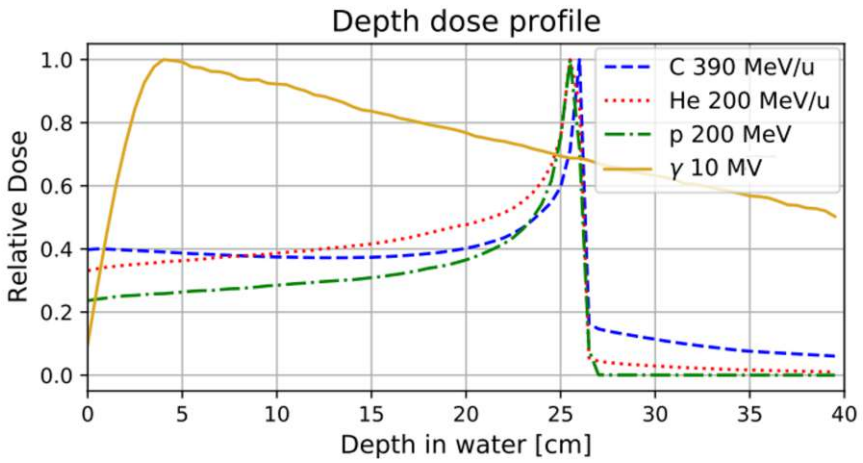

Figure 2.5: The depth-dose curves for 390/u MeV carbon (royal blue), 200 MeV/u helium (red), 200 MeV protons (green) and 10 MV photons/x-rays (ocre). Protons have a constant entry dosage that is smaller than the desired dose and has no exit dose when compared to photons or electrons. Compared to electrons, the dosage fall-off at the end of the proton range is far steeper. In conclusion, the majority of the radiation energy deposited by photons is outside the target, while the majority of the radiation energy deposited by protons lies inside the target and produces no exit dose [96].

Furthermore, it is also possible to observe a difference between the ions themselves. The advantage of carbon ions over protons is that they have less lateral scattering, which causes a sharp lateral dose fall-off around the target. Moreover, projectile fragments form nuclear interactions that comprise the "fragmentation tail" which contributes to dose and energy deposition behind the target volume [97]. Protons, on the other hand, have no additional dose or energy deposition into the neighbouring structures behind the target volume. Range uncertainties and the widening of the Bragg peak are caused by fluctuations in the energy loss of individual ions (also known as "energy straggling").

[5] For ions heavier than protons, there is always a fragmentation tail, which contributes to a non-vanishing exit dose.

[6] 10 MV is the convention for the acceleration voltage of the electrons accelerated in the first place which then generates photons in the tungsten (or other high-Z) target in the accelerator head.

Protons have a wider Bragg peak compared to carbon ions because their energy straggling is higher by a factor of 3.5. For practical reasons, ripple filters [7] are often added to the carbon-ion beam line to broaden the Bragg peak and minimize the number of energy layers needed to provide uniform dose distributions to the target in ion beam therapy [98] (see figure 2.6 below to compare the characteristics of photon, proton and carbon ion beams in terms of their physical characteristics, advantages and disadvantages).

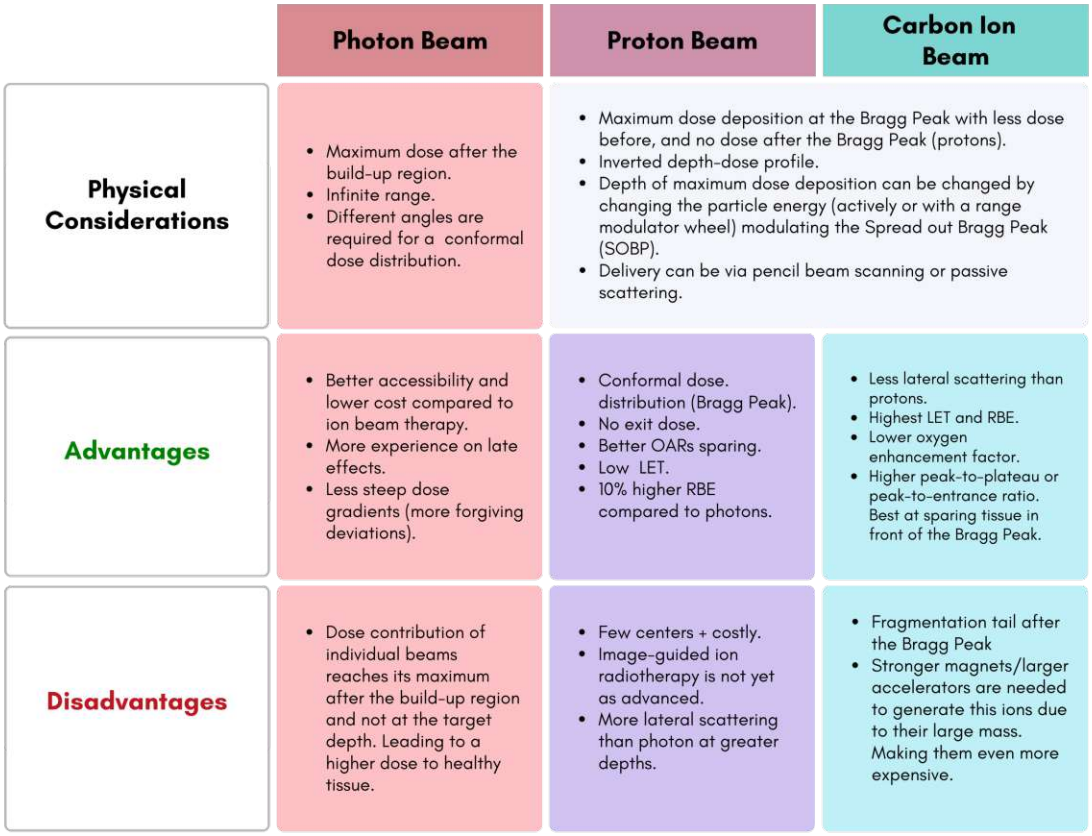

Figure 2.6: Photon, Proton, and Carbon-ion beam therapy comparison in terms of their advantages, disadvantages and their physical considerations [99].

2.3.1 Particle Interaction Mechanisms

Every particle in an ion beam will ultimately interact with nearby matter, whether directly or through secondary interactions or decay products. Furthermore, the type of event is directly dependent on the particle type and energy (see table 2.1 below).

High-energy protons can be used as an example to demonstrate the complexity of particle-matter interactions. To a first-order approximation, protons often engage in inelastic Coulomb interactions with atomic electrons, which causes them to have a continuous loss of kinetic energy, because the mass of a proton is 1832 times larger than that of an electron, and most protons move almost in a straight line trajectory.

[7] Energy modulation components (located at the nozzle) used to broaden the Bragg peak to get smoother output, denominated SOBPs

[8] For ions heavier than protons.

Interaction Type	Interaction Target	Ejectiles	Influence on projectile	Dosimetric Manifestation
Inelastic Coulomb Scattering	Atomic electrons	Primary proton, ionization electrons	Quasi-continuous energy loss	Energy loss determines range in patient , secondary electron production
Elastic Coulomb Scattering	Atomic nucleus	Primary proton, recoil nucleus	Change in trajectory	Determines lateral penumbral sharpness
Non-elastic nuclear interactions	Atomic nucleus	Secondary protons heavier ions, neutrons and gamma rays	Removal of primary protons from beam, fragmentation tail [8]	Primary fluence, generation of stray neutrons, generation of prompt gammas for in vivo radiation
Bremsstrahlung	Atomic nucleus	Primary proton, Bremsstrahlung photon	Energy loss, change in trajectory	Negligible

Table 2.1: Summary of proton interaction types, targets, ejectiles, influence on projectile and selected dosimetric manifestations [100].

In contrast, a proton encountering an atomic nucleus undergoes a repulsive elastic Coulomb contact that, because of the nucleus's substantial mass, causes the proton to deviate from its initial straight-line trajectory. Although less frequent, inelastic nuclear interactions between protons and the atomic nucleus (see image 2.7 below) have a considerably more significant impact on the fate of a single proton. When a nuclear reaction occurs, the projectile proton penetrates the nucleus, which then releases one or more neutrons, deuterons, tritons, or heavier ions. Finally, as the particle energy decreases, other processes become more dominant in occurrence: Compton scattering, photoelectric effect, and ionization losses of charged particles. However, proton Bremsstrahlung is theoretically conceivable but has a small impact at therapeutic proton beam intensities [100, 101].

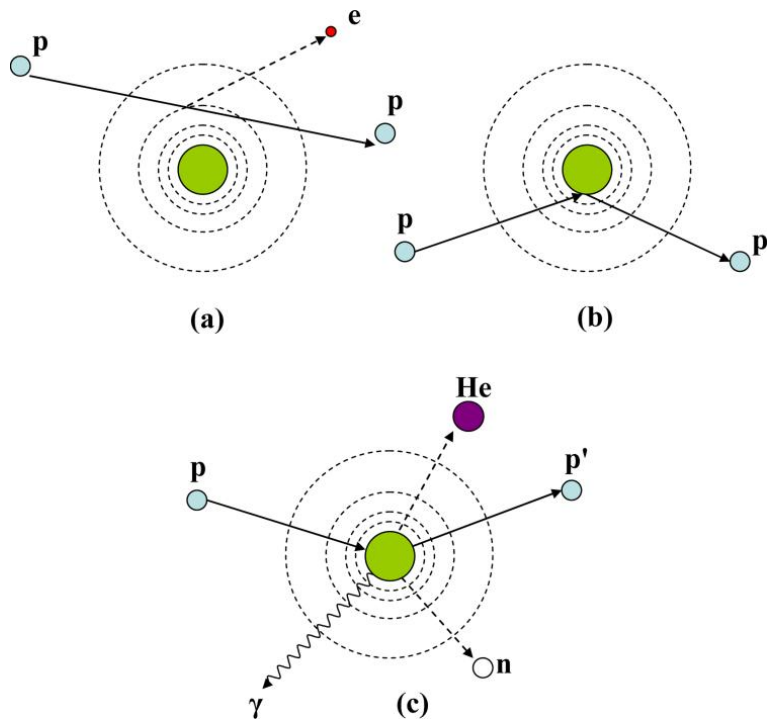

Figure 2.7: Proton interaction processes are depicted schematically as follows: (a) energy loss through Coulomb interactions, (b) trajectory bending due to repulsive Coulomb scattering with the nucleus, and (c) removal of the initial proton and production of secondary particles by non-elastic nuclear interactions. (He: Helium, n: neutron, e: electron, g: gamma rays [100].

2.3.2 Linear Energy Transfer

The (unrestricted) linear energy transfer (LET) is the average amount of energy that is lost along an ionizing particle's trajectory (dE_L) per unit path length due to electronic interactions and is defined by the equation[102, 103]

$$\text{LET} = \frac{dE_L}{dl}. \tag{2.1}$$

This quantity is positive and directly dependent on the nature of radiation and the material being traversed. Its importance relies on the fact that this quantity is used to determine the biological impact of radiation exposure.

Although Newton is the proper SI unit for LET, it is most frequently represented in terms of J/m, MeV/mm or keV/μm, which stand for Joules per meter, mega electron volt per millimetre or kilo electron volt per micrometre, respectively. The LET of a charged particle is approximately given by the following formula [9] [104]

$$\text{LET} = \frac{Q^2}{E_k}. \tag{2.2}$$

Therefore, LET is proportional to the square of the charge of the particle Q^2 and inversely proportional to the particle's kinetic energy E_k. Based on its LET, radiation can be categorized into low and high LET radiation.

It can be immediately inferred from equation 2.2 that radiation consisting of particles with a higher charge, such as, e.g., carbon ions, does have a higher LET than, e.g., protons or electrons. As for uncharged particles, the LET is not defined, strictly speaking, no LET can be assigned to photon and neutron radiation. If the concept of LET is used for uncharged particle radiation, the LET is always associated with the secondary charged particles. Photon radiation, for which the secondary charged particles generated are electrons, would in this case effectively be categorized as low LET radiation.

A high LET will cause the radiation to lose energy more rapidly, thereby limiting penetration depth and reducing the dose to the distal part of the trajectory. Structures close to the particle track may sustain severe damage due to the increased concentration of deposited energy leading to double-strand DNA breaks (DSBs).

Low LET on the other hand is less likely to produce irreparable damage at the same given volume of tissue, as it mostly induces DNA damage that can be repaired with a high probability, such as single-strand DNA breaks (SSBs). A consequence of the higher probability for DSBs associated with high LET radiation is a higher number of chromosomal aberrations compared to low LET radiation, which are not only an indicator for radiation damage but also a main factor for radiation-induced cell death [105, 106].

[9] Exact LET depends on the applicable interaction cross sections.

2.3.3 Stopping Power

The stopping power is a physical quantity that refers to the force that causes kinetic energy loss in charged particles (e.g., alpha particles, protons, and deuterons) as they interact with matter. It is heavily influenced by the type of radiation, the energy, and the composition of the material or absorber medium of interaction. The stopping power of a medium is expressed in general terms as follows [107]

$$S(E) = -\frac{dE}{dx}, \tag{2.3}$$

where E is the energy of the primary particle. In SI units, it is expressed in Newtons [N], but is typically stated in different quantities, such as MeV/mm or similar. Furthermore, this quantity is intrinsically related to LET. The energy loss caused by electronic interactions is called the electronic stopping power S_{el} and is identical to the (unrestricted) LET.

Although most secondary electrons generated by charged primary particles have relatively low energy, some secondary electrons - the so-called delta rays - do have enough energy to cause secondary ionizations. Due to the higher energy of these delta rays, they have a larger range than most secondary electrons and can deposit dose at a greater distance from the primary particle track.

Many studies concentrate on the energy transmitted along the primary particle track and hence ignore interactions that result in delta rays with energies greater than a specific limiting threshold Δ. Since higher energy indicates a wider range, this energy restriction is intended to prevent secondary electrons that transfer energy away from the original particle track. This approach facilitates analytical assessment but neglects the non-linear delta ray path and the directional distribution of secondary radiation.

To only consider the energy transferred to secondary electrons below a certain energy threshold (and therefore maximum range) one can define the restricted LET

$$L_{\Delta} = \frac{dE_{\Delta}}{dx}, \tag{2.4}$$

where dE_{Δ} is the charged particle's energy loss caused by electrical collisions as it travels a distance dx, neglecting all secondary electrons with kinetic energies larger than Δ. If Δ tends towards infinity, then there are no electrons with larger energy, and the LET becomes unrestricted, corresponding to the electronic stopping power.

2.3.4 Bethe-Bloch Equation

The Bethe-Bloch equation gives the mean rate of energy loss (stopping power) product of Coulomb interactions (e.g., ionization and electron orbital excitation) of heavy charged particles as they pass through the medium of the absorber. However, this formula has been refined over the years to account for bremsstrahlung radiative energy losses. These are quite significant when absorbers with a high atomic number Z are subjected to the interactions of beta and high-energy electrons. The latest and most clear derivation is provided by Tsoulfanidis (1995) as the following for heavy charged particles (e.g., protons, deuterons, and alpha particles) [107, 108]

$$\frac{dE}{dx} = 4\pi r_e^2 z^2 \frac{m_e c^2}{\beta^2} NZ[ln(\frac{2m_e c^2}{I}\beta^2\gamma^2) - \beta^2]. \quad (2.5)$$

Where:

- dE/dx is the particle stopping power in MeV/m
- r_e is the classical electron radius $r_e = \frac{1}{4\pi\epsilon_0}\frac{e^2}{m_e c^2} \approx 2.818794 \cdot 10^{-15}\ m$
- z is the particle charge with $z = 1$ for p, d, $\beta+$, and $\beta-$ and $z = 2$ for α
- $m_e c^2$ is the rest energy of the electron (0.511 MeV)
- N is the number of atoms per m^3 in the absorber material through which the charged particle travels $N = \rho \cdot (\frac{N_A}{A})$ where ρ is the absorber density, N_A is Avogadro's number ($(6.022 \cdot 10^{23}$ atoms/mol)) and A is the area.
- A and Z are the atomic weight and atomic number, respectively, of the absorber.
- $\gamma = \frac{T+Mc^2}{Mc^2} = \frac{1}{\sqrt{1-\beta^2}}$ where T is the particle kinetic energy in MeV.
- M is the particle rest mass (e.g., proton = 931.5 MeV/c^2, deuteron = 2(931.5) MeV/c^2, alpha particle = 4(931.5) MeV/c^2, and $\beta-$ or $\beta+$ = 0.511MeV/c^2.
- β is the relative phase velocity of the particle = v/c, the velocity of the particle in the medium divided by the speed of light in a vacuum = $\sqrt{1-(1/\gamma^2)}$.
- I is the mean excitation potential of the absorber in units of eV and can be approximated by the equation: $I = (9.76 + 58.8Z^{-1.19}) \cdot Z$ when $Z > 12$.

The Bethe-Bloch equation describes the mean energy loss and its importance in the field of high-energy ion beam radiotherapy relies on studying and forecasting stopping powers cross sections for heavy ions. This was possible after the corrections on the original work between Bethe's quantum theory of the stopping of charged particles in matter and Bohr's classical theory [109, 110]. This equation is also directly related to the Bragg peak, as a particle slows down, the rate of energy loss and its kinetic energy will change with a trend described by $1/\beta^2$ hence, more energy per unit length will be deposited at the end of the trajectory. If this trend was plotted as a function of penetration depth, the amount of ionization at the end of the track would increase (Bragg curve). In the end, dE/dx drops quite significantly since electrons are picked up by the particle. This property is used in medical applications to spare healthy tissue and deposit the maximal energy at the most distal segment of the path (see figure 2.8).

2.4 Beam Delivery Methods

In the upcoming section Passive Scattering (PS) and Pencil Beam Scanning (PBS) beam delivery methods will be explained. The PS approach utilises passive mechanical devices e.g. range modulator, which can be a rotating wheel of variable thickness along the particle trajectory to disperse the initial Gaussian-distributed beam to form a broadened but homogeneous beam distribution resulting in smooth SOBP that will be later delivered to specific targets. Whereas, the PBS approach utilises active components e.g. magnetic

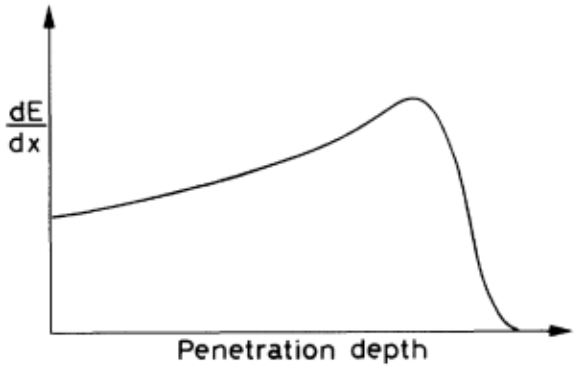

Figure 2.8: General Bragg curve, depicting the variation of dE/dx as a function of the penetration depth of the particle in matter, maximum ionization occurs at the end of the kinetic trajectory [111].

quadrupoles and scanning magnets in x and y directions that are used to steer the beam for each energy layer [112].

2.4.1 Passive Scattering

Passive scattering is a beam delivery method in which scattering and range-shifting high-Z (atomic number) components (see figure 2.9) are employed to spread the beam over a target. These components increase dose conformity and distribution without significant energy degradation. The first element in the beamline is the range modulator wheel or ridge filter, which contains segments of different thicknesses that shift the pristine Bragg peak to a different depth, producing the spread-out Bragg peak (SOBP).

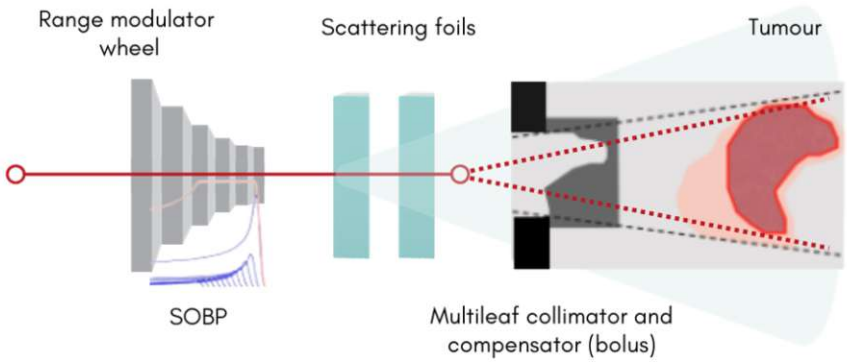

Figure 2.9: Passive elements (collimators and compensators) conform the dose to the target volume. The first element is the range modulator wheel or ridge filter (dark gray), followed by the scattering foils (light blue) and the MLC (black) at the end [113].

The next elements are the scattering foils that are used to scatter the beam laterally, and the multileaf collimator (MLC) which adapts the field to the cross-section of the target. Finally, the range compensator or bolus adapts the range of the SOBP to the distal edge of the target, but it does not account for different target thickness [114].

2.4.2 Pencil Beam Scanning

Pencil beam scanning (PBS) is an advanced "active" beam delivery method used to treat complex and small target morphologies with a high level of precision up to a few millimetres. Furthermore, it provides improved dose conformity to the target and reduces the demand for field-specific devices (apertures and range compensators) because compared to passive approaches, it lowers the patient's exposure to secondary neutron radiation generated form primary proton interactions that occur with multiple scattering components (see figure 2.10) [112].

In simple terms, it works in the following way: The beam is guided by magnets to produce a unique, 3D arrangement. Variable beam energy is used to change the depth of the Bragg peak, thereby scanning the volume layer by layer. Following that, the delivery is mediated by fast scanning control magnets which deflect the beam in lateral directions to scan over each layer, and at last, the beam monitor surveils the spatial configuration of the beam to provide the right intensity and position feedback[115]. The primary benefit of PBS is the ability to modulate the field by individually regulating the position and intensity of each ion beam. PBS is the only method that delivers very inhomogeneous treatment volumes, which enhances dose shaping (conformality).

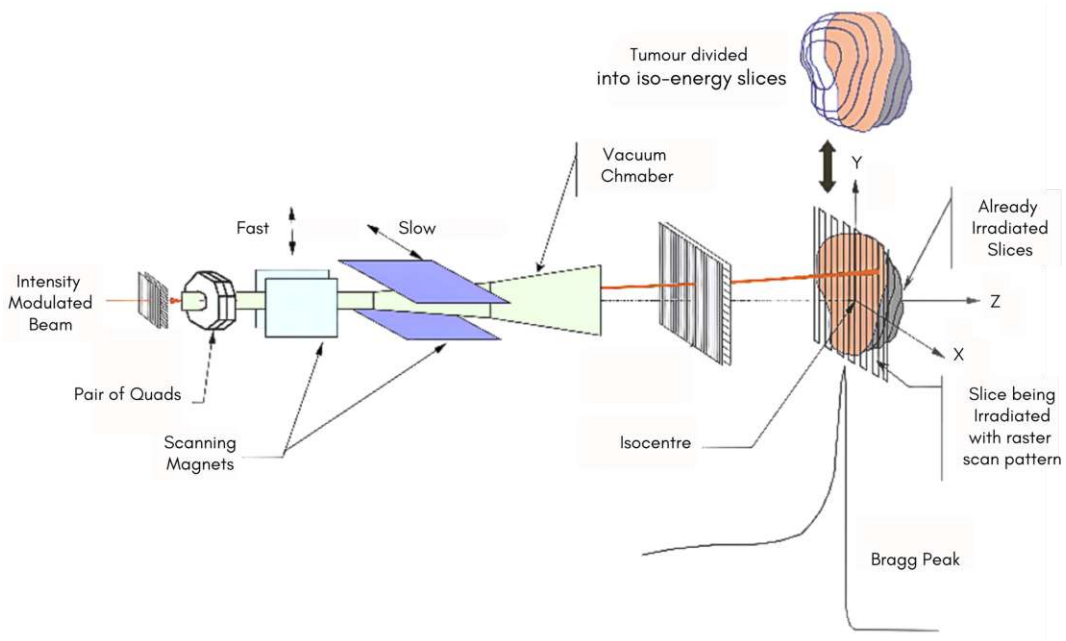

Figure 2.10: Layers of equal particle ranges are cut into the target volume (a tumour for example) and covered by a net of individual ion beam placements. The beam is magnetically steered across each unique beam point for each energy [116].

2.5 Relevant ICRU Guidelines

The ICRU reports provide standardized guidelines and nomenclature for target volumes (CTV, ITV, PTV etc.), organs at risk (OAR), and planning organ at risk volumes (PRVs) in radiation therapy. The taxonomy also includes technical directives for specifying laterality and margins for various structures. Furthermore, such documents provide rules for basic structure naming, as well as non-standard structures used mainly for plan optimization or

evaluation such as rings, islands of dose avoidance, and islands where additional dose is needed (dose painting)) are identified separately [117]. In this section, only the pertinent definitions for a stereotactic radiotherapy treatment approach will be illustrated in figure 2.11.

2.5.1 ICRU Reports 50 and 62 - Target Volume Concepts

Reports 50 (1994) and 62 (1999) offer guidelines regarding dose prescription, reporting and target definitions (including dose-volume and target-volume specifications) necessary to perform radiation therapy. The following definitions are key to understanding treatment planning and optimization (see figure 2.11) [118–120].

- **GTV - Gross Tumour Volume:** volume that contains the visible or clinically detectable tumour (either by imaging or examination).
- **CTV - Clinical Target Volume:** volume to which the radiation treatment will be delivered. This includes the GTV as well as neighbouring areas of particular clinical risk including any microscopic involvement.
- **ITV - Internal Target Volume:** this volume includes a margin to account for physiological movements like cardiac motion. The margin required to compensate for organ movement is known as the internal margin (IM) and may vary in height, breadth, and depth based on the anatomical location, this quantity is derived from the 4DCT. In case gating is used, then the ITV can be considerably reduced.
- **PTV - Planning Target Volume:** this volume is an an expansion based on the ITV to account for external treatment uncertainties. It is recommended to reduce external factors that might influence the treatment outcome, as a result, it would be possible to reduce PTV expansions. It is important to highlight that for accuracy in reporting the PTV margin should not be compromised even if it overlaps with other PTVs, OARs, and PRVs. Hence, priority criteria in the planning system should be applied, or the CTV may be split into sub-regions with singular prescription doses, to provide sufficient dose sparing on the OAR and target coverage.
- **OAR - Organs At Risk:** these are volumes established on organs which are highly susceptible to radiation. Physicians together with the Medical Physicists place constraints on the beam arrangement and dose to be delivered, since OARs may have different radiation tolerance levels to their histological nature.
- **PRV- Planning Organ at Risk Volume:** volume that accounts for uncertainties also of OARs safety margins.

2.5.2 ICRU Report 78 - Proton Beam Prescription Principles

ICRU report 78 (2007), in addition to the IAEA-TECDOC-1560/Sec- 4.3 [122] provides a detailed description of the radiobiological, physical, technological, treatment planning, and clinical elements of proton beam therapy [123]. The dose prescription principles for proton beam therapy aim to deliver 95% of the isodose to the PTV. The dose prescription is always given to the entire treatment volume (TV) and after performing the dose optimization in each volume element of the TV the yield variation shall not exceed 2—3% from the

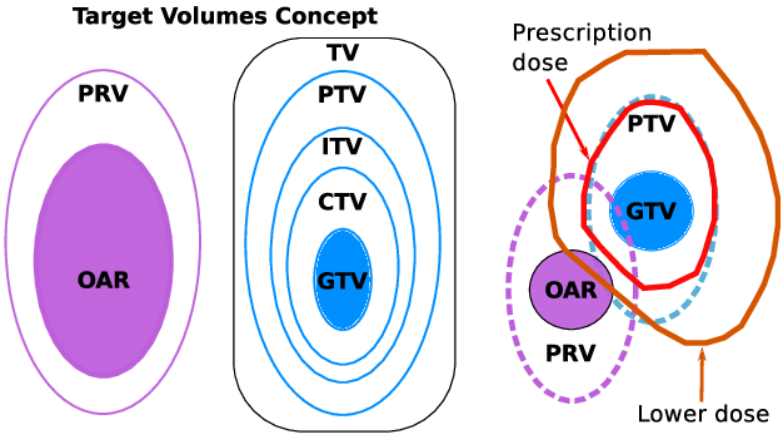

Figure 2.11: ICRU applied concepts; GTV, CTV, ITV, PRV, and PTV, as well as the OARs are shown. Additionally, on the right, a potential configuration of a target near an OAR is illustrated. The final dose computation may be impacted by overlapping volumes, which can result in inadequate PTV coverage or undesirable dose deposition levels for the OAR [121].

prescribed dose. The biologically effective dose D (RBE) is always used for optimization in the TPS, so that the product of dose and relative biological effectiveness is homogeneous throughout the entire TV and it should be covered by at least 90% of the indicated dose. Hot and/or cold spots should have a diameter below 2–3 mm; the only exception to the rule is when an OAR is being used (leading to cold spots) or a patch field technique is unavoidable (leading to hot spots). When compared to IMRT or conventional treatment, the uniformity of dose distributions is often substantially better for ions.

2.6 Absorbed Dose

The amount, referred to as the absorbed dose, is an essential quantity for radiation therapy, it is defined as the amount of energy that has been deposited per unit mass in the irradiated target. Its dimensions are in joules per kilogram, and the standard unit is the Gray (Gy), hence 1 Gy = 1J/kg. Moreover, the radiobiological and clinical impacts are directly correlated with the amount of absorbed dose, regardless of the radiation type and the biological effect's nature. Therefore, this unit has to be specified when prescribing and reporting therapeutic irradiation, together with the point(s) or volume(s) where the absorbed dose is administered as well as the irradiation conditions. Also, the absorbed dose is dependent on the following features: dose administered per fraction, dose rate, overall time and other time-dose relations, radiation quality and irradiation conditions (e.g. degree of oxygenation or temperature). As a result, when comparing or combining radiation treatments carried out under variable conditions, weighting of the absorbed dose is required, and weighting factors (or functions) must be included for accuracy [124].

2.7 Relative Biological Effectiveness

Relative Biological Effectiveness (RBE) is defined as the ratio of a photon dose (Co-60 γ rays are taken as the reference radiation quality) relative to a dose of any other radiation needed to achieve the same biological effect. What's more, this quantity allows for

comparison and estimating possible effects amongst different RT modalities. Which may fluctuate between early and late responses after therapy and depends on radiation type, energy, dose, dose per fraction, fraction number, cell or tissue type being irradiated, and the early vs. late reactions to therapy. RBE generally rises with decreasing dose and can occasionally be greater for late effects than for early effects, particularly at low doses [124].

Current proton beam therapy treatments are based on physical dose estimations, with a constant RBE value of 1.1 often assumed. Nonetheless, IAEA-TRS No. 461 and ICRU 78 state that RBE tends to have a slight increase at the distal part of the spread-out Bragg peak (SOBP), due to an increase in LET. This slight increase has further implications; the effective range of the proton beam is extended by 2 mm for 160–250 MeV and about 1 mm for 60–85 MeV proton beams in the dose fall-off region. Hence, the typical RBE value taken is 1.0 or 1.1 for protons, with almost no significant difference while for carbon ions (heavier compared to protons) the RBE distribution in the target volume varies between 2 and 3.5 [125] utilising other radiobiological models like LEMI or MMKM. The RBE value is assigned to the distal part of each SOBP and the entire ion path, irrespective of its size. This model is based on extensive clinical neutron treatment expertise and conclusions derived from a comprehensive history of radiobiological experiments performed at Berkeley [126] in the USA, HIMAC in Japan [127] and GSI in Darmstadt Germany [127]. The main quantity in particle therapy which is used to prescribe dose to target and OARs is the RBE-weighted dose (see figure 2.12). The model, its parameters, and the steps needed to modify it for use in clinical settings all influence the RBE. An RBE-weighted fractional dose (d) and number of fractions (nf) [10] must be determined by the radiation oncologist taking into account the desired outcome of the treatment as well as the uncertainty associated with the RBE. The clinical response is determined by the RBE-weighted total dose-distribution, or DRBE, which is produced by combining this prescription with the model-based RBE [126].

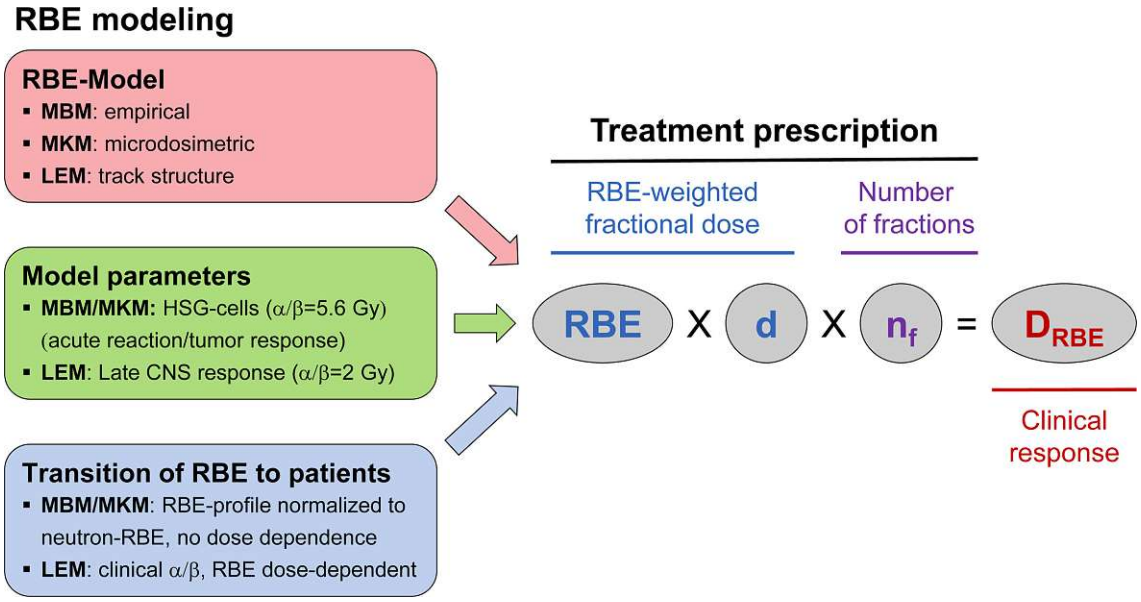

Figure 2.12: Elements of treatment prescription and RBE modeling.

[10] In our case we are dealing with a single fraction treatment, however in multi-fractionated treatments, this quantity highly affects the RBE.

2.8 Interplay Effect and Uncertainties for Moving Targets

In general, the administration of radiation to moving targets imposes an additional challenge. For ion beam therapy, changes with respect to the beam range induced by the target or entry channel must be considered. Whereas this has far less influence on photon treatments [128]. Moreover, large dose errors may result from changes in the Bragg Peak location, and this is especially true for small targets with short spread out Bragg Peaks (SOBPs) where the ratio of dose in the peak to the plateau of the target's profile is higher. If active scanning is employed, the beam's motion across the target occurs in several instances on similar time scales as the target's intrinsic motion, resulting in interface effects, or the so-called "interplay effect". The interplay effect is defined as the difference between the absorbed dose volume measured during motion and the volume resulting from a stationary measurement convolved with the motion function. It typically introduces stripe or checkerboard patterns of hot vs. cold spots [129]. Therefore, motion mitigation and specialized 4D-RT planning and delivery techniques are vital for particle therapy [130]. Furthermore, there is a lack of long-term information on cardiac exposure in individuals exposed to ions, which should be examined in the future [76].

At the moment, the following 4D-RT motion management techniques are available, they can be used individually or in combination[131]. These techniques can be classified into two types: passive and active. The first type consists of adding additional target margins, a 4D treatment planning approach and rescanning. The second type involves bread-holding techniques, gated treatment, target tracking and signal triggering with additional devices and regulation of the respiration during beam delivery [87, 128, 132]:

- **Motion Encompassing:** the internal target volume (ITV) is defined including the clinical target volume (CTV), which varies in position, shape, and size with an asymmetric internal margin (IM) surrounding it. Which is set to compensate for dynamic variations (respiration, organ filling, swallowing, heartbeat, and gastrointestinal motility). Then every volume is referenced to the patient coordinate system.
- **Breath Holding:** combining self-held, active breathing techniques using spirometers and valves with various respiratory monitoring techniques. In some cases forced breathing with continuous positive airway pressure (CPAP), is advised to reduce one degree of motion.
- **Gating/Triggering:** at the present time there are two approaches; either by an ECG or a breathing surrogate. The first is beam-on during a specific stage of the cycle, also known as the "gating window". The second one may be phase, amplitude, or displacement-based signal gating. Gating can be limited by the particle spill length/pause, long treatment times, ambiguous definition of the gating window, and triggered beam delivery. As an example, in figure 2.13, it is possible to observe how a beam can be gated for irregular respiration curves identified during the respiration cycle.

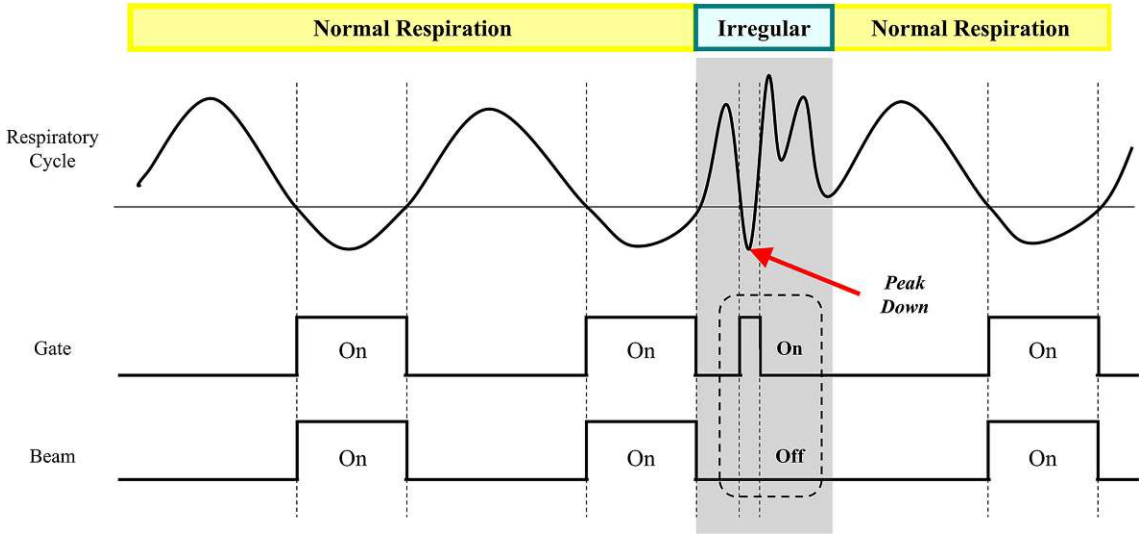

Figure 2.13: Schematic illustration to exemplify the phase-gated beam delivery with an irregular breathing pattern (beam interruption). The shaded area shows the moment that the beam was OFF when the gating was ON.[133].

- **Tracking:** online beam adjustment based on a known dynamic trajectory for the target (requires real-time imaging). Currently, there are no commercial products or official protocols available, but there is an emerging need to mitigate motion uncertainties. To compensate for morphology and position changes of the target, especially for the beating heart.
- **Rescanning:** specific for proton/ carbon ion beams it consists in applying the scanning pattern split into several passages across the target per fraction. It is mainly designed to remove or greatly reduce the motion scanning interplay. This is currently done at MedAustron [134].

Particularly for VT radiotherapy with ions, there are no official guidelines on how to account for cardiac motion, just suggestions based on the expertise and approach of different research groups and clinics. In Europe, some efforts are being consolidated by the STOPSTORM consortium, but the available information is mostly on STAR. In consequence, it is of utmost importance to envision strategies to improve accuracy, sparing healthy tissue as much as possible, account for the interplay effect (spot position and target volume are variables over time), and range uncertainty based on the local availability of resources [92]. Simultaneously, the inherent inaccuracy in translating CT HUs values to particle-stopping powers has to be addressed since irregular motion will severely affect range prediction and dose delivery. Ion CT is a way to measure the stopping power directly, without the need to extrapolate from HU [135, 136]. When compared to photons, the influence on the dose distribution will be much larger for particles. Thus, accounting for target motion variation and robust optimization techniques together with the exploration of new gating and triggering techniques and devices must be addressed to reduce uncertainty [76].

2.9 Basic Principles on Particle Acceleration Technology

2.9.1 Synchroton Acceleration Technology

There are many different types of particle accelerators which can be used in medicine. The main ones are LINAC, cyclotrons and synchrotrons, which are sometimes used in combination. Each of them has specific advantages and disadvantages. For each type it is possible to analyze factors such as beam intensity, profile, particle types or energy consumption rate; allowing a comprehensive technical comparison between the available systems.

Synchrotron technology, although generally bigger and more complicated than the other two accelerator modalities, has several advantages. First and foremost the LINAC can generate X-rays and high-energy electrons for medical purposes, while the cyclotron on the other hand is capable of generating protons for therapy and radiopharmaceuticals [137]. These two technologies are usually designed for a specific particle type, whereas a synchrotron can accelerate a range of different particles without the use of energy degraders [11]. Synchrotron accelerators have also significantly lower particle losses, which translates to less activation, background radiation, shielding etc. It uses less energy, which is a significant cost-driver in the accelerator system [139].

The term "synchrotron" refers to a fixed closed loop or ring accelerator configuration. Its name derives from the Greek "sýnchronos", which stands for "simultaneously". These circular accelerators vary the electric and magnetic fields simultaneously with the particle beam as it gains energy and speed. These devices are designed to accelerate charged elementary particles or ions to relativistic speeds, giving them extremely high kinetic energies while inducing variations in the guiding magnetic field to adjust for the increasing relativistic mass [140]. The main building blocks of a synchrotron are the magnetic systems that supply the bending and focusing fields, together with the acceleration radiofrequency system which operates under vacuum conditions.

The kinetic energy (defined in equation 2.6) of the particle to be accelerated increases with each pass through the acceleration voltage [141].

$$\Delta E = q \cdot U. \tag{2.6}$$

The velocity v acquired by the particle results from the following relativistic consideration (see equation 2.7 below, where c is the speed of light.

$$v = c \cdot \sqrt{1 - \frac{1}{(\frac{E_{\text{kin}}}{E_0} + 1)^2}} \tag{2.7}$$

The Lorentz force $\vec{F_{\text{L}}}$ acts as the necessary centripetal force $\vec{F_{\text{ZP}}}$ for the circular path. Therefore, the following applies to the amount of the Lorentz force.

[11] Plastic materials of variable thickness and widths that decrease the range of protons to achieve differential weighting of the shifted Bragg peaks to create SOBPs beams suitable for treatment at different depths [138].

$$\vec{F_{\mathrm{L}}} = \vec{F_{\mathrm{ZP}}} \Leftrightarrow q \cdot v \cdot B = \frac{m \cdot v^2}{r} \Rightarrow r = \frac{m \cdot v}{q \cdot B} \tag{2.8}$$

Where the relativistic mass would be defined as follows

$$m(v) = \frac{m_0}{\sqrt{1 - (\frac{v}{c})^2}}. \tag{2.9}$$

The synchrotron has low secondary neutron and scatter radiation production due to the lack of a beam degrader, which reduces the danger of undesired scattered radiation and provides a much "cleaner" beam. At the end of the accelerator's beam extraction pathway, the chopper system is located. These systems are essential to provide the ion beams with key temporal parameters to operate the extraction at will. This magnetic dipole device is part of the accelerator's pulsing system in the extraction line and it is used to introduce an assured time structure on an ion beam. When the chopper is ON it makes a closed-orbit that is bypassed by a dump block, mounted inside the vacuum chamber. When the chopper is OFF, the beam is then stopped by the dump block (see figure 2.14) [142, 143].

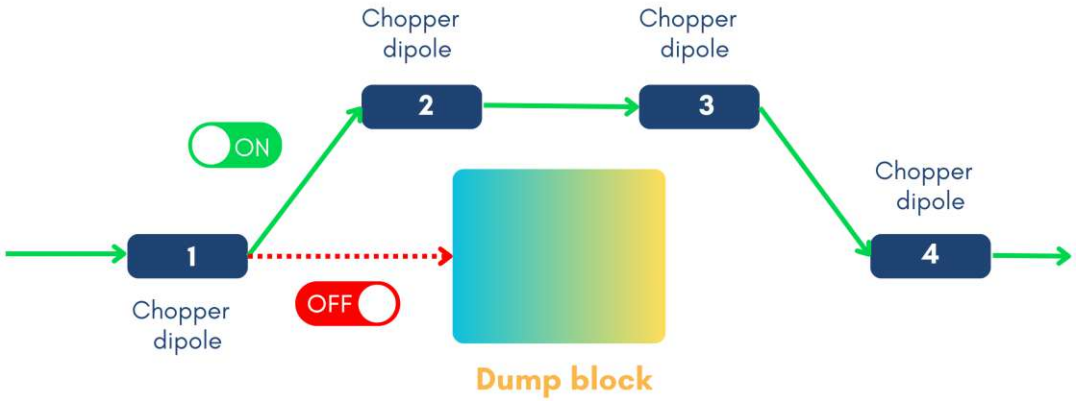

Figure 2.14: Accelerator beam chopper operation ON/OFF mode (Modified, created with Canva) [143].

The chopper is used to produce beam-free periods for experimental requirements such as the time-of-flight (TOF) technique, to lower the duty cycle and hence restrict the average power deposition for sensitive machine components, or low-loss injection or extraction (only for circular accelerators) [142]. However, another operation mode for the chopper in clinical accelerators is to receive a trigger signal that would modify its state, and as a result gate the beam to a particular time stamp related to a physiological condition (e.g. respiration phase, heartbeat phase) that would act as a flag variable for the beam in-room delivery.

2.9.2 MedAustron Particle Therapy and Acceleration Physics Facility

MedAustron [144] is a synchrotron-based accelerator complex for cancer treatment (IR1-IR4 [12] as well as for clinical and non-clinical research (IR1) with protons and other light ions, as depicted in figure 2.15. It is one of only six multi-ion facilities worldwide [145]. The accelerator complex is based on the CERN-PIMMS study and its technical implementation

[12] In-house nomenclature for "Irradiation Rooms", IR2, IR3, IR4 are used for clinical purposes and IR1 for research.

was first performed by the Italian CNAO foundation in Pavia [146]. At an energy of 8 keV/u, protons, carbon and helium beams are extracted from their respective ion sources of H_3^{1+}, C^{4+} and light ions [147, 148]. The particles are then delivered to the Low Energy Beam Transfer Line (LEBT) after passing via a spectrometer magnet to choose the appropriate charge state and filter out undesirable ion species. The beam is then pulsed, injected, and accelerated to 7 MeV/u in the linear accelerator (LINAC) and afterwards passed on to the accelerator ring (synchrotron) where it is accelerated further until the final desired energy is reached. The MedAustron Particle Accelerator (MAPTA) can deliver protons for medical treatment from 62.4 MeV to 252.7 MeV and carbon ions from 120 MeV/u to 402.08 MeV/u. For research purposes, it is even possible to accelerate protons up to 800 MeV. The particles are extracted using a betatron core-driven slow extraction method at the required energy. The beam is moved through the High Energy Beam Transfer Line (HEBT) into one of the four irradiation rooms following extraction from the Main Ring. Activities related to non-clinical research (NCR) take place in the first room, IR1. It is largely utilised by the Vienna University of Technology (TU Wien), the Medical University of Vienna (MedUni Wien), and the Institute for High Energy Physics of the Austrian Academy of Sciences (HEPHY). Clinical therapy is carried out in IR2, IR3, and IR4, the other three irradiation rooms. While IR3 only has a horizontal beamline, IR2 may emit radiation both horizontally and vertically. In addition in IR2 and IR3 $p+$ and C ions are available. In IR4, a proton gantry [13] is offered. The main research activities are in the fields of medical radiation physics, radiation biology, and experimental acceleration physics.

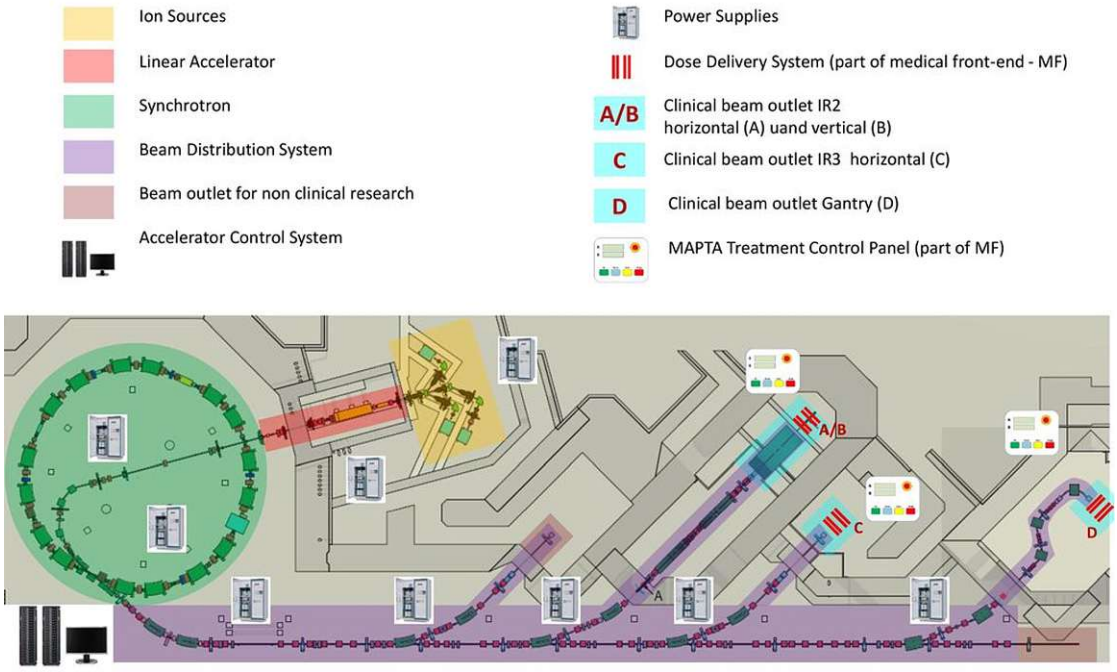

Figure 2.15: The accelerator layout of the MedAustron facility, illustrates the synchrotron hall (SH-Green), injector hall (IH-Red+Yellow), and the four irradiation rooms IR1-IR4. (The vertical beam line in IR2 is a projection) [149].

[13] A rotating frame that houses the collimators, detectors, and x-ray tube in a radiation therapy plus the last bending magnets to make the beam go around the patient. This last trait is characteristic of high energy ion beam therapy and it is different concerning photon therapy gantries.

CHAPTER 3

Method Development

3.1 Literature Review

The theoretical background and current state-of-the-art regarding this work were collected via a comprehensive and systematic literature review. Through the search of recurrent keywords (e.g., “ventricular tachycardia”, “VT radioblation”, “stereotactic ablative radiotherapy of ventricular tachycardia”, “STAR treatment planning”, “ablation with ion beams”, “ablation with photons”, “ablation with protons”, “synchrotron technology for medical appliances”, “cardiac ablation” etc).

In addition, authors, and institution names in common were also observed to identify serial publications on the VT radiotherapy ablation topic. Google Scholar, PubMed, Scopus, and the e-library catalogues of the Technical and Medical Universities of Vienna were utilized as search engines for reliable repositories of scientific literature. 114 publications were collected and 93 thoroughly revised and used as a basis for this research dating from 2013 until the last quarter of 2023. Including scientific and peer-reviewed articles, meeting abstracts, proceeding papers, editorial material, scientific letters, congress presentations, and even early access publication material, considering the past, present, and potential advancements in VT radiotherapy, compensation of cardiac dynamics, and treatment delivery workflow.

Most of the resources were condensed in Web of Science for a better overview. Which is a tool that allows further inspection, such as tracing cross-references, author affiliation, global distribution of the institutions involved in particular research, topics, common keywords, and related research funds. The core material regarding this topic mainly originates from papers and surveys (e.g., RAVENTA, Germany) published by the members of the STOPSTORM consortium. In addition to the literature search, internal manuals, and local shift documentation files were also used to conduct this thesis.

3.2 Sources of Applied Knowledge and Collaborators

Regular interdisciplinary meetings were held throughout this research between different organizations and departments encompassing the following fields: medical physics, accelerator physics, cardiology, radiation oncology, and biomedical engineering. Both local and external professionals were consulted to obtain information about their hands-on experience and validate our envisioned workflow step-by-step; from extraction to delivery in terms of the local capabilities and resources. To achieve this, a network of collaboration synergies between the following institutions and professionals was created:

- **Claus-Stefan Schmitzer (Head of Acceleration, Vacuum Technology, Ion Sources and Diagnostics (AVID) | MedAustron):** Ion sources, radio-frequency systems, linear accelerator, accelerator cavities, international research, and novel development networks.
- **Markus Stock (Head of Medical Physics | MedAustron):** Head of Medical Physics in-house, expert, and full professor in Medical Physics for Particle Therapy.
- **Piero Fossati (Radiation Oncologist | MedAustron):** In-house Radiation Oncology Specialist, Scientific Director, Carbon Program Director, and full professor for Radiation Oncology in Particle Therapy.
- **Svetlana Marić (Medical Device Engineer| MedAustron)**: Gating project lead, expert in compliance and medical device regulations.
- **Martina Fuß (Medical Physicist | MedAustron)**: Clinical Medical Physicist, with research experience in Particle Therapy with a focus on radiobiology, mechanistic modelling, and alternative ions.
- **Lukas Fiedler (Cardiologist | Landesklinikum Wiener Neustadt):** Specialist in internal medicine, angiology, rhythmology, and electrophysiology.
- **Adriano Garonna (Accelerator Physicist | EBAMed):** Co-Founder and Director of EBAMed, a Swiss company creator of unique External Beam ablation medical Devices specializing in non-invasive and automated treatment of heart arrhythmias with protons. Provider of literature on cardiac radioablation and motion management.
- **Oliver Blanck and Melanie Grehn (Medical Physicists | University Hospital Schleswig-Holstein, University of Kiel| UKSH Radiation Therapy Clinic, Germany):** Active members of the STOPSTORM consortium and leaders of The multicenter RAdiosurgery for VENtricular TAchycardia (RAVENTA) study (NCT03867747). Providers of STAR clinical expertise, literature on cardiac radioablation and EAM target migration.
- **Jingyang Xie (Institute of Robotics and Cognitive Systems | University of Lübeck, Germany):** Software developer of the CARDIO-RT tool, collaborator of the STOPSTORM consortium, and RAVENTA. Specialized in VT and EAM Medical Imaging and Processing. Provider of support for EAM raw data processing.

3.3 Technological Assessment

In parallel, a technological compatibility and interoperability assessment of the in-house systems was performed. With a special focus on the the gating interface (currently under development) which will act as a gateway between the accelerator and external triggering/gating devices. A exploration of the technical characteristics and potential benefits of available surface scanners at MedAustron and a novel ultrasound cardiac probe from EBAMed was performed. The other major focus was on assuring compatibility between RayStation treatment planning system (TPS) software, and clinical datasets (mostly DICOM and other non-standard formats) amongst participating facilities. A list of potential improvements and bottlenecks was identified to ultimately test, incorporate, and implement a brand-new treatment at MedAustron in the future.

3.4 Case Study and Electroanatomical Mapping Data

An anonymous set of cardiac CTs and the patient's respective electroanatomical mapping (EAM) dataset [1] taken during invasive VT radiofrequency ablation procedures (RFCA) with the EnSite Precision Sytem by Abbott were provided for analysis [2]. In addition, 3 different planning CTs with VT target contours and their respective substructures were provided by collaborators, [3] the contours were drawn by the medical doctors participating in the RAVENTA treatment planning benchmark study. Both sets (for characteristics overview see table 3.1) were used to have a deeper comprehension of the target volumes, contours, potential doses applied to the target, and implications of the motion margins to be applied to the target.

These datasets were key in order to be able to generate our in-house VT workflow. Three different treatment plans were generated for the given contours based on the RAVENTA TP recommendations and our in-house ion-beam therapy planning approach [4]. In the end, the treatment plans were compared in terms of dose distribution and loaded into a simulation tool to evaluate the burden on the synchrotron and estimate the in-room and treatment delivery time.

	Dataset A	**Dataset B**
Specifications	1 set of Cardiac CT and EAM	3 sets of cardiac CTs + 4DCTs with their respective target and substructure contorus
Format	DICOM and 20 CSV files	DICOM

Table 3.1: Specifications and formats of the data used for image compatibility analysis and treatment planning case studies.

In figure 3.1, it is possible to observe four standard medical imaging planes of the heart: left lateral (LL), right lateral (RL), anterior posterior (AP), and posterior anterior (PA). On the image we observe the EAM data for the left ventricle of a patient obtained with the EnSite Precision cardiac mapping system by Abbott.

[1] Medical imaging data that shows a 3-D structure, the voltage and timing of signals of the heart. These maps are used to understand and treat VT. Please refer to section 3.8 for more information.

[2] Courtesy of Dr. Lukas Fielder, Cardiology Department at Landesklinikum Wiener Neustadt.

[3] Courtesy of Dr. Oliver Blanck and Dr. Melanie Grehn, Saphir Radiochirurgie Zentrum in Germany.

[4] Please note that no patients were treated in the scope of that project.

The areas highlighted in in purple colour are regions of normal conductivity and timely activation, while the areas marked with gray, indicate critical conductivity and late activation (in mV). Anything in between purple and gray on this scale, indicates abnormal conductivity and delayed activation. The different shares of red dots on the image, indicate the duration of to the RF (in seconds).

In figure 3.2, we observe the graphical representation of the left ventricle (blue) obtained via Matlab scripting, also in clinical standard views (LL), right lateral (RL), anterior posterior (AP), and posterior anterior (PA). As well as the ablation points (red) obtained form the Abbott, EnSite Precision cardiac mapping workstation raw data extraction files.

Figure 3.3 shows the CT data form the same patient that underwent the RFCA and the EAM during a interventional radiology procedure. At the top of this figure (coronal scout view) the chest of the patient is shown, where the ECG external cables and the internal ICD and its respective leads can be seen. At the bottom of this figure (axial plane) the heart of the patient is visible (four chambers) and the internal ICD leads causing an artifact in the image are shown.

In figure 3.4 it is possible to depict an example of the contorus including targets, cardiac substructures and other organs drawn by the medical doctors participating in the RAVENTA study. Furthermore, the ICD (inducing the spikey pattern noises in the planning CT) and ECG leads were highlighted with the white arrows.

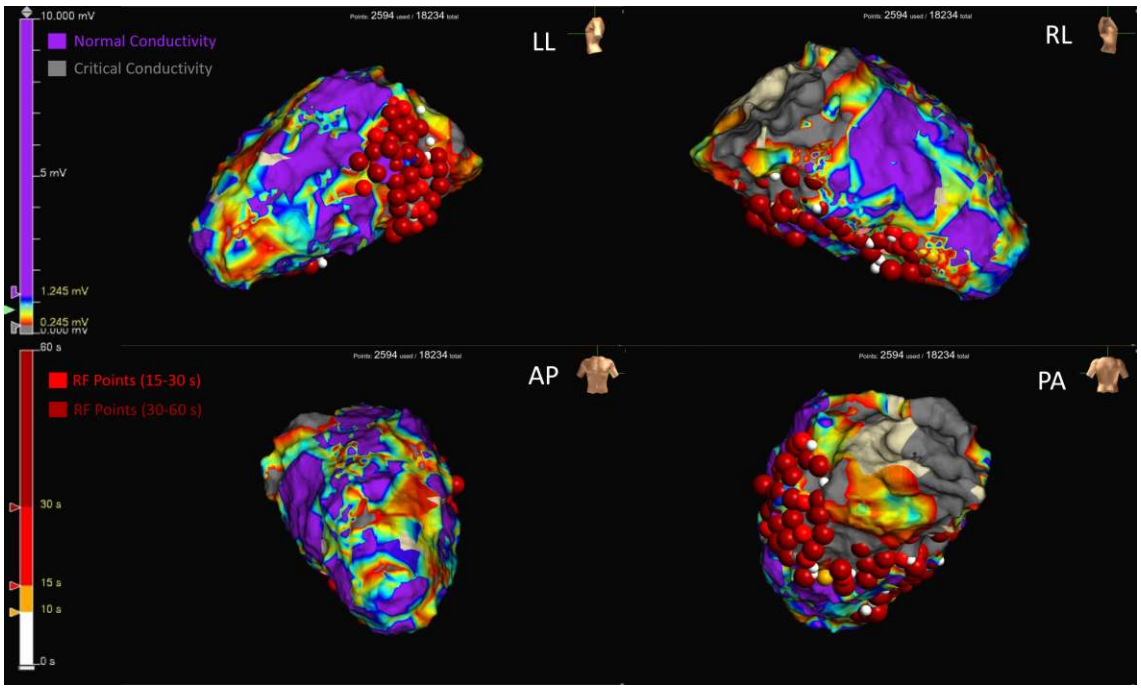

Figure 3.1: EAMs most relevant areas as displayed by the Precision cardiac mapping system by Abbott. The red balls indicate RF ablation regions during interventional procedures. Whereas the purple and grey areas indicate where the VT is running or normal tissue exhibiting enough electrical potential for proper circulation. The scales for both the voltage used for the catheter probe and the circulating voltage in the heart are located on the left side of the image.

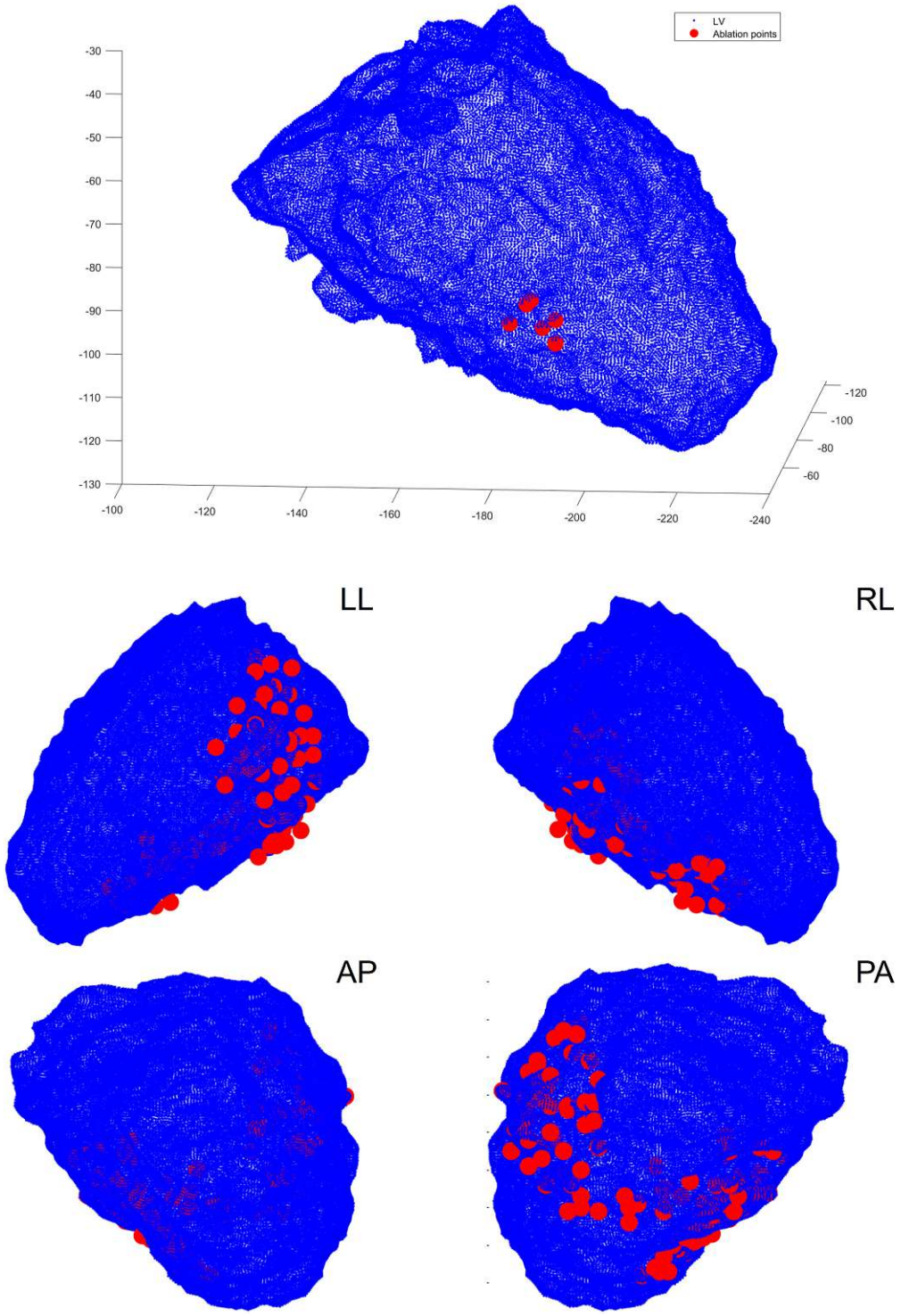

Figure 3.2: Example of graphical representation of the 3D cloud-like arrangement of points contained in the EAM form a VT patient at the Landesklinikum Wiener Neustadt cardiology department. This map was generated with a Matlab script with the LV point cloud and other available data form the EAM file.

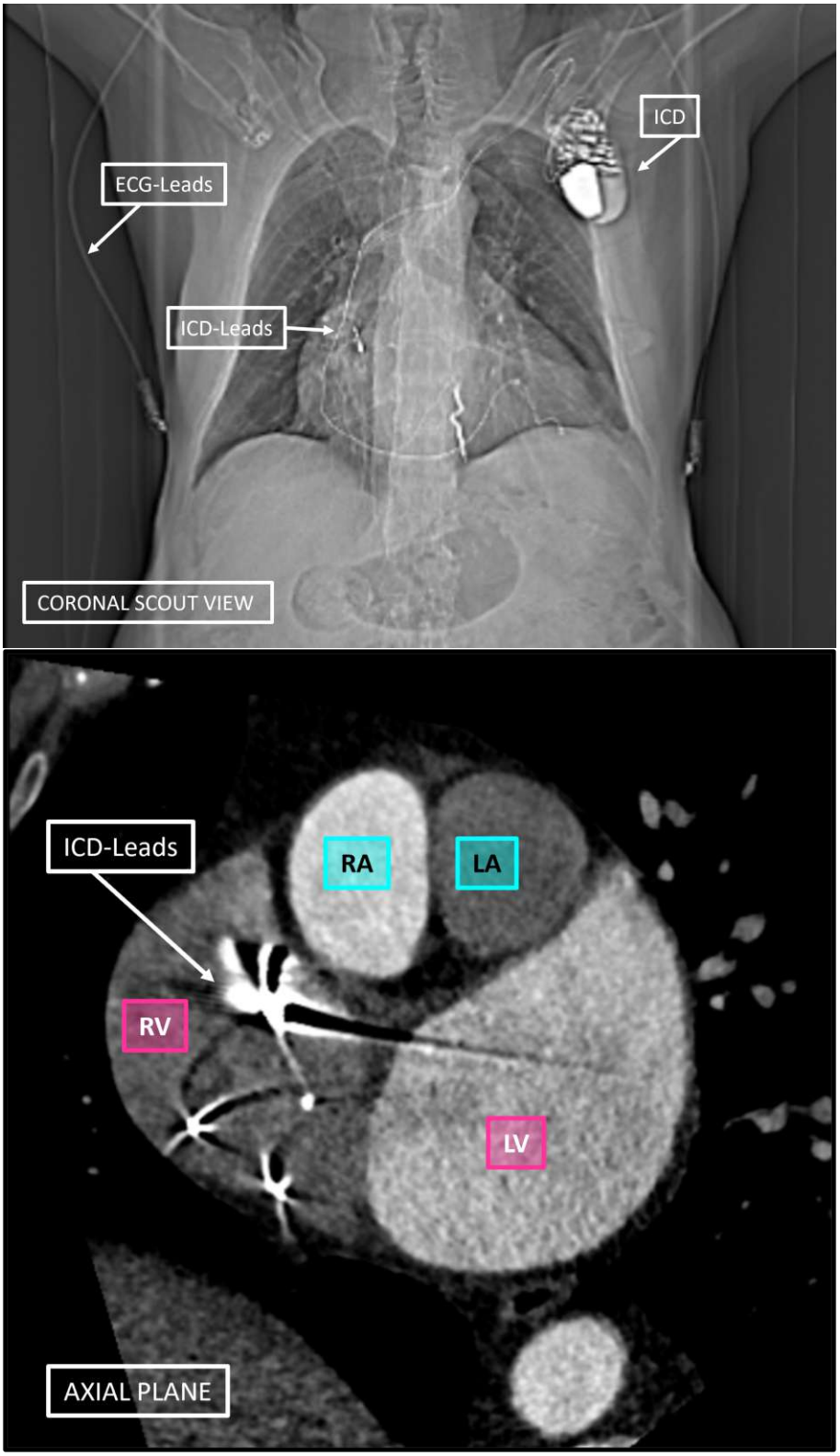

Figure 3.3: CT data form the Landesklinikum Wiener Neustadt. On the coronal plane, it is possible to observe the ICD, its leads and some ECG external cables. On the axial plane, the atria (RA and LA) and ventricles (RV and LV) are visible with the internal location of the ICD leads.

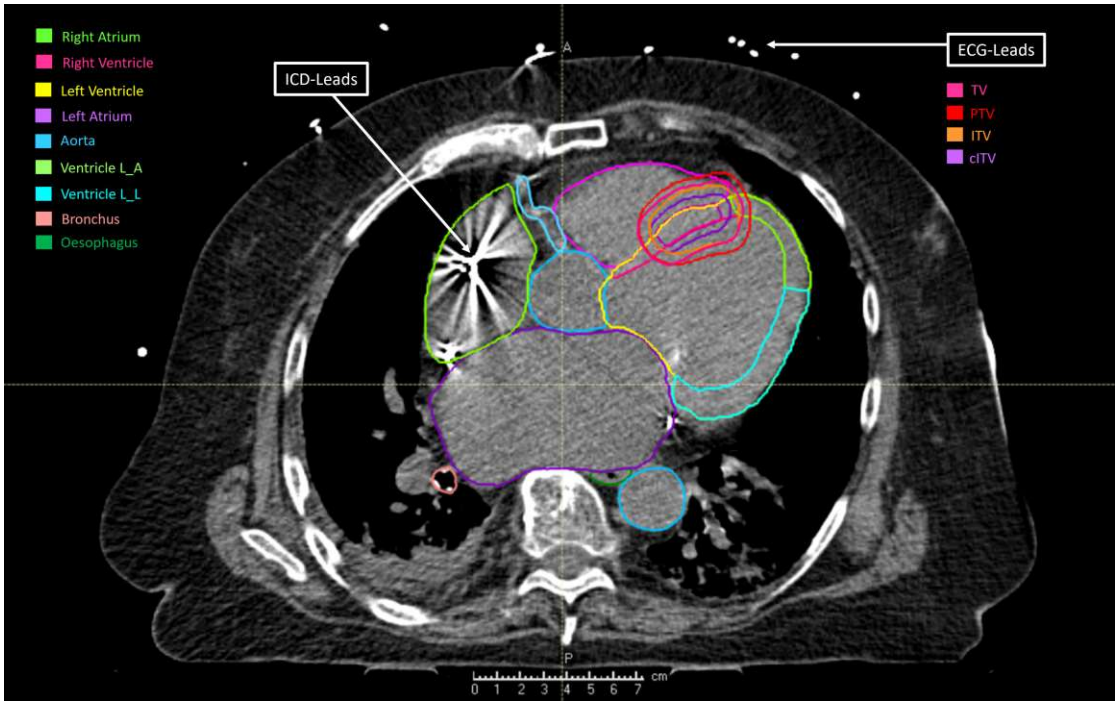

Figure 3.4: Example of a planning CT (axial plane) with the contours drawn by the medical doctors participating in the RAVENTA study in Germany. Here it is possible to observe the different cardiac structures (atria, ventricles, and ventricle walls), some OARs (bronchus and oesophagus), target delineations (TV, PTV, ITV, CITV), and the internal ICD leads causing major artefacts in the image.

3.5 Synergies between MedAustron and other Institutions

To develop a tailor-made medical VT workflow, all the resources available from the network of collaborators were identified and allocated. Then, the tasks to be accomplished were outlined and discussed in regular meetings with the pertinent members of the network of internal and external collaborators.

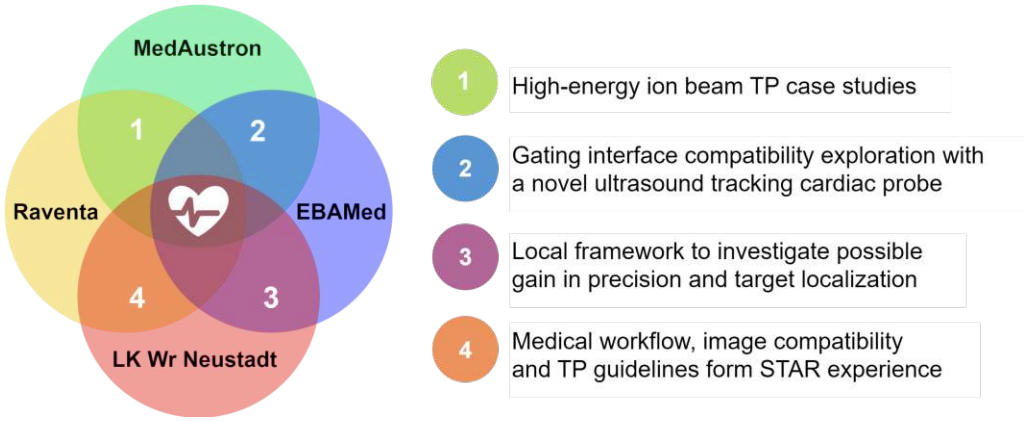

Figure 3.5: Venn diagram depicting the project synergies to potentially achieve VT-RT treatments at MedAustron. The overlapping areas show the specific technical aspects of collaboration between the institutions and participants.

In the end, a workflow proposal was created based on the available resources, state-of-the-art literature, multidisciplinary experience and resources available at the different involved parties. In figure 3.5 a Venn diagram illustrates all the collaborators involved for the development of this thesis. The center of the figure represents the VT medical workflow, and the overlapping areas show the technical aspects and individual contributions.

Other factors such as compatible ongoing research projects at other centres were considered as a basis for future local testing, evaluation and eventual implementation (in stages), and possible deployment for clinical use in the upcoming years at MedAustron.

3.6 Accelerator Gating Technological Assessment

The GID was originally designed as a medical device to gate the beam for the MedAustron Treatment Environment for Ocular diseases (MATEO). However, its compatibility with other external instruments is of interest due to the potential expansion of treatment options for moving targets. In the upcoming section, its structure, operability, and functionality will be discussed. In the end, limitations and requirements will be stated to integrate extrinsic devices with their respective signals as triggers (e.g. cardiac probe) to gate the accelerator chopper [5] to a particular state reflected as a time stamp.

3.6.1 Gating Interface

The MedAustron gating interface device (GID) is an ongoing implementation project to commission a medical interface device able to couple external devices that can send a trigger input to the MedAustron Particle Therapy Accelerator (MAPTA). In figure 3.6 external gating devices and environments (MATEO, any surface scanner and the EBAMed cardiac probe) are shown as inputs to the GID. Input signals form gating devices communicate with the Dose Delivery System Interlock Gateway, and the the Demultiplexer. Finally, via the MedAustron Particle Therapy Accelerator Treatment Control Panel the accelerator chopper state can be changed form open to close state.

3.6.2 Interface Operation Overview

A 10-pin optical fibre connector bridges the gating and monitoring system with the Gating Interface Device (GID) (see figure 3.7 for pin configuration diagram). Incoming Veto signals (Veto in A/B) are sent by the GID into the Dose Delivery System Interlock Gateway (DIG) and the MedAustron Particle Therapy Accelerator Treatment Control Panel (MTCP), which is a piece of hardware user interface of MAPTA located outside of the treatment room enabling the operators to start, stop, and interrupt irradiation. The gating interface device is ignited by an entire sequence of actions elicited by “Raycomand”, which is the central treatment control system (TCS) that loads the treatment plan into the accelerator and controls the whole in-room workflow in addition to the treatment delivery sequence via MedAustron Delivery and Allocation Manager (MADAM).

MADAM is a software originally developed by radART and currently managed and upgraded in-house, that manages the functioning of MAPTA and serves as the single,

[5] Device that controls the extraction of the beamline by introducing an assured time structure on an ion beam [142]. For more information see section 2.9.1.

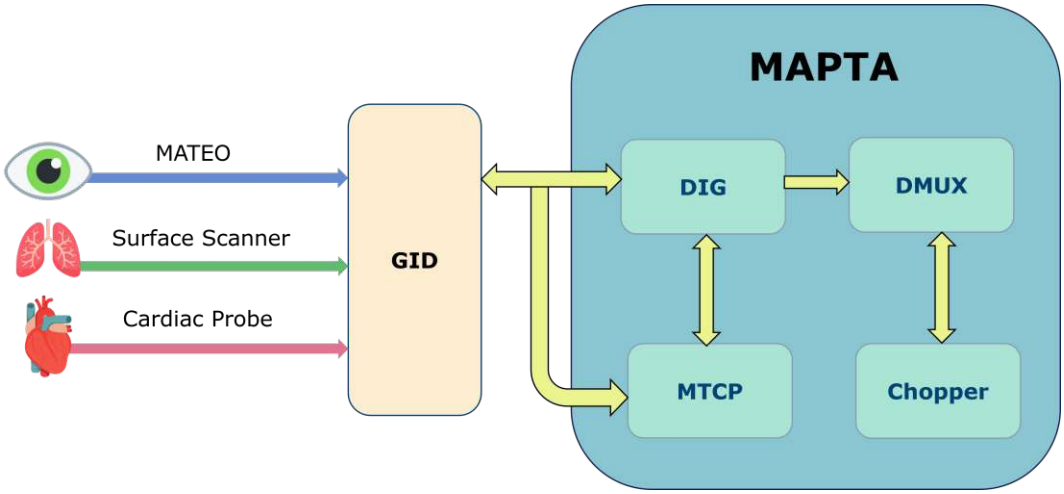

Figure 3.6: External gating devices and environments connected to the Gating Interface Device (GID), which communicates with MAPTA, the DMUX and the DIG via the MTCP. As a result, the chopper can be opened or closed at demand from an incoming triggering signal propagated by external devices [150].

bi-directional virtual point of contact between MAPTA and connecting RayCommand platform for clinical usage of the machine. MADAM can be seen as a software representation of the MAPTA medical frontend. Moreover, it can be understood as a "state machine" controlled by the MedAustron Control System (MACS), which coordinates all functional components of the particle accelerator for beam generation purposes.

MADAM and MACS revise the following states to be TRUE in sequence before determining the position of the chopper:

1. Beam line not occupied
2. No treatment ongoing
3. Treatment ready and valid
4. No interlocks
5. No Veto

Subsequently, all the in-room components like the robotic arm, the patient table, the X-ray system for positioning, will be checked and their status reported as feedback to MADAM and RayCommand software. Then MADAM will propagate this "ready" signal coming from the in-room devices and the Dose Delivery System (DDS). It will also check for interlocks that can be faults in the geometry, plan constraints related to dose, or even software failure. Then, two output signals from the DIG (Veto OUT A/B) serve as feedback to the gating monitoring system and guide the Veto to the DMUX. This device is used to verify the state of the beamlines and determine which one of them is currently being occupied.

Once all of this is checked, and no faults are detected or dose restrictions violated, the "START" signal (optical) will go to the MedAustron Control System (MACS) and activate within 120 seconds the accelerator and its relevant components to yield the desired ion beam for the required treatment plan.

The GID signal states and arguments sent to MAPTA after the DMUX are as follows [151]:

- **Veto IN (A/B):** dose Delivery System Interlock Gateway (DIG) input that indicates if the gating monitoring system allows irradiation to the target at the moment or not.
- **Veto OUT (A/B):** DIG redundant feedback that crosschecks if a Veto signal has been received or not.
- **Permanent light:** a permanent light is always sent from the DIG from the DDS rack and into the gating monitoring system. Unless the gating is activated, then the state and the signal must be changed to "gating enabled".
- **Gating enabled:** MTCP input that uses the gating-enabled lamp to show whether or not the gating is currently active. Then it is converted from an optical signal to a 24 V electrical TTL pulse.

In parallel, the GID sends the MTCP the "gating enabled" signal from the gating monitoring system, allowing the user to know whether or not the accelerator is ready to perform the gating. Simultaneously, the DIG checks if the treatment is ongoing, interrupted, or terminated. To this day, there are four more fibres available for future use and integration of new devices.

Currently, only the MedAustron Treatment Environment for Ocular Diseases (MATEO) and the Catalyst Surface Scanner are designed to be connected to the GID autonomously (one at a time). Each one of these devices has its graphical user interface (GUI) and control to interact with the user. Finally, if the gating is not in use, a permanent UN-VETO is applied to the DIG through a permanent light [6]. Pin 1 of the 10-Pin optical connector is attached to the FO/TTL converter in the DDS rack for gating off, leaving some fibres available for future use, the current setup can be seen in figure 3.7 below.

[6] Optical signals have faster propagation compared to others (e.g. electrical) in addition all in-house components have electrical connectors. As a result, there is no need for converters or any other electronics in between.

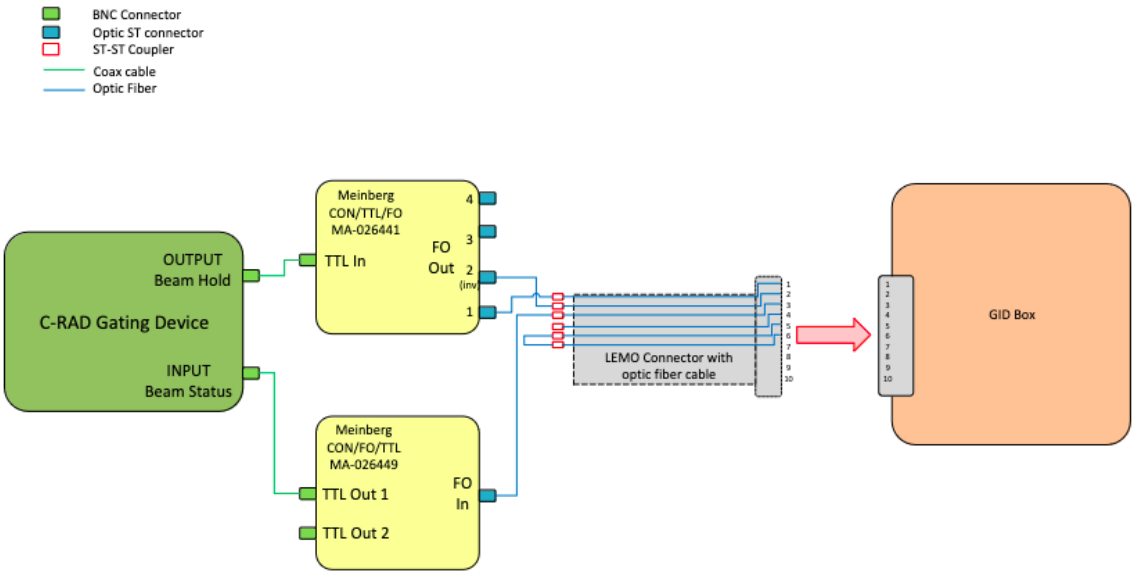

Figure 3.7: Current Surface Scanner set-up in IR2 [152].

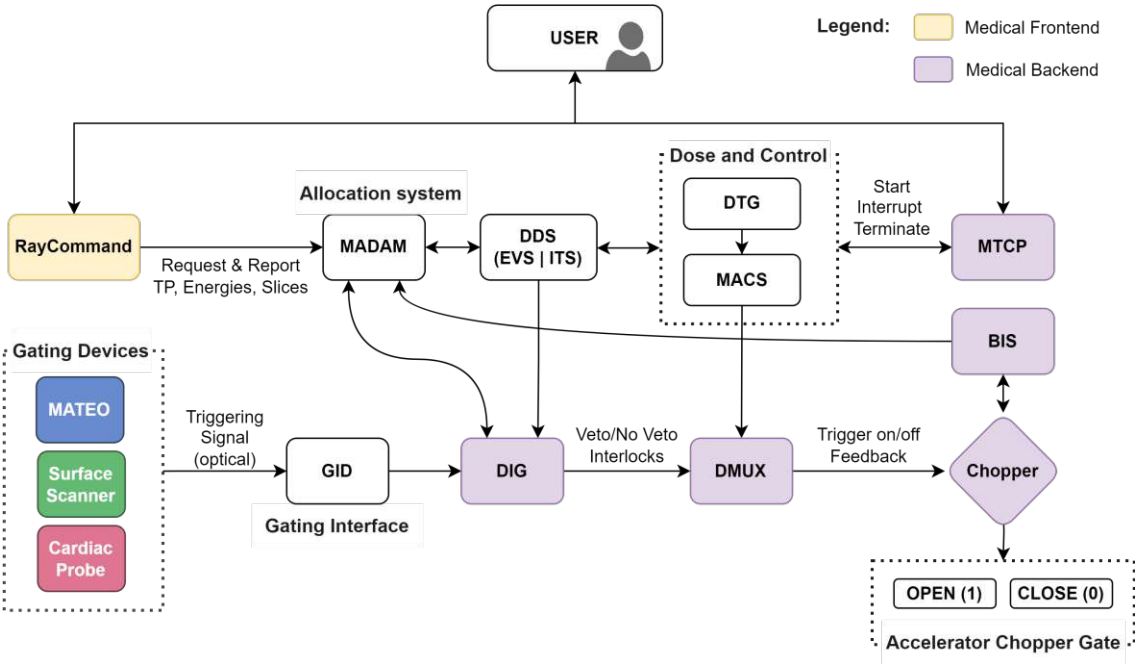

Figure 3.8: Basic signal propagation and communication of the Gating Interface device and surrounding control systems of the MedAustron Particle Therapy Accelerator (MAPTA) to trigger the chopper at the end of beam extraction to a specific time stamp (created with draw.io).

The GID control workflow to the accelerator chopper begins with the transmittance of the treatment plan (TP) via RayCommand software (see figure 3.8, top section, yellow square). The required energies, slices, beam position, etc. are also transmitted for allocation. Following that, the required in-room equipment is activated based on the TP specifications and the type of gating that is required from one or more of the available external devices. MADAM and MACS request the status of the beamline and all the in-room components (as specified in the checklist above) to continue or interrupt the signal propagation.

Next, the system runs a dose control check-up via the dose delivery system (DDS) aided by the energy verification system (EVS) + independent termination system (ITS) and the dose delivery system timing gateway (DTG).

When constraints are violated, an interlock or warning signal will propagate immediately and remain until the system is resolved and in "ready" state again. Then, with the MTCP, the treatment can be started, terminated, or interrupted. Eventually, MACS will communicate with the DMUX and emit a trigger on/off signal to open/close the chopper at demand. This action is constantly surveilled by the beam interlock system (BIS) in case irradiation needs to be interrupted. The general system architecture overview and communication can be seen in figure 3.8 [152].

3.6.3 Gating Signal States and Constraints

Following EBG MedAustron GmbH internal internal documentation and standards [151].

- **Timing:** when the Veto IN signals (Veto IN A/B) signals are being switched, they must reside in the new stable state for a maximum of 200 ns, from the start till the end of a change concerning the first signal. If both of the signals do not remain in the stable state for at least 1.5 µs at the same time, the DIG will trigger a Veto or Un-Veto signal. The wavelength for the signals should be 850 nm, following the DIG in-house specifications.

- **Signal Consistency:** Veto OUT indicates if a current Veto is being received, and it is partly independent of Veto IN. The Veto source does not necessarily come from the gating monitoring system, it may be any signal or event from the Dose Delivery System (DDS), the Irradiation Room Safety System (the IRSS), and the Energy Verification System (EVS). These signals (Veto IN A/B) are then sent to the DMUX and the gating monitoring system.

  In case the gating monitoring system sends a Veto IN, it must be indicated by Veto-OUT. Furthermore, the "gating enabled" signal will remain active as long as the gating monitoring system is connected to the GID, regardless of the treatment state.

- **Signal Levels:** two optical lines are used for Veto IN and Veto OUT, indicated with light on (high) and light off (low) in tables 3.2 and 3.3. Where, all their possible states and their respective possible combinations are listed below.

  Only one optical line is required for the gating-enabled signal, then it is transduced into an electrical signal before being passed to the MTCP. The 24 V signal refers to a light that is on (high), whereas 0V represents the opposite case (low). The table below (3.4) presents all the possible states for "gating enabled".

Veto IN A	Veto IN B	Meaning
0 - light off	0 - light off	Fault, generate interlock
0 - light off	1 - light on	Veto
1 - light on	0 - light off	No Veto
1 - light on	1 - light on	Fault, generate interlock

Table 3.2: Possible state combinations for Veto IN.

Veto OUT A	Veto OUT B	Meaning
0 - light off	0 - light off	Veto
0 - light off	1 - light on	Fault, generate interlock
1 - light on	0 - light off	Fault, generate interlock
1 - light on	1 - light on	NO Veto

Table 3.3: Possible state combinations for Veto OUT.

Gating Enabled (Optical)	Gating Enabled (Electrical)	Meaning
0 - light off	0 V (TTL)- low	Gating not active
1 - light on	24 V (TTL) - high	Gating active

Table 3.4: Possible state combinations for gating enabled.

3.6.4 Compatibility with External Devices

The MedAustron Gating Interface will soon be part of the CE-certified medical device MAPTA. At the moment, it has been used for experimental testing only with a frequency/pulse generator and the surface scanner (The Catalyst, C-RAD). Eventually, it will become clinical once end-to-end testing is performed that will prove the device to be safe and efficient. So far, the response time has been measured, which is around 5 ms. The pathway starts from the moment the signal is sent to the accelerator and controls the chopper to command, meaning that at the moment, there is not a completely quantified overall latency of the system. Due to its modular design, external devices with their own GUI can be plugged into the GID. Ideally, the following technicalities must be considered to ensure interoperability [151]).

Requisites:

- Connectors from any gating or triggering device to the GID must be optical 62.5/125 μm optical fibre, LEMO 10 pin, 7 m length connectors), and the electrical signal communication should be managed via TTL electrical pulses.
- The treatment planning must contain data requesting a specific gating device, ideally via a DICOM modality worklist [7].

  This is because during the treatment planning stage, different machine models can be selected to indicate a part of the body that will be irradiated. If a gating environment and device would be required, then in the treatment plan itself it would be needed to specify the desired gating functionality for any external probe.

[7] Function that integrates modalities, image acquisition tools, archives, DICOM and non-DICOM, on-premise and remote locations to the healthcare company into a single scheduling database that becomes a Worklist Server for Radiology [153].

- Adherence to the in-house pin configuration (see table 3.5 below).

Pin	Signal	SRC	DST	Signal
1	Veto in A	Gating monitoring system	DIG (Gating Veto A)	Optical
2	Veto in B	Gating monitoring system	DIG (Gating Veto B)	Optical
3	Veto out A	DIG (Veto)	Gating monitoring system	Optical
4	Veto out B	DIG (Veto or CAT A)	Gating monitoring system	Optical
5	Gating enabled	Gating monitoring system	MTCP	Optical/Electrical
6	Gating active	Permanent light	Gating monitoring system	Optical
7–10	Further use	-	-	-

Table 3.5: Pining and signal overview form source (SRC) to destination (DST) component.

Restrictions:

- Pulses shorter than 1 μs are ignored by the DDS, hence any utilised pulse to illicit any action must be longer than this value.
- The integration period to calculate the particle rate is configurable on the DDS and is typically set to 1 ms. If the particle rate exceeds the preconfigured threshold, the DDS-Beam-Detected signal is activated. As a result, when the Veto changes, a typical delay of 1—2 ms can be observed by the gating system before the DDS-Beam-Detected signal is activated or deactivated.
- When the gating system activates the Veto signal (disallow beam) it takes 30—100 μs (depending on the particle type and energy) to turn the beam off.
- When the gating system deactivates the Veto signal (allow beam) it takes 30 μs to several seconds before the beam arrives at the dose delivery monitor (gas chamber detector) custom made for MedAustron (depending on the accelerator state and the current extraction phase).

3.7 Cardiac Gating and Target Tracking

EBAMed SA is a Swiss start-up company that is developing an ultrasound (US) based motion management system dedicated to the treatment of cardiac arrhythmias using radiation. The device is not yet clinically available but first published data [92, 93] highlights the potential of this technology. The device produces clinically relevant real-time B-mode ultrasonic images [8] to monitor the heart, automatically computes cardiac displacement, and send an alert to the operator in case the target is found out of range or not compliant with predefined geometrical limits. The device must be used for therapy planning imaging acquisition with the planning CT [9] and during treatment delivery. In the subsection below usage, setup of the device and required systems to potentially integrate this device into the medical workflow at MedAustron will be described.

[8] US brightness mode (B-mode), where a 2D image is produced by a range of transducer elements scanning a plane through the body [154].

[9] Equipment available at MedAustron: CT-sim Brilliance, Phillips

3.7.1 Acquisition System Set-up

A custom-made echocardiographic probe must be placed on the chest of the patient (ideally supine and arms up) using a mechanical probe fixation system around the thorax of the patient (see figure 3.9 panel A) and gel for better conductivity. The probe has passive spherical references that are tracked with an infrared camera (Polaris Vega® XT, NDI, Ontario, Canada) to track the probe position in the room. Then the US system records 2D B-mode images at 40 Hz on two orthogonal planes.

Following that, ECG electrodes are also placed at the level of the left anterosuperior iliac spine and on the root of both upper limbs (see figure 3.9 panel B, top and bottom respectively), the emitted signal is processed to automatically identify the R-waves signal, which will be later used as a marker to determine the cardiac contraction. The obtained ECG and the US signals are then integrated and processed in real-time to determine the heart current position. The probe can be positioned either in apical position or in parasternal position (see figure 3.9 panel B, bottom).

A feasibility study performed on 24 Ventricular Tachycardia patients [92] has shown that transthoracic echocardiographic imaging on real-life subjects in treatment position delivers images of sufficient quality for heart motion assessment. In addition, a treatment planning study [93] showed that the ultrasound probe position needs to be considered for treatment planning, but that this additional constraint does not prevent to obtain a clinically acceptable treatment plan.

After being analyzed, the data is transferred to a workstation that is integrated into the probe's optical localization system and "Demonstrator 2", offering the operator GUI live information on ECG tracing, echocardiography pictures, and details on the probe's location are used for critical decision-making during diagnostic imaging or the treatment delivery. The EBAMed system (see figure 3.10) would need to be connected to the MedAustron GID that communicates with MAPTA via LEMO optical connectors following the in-house pin configuration to be able to send TTL pulses in a bidirectional manner and gate the beam chopper to the cardiac motion in real-time.

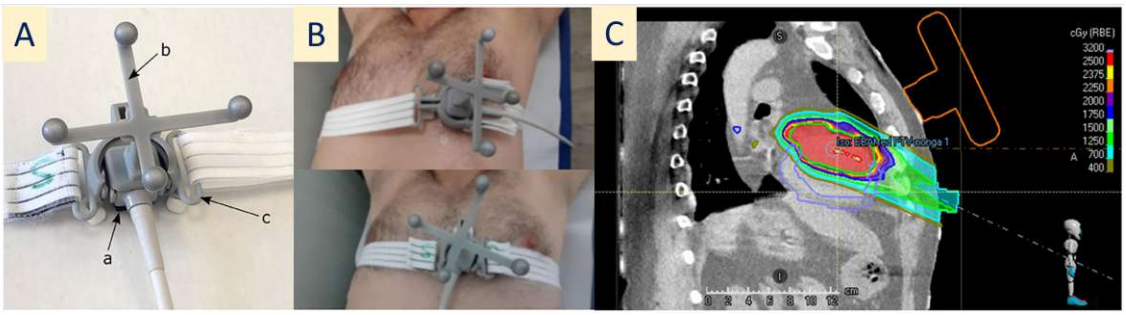

Figure 3.9: Panel A shows the EBAMed ultrasound prototype, panel B shows the two different placements of the probe for data acquisition and panel C shows the treatment planning system with the target and contour that accounts for the probe on the chest of the patient for treatment delivery [92, 93].

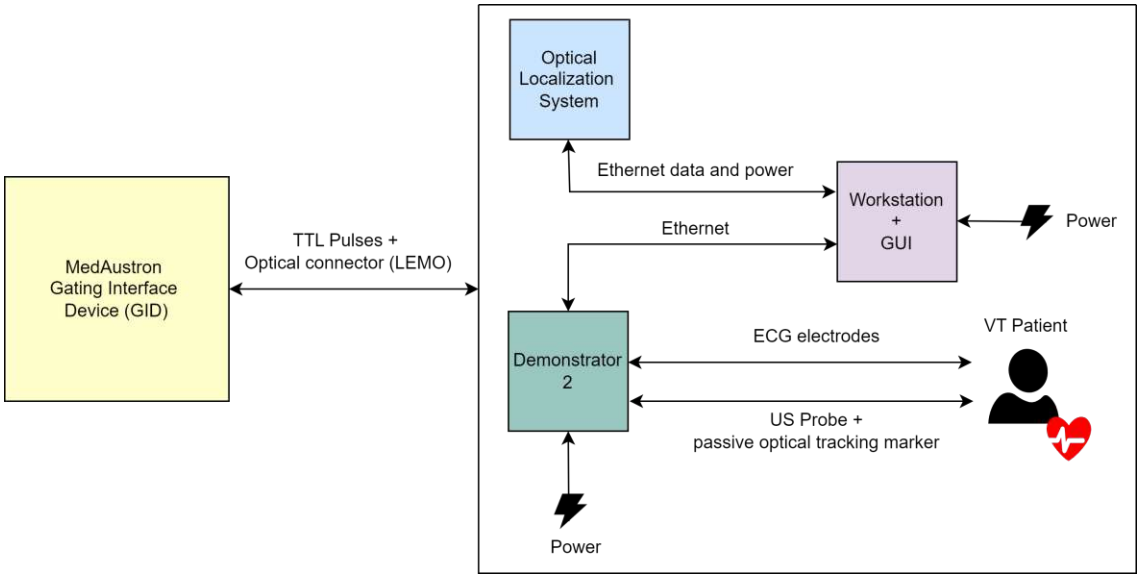

Figure 3.10: Schematic portraying the EBAMed acquisition environment and its flow connected to MedAustron GID which is then communicating to MAPTA in a bidirectional fashion (modified) [92].

3.7.2 Signal and Image Processing Aided by Artificial Intelligence

The EBAMed System relies on Artificial Intelligence (AI) algorithms to to process the ultrasound images and extract heart motion information. Their published approach was based on two layers of neural networks, which were trained on a publicly available database of 500 cardiac patients and evaluated via a 5-fold cross-validation method. The first layer extracts spatial and short-term temporal characteristics from the US sequence using a multi-stage 3D causal convolution network. The second layer is comprised of a single-dimension (1D) temporal convolution neural network. As a whole, it can automatically determine the associated cardiac cycle phase for every US picture taken and estimate how far the image has moved in relation to a reference cycle.

An arbitrary-length US series is received as input and produces one cardiac phase for each ultrasound picture in the sequence. Once this is identified, the heart displacement is measured in three orthogonal directions by rigid registration between the real-time US acquisition and the reference image for the matching cardiac phase. The reference and real-time ultrasound pictures are concatenated and then run through many convolution blocks before feature map averaging. As a result, the output of the network may be utilised to provide the displacement of the heart in 3D space as each (heart) pixel inside the pictures is known in 3D space because of the optical localization mechanism [92]. The system can thus be used to monitor heart motion (see figure 3.11) and gate the beam accordingly.

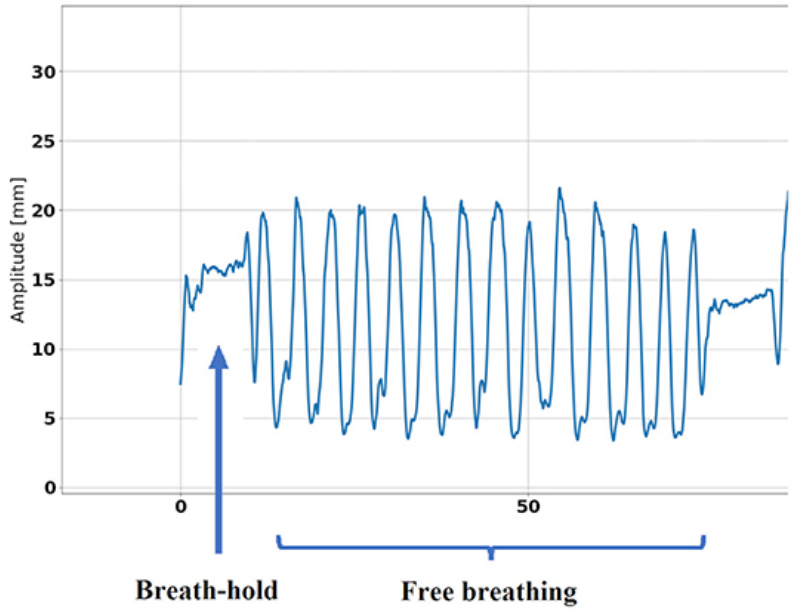

Figure 3.11: Example of heart displacement measured by the EBAMed US system [92].

3.7.3 Problems and Suggestions for Future Improvements

The compatibility of the GID and the EBAMed probe has been addressed only at the theoretical level based on scientific literature, and local documentation. Further investigation and testing would be required to estimate the time frames for collocation on the patient and modelling of the probe in the TPS. Another aspect that must be tested in the future and before irradiation shall be the benefits of this device, the influence of the presence of the probe and how it would affect the medical workflow and the 4DCT acquisition. The impact of the US probe with the potential beam directions in TP in accordance with various target locations is another factor that needs to be better investigated. Other assessments like gain in treatment precision, signal acquisition, instrumentation and latency determination between the motion management system, the GID and MAPTA would also be required to ensure integration with the local environments and time viability (critical for VT patients). Another aspect that must be considered for integration and testing is the electronics. LEMO optical cables should be the physical communication pathway between the GID, MAPTA and the US cardiac probe. Furthermore, signal transduction should be performed via TTL pulses.

At the moment RayWorld (TPS software environment) is not using the gating tag embedded in the DICOM standard, this is the reference for the software to indicate that there is an external trigger and an external gating device incorporated in the environment (which would need to be communicated via RayCommand). In addition, no cardiac CT protocol is commissioned in-house. Hence, a new development project between MedAustron and RaySearch Laboratories would be required. Having this feature available within RayCommand would not only be adequate for the cardiac probe but also for any other external trigger signals from available gating devices (like the surface scanners or the MATEO environment. Finally, the US system needs to be DICOM and CE compliant, which means that the GUI software of the external devices must have the “DICOM modality worklist” feature available.

3.8 EAM Target Migration to Planning CT

In this section, the EAM target migration to the planning CT will be discussed. Electroanatomical mapping (EAM) is an electrophysiological study that records intracardiac electrical activation signals at a heart chamber of interest for arrhythmia mapping during RFCA fluoroscopic guided procedures. As a result, a 3D object is generated (see figure 3.2) encompassing chamber geometry and conductivity activation, which is then registered with a CT to have an anatomical reference. This map is used in VT radiotherapy planning for identifying the arrhythmogenic substrate and aid target contouring.

The transfer of the target region from the EAM to the CT is mostly done manually. There have been several proposed in-house solutions (approximately 15 different workflows proposed until today) for EAM target migration to the planning CT, but most of them rely on specific data formats [44, 47, 155–158] and platforms. What is more, not all of them are open to the public for general use and hence lack of CE-approval. To allow for the quality assurance of the target transfer from EAM to CT the CARDIO-RT software package was developed by the research unit of the Institute for Robotics and Cognitive Systems at the University of Lübeck in Germany in the course of the RAVENTA trial [159].

It is a stand-alone cross-platform solution for data presentation, EAM registration and target transfer to the planning CT, which implements three different methods for target transfer, whose results can be compared to each other and that of other transfer methods: 3D-3D, 2D-3D, and 17-segment registration (see table 3.6).

CARDIO-RT is not a system for clinical decision making, but rather for assessing the quality of the target transfer carried manually or with other methods and for making suggestions for delineating the target in the planning CT.

Registration Method	**System**	**Prerequisites**
3D-3D	Biosense Webster, Carto 3 System and Boston Scientific, Rhythmia System Only	.mesh geometry data files plus LV contours in DICOM
2D-3D	All mapping systems	2D EAM screenshots plus LV contours in DICOM
17 Segment	All mapping systems	LV contours in DICOM format

Table 3.6: Overview of the current EAM-CT registration methods and their respective data prerequsities for the CARDIO-RT QA tool [159]).

In the 3D-3D registration method, the EAM and the cardiac CT are registered as 3D structures. As for this method the original 3D mesh of the EAM is needed, it has the disadvantage of having to deal with the different data formats used by different cardiac mapping systems (Boston Scientific, Rhythmia System [.mat or Matlab.m], Biosense Webster, Carto 3 System [.mesh or,mesh + _car.txt], Abbott Laboratories, EnSite System [.xml]). It is also important to highlight that the cardiologist must define the low conductivity scale used.

- The EAM and the cardiac CT are registered by aligning the thoracic aorta and the left ventricle as they are delineated in the CT and visible in the EAM. The approximate alignment is done by manual shifting and rotation and afterwards refined using an *iterative closest point* algorithm.
- The good pace map locations [10] defined in the EAM are projected onto the left ventricle, as it is defined in the cardiac CT.
- A transmural 3D target volume is created by defining a margin around the projections of the good pace map locations that reach at least 2 mm beyond the outermost ablation point and extending the target region along the depth of the myocardial wall (see figure 3.12).

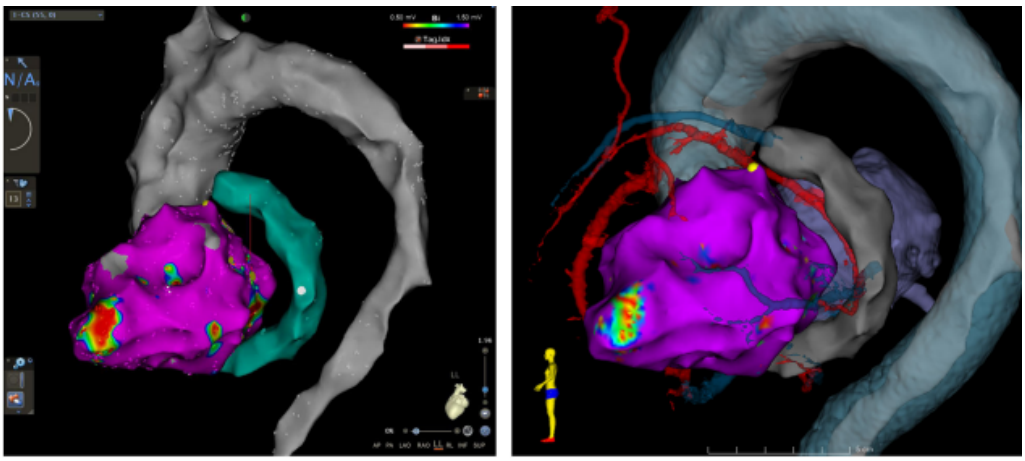

Figure 3.12: EAM 3D-3D integration. On the left, it is possible to depict the EAM and on the right, the corresponding view after import and registration to the cardiac CT in 3D Slicer as proposed by S. Hohmann et al. [156].

The 2D-3D registration method is based on first drawing the target contours on screenshots of the EAM and then registering the screenshots with the planning CT (see figures 3.13 and 3.14 which are screenshots of the registration between the EAM and the planning CT) to generate the corresponding 3D target volumes within the myocardial wall.

- Screenshots of the Electrophysiological Mapping from different perspectives(i.e., Anteroposterior, Posteroanterior, Superior, Inferior, Right Lateral and Left Lateral) are generated.
- On each screenshot a contour for the part of the target visible on the respective screenshot is drawn by the cardiologist.
- The screenshots are registered with the cardiac CT. For this, the left ventricle, which is contoured in the planning CT, is projected onto the screenshot and this projection is then manually shifted and scaled until it coincides with the left ventricle as it can be seen in the screenshot of the EAM (see figure 3.13).

[10] Areas of low conductivity in the heart that could be included for RT ablation where the VT is more likely to be found.

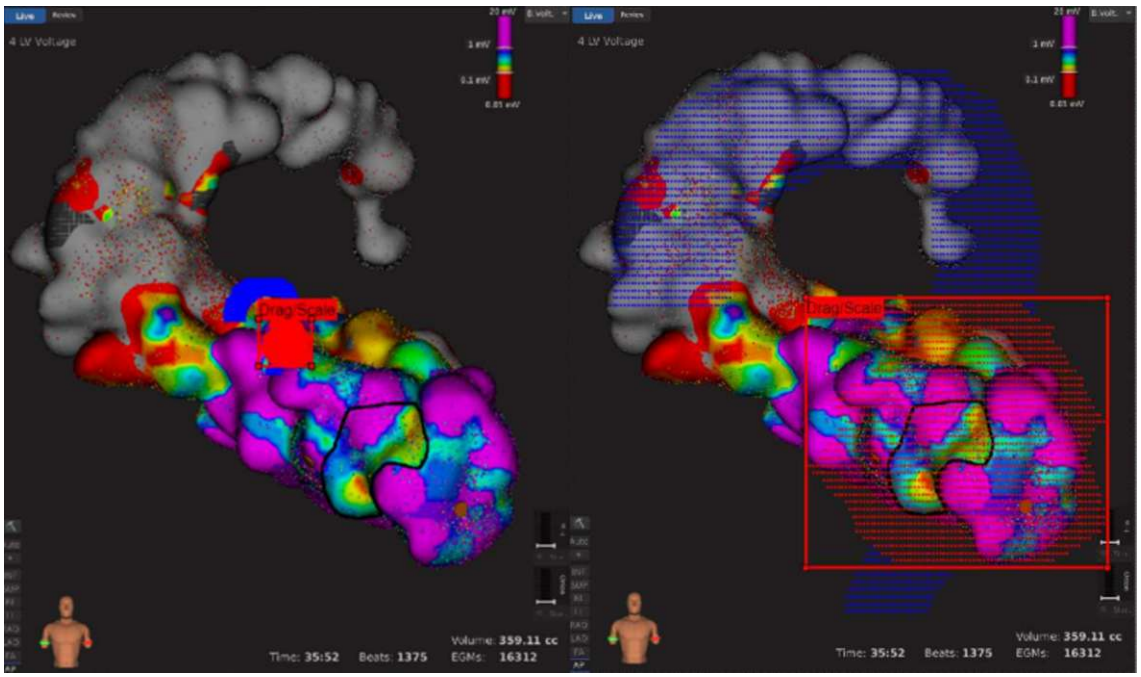

Figure 3.13: Registration of screenshots with the cardiac CT by shifting and scaling the left ventricle (Taken from the CARDIO-RT Software Instruction Manual, Institute for Robotics and Cognitive Systems, University of Lübeck, Lübeck, Germany, 2023).

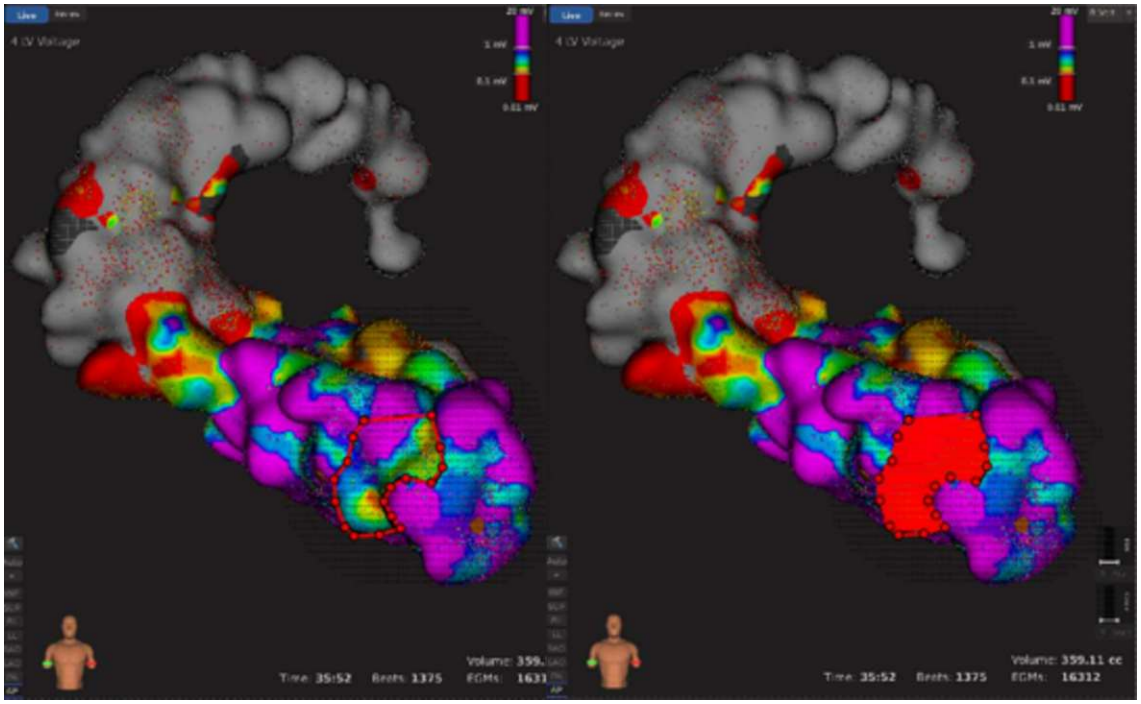

Figure 3.14: Generation of polygonal chain and 2D target area on the cardiac CT (Taken from the CARDIO-RT Software Instruction Manual, Institute for Robotics and Cognitive Systems, University of Lübeck, Lübeck, Germany, 2023).

- To generate a 2D target area within the screenshot, the target contour is first approximated by a polygonal chain that is drawn by manual selection of its vertices and then the area bounded by the polygon is determined by an algorithm (see figure 3.14).

- The 3D target volume is extrapolated from the 2D area by extending it into the myocardial wall (see figure 3.14).

Another alternative is applying a 17-segment heart model as proposed by the AHA [160]. In this model the ventricle is split into three equal sections, base, mid-cavity, and apex, then it is segmented into 17 fractions which include 4 apical segments, 6 basal segments, 6 mid-cavity segments, and segment 17, which is the actual apex. Specific coronary artery regions relate to each one of the 17 segments (see figure 3.15). This model has been used for harmonization in cardiac imaging [161].

- A 3D 17-segment model is registered semi-automatically with the LV contour of the CT.

- After the registration is finished, the surface of the LV is partitioned into 17 segments (see figure 3.16).

- The segmentation of the LV contour can then be used to describe a target region in the CT.

The main drawback of this approach is that by using the segments to describe the target, the target region is expanded more than necessary. Also, there is no direct registration of the EAM and no visualization [162, 163].

A comparison between targets acquired by manual transfer and those generated by 3D-3D and 2D-3D registration using CARDIO-RT showed considerable differences, even though the manual transfer had been performed by an interdisciplinary team with very high expertise [159]. As for the evaluation of the CARDIO-RT software, the target transfer for each case was only done by one centre, it can not be investigated to which extent the difference between the manually and the semi-automatically transferred target regions can be attributed to uncertainties in the manual transfer process. However, in another study done as part of the RAVENTA, the variability of the manual target transfer process has been investigated by comparing the target volumes manually generated by five different centres for a fixed set of patients. Apart from differences already present due to different delineations on the EAM as done by the different centres, the study clearly showed an increase in target region variability due to uncertainties in the transfer process from the EAM to the CT[45].

This provides evidence that automated or semi-automated VT target transfer methods could reduce the variability relative to the manual transfer methods. Until now these methods can only be applied to improve the target transfer using them for target suggestions or as part of a quality assurance process.

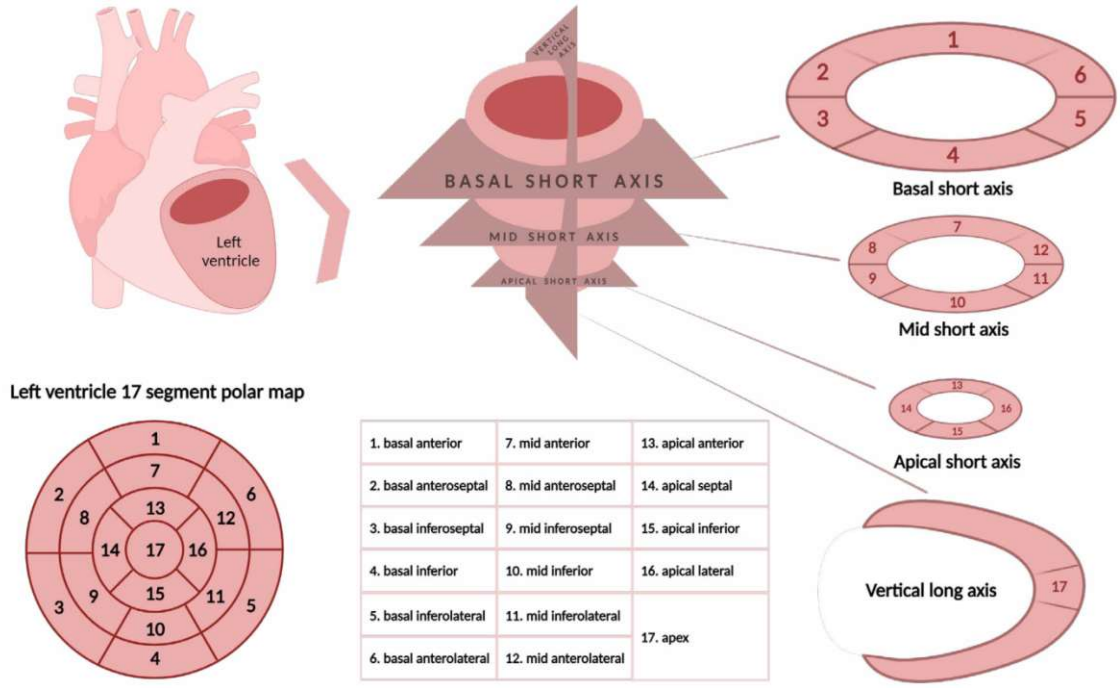

Figure 3.15: American Heart Association's (AHA) 17-segment model for left ventricle (LV) segmentation, nomenclature, and a 17-segment polar map [164]).

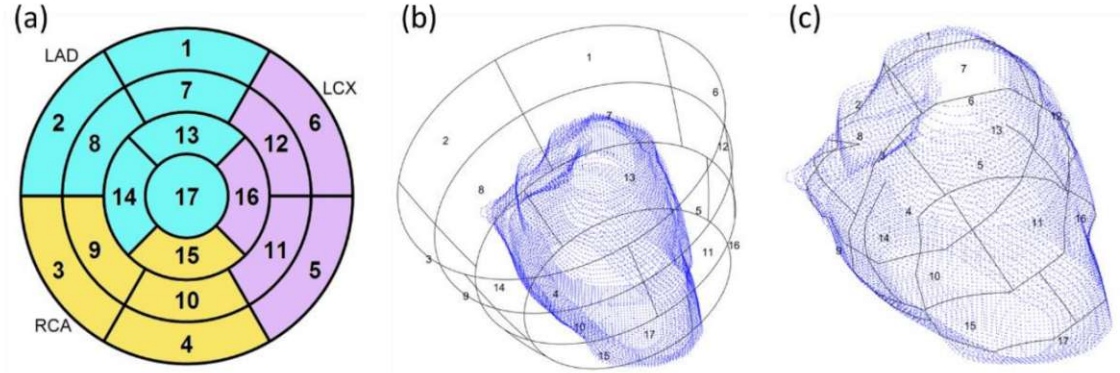

Figure 3.16: (a) The 17-segment model with numbers identifying the LV segments; (b) The LV contours with the 17-segment model generated in the CT coordinates; (c) The LV contours overlaid with the 17 segments. Abbreviations: left anterior descending artery (LAD), left circumflex artery (LCX), right coronary artery (RCA) [159]).

3.8.1 Problems and Suggestions for Future Improvements

There is no standardised tool or direct procedure to migrate the targets from the EAM to the planning CT and most of the centres perform this task manually. VT target definition depends on several sources of information, with low voltage generally being an indication for VT scar. All ECGs must also be revised to localize where the VT isthmus is. The intricate constructions known as VT isthmuses have numerous entries, exits, and activation dead ends in the cardiac conductivity pathway. Functional block sections (very low conductivity zones in the EAM) are commonly used to define the isthmus, and a VT "critical zone" may contain many VT circuits.

This has a direct and significant impact on correct substrate mapping, and improved techniques to properly identify VT critical zones for targeted radioablation may improve treatment outcomes [165].

Currently EAM to CT target transfer is mostly based on either manual transfer techniques or in-house methods that are not open to the public. Using semi-automatic target transfer based on 3D-3D, 2D-3D, and 17-segment registration, as implemented in CARDIO-RT, allows for improvement of the quality of the target transfer by providing suggestions for delineations of target contours on the CT and QA for the transfer process itself. During the development of this thesis, there was an ongoing collaboration with Jingyang Xie from the Institute for Robotics and Cognitive Systems at the University of Lübeck in Germany. Together, Matlab scripts were generated to be able to read the EAM data provided by the Landesklinikum Wiener Neustadt. However, it seems that the extraction of these data was incomplete as it lacks certain information like all the ablation points that were made during the RFCA. We easily noticed this by comparing the screenshots (see figure 3.1) and the plot generated via Matlab scripts from the extracted files of the Abbott EnSite Precision System (see figure 3.2).

Hence it was not possible under the scope of this thesis to already provide a solution for target migration with the provided data from the Landesklinikum Wiener Neustadt. To be able to migrate the EAM targets in a correct and standardised manner the following details shall either be amended or taken into consideration:

- There might be distortions between the CT used for the cardiac interventions and the planning CT. Injection of contrast media results in different attenuation, hence different HUs. This leads to problems in geometrical compatibility when performing image registration. Hence the MPs must be able to apply deformable registration to account for the image geometrical disparities of the image.

- The data transfer between Landesklinikum Wiener Neustadt and MedAustron requires further analysis. The aim should be to have an SOP to eventually achieve direct, fast and consistent file exchange. Furthermore, the data formats utilised must be compatible across the environments for diagnosis, therapy planning (e.g., CARDIO-RT and RayStation), and treatment delivery.

- Further exploration on the EAM extraction formats of the Abbott Laboratories, EnSite System available at the Landesklinikum Wiener Neustadt cardiology department is needed. Streamlining this process will provide a clear workflow and mechanisms to potentially use this data for target migration.

- The CARDIO-RT software is available to the public for research purposes and modifications to the algorithm can be made to meet specific compatibility requirements.

- CARDIO-RT requires the following data: Screenshots of the EAM data from standard projection views (i.e., AP, PA, SUP, INF, RL and LL) with marked VT target; DICOM-RT Structure Set file containing the heart structures (i.e., LV, aorta, etc.); Cardiac CT which is registered with the planning CT, or the original CT with the corresponding DICOM RE registration file; and the planning CT.

- Another possibility might be to explore the solutions offered by external companies. Liryc is a heart rhythm disease institute that specializes in heart disorders like VT. Through their research project "Map in Heart" funded by the European Research Council (No. 899539), they offer advanced image processing software for VT. Nevertheless, it must be kept in mind that outsourcing services and adding layers of complexity will have a toll on the workflow [166].

3.9 MedAustron VT Ablation Medical Workflow

Throughout this section, the envisioned medical workflow to be implemented at MedAustron will be detailed step-by-step; from diagnostics and patient selection, to beam delivery. The presented structure includes the available technology and resource requirements; estimated time and involved personnel are also considered. At the end of this section, challenges, bottlenecks and possible "show-stoppers" will be outlined as a reference for the future.

3.9.1 VT Diagnosis and Patient Selection

Patients that present acute symptoms and persistent, focal, and/or re-entrant VT (wide QRS complex and reduced ejection fraction ($\leqslant 20\%$)) [167] even after first-line treatments such as ICD and RFCA are potential candidates for VT-RT with ion beams. Especially if the patients presented > 3 VTs or external defibrillation in the last 24 hours (A.K.A electrical storm) [17, 77]. The diagnosis, treatment viability, and death criticality assessment are performed by the cardiologist and the electrophysiologist within an hour. After carefully evaluating a baseline ECG in addition to any other medical imaging studies available at the time (e.g. CT, previous CMR, PET-CT, Mitigated Acquisition Scan (MUGA with Tc-99m). Once the patient's status has been identified, the patient will be referred to MedAustron for treatment.

3.9.2 Electroanatomical Mapping (EAM)

Electroanatomical Mapping (EAM) is the 3D medical imaging modality that will be employed to record and track cardiac activation signals. With it, information about the VTs concerning their anatomic location within the chambers of the heart is obtained. Furthermore, the cardiologist and the electrophysiologist can use the exact location and orientation of the catheters inside the heart, to tag relevant anatomical landmarks, record ablation lesions, and visualize signal activation, voltage, or scar pathways. These 3D structures will be obtained employing one of these two mechanisms available at the Landesklinikum Wiener Neustadt cardiology department:

- **Invasive EAM (standard):** Obtained from previous RFCA minimally invasive surgical interventions utilising the EnSite Precision Navigation System and catheters by Abbott, [168]. This procedure is performed under anaesthesia in the Fluoroscopy Operating Room (A.K.A. CatLab) (see image 3.17). The involved professionals for this procedure: 1 cardiologist, 1 instrumentalist nurse, 2 interventionist nurses, 2 radiographers, 3–4 Abbott technical operators, and 1 anaesthesiologist. Time-wise, it is variable and highly dependent on the team's experience and case complication, on average it takes between 4–6 hours for the team at the Landesklinikum Wiener Neustadt to complete the procedure. All patients who will be referred to MedAustron will have an EAM available from their previous interventional procedure.

Figure 3.17: On the left side of the image EnSite Precision navigation system that the cardiologists use to map the physiological endpoints of the heart and ablate in the areas of lowest conduction. On the right side of the image, an example of how the medical doctors visualize the EAM inside the operation room which allows for deciding on how and when to approach the VT [169].

- **Non-Invasive EAM (optional):** Obtained from a dense 252 superficial electrode configuration provided by the CardioInsight™ Vest by Medtronic [170]. To derive EAM information, the vest must be properly placed and secured with surgical tape on the chest of the patient and then he or she must be laying flat (supine) in a resting position. Next, the patient can be transferred to the radiology department for the CT acquisition, as a last step, ECG signals will be recorded independently with the workstation and then utilised to create the potential and activation maps [171] (see image 3.18). The involved professionals for this task are 1 cardiologist, 1 nurse, and 2 radiographers. The estimated time for its execution is between 60 and 90 min. This type of mapping would only be performed if determined necessary by the cardiologist due to missing or poor data acquisition from the interventional procedure.

To be able to migrate the identified VT lesion (target) locations for therapy planning, the operator of the EnSite Precision System at Landesklinikum Wiener Neustadt must extract the EAM data as a .mesh file and the CT used for the RFCA in DICOM format respectively and provide them to MedAustron.

3.9.3 4DCT Imaging for Dose Calculation and Contouring

Once the patient has been referred to MedAustron and the lesion has been localized by the cardiologist aided by the EAM, it is possible to perform the 4DCT simulation with the in-house CT-sim Brilliance Big Bore, Phillips. This device has certainCT protocols commissioned to convert Hounsfield Units (HUs) into mass-stopping powers (this conversion occurs within the TPS). This study aims to generate the planning CT that will be used to identify the arrhythmogenic substrate within the patient's anatomy and it has to be performed under the following conditions and specifications:

- **Patient positioning:** the patient can be placed head-first supine prone or decubitus, hands up or to the side (only when the first constraint can not be fulfilled). Minding that this step is strictly conditional on the acuteness of the patient's condition and tolerance to particular movements.

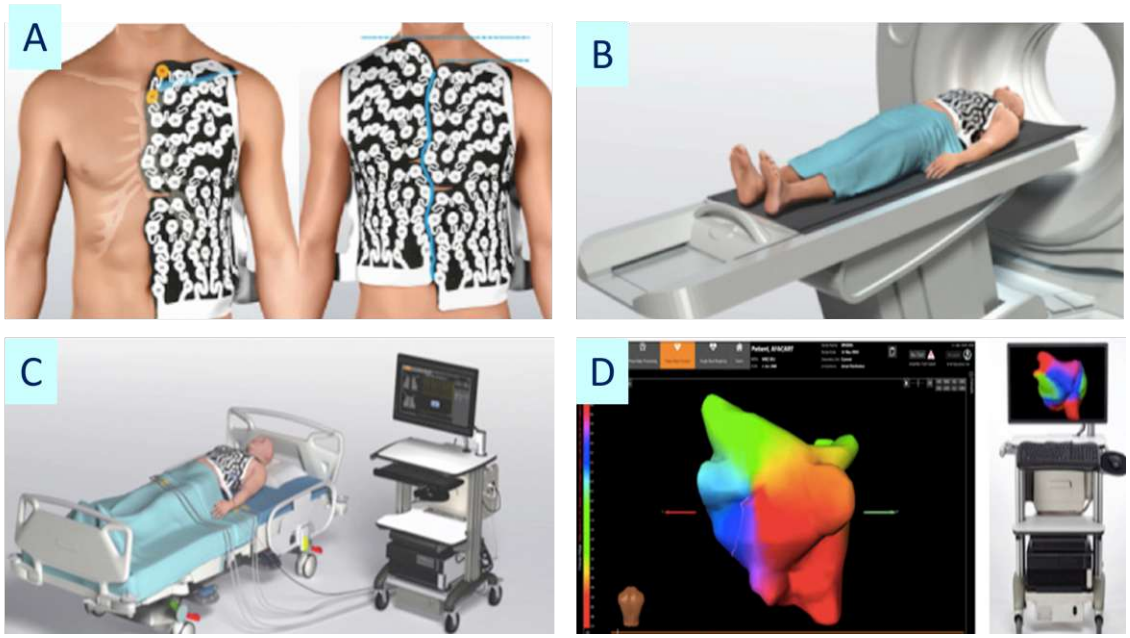

Figure 3.18: Example of the noninvasive EAM procedure, (A) the patient is prepared and the vest is placed on the chest with the depicted placement, (B) the patient is taken to the CT for imaging wearing the vest here the heart-torso geometry will be obtained, (C) then the patient is laid to rest for some minutes and the workstation acquires additional ECG signals. (D) At last the beats where the VT is running are selected to create EAM mapping data [171]).

- **Immobilization Devices:** the patient would be placed on the mammo-board, which is a fixation device where the patient lays supine and holds a pair of tubes above their head, allowing for comfort and better gantry angles. This device also reduces involuntary movements from the patient and geometrical uncertainty.

  In addition, a thermoplastic mask will be placed over the chest of the patient and the remaining gaps along the sides of the patient will be filled with vacuum cushions or Moldcare fixation devices.

- **External Monitoring Devices:** all the leads and cables from external monitoring devices (e.g. ECG leads or the EBAMed US probe) should be tied together and taped to the side of the patient, to avoid additional noise and artefacts in the images to be used for therapy planning.

- **Parameters:** slice thickness of at least 2 mm and performed following the in-house MedAustron 4DCT commissioned protocol. Where the CT is reconstructed at the following different phases of the respiration cycle: 0%, 25%, 75%, and 100%.

- **Breathing technique:** deep inspiration-breath-hold (DIBH) is suggested, but it can be used as a stand-alone technique or in combination with any of the following: reduced respiration motion via abdominal compression, and continuous positive airway pressure (CPAP). When available, jet ventilation (direct delivery of oxygen via a high-pressure jet ventilator) under anaesthesia could be arranged.

The technique of choice is discussed between the radio oncologist and the cardiologist and it is strictly related to the criticality of the patient's condition and bound to the availability of equipment and critical survival time impediments.

- **Surface Tracking and Respiratory Gating:** via Real-time surface scanning (optical) offered by the Catalyst, C-rad surface scanner. With this device, it is possible to obtain non-rigid deformable models for respiration displacement computed at 6 degrees of freedom with isocentric shifts.

The estimated time for this procedure is 150 min, considering machine set-up, surface scanning, positioning, and acquisition. The required personnel to execute this stage are 2 RTTs, 1 RO, and 1 MP.

3.9.4 Treatment Planning and Patient Modelling

RayStation Treatment Planning System will be utilised to create a tailored plan for the patient, compliant with the following criteria and constraints and based on the "MedAustron General Plan Generation Guidelines", last updated in 2020:

- **Treatment aim:** total clinical VT suppression via the induction of myocardial scar formation, fibrosis, depolarization and protein activation (connexin-43 and NaV 1.5 [172]).
- **Dose to the target:** single fraction between 30 and 32.5 Gy to the 98% of the TV and reported to the median dose (D50%) as indicated in ICRU 78.
- **Dose to ICD:** maximum dose to ICD main electronics 2 Gy, and 15 Gy max. dose for the leads inside the chambers [173].
- **Target contouring:** ITV approach and additional geometric margins to control the dose distribution with a ring.
- **Set-up margin:** 3–5 mm in 3 orthogonal directions.
- **Extra-cardiac organs at risk:** the most critical organs to be spared (based on photon experience [58]) are the lungs, oesophagus, stomach, trachea, bronchus, and the skin. These structures must not exceed between 14 and 16 Gy (RBE). Ideally 15 Gy and below 25 Gy when the structure is compromised.
- **Cardiac substructures to be spared:** valves, coronary arteries, and the AV node, at most 25 Gy (RBE) should reach these volumes.
- **EAM target migration to planning CT:** 2D-3D registration method will be used to localize the clinical VT and the previous ablation points. These 2D EAMimages will be used as a reference for contouring the lesion in the TPS.
- **Range uncertainty:** ±3.5% for CTV motion due to heartbeat and breath-hold variability. This parameter is added to compensate for intrinsic uncertainties like CT calibration, end of range RBE [174], artefacts, etc.
- **Reference segment of the respiration cycle:** end of the expiration phase.

- **Cardiac Probe Reference Modeling:** The localization of the US probe should be modeled in the TPS as a cube of 2×2×2 cm. An isotropic safety margin of 10 mm must be added to account for uncertainties in relocating the probe during the treatment, including variables related to respiration and breath-hold variances [93].

- **Reference cardiac phase:** R-R interval cycle [93] in case of ECG US gating with the EBAMed Cardiac Probe.

The required personnel for this stage are 1 radiation oncologist, 1 radiographer, 1 cardiologist, and 1 medical physicist. The estimated procedure time is between 90 and 120 minutes.

3.9.5 Dose Distribution and Plan Generation

At the last stage of treatment planning, the medical physicist will send the best achievable plant together with the final dose calculations to the radiation oncologist for approval.

- **Beam geometry:** at least 3 beams in arc-like angles, dependent on case-by-case and lesion localization (most common in the septum of the heart between the chambers).

- **Particle Type and Delivery Technique:** protons, pencil beam scanning and no additional range shifters (only added if the depth is very shallow, less than < 3.5 cm).

- **Optimization:** 4D Robust Minimax Tool (with the 4DCT) and Franciska Lebbink Interplay Effect Optimization Tool and interplay evaluation; both implemented into RayStation. D_{50}, D_{95}, D_{98} (near minimum dose), average dose, target dose conformity, and homogeneity.

- **Reporting dose statistics**: D_1, D_2 (near max dose),

The required personnel for this stage are 1 radiation oncologist and 1 medical physicist, and the estimated procedure time is between 60–90 min.

3.9.6 End-to-end Testing

This test will be performed once during the commissioning process before establishing VT irradiation at MedAustron. The required instrument to conduct this test is the 4D CIRS Dynamic Phantom following the in-house protocol, mimicking the whole workflow under the same conditions and setups used for treatment. For moving targets, an in-house designed holder that is placed inside the phantom (see figure 3.19) is filled with alanine pellets [11], inserted into the 4D phantom and scanned. Afterwards, these pellets are sent to a laboratory for measurement and a report is generated from which the treatment delivery accuracy is addressed. This test as a whole takes approximately 14 hours to be performed and involves 1 medical physicist and 1 radiographer.

[11] The number of the main free radicals produced during radiation is measured by an alanine dosimeter. This measurement is proportional to the absorbed dose. The advantages of alanine pellets for medicinal applications include their small size and water-equivalent composition [175]

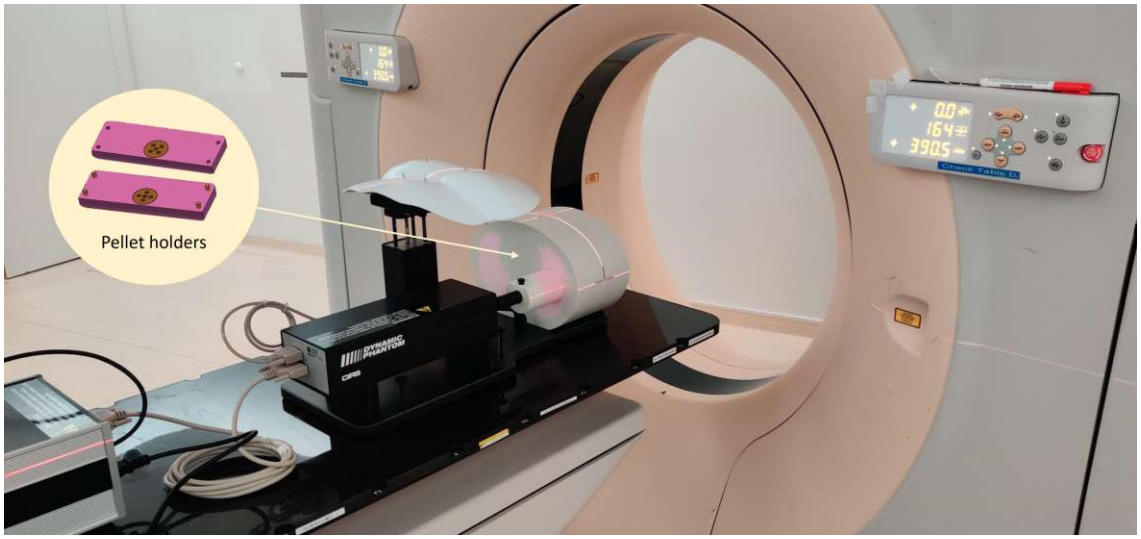

Figure 3.19: End-to-end testing setup with the 4D CIRS Dynamic Phantom, and the double layered pellet holders to be irradiated with the CT-sim Brilliance Big Bore form Phillips.

3.9.7 Plan Verification - Patient-Specific Quality Assurance (PSQA)

This parametric test identifies deviations between the planned and the delivered dose for every field for each patient. The proposed plan must have been previously discussed and approved during the "Treatment Planning Conference", which is a regular decision-making meeting amongst a team of experts at the department. Only then, it is exported to the clinical database (RayCare TCS, PACS), and a virtual water phantom [12] is used to simulate treatment delivery. After the simulation, the physical test is carried out with the real water tank (PTW MP3-P), 24 Pinpoint ICs [13], (as seen in figure 3.20), and other instruments like a thermometer and a barometer are used to measure in reproducible conditions. For this procedure tissue equivalence to water calculations must be made for this test [176]. The entire procedure takes on average 2 hours and requires 1 medical physicist and 1 radiation technology technician.

[12] A computer-generated simulator of the real water phantom that reproduces the physical characteristics of the PTW MP3-P water tank is imported from the RayPhysics suite in the QA preparation workspace of RayStation.

[13] 3D chamber arrangement that allows measuring a 3D dose distribution.

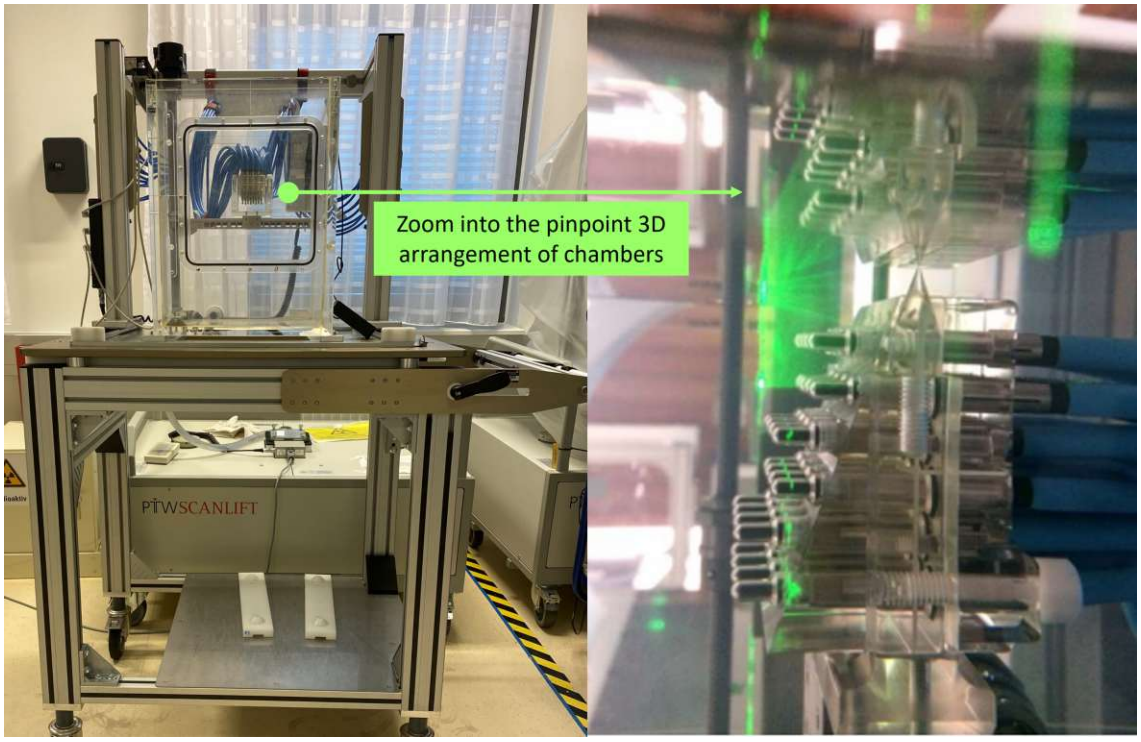

Figure 3.20: PTW MP3-P water tank on the PTW Scanlift device and the 3D pinpoint chamber layered array.

3.9.8 Treatment Delivery

The patient will be taken into the treatment room and positioned the same as in the planning CT, including immobilisation devices and the cardiac US probe with its antenna wearable belt, and workstation. Before irradiation, the patient position verification will be carried out via 3D matching cone beam computed tomography (CBCT). Small corrections can be made for mismatched positioning with the help of in-room lasers. The plan will then be loaded to MAPTA and controlled by the medical frontend and the console. When the cardiac probe is used, it should be set and placed on the chest of the patient as described in figure 3.9 panel B for transthoracic real-time cardiac motion monitoring.

The optimal gantry solid angles must account for the US probe, the holder, and the localization marker (see figure 3.9 panel A). If the target within the myocardium is out of the field of interest, the EBAMed system (more details in section 3.8) will send an alarm to the operator and stop the beam. Once all the settings are in place, and no interlock signals are triggered the treatment can be initiated. Once it is over, the immobilisation and monitoring devices will be removed from the patient and they will be sent back to the hospital. The required personnel is 1 radiation oncologist, 1 medical physicist, and 2 radiographers and the estimated time for this entire stage is about 45 minutes.

3.9.9 Post-treatment Evaluation

The treatment will be considered successful if the symptoms are eliminated and no new ones appear. Evaluation of long-term toxicities, for good measure imaging after 3 months is strongly advised.

3.9.10 Problems and Suggestions for Future Improvements

On average the "fast" treatment planning time in-house is between 4 and 5 days, which might not be quick enough to treat VT patients due to their life-threatening condition. Hence, after several discussions with the group of experts it was envisioned that ideally, the entire medical workflow has to be performed within three days. On day one, the patient is identified as a potential candidate for ion therapy after RFCA and sent to MedAustron with their pertinent EAM and CT files (in proper formats, as discussed in section 3.8) which would then be used for migrating the targets to the planning CT. This patient must also undergo a CT-sim image acquisition in-house to obtain a mass stopping power calibrated CT that will be used for planning. On day two, the treatment planning, and the PSQA should be performed as described in the current guidelines. it is yet to be discussed if all the in-house clinical guidelines shall remain the same, be modified or even eliminated from the workflow due to the time burden. Finally, on day three the treatment should be delivered to the patient. Keep in mind that during delivery any external leads or cables shall be kept on the side and avoid laying on the chest of the patient (especially in a chaotic manner) since this will induce noise and interrupt the proper functionality of the surface scanner. Furthermore, this practice would also lead to adequate dose distribution outcomes.

The effects of high-energy ion beam therapy for VT are still unexplored, so far the most comprehensive information on VT-RT is provided by a series of publications derived from the RAVENTA study, where 10 patients have been reported alive, with a significant reduction on their arrhythmia and complications after STAR photon treatment within a multi-centre multi-platform clinical trial. Precise characterization of the dose required to induce fibrosis is required for determining appropriate dose levels in future clinical treatment of VT patients. Regarding the "appropriate" dose for this treatment, there are papers on animal irradiation (pigs and explanted hearts) with carbon ions from Immo Lehmann et al. and Douglas Packer et al., where some dose–effect data are provided [74]. How much dose is needed to treat VT is still under debate.

Almost all patients have been treated with 25 Gy, although animal work showed that 32 Gy or more are needed. The research group at the Mayo Clinic in the USA has treated 8 VT patients with protons using 30 Gy. The results were presented as an abstract at the last HRS congress [177] and they will publish a paper on this matter soon. CNAO has published a paper from their 1 patient experience [81], also irradiated with protons at 25 Gy. To this date, no follow-up literature is available from this centre and also by far only one patient is insufficiently conclusive.

In addition, it is known amongst the scientific community working on this topic that the CHUV in Switzerland has treated one patient with less than 25 Gy with poor results, but the information from this case has not been made public yet. In addition, the best particle type is yet to be defined, and further investigation and biological studies on the gains, advantages and disadvantages are lacking. What can be said at the moment is that protons seem to be the most feasible option, primarily because this beamline has a gantry available at MedAustron to offer vast geometrical arrangements and variations that could adjust to patient requirements and conditions.

CHAPTER 4

Treatment Planning Case Studies

The leads of the multi-centre benchmark study (RAVENTA [178]) in Germany, provided 3 sets of retrospective patient [1] data. These are comprised of the following elements: planning CT, the respective 4DCT, the targets (TV, PTV, CITV) and the OARs contoured by the participating cardiologists (medical doctors) and radiation oncologists. For each case, treatment plans were developed, the contours were used to generate a TP for proton therapy utilising the suggested clinical goals, constraints and doses published in the RAVENTA treatment planning and contour trial and other publications by O. Blanck et al. [58], A. Kluge et al. [49] and Perrin et al. [93]. Please note that no patients were treated under the scope of this thesis.

The OARs for this type of treatment are the trachea, the bronchus, the oesophagus and the stomach, which must be kept below 12–14 Gy (D_0.03cc.). Additionally, the dose received by the skin must be below 10 Gy dose at 0.01 cm^3 volume. For the sensitive cardiac substructures, the coronary arteries must receive below 20 Gy (D_0.03cc.). The ICD main electronics must not surpass 2 Gy dose at 0.1% volume, and for its leads, a dose below 15 Gy (D_0.03cc.) is considered acceptable, although based on photon TP experience, it is not always achievable [173] due to overlapping with the target. The dose perception was 32 Gy or 25 Gy median dose (D50%), and minimum dose 31.36 Gy to 95% of TV and 24.5 Gy to 95% of the PTV. For this type of treatment, the cardiac substructures listed below should be spared to avoid stenosis induced by radiation (in addition their function is explained to provide context). Critical damage might occur at doses above 25 Gy (single fraction) in cardiac substructures (arteries), which could lead to life-threatening radiation toxicities [179]. The nomenclature used and the functionality of the cardiac substructures (arteries) in question will be stated below.

- **Aorta Ascendens (A_Aorta):** this is a section of the aorta that starts at the top of the left ventricle's base and ends behind the left half of the sternum, level with the lower edge of the third coastal cartilage. Its main function is to supply the entire body with oxygenated blood.
- **Left anterior descending artery (A_LAD):** this is a branch of the left coronary artery and its main function is to supply the left ventricle.

[1] No patients were treated under the scope of this thesis.

- **Circumflex Artery (A_LCX):** this is the branch of the left coronary artery, it supplies blood to the left atrium.
- **Left Main Coronary Artery (A_LM):** this branch supplies blood to the left ventricle and the left atrium.
- **Pulmonary Artery (A_Pulmonary):** this structure carries hypoxic blood from the right side of the heart into the lungs.
- **Right Coronary Artery (A_RCA):** this pathway supplies the interventricular septum, the right ventricle and the atria of the heart.

			Case 1		Case 2		Case 3	
Priority	**ROIs**	**Clinical Goal**	**Dose [Gy]**	**Pass**	**Dose [Gy]**	**Pass**	**Dose [Gy]**	**Pass**
1	A_Aorta	At most 25 Gy (RBE) dose at 0.03 $cm3$ volume	0.06	Y	0.01	Y	24.35	Y
1	A_LAD	At most 25 Gy (RBE) dose at 0.03 $cm3$ volume	23.99	Y	22.06	Y	24.77	Y
1	A_LCX	At most 25 Gy (RBE) dose at 0.03 $cm3$ volume	0.01	Y	0.00	Y	24.88	Y
1	A_LM	At most 25 Gy (RBE) dose at 0.03 $cm3$ volume	0.00	Y	0.00	Y	15.47	Y
1	A_Pulmonary	At most 25 Gy (RBE) dose at 0.03 $cm3$ volume	4.75	Y	0.00	Y	25.14	N
1	A_RCA	At most 25 Gy (RBE) dose at 0.03 $cm3$ volume	0.01	Y	0.00	Y	0.16	Y
1	Oesophagus	At most 14 Gy (RBE) dose at 0.03 $cm3$ volume	0.00	Y	0.00	Y	0.04	Y
1	ICD	At most 2 Gy (RBE) dose at 0.10% volume	0.00	Y	0.00	Y	0.00	Y
1	Stomach	At most 14 Gy (RBE) dose at 0.05 $cm3$ volume	13.73	Y	0.01	Y	0.03	Y
1	Skin	At most 10 Gy (RBE) dose at 0.01 $cm3$ volume	8.25	Y	7.72	Y	10.01	N
1	Trachea	At most 14 Gy (RBE) dose at 2% volume	0.00	Y	0.00	Y	0.01	Y
1	Bronchus	At most 14 Gy (RBE) dose at 2% volume	0.00	Y	0.00	Y	2.16	Y
2	PTV	At least 24.50 Gy (RBE) dose at 95% volume	24.46	N	23.33	N	23.47	N
2	TV	At least 31.36 Gy (RBE) dose at 95% volume	31.58	Y	31.56	Y	30.88	N
2	PTV	At least 95% volume at 24 Gy (RBE) dose	94.58%	N	89.29%	N	87.98	N
2	TV	At least 95% volume at 31.36 Gy (RBE) dose	98.82%	Y	97.50%	Y	92.82	N
2	TV	At most 1% volume at 33.60 Gy (RBE) dose	0.00%	Y	0.00%	Y	0.00%	Y

Table 4.1: Comparison of the clinical goals after optimizer calculations via the TPS (RayStation) for the 3 cases derived from the multicenter RAVENTA benchmark study in Germany. When the clinical goals are met, the passing criteria are defined as Y (Yes) and N (No) for the opposite case.

In table 4.1 above it can be observed that all the clinical goals marked as priority 1 [2] were met with one exception for Case 3. Where an overdose of 0.14 Gy for the pulmonary artery is present due to an overlap of the respective OARs with the anatomical location of the target. Although there is a small dose surplus, it is still considered clinically acceptable. The clinical goals were stated and physical cost functions were added and adjusted when compromised accordingly to achieve the goals as effectively as possible.

The position of the patient in the external datasets received (CT scans) was head first supine. In addition, it should be noted that patient positioning would be slightly adapted at MedAustron depending on the gantry angles available at the time of implementation. The radiation type selected was protons and the treatment delivery technique PBS with an RBE model with constant 1.1. In the upcoming sections below, each case will be analysed in terms of its respective dose distribution, limitations, and outcome. As a final note, the cases will be compared and future treatment planning recommendations will be outlined.

[2] If these goals are not met, fatal consequences are expected (e.g., artery perforation, fistula in the stomach, etc.). This prioritization comes from the RAVENTA TP benchmark study.

4.1 Case 1

This plan delivers 3 beams with the configurations and beam-on time simulation estimations stated in table 4.2.

Configuration	Weight[%]	Delivery Time [min:sec]
b1g35c270	36.23	5:26
b2g35c0	32.06	4:54
b3g80c5	31.71	4:46

Table 4.2: Case 1 beam parameters and delivery estimations after simulation. Where b refers to the beam number, g refers to the gantry angle and c refers to the couch angles with respect to the isocenter.

Regarding the entire plan, the beam-on estimation results in a total of 15 minutes and 6 seconds. The beam-occupation considering beam-line allocation and activation time to deliver this plan is estimated to be 19 minutes and 11 seconds. The minimum in-room time estimation is 40 minutes and 10 seconds. In reality, this estimation would be highly dependent on patient condition, positioning, immobilization device placing and whether or not motion management techniques would be utilised.

For this case, all the clinical goals marked as priority 1 were achieved, whereas for the ones marked as priority 2, there is a slight difference. For the PTV (pink curve, there is a small "shoulder" that corresponds to the dose fall-off between the 32 Gy and 25 Gy dose levels) and the TV (lila curve, close to a step function) there is a small region under dosed and slightly less target coverage because there are implants in the target (ICD leads). There are also ECG leads placed externally over the chest of the patient. However, the final dose distribution and coverage are acceptable for treatment, this can be observed via the DVH curve [3] (see figure 4.1) and images on different planes of the dose distribution below (see figure 4.2 for the transversal dose distribution, figure 4.3 for the coronal dose distribution, and figure 4.4 for the sagittal dose distribution). Also, in figure 4.1 we can observe that the target dose was reached for the TV and PTV. The rest of the OARs present a steep dose fall-off which indicates excellent organ sparing.

Based on the results of this case, it is highly recommended in the future to avoid chaotically placing cables over the chest of the patient. All the external devices, markers, and cables (see figure 4.5) must be placed on the sides and secured with surgical tape avoiding the heart region as much as possible. Because when such structures cross paths with the beam arrangements, it introduces extra uncertainties in the HUs to density conversion (which will be then used for conversion into stopping power), and additionally can lead to electrical interference in the ECG signal or any other monitoring systems.

ICD leads inside the patient can produce large artefacts (see figure 4.2, white stripe pattern). These regions are not suitable for dose calculation due to the large imprecisions originating from the artefacts. Therefore, it is generally avoided to cross artefact regions with the proton beam. For optimization purposes, geometrical subtraction via ROI algebra was performed to improve the dose uncertainties and avoid direct irradiation through the ICD lead region.

[3] Graphical representation of the radiation dose delivered to any defined volume. These curves are commonly used as tools to aid the evaluation of treatment plans. [180].

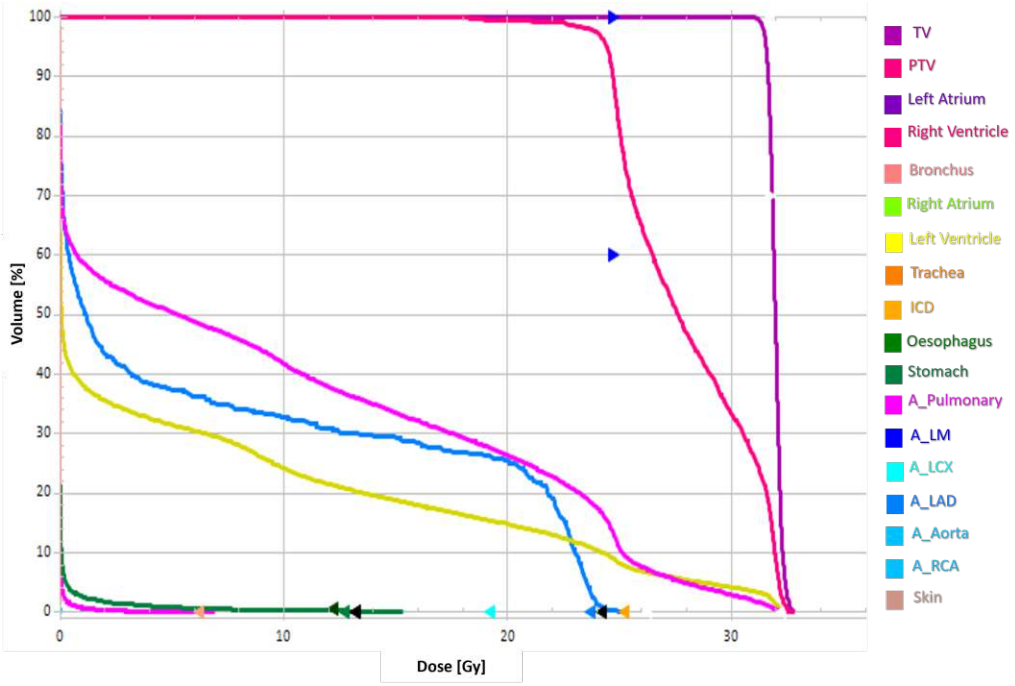

Figure 4.1: Case 1 dose-volume histogram with the respective OARs, TV and PTV.

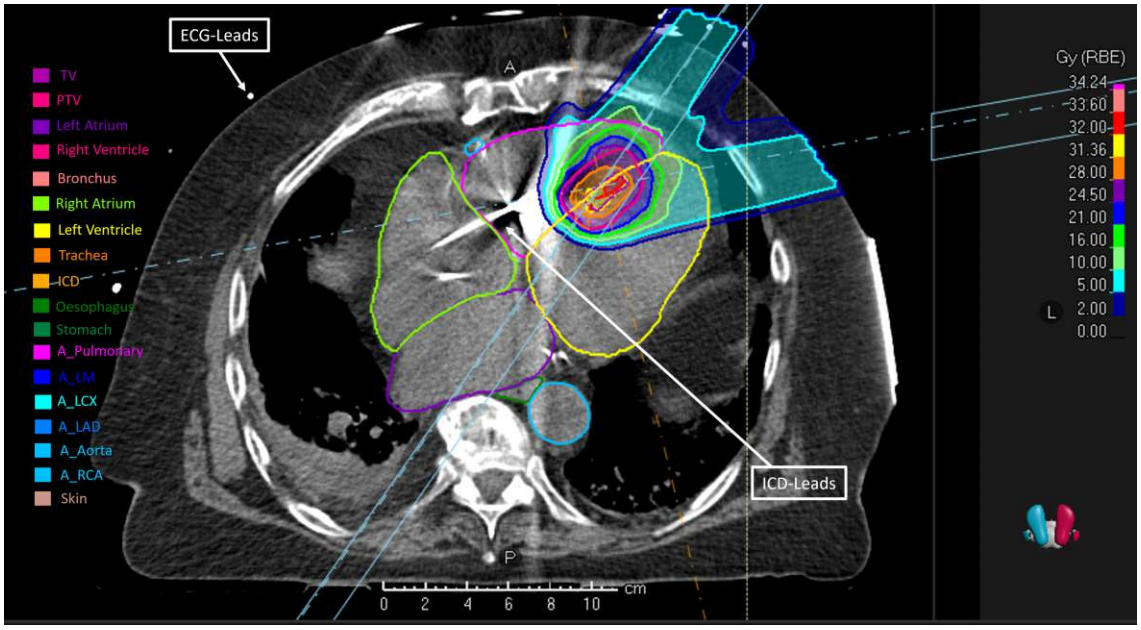

Figure 4.2: Case 1 TP transversal dose distribution.

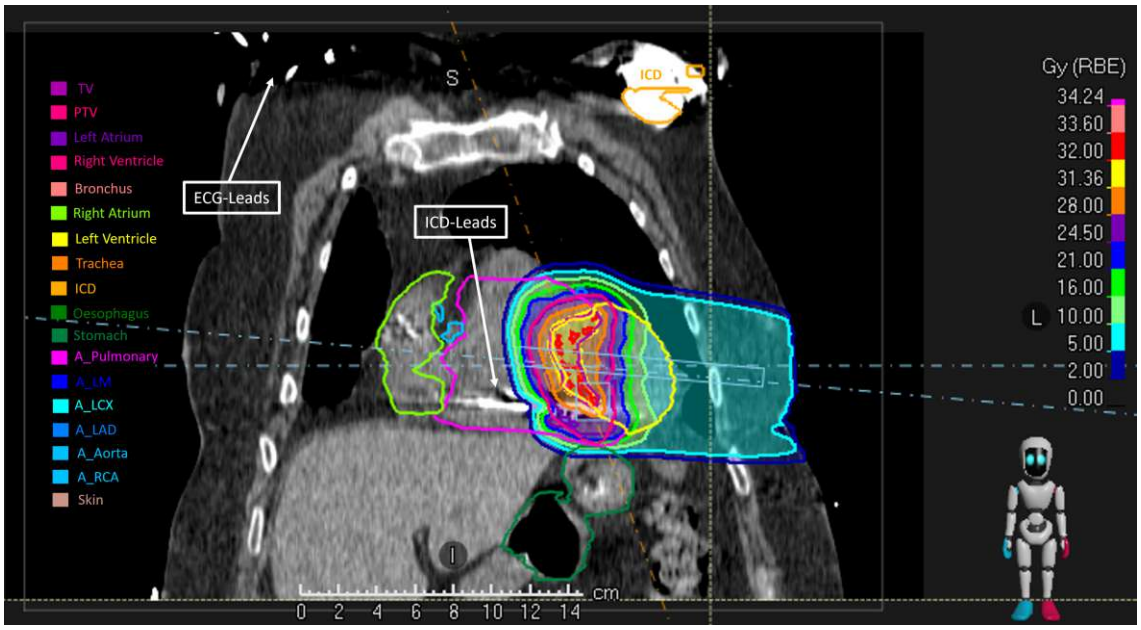

Figure 4.3: Case 1 TP coronal dose distribution.

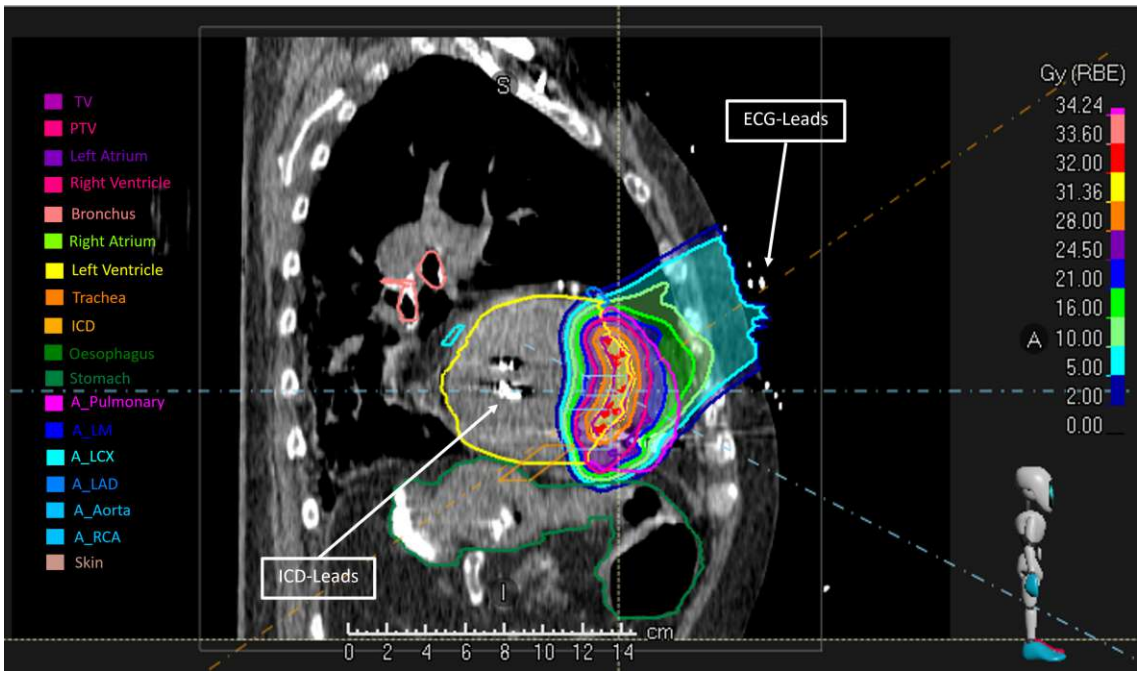

Figure 4.4: Case 1 TP sagittal dose distribution.

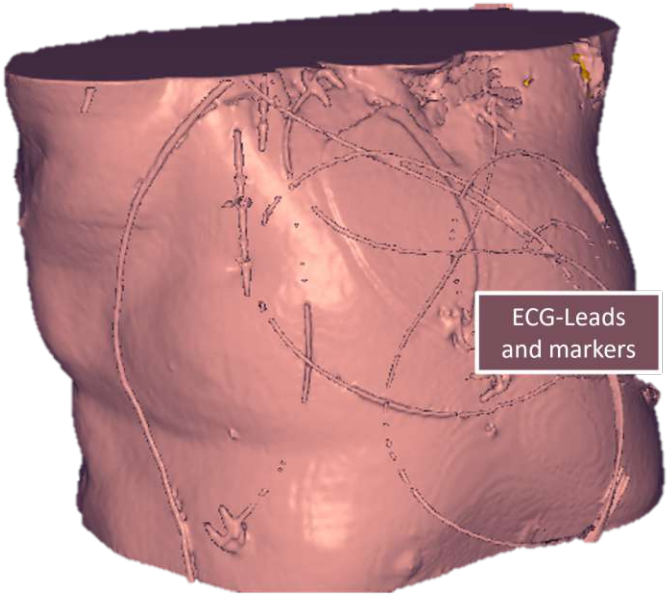

Figure 4.5: Volume rendering displaying all the external ECG lead cables all over the chest of the patient.

4.2 Case 2

This plan delivers 3 beams with the configurations and beam-on time simulation estimations stated in table 4.3.

Configuration	Weight[%]	Delivery Time [min:sec]
b1g35c270	39.77	5:18
b2g40c0	32.20	4:18
b3g70c10	28.03	4:06

Table 4.3: Case 2 beam parameters and delivery estimations after simulation. Where b refers to the beam number, g refers to the gantry angle and c refers to the couch angles with respect to the isocenter.

Regarding the entire plan, the beam-on estimation results in a total of 13 minutes and 42 seconds. The beam-occupation considering beam-line allocation and activation time to deliver this plan is estimated to be 17 minutes and 46 seconds. The minimum in-room time estimation is 38 minutes and 29 seconds. This patient had a LVAD, which means that this patient had a severe cardiac condition that most likely requires extra in-room time due to complications in positioning since they might present shortness of breath and very limited mobility. In addition, the device has an external “drive line” (cable) coming from the upper abdomen connected to a controller device, a series of cables and a power supply that must be kept out of the beam path to avoid damage and eventual failure induced by radiation (see figure 4.6).

For Case 2, all the clinical goals marked as priority 1 were achieved, whereas for the ones marked as priority 2, there is a slight difference because a compromise had to be made between sparing the critical OAR constraints and target coverage.

In addition, this was a very complicated case, due to the implanted left ventricular assist device LVAD, which is a life-saving mechanical bypass between the aorta and the left ventricle [172]. This device aims to provide a higher QOL while patients await a heart transplant or remain with the device after a fatal diagnosis. Being a metal and electrical device, similar to the ICD leads of Case 1, it was generally avoided to cross the device and artefact region with the proton beam, leading to a partial underdose of the PTV. It is of high importance to choose the optimal beam angles in order to avoid overlapping of the beam with any implant.

Despite the presence of this device, the TV (lila curve, step function) was fully covered, whereas the PTV (red curve, small "shoulder") was slightly undercovered in the overlap region (see figure 4.7). The rest of the OARs present a steep dose fall-off which indicates excellent organ sparing.

Several components from the LVAD overlap with the target. However, the final dose distribution sown for this case, was the best possible compromise between priority 1 organ sparing and the maximum achievable coverage. This can be observed via the images on different planes of the dose distribution (see figure 4.8 for the transversal dose distribution, figure 4.9 for the coronal dose distribution, and figure 4.10 for the sagittal dose distribution).

Due to the high mortality outcome of the patients that are subject to LVAD, there is a scarce amount of case study reports collected and limited clinical experience. However, some literature is available for VT stereotactic photon RT. In Europe, it is available via the STOPSTORM consortium and the RAVENTA record collection, because they do not rule out these patients from the trials. In a recent publication (February 2023) by F. Mehrhof et al., it was stated possible to haemodynamically stabilize two of these patients almost immediately after therapy, in one case even for several months before fatal bleeding, whereas the other patient eventually perished due to sudden heart failure. in addition, no toxicities were reported [172].

However, target identification and migration remain a big challenge for patients with a LVAD, because of the significantly reduced contact between the probe and the endocardium during the invasive EAM procedures. To this date, there are no available cases of this type of patients undergoing ion-beam treatment and the radiobiological effects of VT-RT and not yet understood, especially long term.

Based on the results of this case, it is highly recommended for the future to develop a specific treatment planning clinical guideline for VT treatments with ions, in close collaboration with the cardiologists and the radiation oncologists involved. Encompassing patient positioning options depending on patient tolerance and treatment planning strategies that account for assistive devices and implant checks. Given that all of these factors have a severe impact on the treatment dose calculation and outcome. This will make the immobilization assessment, treatment planning and implant monitoring (ICD, LVAD) agile, helping the staff to be prepared and respond fast even under critical circumstances.

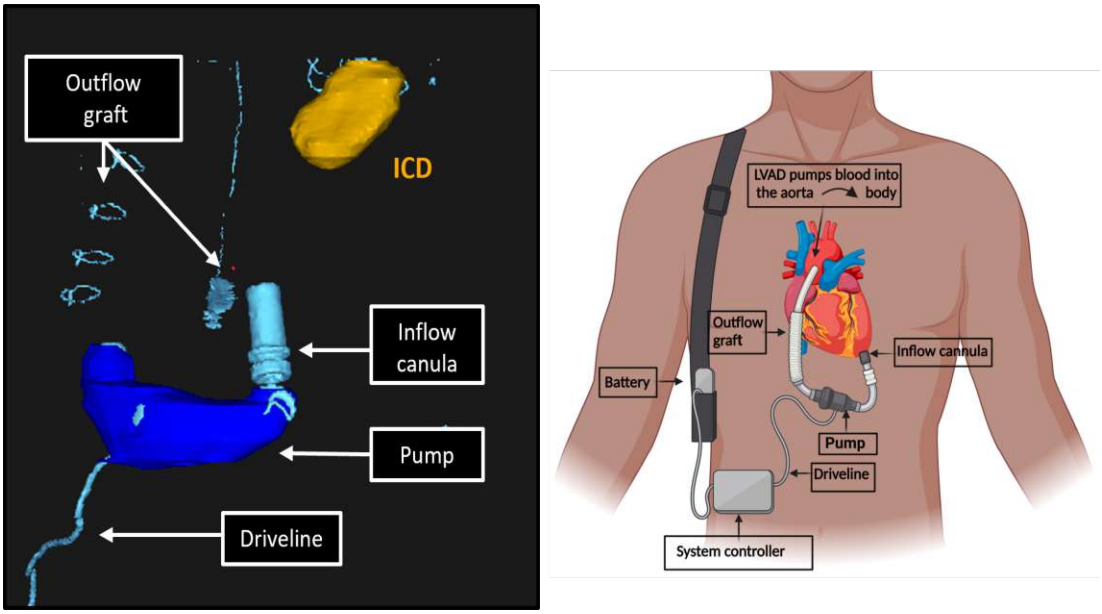

Figure 4.6: Volume rendering displaying the LVAD inside the chest of the patient, on the right a schematic of such device is shown side-by-side as reference (Image from H. Alnsasra, 2023 [181]).

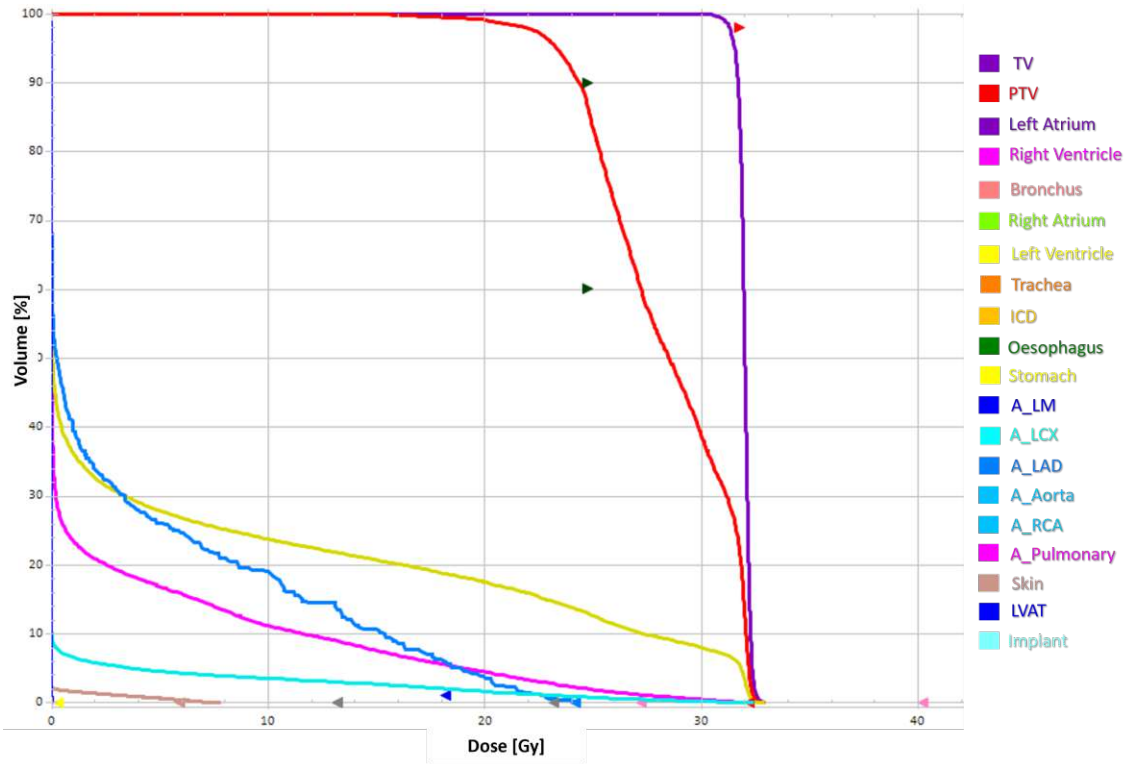

Figure 4.7: Case 2 dose-volume histogram with the respective OARs, TV and PTV.

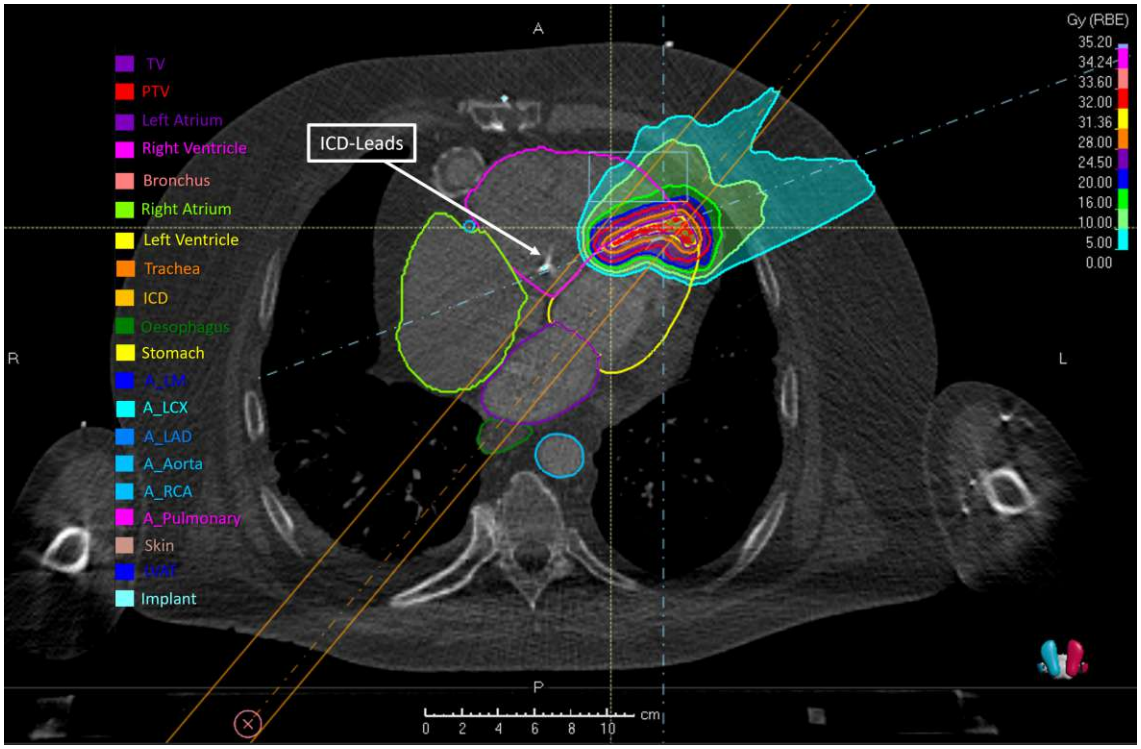

Figure 4.8: Case 2 TP transversal dose distribution.

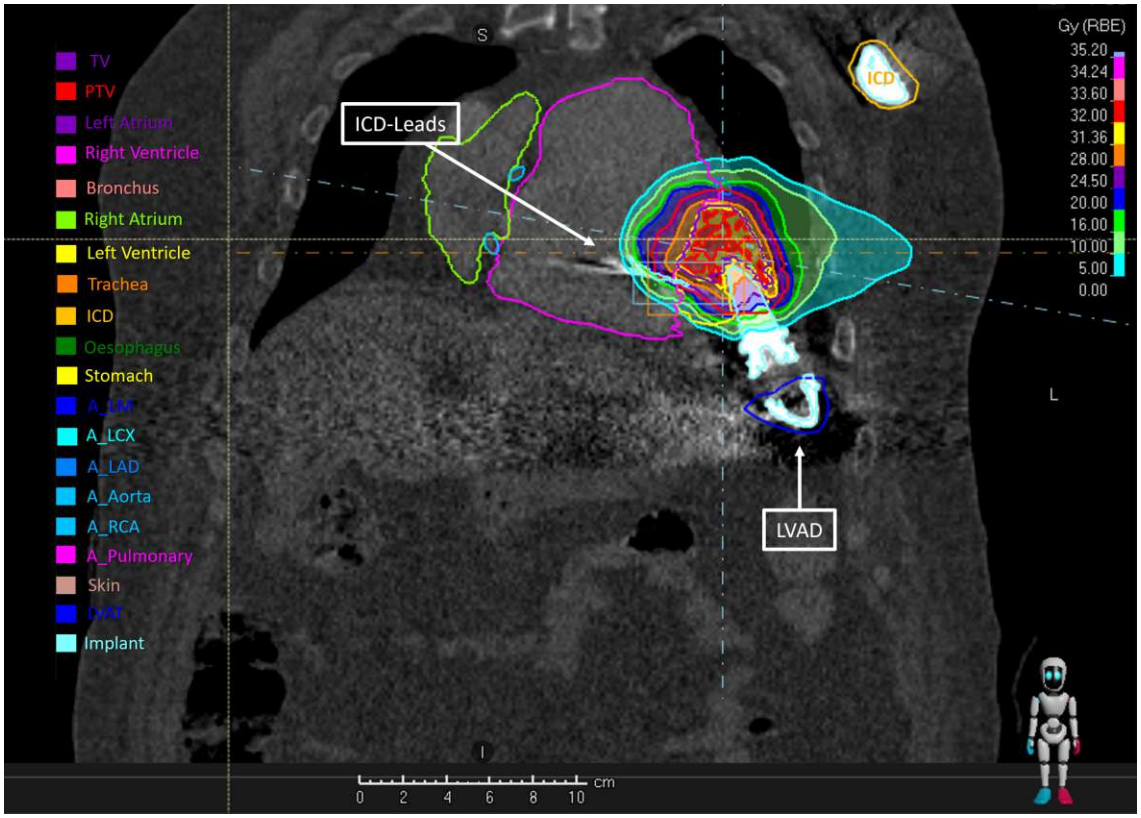

Figure 4.9: Case 2 TP coronal dose distribution.

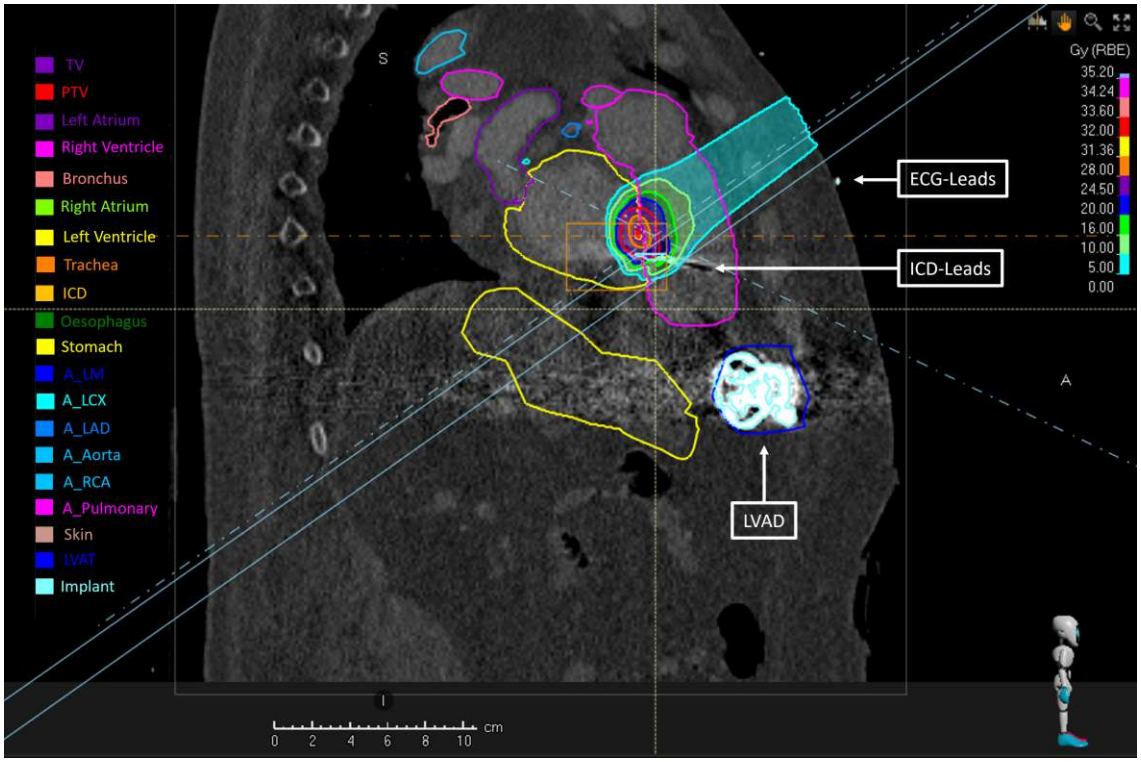

Figure 4.10: Case 2 TP sagittal dose distribution.

4.3 Case 3

This plan delivers 3 beams with the configurations and beam-on time simulation estimations stated in table 4.4.

Configuration	Weight[%]	Delivery Time [min:sec]
b1g40c230	34.27	6:19
b2g25c0	31.96	5:41
b3g70c10	33.76	5:39

Table 4.4: Case 3 beam parameters and delivery estimations after simulation. Where b refers to the beam number, g refers to the gantry angle and c refers to the couch angles with respect to the isocenter.

Regarding the entire plan, the beam-on estimation results in a total of 17 minutes and 39 seconds. The beam-occupation considering beam-line allocation and activation time to deliver this plan is estimated to be 21 minutes and 42 seconds. The minimum in-room time estimation is 43 minutes and 13 seconds.

In this case, the lesion is also situated on the left ventricle at the septum. There was an overlap with the PTV and the pulmonary artery, leading to a slight overdose. For the rest of the arteries, their dose is very close to their constraints. No hot spots had to be amended for this plan and with the right beam angle it was possible to deliver the prescription dose (see figure 4.12 for the transversal dose distribution, figure 4.13 for the coronal dose distribution, and figure 4.14 for the sagittal dose distribution).

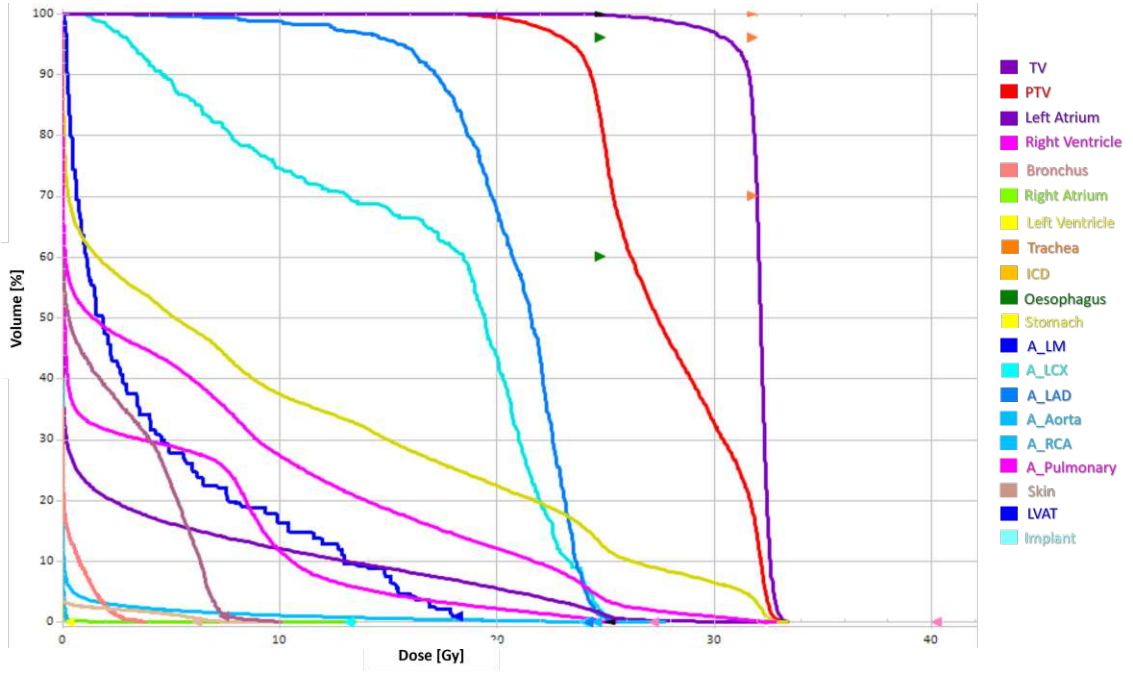

Figure 4.11: Case 3 dose-volume histogram with the respective OARs, TV and PTV.

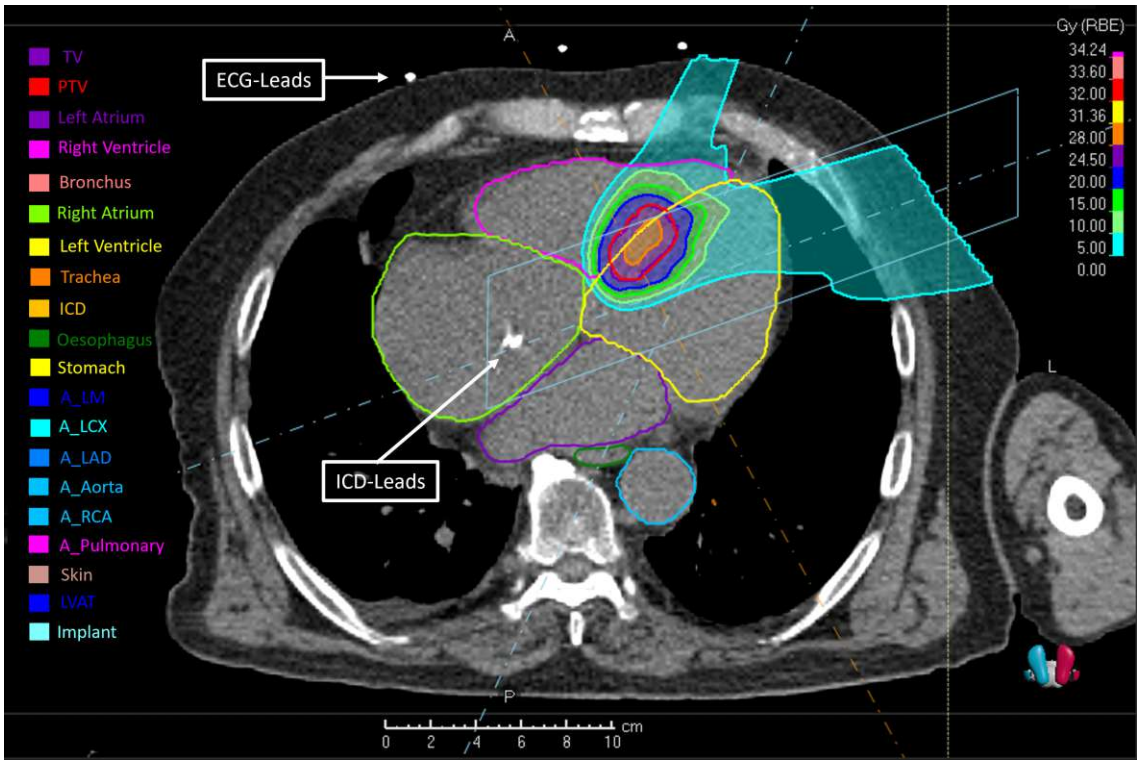

Figure 4.12: Case 3 TP transversal dose distribution.

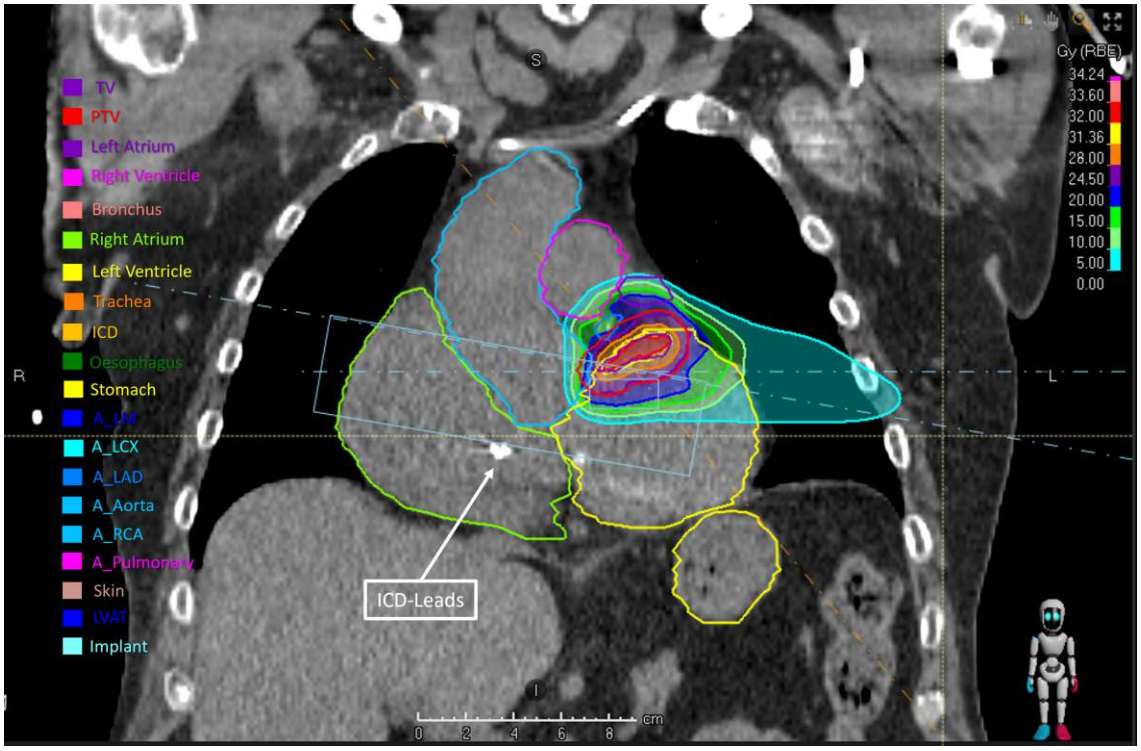

Figure 4.13: Case 3 TP coronal dose distribution.

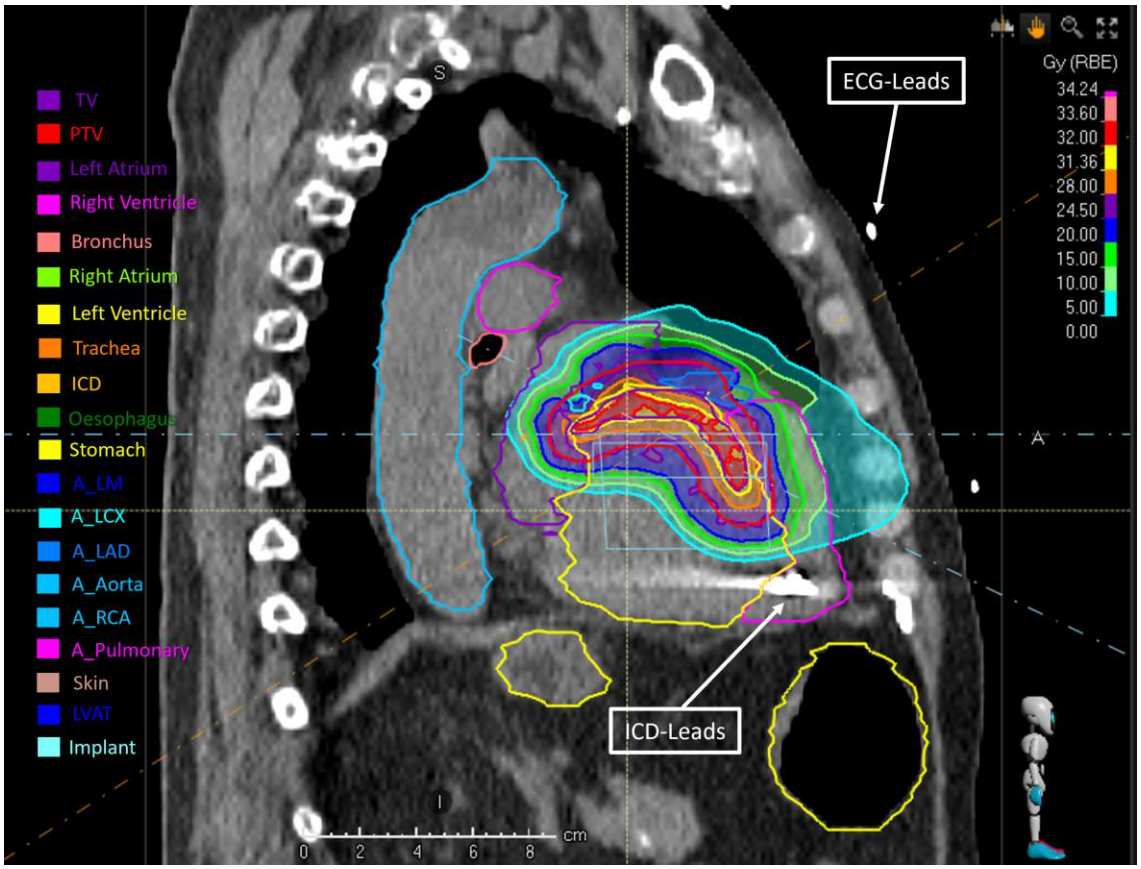

Figure 4.14: Case 3 TP sagittal dose distribution.

4.3.1 Case Study Treatment Plan Comparison

In figure 4.15 it is possible to observe the cardiac substructures (OARs) and the dose level comparison across the 3 Cases. For Case 3 (light green), we depict higher doses close to 25 Gy compared to Cases 1 (purple) and 2 (turquoise), because the aorta ascendens (A_Aorta), left anterior descending artery (A_LAD) was always close to the targets across the cases, circumflex artery (A_LCX), left main coronary artery (A_LM) and pulmonary artery (A_Pulmonary) were very close or overlapped with the target.

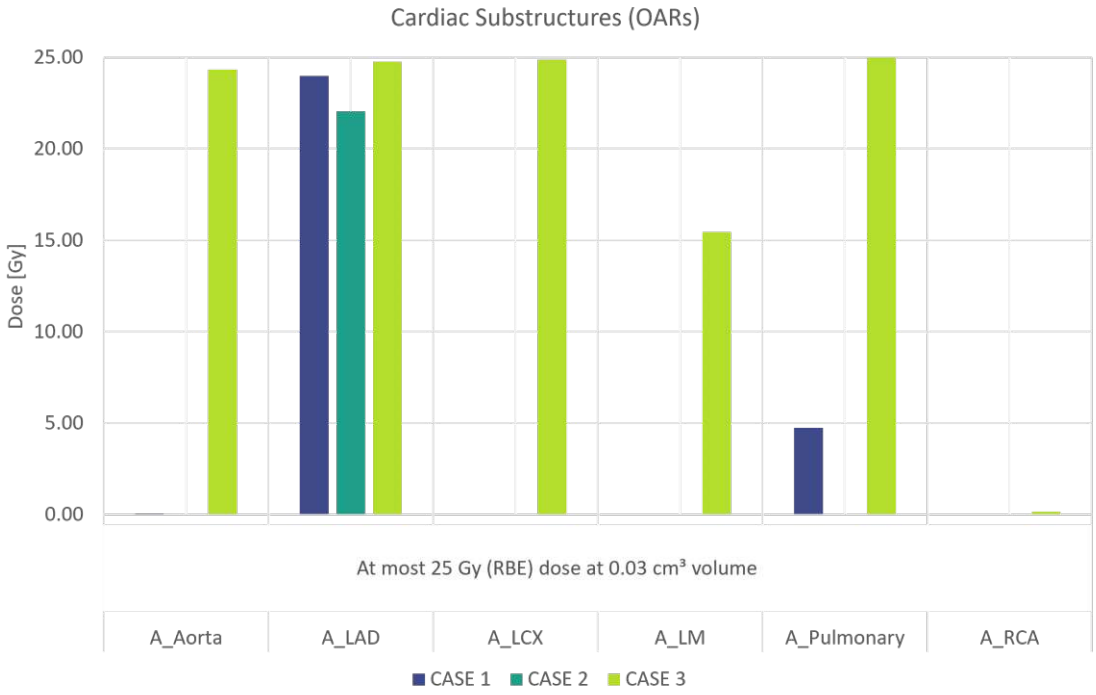

Figure 4.15: Cardiac Substructures (OARs) to be spared dose comparison in terms of the defined clinical goal for Case Studies 1–3.

Due to proximity, to the heart, other structures were assigned as OARs based on the RAVENTA study. Such structures were: The bronchus and the stomach followed by their distal elongations which are the trachea, and the oesophagus respectively. The skin was added to measure the amount of dose that could potentially reach the surface and possibly result in erythema with such single-fraction treatments. In figure 4.16 we can observe the dose levels stated in the clinical goals across the 3 different cases. For Case 3, 2.16 Gy was reported in the bronchus, but it is certainly far beneath the limit.

For Case 1, although a dose of 13.73 Gy was reported at the stomach, it is still under the tolerated threshold. Along the 3 cases dose reaching the trachea was negligible and different dose levels were reported for the skin.

Variability is highly dependent on how deep the target is located and if the beam angles are widely spaced. Hence, the deeper the target and the closer the beam angles, the higher the dose (for more details, see the plan reports in the Appendix).

The target coverage regarding the TV and the PTV was good enough to be clinically acceptable. In some cases, the coverage was not complete, due to intrinsic artefacts in the planning CT originating from the ICD leads and the LVAD in particular for Case 2 (see figure 4.17).

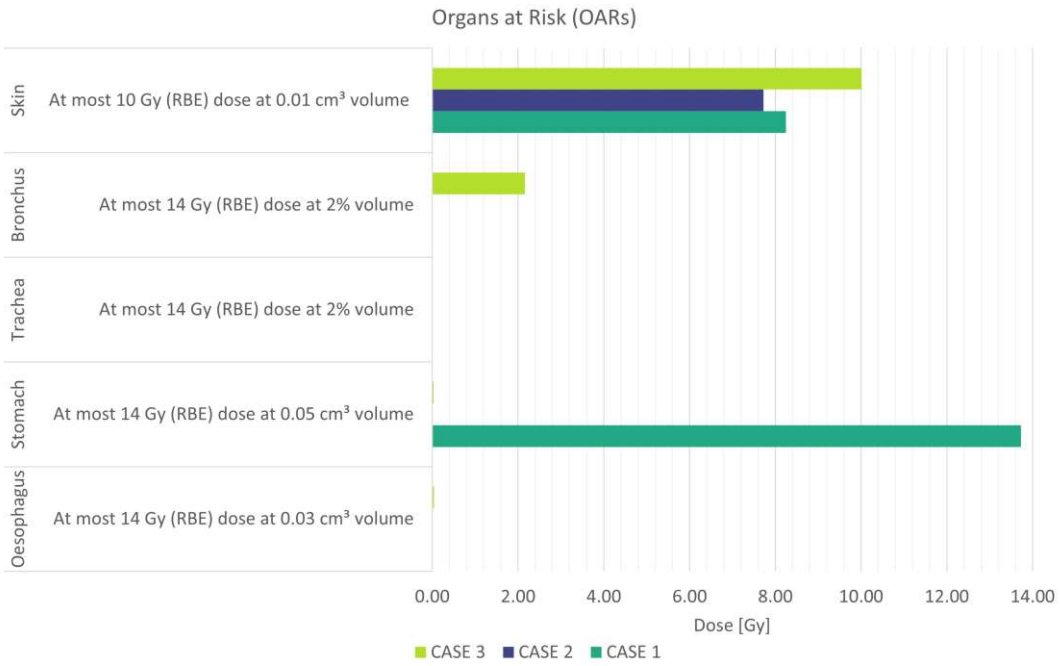

Figure 4.16: Organs at risk (OARs) close to the anatomical location of the heart inside the chest cavity of the patients. Other structures like the lungs or the spinal canal were not included in this table because the dose reaching those organs was negligible.

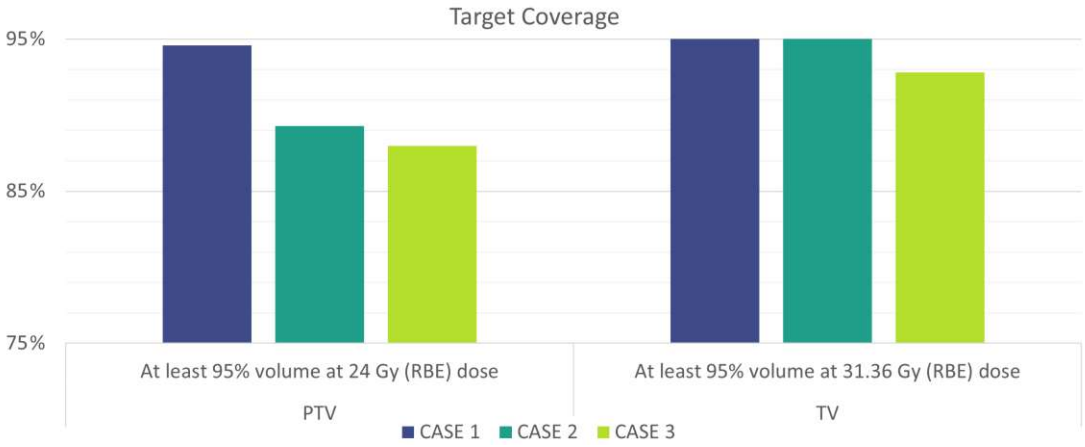

Figure 4.17: Target coverage for the PTV and TV based on the RAVENTA TP recommendations for photon stereotactic therapy.

Naturally, this also had a toll for the dose reaching the targets (see figure 4.18) and its distribution. Nevertheless, after a few adjustments, it was possible to improve the target dose outcome. In figures 4.17 and 4.18 in addition to table 4.1 and the 2D dose distributions it is possible to understand the following:

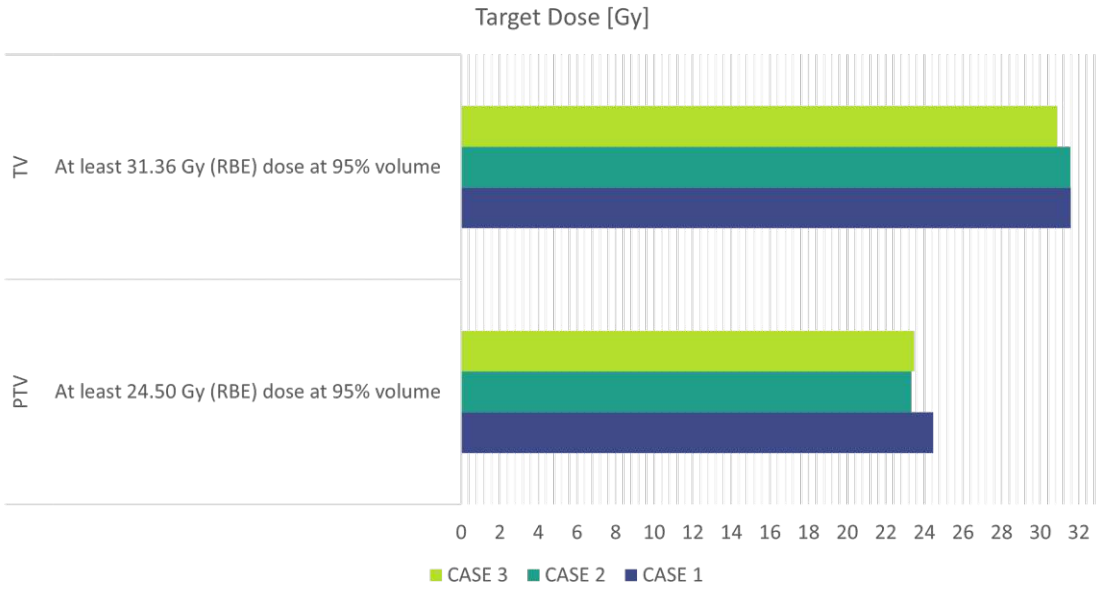

Figure 4.18: Target Dose for the PTV and TV based on the RAVENTA TP recommendations for photon stereotactic therapy.

- In Cases 1 and 2, there was an overlap between the TV and the ICD leads or LVAD inside the patient. Resulting in less dose and target coverage.
- In Case 3, there was an overlap between the arteries and the TV leading to an increase in organ doses and a decrease in target coverage.

4.3.2 Case Study Recommendations and Conclusions

For these three cases, proper target coverage was achieved regardless of severe artefacts in the planning CT originating from the ICD leads and the LVAD. Due to the ion Bragg Peak properties, the dose to the lungs was always kept to a very small and restricted volume. The beams never reached the spinal canal of any of the patients, this can be observed in any of the 2D dose distribution displays. The outlined OARs mostly remained under the proposed limits, with some exceptions where a compromise had to be made to accomplish all the clinical goals in the best possible manner. To be very efficient, a TP template shall be made based on the outlined treatment dose, clinical goals, most typical lesion location (myocardium of the left ventricle. Rarely also in the right ventricle).

Across the 3 cases, a small variation was observed in such parameters and the ICD was never crossed by any beam and the dose deposited to it was always zero. In addition, a detailed clinical guideline shall be streamlined to make the patient set-ups, assistive device localization and positioning agile and understandable to everyone at the clinic, even under critical circumstances. This protocol should also include all the imaging and additional system specifications and decision-making diagrams. Which would serve as a tool to assist problem resolution in case of ICD failure, presence of anaesthesia, beam triggers, and motion management techniques.

The most difficult issue when aiming to target small, and dynamic cardiac substructures with high-energy ion beams (like the septum) is particle range uncertainty. Irregular motion and artefacts present in the image used for planning could affect range prediction in addition to general uncertainty in the conversion of CT numbers to particle stopping powers. Compared to photons, the influence on the dose distribution will be far larger for particles. Furthermore, it is considerably more difficult to identify range changes during irradiation than it is to detect geometric motion during treatment [94]. The treatment dose and the biological effects of VT-RT are still under debate since they are not entirely understood by the community of scientists working in this particular area. In animal models, radiation doses have been demonstrated to induce fibrosis and scarring in previously injured cardiac regions [182]. However, throughout recent studies, a radiation-induced protein activation involving connexin-43 and NaV1.5 chain has been observed. This leads to very quick, although not instantaneous, modifications in aberrant cardiac rhythms [52].

Treatment planning for VT indications was proven possible with the available tools and resources at MedAustron. Nevertheless, many details and further testing are required before it becomes available for experimentation and clinical use. The proper dose and the potential benefits of gating and triggering for this treatment are still under debate, thus future efforts towards implementation should focus on the following aspects:

- Characterising the dose required for lesion creation/protein activation is and determining appropriate dose levels in future clinical treatment of VT patients.
- Addressing image compatibility and DICOM worklist compliance between triggering/gating tools MAPTA and the TPS.
- Developing a standardised protocol for EAM target transfer to the planning CT based on the currently available options either with open source tools or outsourcing the service.
- For clinical use, rescanning (currently preformed at MedAustron) would need to be made to reduce the uncertainties from the interplay effect. However, if gating is added, this would no longer be required.
- Exploring functional imaging techniques such as MUGA scans as a possible option for target identification and contouring.
- Testing EBAMed US cardiac probe with the GID and evaluating the potential benefits in precision.
- Investigating the effects of radiation-induced connexin-43 and NaV1.5 protein activation chains or the radiation induced fibrosis and their effects (long term and short term) on cardiac conductivity [4].
- Comparing different particle types for treatment (protons vs. carbons. vs helium).
- Simulating the entire workflow and eventually irradiating an anthropomorphic phantom able to mimic cardiac and respiration dynamics.

[4] At the moment radiation induced fibrosis is only well characterised for photons, but there is no sufficient data for protons.

CHAPTER 5

Conclusion and Future Work

In the scope of this thesis, a novel workflow for VT-RT at MedAustron was developed. Considering the aspects from accelerator beam extraction (moment that the chopper opens) to in-room delivery, a list of potential technical solutions and improvements was also outlined. Recommendations encompass TP, beam gating, signal triggering, and cross-platform image processing and compatibility required to perform VT ablation treatments with high-energy ion beams at MedAustron. The results from the technical assessment unveiled the missing tools and gaps to be filled prior to implementation. As a result, this work proposes a path towards finding solutions taking into account the clinical relevance within the local framework, available synergies and resources, so that this treatment modality could eventually become available for research, and testing.

Future directions would be to implement a standardised methodology to extract and use the EAM data for TP, streamline the entire workflow, explore the effects of different particles, and determine the best dose threshold to achieve myocardial scar formation, fibrosis, depolarization or protein activation (connexin-43 and NaV 1.5). It would be of particular interest to quantify the burden of the interplay effect and how it affects the treatment by comparing the results in the presence and absence of beam gating, signal triggering, and tracking devices that account for cardiac pace and respiration dynamics under a clinical setting by irradiating a 4D anthropomorphic phantom. There are no published studies on medical workflow, gating or VT TP comparison for ion therapy so far. Only one patient has been treated at CNAO in Italy with protons and a few at the Mayo Clinic in the USA and at Heidelberg in Germany, but their results are not available to the public and the target dose or the optimal considerations remain unclear. Making it an excellent opportunity for future collaboration with the STOPSTORM consortium and standardization of the technique with similar centres worldwide. With the right directions, it would be possible to perform cell-line and animal irradiation, so that in the future we could potentially achieve clinical trials and eventually a life-saving treatment.

CHAPTER 6

Appendix

```
% Script for plotting the LV point cloud and RF ablation points

% Read the LV point cloud from the file Model_Groups.xml
XMLdata = readstruct('Model_Groups.xml');
LV = str2num(XMLdata.DIFBody.Volumes.Volume.Vertices.Text);

% Read the ablation points from the file AutoMarkSummaryList.csv
ablation_points = readmatrix('AutoMarkSummaryList.csv');
ablation_points = ablation_points(:, 8:10);

% Remove the rows containing element "Inf" or "NaN"
rowsWithNaNOrInf = any(isnan(ablation_points) | isinf(ablation_points), 2);
ablation_points(rowsWithNaNOrInf, :) = [];

% Plot the point clouds
f = figure;
plot3(LV(:,1), LV(:,2), LV(:,3), '.b');
hold on;
plot3(ablation_points(:,1), ablation_points(:,2), ablation_points(:,3),
'.r','MarkerSize',50);

legend('LV', 'Ablation points');
hold off;

% Visualize the 3D model from four standar projection views
% Visualize the 3D model from LL view
view([90, 0]);

% % Visualize the 3D model from RL view
% view([-90, 0]);

% % Visualize the 3D model from AP view
% view([0, 0]);

% % Visualize the 3D model from PA view
% view([180, 0]);
```

Patient name	Stopstorm benchmark case 1 zzz_Test1_ACH	Report creation time	05 Dec 2023, 16:20:50 (hr:min:sec)
Patient ID	zzz_Test1_ACH	Plan last save time	05 Oct 2023, 11:02:16 (hr:min:sec)
Treatment plan name	VT_STOPSTORM_case1_3beams	Plan approved by	-
Plan and structure set approved	No	Plan approval time	-

Plan Report

Patient data

Patient ID	zzz_Test1_ACH
Patient name	Stopstorm benchmark case 1 zzz_Test1_ACH
Patient gender	Male
Patient birth date	
Case data	
Case name	Case 1
Physician	-
Body site	-

Treatment plan data

Treatment plan name	VT_STOPSTORM_case1_3beams
Plan last save time	05 Oct 2023, 11:02:16 (hr:min:sec)
Planned by	
Number of beam sets	1
Treatment plan approval data	
Approved	No
Approved by	-
Approval time	-
Plan comment	
Total dose image set	Planning CT
External ROI	External

General data

Treatment planning system	RayStation 11B (12.1.0.1221)
Report creation time	05 Dec 2023, 16:20:50 (hr:min:sec)
Template name	2022-04-25_PlanReportTemplate_11BSP1
Patient coordinate system	IEC 61217

ROI properties

Name	Material	Mass density [g/cm³]	RBE cell type
tissue_override	Tissue soft	1.000	

Beam set overview

Beam set name	VT_STOPSTORM_c_1
Treatment technique	Pencil Beam Scanning
Treatment unit	G_IR3_p_11A
Planning image set	Planning CT
Patient treatment position	HFS : Head First Supine
Number of beams	3
RBE model	Constant 1.1, Constant factor

Warnings [VT_STOPSTORM_c_1]

Warnings confirmed at report creation by: MEDAUSTRON\AC1.

- There are spots with meterset values above the machine default for beams: b1g35c270, b2g35c0, b3g80c5
- The following prescription is not fulfilled.
  Prescription: 25.00 Gy (RBE) x 1 fx = 25.00 Gy (RBE)
  Median dose (D50%)
  ROI: PTV_MA
  Computed dose: 27.64 Gy (RBE) x 1 fx = 27.64 Gy (RBE)
  Relates to beam set dose
- The ROI 'tissue_override' has a material override but the ROI is not defined on image set 'Planning CT'.
- The following image sets have original patient ID different from patient:
  CT Image Planning CT: 28 Nov 2018, 13:00:22 (hr:min:sec) was 'zSTOPBM01'

Patient name	Stopstorm benchmark case 1 zzz_Test1_ACH	Report creation time	05 Dec 2023, 16:20:50 (hr:min:sec)
Patient ID	zzz_Test1_ACH	Plan last save time	05 Oct 2023, 11:02:16 (hr:min:sec)
Treatment plan name	VT_STOPSTORM_case1_3beams	Plan approved by	-
Plan and structure set approved	No	Plan approval time	-

Beam set report

Beam set data

Beam set name	VT_STOPSTORM_c_1
Modality	Protons
Treatment technique	Pencil Beam Scanning
Treatment unit	G_IR3_p_11A
Commission time	12 Jul 2021, 09:55:32 (hr:min:sec)
Number of beams	3
DICOM plan UID	1.2.752.243.1.1.20231005110216960.7000.80303
Planning image set	
Name	Planning CT
Image modality	CT
Imaging system	Generic CT 20 Jul 2011, 15:25:00 (hr:min:sec)
Patient scanning position	HFS
Series date and time	28 Nov 2018, 13:20:06 (hr:min:sec)
Acquisition date and time	-
Is a converted image set	No
Patient treatment position	HFS : Head First Supine
Dose calculation algorithm	Monte Carlo, Version 5.3 Tot. ions: 70189056
RBE model	Constant 1.1, Constant factor
Density calculation algorithm version	2.1
Number of fractions	1
ROI(s) with material override	tissue_override
Beam set approval data	
Approved	No
Approved by	-
Approval time	-
Structure set UID	1.2.752.243.1.1.20231005101544570.3800.47745
Structure set approval data	
Approved	No
Approved by	-
Approval time	-

Beam data overview [Isocenter: VT_STOPSTORM_c_1 10_moved 1, **R-L:** 12.83 cm, **I-S:** -119.70 cm, **P-A:** -11.80 cm**]**

#	Beam name	Gantry angle [deg]	Couch rotation angle [deg]	Snout ID / position [cm]	Air gap Min / CAX [cm]	Range shifter	Beam meterset [10^6 NP/fx]
1	b1g35c270	35.0	250.0	HBL_Nozzle / 64.80	16.00 / 21.26	No	181703.2562

Beam data overview [Isocenter: VT_STOPSTORM_c_1 8_moved 2, **R-L:** -16.16 cm, **I-S:** -100.51 cm, **P-A:** -14.08 cm**]**

#	Beam name	Gantry angle [deg]	Couch rotation angle [deg]	Snout ID / position [cm]	Air gap Min / CAX [cm]	Range shifter	Beam meterset [10^6 NP/fx]
2	b2g35c0	35.0	0.0	HBL_Nozzle / 64.80	16.00 / 17.26	No	160812.3903

Beam data overview [Isocenter: VT_STOPSTORM_c_1 7, **R-L:** -22.90 cm, **I-S:** -98.00 cm, **P-A:** 12.27 cm**]**

#	Beam name	Gantry angle [deg]	Couch rotation angle [deg]	Snout ID / position [cm]	Air gap Min / CAX [cm]	Range shifter	Beam meterset [10^6 NP/fx]
3	b3g80c5	80.0	5.0	HBL_Nozzle / 64.80	20.00 / 25.10	No	159053.3313

Objectives

Dose	Function	ROI	Description	Robust	Weight	Value
	Physical composite objective					
Plan (RBE)	Min dose	PTV-stomach	Min dose 25.00 Gy (RBE)	No	100.00	0.0427
Plan (RBE)	Max dose	PTV-clTV	Max dose 25.00 Gy (RBE)	No	90.00	
Plan (RBE)	Uniform dose	PTV-stomach	Uniform dose 25.00 Gy (RBE)	No	50.00	0.0345
Beam set (RBE)	Min DVH	PTV-stomach	Min DVH 25.00 Gy (RBE) to 60.00% volume, All beams	No	40.00	0.0011
Beam set (RBE)	Max dose	PTV-stomach	Max dose 40.00 Gy (RBE), All beams	No	40.00	7.8560E-4
Plan (RBE)	Max dose	ring	Max dose 24.00 Gy (RBE)	No	10.00	1.2527E-4
Plan (RBE)	Max EUD	ring	Max EUD 9.40 Gy (RBE), Parameter A 1	No	6.00	0.0000
Plan (RBE)	Dose fall-off	ring	Dose fall-off [H]31.50 Gy (RBE) [L]20.00 Gy (RBE), Low dose distance 1.00 cm	No	4.00	0.0015
Plan (RBE)	Min dose	TV_expanded	Min dose 32.00 Gy (RBE)	No	120.00	
Plan (RBE)	Max dose	TV_expanded	Max dose 32.00 Gy (RBE)	No	90.00	0.0022
Plan (RBE)	Uniform dose	TV_expanded	Uniform dose 32.00 Gy (RBE)	No	80.00	0.0192
Beam set (RBE)	Min DVH	TV_expanded	Min DVH 32.00 Gy (RBE) to 70.00% volume, All beams	No	50.00	0.0039
Beam set (RBE)	Max dose	TV_expanded	Max dose 46.00 Gy (RBE), All beams	No	60.00	0.0000
Plan (RBE)	Max DVH	tentative_skin	Max DVH 6.00 Gy (RBE) to 0.05% volume	No	10.00	0.0016
Plan (RBE)	Max dose	Stomach	Max dose 12.50 Gy (RBE)	No	40.00	2.6300E-4
Plan (RBE)	Max DVH	stomachPRV	Max DVH 12.00 Gy (RBE) to 0.50% volume	No	20.00	2.5162E-4
Plan (RBE)	Max DVH	implant	Max DVH 19.00 Gy (RBE) to 0.10% volume	No	5.00	7.1711E-6
Beam set (RBE)	Max dose	ring	Max dose 13.00 Gy (RBE), Beam 'b1g35c270'	No	10.00	4.7693E-5
Beam set (RBE)	Max dose	ring	Max dose 13.00 Gy (RBE), Beam 'b3g80c5'	No	10.00	1.8486E-4
Plan (RBE)	Max dose	A_LAD	Max dose 23.50 Gy (RBE)	No	15.00	3.8506E-4
Plan (RBE)	Max dose	hotspot_out	Max dose 26.00 Gy (RBE)	No	5.00	6.1476E-4
Beam set (RBE)	Max dose	ring	Max dose 13.00 Gy (RBE), Beam 'b2g35c0'	No	10.00	2.7731E-6

Constraints

No constraints defined

Patient name	Stopstorm benchmark case 1 zzz_Test1_ACH	Report creation time	05 Dec 2023, 16:20:50 (hr:min:sec)
Patient ID	zzz_Test1_ACH	Plan last save time	05 Oct 2023, 11:02:16 (hr:min:sec)
Treatment plan name	VT_STOPSTORM_case1_3beams	Plan approved by	-
Plan and structure set approved	No	Plan approval time	-

Prescription

Primary prescription

Treatment site	TV
Prescription type	Median dose (D50%)
Prescribed dose	32.00 Gy (RBE) x 1 fx = 32.00 Gy (RBE)
Dose type	Relates to beam set dose
Fulfillment	Fulfilled (32.00 Gy (RBE) x 1 fx = 32.00 Gy (RBE))

Treatment site	PTV_MA
Prescription type	Median dose (D50%)
Prescribed dose	25.00 Gy (RBE) x 1 fx = 25.00 Gy (RBE)
Dose type	Relates to beam set dose
Fulfillment	Not fulfilled (27.64 Gy (RBE))

Nominal contributions

	Treatment site: **Prescription type:**	**TV** **Median dose (D50%)**	**PTV_MA** **Median dose (D50%)**
Beam no.	Beam name	Nominal contribution/fx [Gy (RBE)]	Nominal contribution/fx [Gy (RBE)]
1	b1g35c270	11.59	9.06
2	b2g35c0	10.26	8.01
3	b3g80c5	10.15	7.93
-	Total:	32.00	25.00

Nominal contribution can be used to track nominal progress towards a prescription during treatment delivery.
The table presents nominal contribution per beam and prescription.
Nominal contribution is defined as prescribed fraction dose weighted with each beam's relative weight (based on beam meterset).

Note: Nominal contribution is unrelated to the calculated beam set dose in RayStation, and is based solely on the prescribed fraction dose. It is not affected by whether the prescription is fulfilled or not.

Note: Nominal contributions will only be DICOM exported if corresponding setting is made in the machine.

Beam collision status

Beam #	Beam name	Collision status	
		Nominal	Within setup margins
1	b1g35c270	Unknown	Unknown
2	b2g35c0	Unknown	Unknown
3	b3g80c5	Unknown	Unknown

Setup margins

Lateral [cm]		Longitudinal [cm]		Vertical [cm]		Yaw [deg]		Pitch [deg]		Roll [deg]	
Lower	Upper	Lower	Upper	Lower	Upper	Lower	Upper	Lower	Upper	Lower	Upper
-2.00	2.00	-2.00	2.00	-2.00	2.00	-3.00	3.00	-3.00	3.00	-3.00	3.00

Patient setup

Localization point
No localization point defined.
Patient setup
No localization point defined.
Patient setup
No localization point defined.
Patient setup
No localization point defined.

BeamsetDoseData

Isocenter name	VT_STOPSTORM_c_1 10_moved 1
Isocenter [cm]	Right-Left: 12.83 Inf-Sup: -119.70 Post-Ant: -11.80
Dose type	RBE
Dose grid resolution [cm]	Right-Left: 0.20 Inf-Sup: 0.20 Post-Ant: 0.20

BeamsetDoseData

Isocenter name	VT_STOPSTORM_c_1 8_moved 2
Isocenter [cm]	Right-Left: -16.16 Inf-Sup: -100.51 Post-Ant: -14.08
Dose type	RBE
Dose grid resolution [cm]	Right-Left: 0.20 Inf-Sup: 0.20 Post-Ant: 0.20

BeamsetDoseData

Isocenter name	VT_STOPSTORM_c_1 7
Isocenter [cm]	Right-Left: -22.90 Inf-Sup: -98.00 Post-Ant: 12.27
Dose type	RBE
Dose grid resolution [cm]	Right-Left: 0.20 Inf-Sup: 0.20 Post-Ant: 0.20

Points of Interest

		Beam isocenters [cm]	Point - isocenter [cm]
Name	**Fiducial 1**	**Right-Left: 12.83**	**Right-Left: -6.66**
Type	**Marker**	**Inf-Sup: -119.70**	**Inf-Sup: 16.58**
Beam set dose [Gy (RBE)]	**19.34 [Interpolated]**	**Post-Ant: -11.80**	**Post-Ant: 30.78**
Location [cm]	**Right-Left: 6.17**		
	Inf-Sup: -103.12	**Right-Left: -16.16**	**Right-Left: 22.33**
	Post-Ant: 18.98	**Inf-Sup: -100.51**	**Inf-Sup: -2.61**
		Post-Ant: -14.08	**Post-Ant: 33.05**
		Right-Left: -22.90	**Right-Left: 29.07**
		Inf-Sup: -98.00	**Inf-Sup: -5.12**
		Post-Ant: 12.27	**Post-Ant: 6.71**

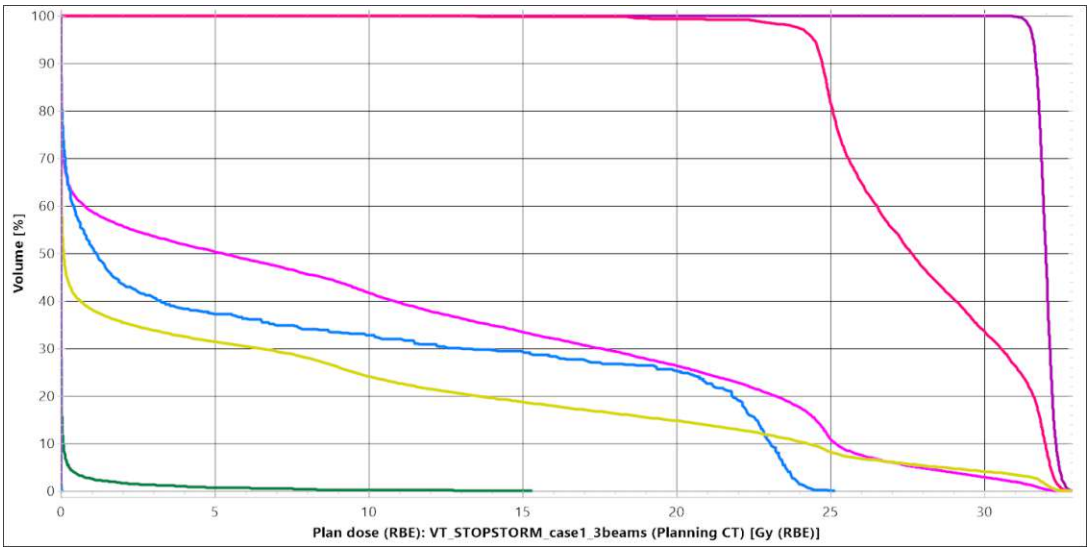

POI dose statistics

Dose	POI	Dose [Gy (RBE)]	Position Right-Left: [cm]	Position Inf-Sup: [cm]	Position Post-Ant: [cm]
Plan dose (RBE): VT_STOPSTORM_case1_3beams (Planning CT)	Fiducial 1	19.34	6.17	-103.12	18.98

ROI dose statistics [beam set dose]

Name	Volume [cm³]	D99 [Gy (RBE)]	D98 [Gy (RBE)]	D95 [Gy (RBE)]	Average [Gy (RBE)]	D50 [Gy (RBE)]	D2 [Gy (RBE)]	D1 [Gy (RBE)]	% outside grid
A_Aorta	308.82	0.00	0.00	0.00	0.00	0.00	0.00	0.01	0
A_LAD	2.12	0.00	0.00	0.00	7.56	1.15	23.92	24.18	0
A_LCX	1.53	0.00	0.00	0.00	0.00	0.00	0.01	0.01	0
A_LM	0.68	0.00	0.00	0.00	0.00	0.00	0.00	0.00	0
A_Pulmonary	185.35	0.00	0.00	0.00	0.03	0.00	0.27	0.64	0
A_RCA	4.57	0.00	0.00	0.00	0.00	0.00	0.01	0.01	0
Atrium_L	323.98	0.00	0.00	0.00	0.00	0.00	0.00	0.00	0
Atrium_R	203.03	0.00	0.00	0.00	0.00	0.00	0.00	0.00	0
AVN	5.84	0.00	0.00	0.00	0.00	0.00	0.00	0.00	0
Bronchus_Main	29.05	0.00	0.00	0.00	0.00	0.00	0.00	0.00	0
cITV	24.88	28.18	28.58	29.19	31.28	31.67	32.48	32.57	0
Colon	311.07	0.00	0.00	0.00	0.00	0.00	0.04	0.07	0
Esophagus	41.91	0.00	0.00	0.00	0.00	0.00	0.00	0.00	0
External	24724.42	0.00	0.00	0.00	0.39	0.00	7.13	10.57	0
Heart	1321.09	0.00	0.00	0.00	3.55	0.00	29.13	31.61	0
hotspot_out	0.45	20.88	20.90	21.71	24.90	24.85	26.92	27.00	0
ICD	42.18	0.00	0.00	0.00	0.00	0.00	0.00	0.00	0
implant	37.71	0.00	0.00	0.00	0.22	0.00	0.75	10.37	0
implants_in_target	0.75	0.02	0.03	0.04	8.90	8.84	21.65	21.88	0
ITV	50.13	20.34	23.01	24.59	28.80	29.39	32.36	32.48	0
ITV_robust	48.15	24.19	24.48	24.77	29.05	29.59	32.37	32.48	0
Liver	1143.94	0.00	0.00	0.00	0.02	0.00	0.01	0.04	0
Lung_L	1469.48	0.00	0.00	0.00	0.45	0.00	8.81	11.07	0
Lung_R	1203.00	0.00	0.00	0.00	0.00	0.00	0.00	0.00	0
PTV_MA	66.78	22.51	23.61	24.46	28.02	27.64	32.31	32.43	0
PTV_original	97.00	8.00	12.84	18.85	26.15	25.44	32.25	32.37	0
PTVcheck	100.26	8.31	12.92	18.78	26.04	25.32	32.25	32.36	0
PTV-cITV	16.86	18.03	18.80	22.74	24.64	24.87	26.35	26.62	0
PTV-stomach	15.95	22.75	23.63	24.12	24.94	24.91	26.38	26.65	0
ring	353.24	0.02	0.03	0.08	9.09	8.73	23.74	24.26	0
SAN	2.35	0.00	0.00	0.00	0.00	0.00	0.00	0.00	0
SpinalCanal	42.69	0.00	0.00	0.00	0.00	0.00	0.00	0.00	0
Stomach	249.33	0.00	0.00	0.00	0.13	0.00	1.58	3.90	0
stomachPRV	381.20	0.00	0.00	0.00	0.26	0.00	3.61	8.31	0
tentative_skin	984.87	0.00	0.00	0.00	0.14	0.00	3.55	6.08	11
test_ITV	30.16	27.10	27.45	28.06	30.85	31.40	32.45	32.54	0
tissue_override									-
Trachea	50.08	0.00	0.00	0.00	0.00	0.00	0.00	0.00	0
TV	10.19	31.34	31.44	31.58	32.00	32.00	32.56	32.64	0
TV_expanded	16.59	30.27	30.55	30.89	31.81	31.89	32.52	32.62	0
V_Venacava_I	11.43	0.00	0.00	0.00	0.00	0.00	0.00	0.00	0
V_Venacava_S	27.39	0.00	0.00	0.00	0.00	0.00	0.00	0.00	0
Valve_Aortic	22.97	0.00	0.00	0.00	0.00	0.00	0.03	0.03	0
Valve_Mitral	7.62	0.00	0.00	0.00	0.00	0.00	0.00	0.00	0
Valve_Pulmonic	10.75	0.00	0.00	0.01	0.69	0.14	5.61	6.60	0
Valve_Tricuspid	5.33	0.00	0.00	0.00	0.00	0.00	0.02	0.02	0
Ventricle_L	392.80	0.00	0.00	0.00	6.06	0.09	31.85	32.09	0
Ventricle_L_A	40.94	0.00	0.00	0.00	6.82	4.18	25.14	26.51	0

Ventricle_L_I	35.87	0.00	0.00	0.00	2.37	0.00	24.92	25.31	0
Ventricle_L_L	48.30	0.00	0.00	0.00	0.14	0.00	1.92	4.64	0
Ventricle_L_S	25.35	0.00	0.00	0.00	22.02	27.99	32.45	32.54	0
Ventricle_R	216.21	0.00	0.00	0.00	9.84	5.20	30.88	31.65	0

External — This ROI is set as the external ROI that defines the outer border of the patient

Beam data

Beam number	1
Beam name	b1g35c270
Beam description	
Gantry angle [deg]	35.0
Couch rotation angle [deg]	250.0
Isocenter [cm]	VT_STOPSTORM_c_1 10_moved 1 - Right-Left: 12.83 Inf-Sup: -119.70 Post-Ant: -11.80
Treatment technique	Pencil Beam Scanning
Number of fractions	1
Beam weight [%]	36.23
Dose calculation algorithm	Monte Carlo, Version 5.3 Uncert: 0.49% Tot. ions: 24772608
Treatment unit	G_IR3_p_11A
Commission time	12 Jul 2021, 09:55:32 (hr:min:sec)
SnoutID	HBL_Nozzle
Snout position [cm]	64.80
Spot tune ID	4.0
Range shifter	No
Range modulator	No
NumberOfEnergyLayers	38
Number of spots	10766
Beam meterset [10⁶ NP/fx]	181703.2562
Min spot meterset [10⁶ NP/fx]	0.9632
Max spot meterset [10⁶ NP/fx]	236.5707

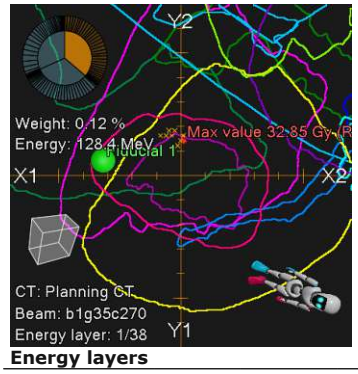

Energy layers

No	Energy [MeV]	Rel. weight [%]	[10⁶ NP/fx]	No. of spots	Spot spacing [cm]	Min spot meterset [10⁶ NP/fx]	Max spot meterset [10⁶ NP/fx]	No. of paintings	NP/spill [10⁶ NP]	Spill [sec]	Deg
1	128.40	0.12	225.7051	8	0.23	1.1594	126.5487	1	20000	10	0.00
2	126.50	2.55	4635.2579	73	0.23	1.2060	236.0409	1	20000	10	0.00
3	124.70	3.42	6208.4538	130	0.23	1.0427	236.3868	1	20000	10	0.00
4	122.80	2.92	5306.0431	182	0.23	1.0132	236.5707	1	20000	10	0.00
5	121.50	2.53	4602.1105	197	0.23	0.9995	236.4950	1	20000	10	0.00
6	120.20	3.32	6024.6672	223	0.23	0.9902	236.5461	1	20000	10	0.00
7	118.90	2.40	4363.1519	250	0.23	0.9874	236.5415	1	20000	10	0.00
8	117.60	2.39	4349.8342	276	0.23	0.9880	236.5426	1	20000	10	0.00
9	116.30	3.66	6645.5026	299	0.23	0.9733	236.4950	1	20000	10	0.00
10	115.00	3.39	6165.0355	325	0.23	0.9662	236.4161	1	20000	10	0.00
11	113.70	3.74	6794.0564	357	0.23	0.9661	236.4189	1	20000	10	0.00
12	112.30	3.28	5964.6391	353	0.23	0.9694	236.4921	1	20000	10	0.00
13	111.60	2.64	4788.2979	338	0.23	0.9632	235.8667	1	20000	10	0.00
14	110.30	3.68	6695.7368	363	0.23	0.9725	236.5134	1	20000	10	0.00
15	108.90	3.56	6466.8786	379	0.24	0.9680	211.8009	1	20000	10	0.00
16	107.50	3.88	7050.0861	399	0.24	0.9713	228.3221	1	20000	10	0.00

17	106.10	3.97	7218.4441	422	0.24	0.9709	230.4012	1	20000	10	0.00
18	104.70	3.99	7240.8820	448	0.24	0.9649	165.8184	1	20000	10	0.00
19	103.30	4.31	7838.9161	441	0.24	0.9792	196.1505	1	20000	10	0.00
20	101.80	3.72	6766.7612	425	0.24	0.9831	224.7495	1	20000	10	0.00
21	100.40	2.99	5427.3267	416	0.24	0.9976	235.6003	1	20000	10	0.00
22	98.90	3.70	6719.3082	426	0.24	0.9711	229.5428	1	20000	10	0.00
23	97.40	3.59	6523.5532	429	0.24	0.9644	196.8811	1	20000	10	0.00
24	95.90	3.60	6535.2171	448	0.24	1.0309	220.8624	1	20000	10	0.00
25	94.30	3.12	5673.7111	440	0.24	1.0423	158.4273	1	20000	10	0.00
26	92.80	2.92	5297.6387	415	0.25	1.0583	146.3173	1	20000	10	0.00
27	91.20	2.48	4504.1177	348	0.25	1.0583	235.4165	1	20000	10	0.00
28	89.60	2.56	4653.8381	325	0.25	0.9708	235.9216	1	20000	10	0.00
29	88.00	2.17	3941.7535	331	0.25	0.9883	184.5615	1	20000	10	0.00
30	86.40	2.31	4193.7457	311	0.25	0.9983	171.3930	1	20000	10	0.00
31	84.70	1.65	3003.7462	246	0.25	1.0387	146.0225	1	20000	10	0.00
32	83.00	1.39	2529.0885	201	0.26	1.0943	110.5793	1	20000	10	0.00
33	81.30	1.25	2263.5197	145	0.26	1.1827	108.6029	1	20000	10	0.00
34	79.60	1.15	2081.9684	128	0.26	1.0864	120.5295	1	20000	10	0.00
35	77.80	0.83	1510.8288	101	0.27	1.1037	68.9303	1	20000	10	0.00
36	76.00	0.35	644.0314	72	0.27	1.2884	74.0484	1	20000	10	0.00
37	74.20	0.23	412.6910	63	0.27	1.3953	19.8945	1	20000	10	0.00
38	72.40	0.24	436.7120	33	0.27	1.4836	28.7898	1	20000	10	0.00

	Patient name	Stopstorm benchmark case 1 zzz_Test1_ACH	Report creation time	05 Dec 2023, 16:20:50 (hr:min:sec)
	Patient ID	zzz_Test1_ACH	Plan last save time	05 Oct 2023, 11:02:16 (hr:min:sec)
	Treatment plan name	VT_STOPSTORM_case1_3beams	Plan approved by	-
	Plan and structure set approved	No	Plan approval time	-

Beam data

Beam number	2
Beam name	b2g35c0
Beam description	
Gantry angle [deg]	35.0
Couch rotation angle [deg]	0.0
Isocenter [cm]	VT_STOPSTORM_c_1 8_moved 2 - Right-Left: -16.16 Inf-Sup: -100.51 Post-Ant: -14.08
Treatment technique	Pencil Beam Scanning
Number of fractions	1
Beam weight [%]	32.06
Dose calculation algorithm	Monte Carlo, Version 5.3 Uncert: 0.48% Tot. ions: 24772608
Treatment unit	G_IR3_p_11A
Commission time	12 Jul 2021, 09:55:32 (hr:min:sec)
SnoutID	HBL_Nozzle
Snout position [cm]	64.80
Spot tune ID	4.0
Range shifter	No
Range modulator	No
NumberOfEnergyLayers	37
Number of spots	6923
Beam meterset [10^6 NP/fx]	160812.3903
Min spot meterset [10^6 NP/fx]	0.9621
Max spot meterset [10^6 NP/fx]	236.5744

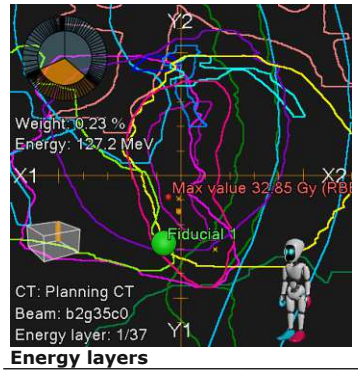

Energy layers

No	Energy [MeV]	Rel. weight [%]	[10^6 NP/fx]	No. of spots	Spot spacing [cm]	Min spot meterset [10^6 NP/fx]	Max spot meterset [10^6 NP/fx]	No. of paintings	NP/spill [10^6 NP]	Spill [sec]	Deg
1	127.20	0.23	365.6706	3	0.30	68.8712	199.6228	1	20000	10	0.00
2	125.30	2.03	3264.0108	27	0.30	2.3740	232.4176	1	20000	10	0.00
3	123.40	4.81	7739.9947	85	0.30	1.0897	236.5744	1	20000	10	0.00
4	122.10	4.35	6993.6142	122	0.30	1.0010	236.5686	1	20000	10	0.00
5	120.90	3.80	6103.8554	148	0.30	0.9897	236.5316	1	20000	10	0.00
6	119.60	3.84	6177.9111	182	0.30	0.9642	236.5687	1	20000	10	0.00
7	118.30	4.10	6588.8358	203	0.30	0.9621	236.5476	1	20000	10	0.00
8	117.00	4.38	7045.5208	225	0.30	0.9667	236.5158	1	20000	10	0.00
9	115.70	4.28	6887.8876	248	0.30	0.9779	236.4866	1	20000	10	0.00
10	114.30	4.07	6549.0126	269	0.30	0.9749	235.3742	1	20000	10	0.00
11	113.00	3.91	6290.5530	280	0.30	0.9670	236.5271	1	20000	10	0.00
12	111.60	3.80	6106.5076	293	0.30	0.9753	236.4984	1	20000	10	0.00
13	110.30	4.09	6571.4067	302	0.30	0.9808	233.5401	1	20000	10	0.00
14	108.90	3.57	5734.6621	309	0.30	0.9670	201.2142	1	20000	10	0.00
15	107.50	3.06	4915.3640	320	0.30	0.9719	185.8816	1	20000	10	0.00
16	106.10	3.66	5879.2598	317	0.30	0.9672	236.3623	1	20000	10	0.00

17	104.70	4.05	6507.4786	326	0.30	0.9741	236.5049	1	20000	10	0.00
18	103.30	4.18	6726.8265	330	0.30	0.9768	236.4706	1	20000	10	0.00
19	101.80	4.92	7908.6472	316	0.30	0.9930	236.2274	1	20000	10	0.00
20	100.40	3.54	5688.2557	288	0.30	1.0117	236.4602	1	20000	10	0.00
21	98.90	3.75	6026.4588	248	0.30	1.0083	234.3804	1	20000	10	0.00
22	97.40	2.52	4051.4582	237	0.30	0.9968	208.2658	1	20000	10	0.00
23	95.90	3.14	5056.2187	217	0.31	1.0117	235.7909	1	20000	10	0.00
24	94.30	2.27	3652.9388	214	0.31	1.0226	188.0548	1	20000	10	0.00
25	92.80	2.41	3882.2922	219	0.31	1.0323	150.4690	1	20000	10	0.00
26	91.20	1.66	2663.5230	189	0.31	1.0217	164.9641	1	20000	10	0.00
27	89.60	1.84	2957.0712	195	0.31	1.0256	166.8984	1	20000	10	0.00
28	88.00	1.67	2693.5512	186	0.32	1.0641	141.9717	1	20000	10	0.00
29	86.40	1.15	1842.6723	151	0.32	1.0659	196.0680	1	20000	10	0.00
30	84.70	1.28	2050.3707	122	0.32	1.0596	143.2481	1	20000	10	0.00
31	83.00	0.84	1356.7226	70	0.32	1.0772	193.8687	1	20000	10	0.00
32	81.30	0.74	1184.6415	53	0.33	1.0550	128.8523	1	20000	10	0.00
33	79.60	0.71	1147.9835	52	0.33	1.0600	98.3984	1	20000	10	0.00
34	77.80	0.60	959.1445	56	0.33	1.1494	78.2557	1	20000	10	0.00
35	76.00	0.47	753.2456	61	0.34	1.3423	80.5007	1	20000	10	0.00
36	74.20	0.28	454.8020	43	0.34	1.3197	82.1811	1	20000	10	0.00
37	72.40	0.02	34.0207	17	0.34	1.3463	6.9817	1	20000	10	0.00

Beam data

Beam number	3
Beam name	b3g80c5
Beam description	
Gantry angle [deg]	80.0
Couch rotation angle [deg]	5.0
Isocenter [cm]	VT_STOPSTORM_c_1 7 - Right-Left: -22.90 Inf-Sup: -98.00 Post-Ant: 12.27
Treatment technique	Pencil Beam Scanning
Number of fractions	1
Beam weight [%]	31.71
Dose calculation algorithm	Monte Carlo, Version 5.3 Uncert: 0.48% Tot. ions: 20643840
Treatment unit	G_IR3_p_11A
Commission time	12 Jul 2021, 09:55:32 (hr:min:sec)
SnoutID	HBL_Nozzle
Snout position [cm]	64.80
Spot tune ID	4.0
Range shifter	No
Range modulator	No
NumberOfEnergyLayers	35
Number of spots	6727
Beam meterset [10^6 NP/fx]	159053.3313
Min spot meterset [10^6 NP/fx]	0.9529
Max spot meterset [10^6 NP/fx]	236.5746

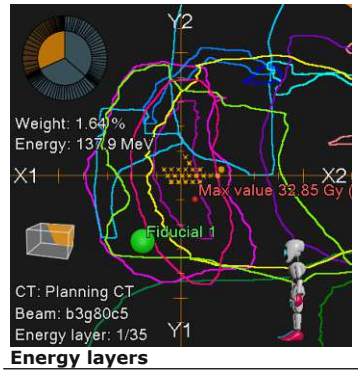

Energy layers

No	Energy [MeV]	Rel. weight [%]	[10^6 NP/fx]	No. of spots	Spot spacing [cm]	Min spot meterset [10^6 NP/fx]	Max spot meterset [10^6 NP/fx]	No. of paintings	NP/spill [10^6 NP]	Spill [sec]	Deg
1	137.90	1.64	2612.9289	22	0.29	43.7842	235.0136	1	20000	10	0.00
2	136.20	3.03	4814.5299	59	0.29	1.1144	235.0183	1	20000	10	0.00
3	134.40	5.89	9367.4839	128	0.29	1.0374	236.0921	1	20000	10	0.00
4	132.60	6.83	10870.9599	188	0.29	1.0322	236.4013	1	20000	10	0.00
5	130.80	7.74	12318.2498	238	0.29	1.0217	236.5695	1	20000	10	0.00
6	129.00	6.54	10400.2477	271	0.29	0.9918	236.5746	1	20000	10	0.00
7	127.20	6.78	10777.8239	279	0.29	0.9648	236.5604	1	20000	10	0.00
8	125.30	6.84	10877.8732	311	0.29	0.9529	236.5734	1	20000	10	0.00
9	123.40	5.87	9334.3592	323	0.29	0.9672	236.5257	1	20000	10	0.00
10	122.10	4.24	6748.9664	312	0.29	0.9771	236.5630	1	20000	10	0.00
11	120.90	4.54	7214.6924	313	0.29	0.9594	236.5332	1	20000	10	0.00

12	119.60	3.54	5635.3624	301	0.29	0.9586	236.4271	1	20000	10	0.00
13	118.30	3.12	4964.2873	301	0.29	0.9603	236.4916	1	20000	10	0.00
14	117.00	3.06	4870.2402	305	0.29	0.9675	236.4305	1	20000	10	0.00
15	115.70	3.28	5218.8298	312	0.29	0.9718	236.0974	1	20000	10	0.00
16	114.30	2.46	3919.8728	293	0.29	0.9683	208.0293	1	20000	10	0.00
17	113.00	2.72	4320.4632	291	0.29	0.9869	235.6805	1	20000	10	0.00
18	111.60	2.50	3976.4281	279	0.29	1.0191	176.7151	1	20000	10	0.00
19	110.30	1.77	2815.9776	261	0.29	0.9899	170.1622	1	20000	10	0.00
20	108.90	2.21	3514.7674	244	0.29	1.0423	167.8206	1	20000	10	0.00
21	107.50	1.78	2833.9454	229	0.29	1.0584	133.7885	1	20000	10	0.00
22	106.10	1.60	2542.2394	212	0.30	1.0447	228.3548	1	20000	10	0.00
23	104.70	2.10	3333.1190	185	0.30	1.0596	194.4507	1	20000	10	0.00
24	103.30	2.04	3242.1851	209	0.30	1.0533	129.3394	1	20000	10	0.00
25	101.80	1.53	2433.1485	206	0.30	1.0362	170.2286	1	20000	10	0.00
26	100.40	1.21	1929.3732	152	0.30	1.0448	121.2422	1	20000	10	0.00
27	98.90	0.80	1280.2739	113	0.30	1.0461	95.1166	1	20000	10	0.00
28	97.40	0.72	1142.4037	72	0.30	1.0898	88.0276	1	20000	10	0.00
29	95.90	0.56	883.9138	61	0.30	1.0664	86.1738	1	20000	10	0.00
30	94.30	0.72	1151.6837	60	0.31	1.0822	152.0989	1	20000	10	0.00
31	92.80	0.84	1331.8530	48	0.31	1.1743	161.1332	1	20000	10	0.00
32	91.20	0.54	862.7089	47	0.31	1.5084	147.4151	1	20000	10	0.00
33	89.60	0.55	879.6795	49	0.31	1.5960	133.6258	1	20000	10	0.00
34	88.00	0.33	518.2353	35	0.32	2.1696	65.3876	1	20000	10	0.00
35	86.40	0.07	114.2249	18	0.32	1.7014	10.3089	1	20000	10	0.00

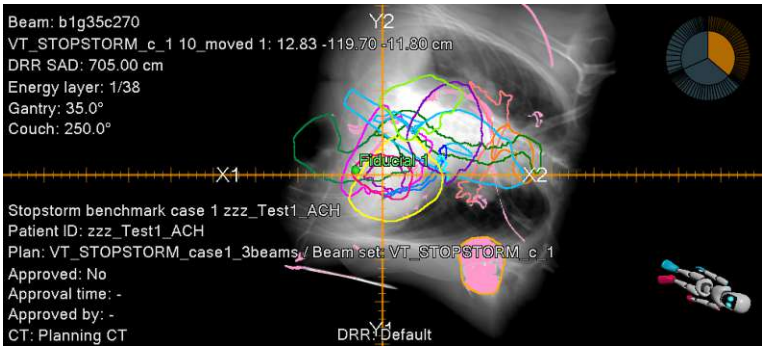

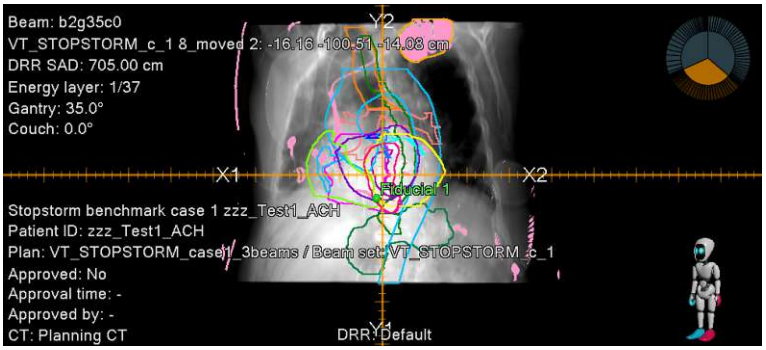

Patient name	Stopstorm benchmark case 1 zzz_Test1_ACH	Report creation time	05 Dec 2023, 16:20:50 (hr:min:sec)
Patient ID	zzz_Test1_ACH	Plan last save time	05 Oct 2023, 11:02:16 (hr:min:sec)
Treatment plan name	VT_STOPSTORM_case1_3beams	Plan approved by	-
Plan and structure set approved	No	Plan approval time	-

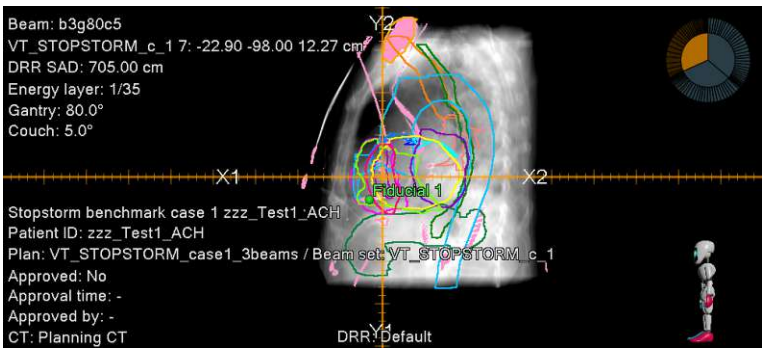

MedAustron	Patient name	Stopstorm benchmark case 2 zzz_Test2_ACH		Report creation time	05 Dec 2023, 16:31:24 (hr:min:sec)
	Patient ID	zzz_Test2_ACH		Plan last save time	06 Nov 2023, 13:51:48 (hr:min:sec)
	Treatment plan name	case2_copy		Plan approved by	-
	Plan and structure set approved	No		Plan approval time	-

Plan Report

Patient data

Patient ID	zzz_Test2_ACH
Patient name	Stopstorm benchmark case 2 zzz_Test2_ACH
Patient gender	Unknown
Patient birth date	09 Aug 1969
Case data	
Case name	Case 1
Physician	-
Body site	-

Treatment plan data

Treatment plan name	case2_copy
Plan last save time	06 Nov 2023, 13:51:48 (hr:min:sec)
Planned by	
Number of beam sets	1
Treatment plan approval data	
Approved	No
Approved by	-
Approval time	-
Plan comment	
Total dose image set	Planning CT
External ROI	External

General data

Treatment planning system	RayStation 11B (12.1.0.1221)
Report creation time	05 Dec 2023, 16:31:24 (hr:min:sec)
Template name	2022-04-25_PlanReportTemplate_11BSP1
Patient coordinate system	IEC 61217

ROI properties

No material override

Beam set overview

Beam set name	case2_copy
Treatment technique	Pencil Beam Scanning
Treatment unit	G_IR3_p_11A
Planning image set	Planning CT
Patient treatment position	HFS : Head First Supine
Number of beams	3
RBE model	Constant 1.1, Constant factor

Warnings [case2_copy]

Warnings confirmed at report creation by: MEDAUSTRON\AC1.

- There are spots with meterset values above the machine default for beams: b2g40c0, b3g70c10, b1g35c270
- The following prescription is not fulfilled.
  Prescription: 25.00 Gy (RBE) x 1 fx = 25.00 Gy (RBE)
  Median dose (D50%)
  ROI: PTV
  Computed dose: 28.55 Gy (RBE) x 1 fx = 28.55 Gy (RBE)
  Relates to beam set dose
- The selected imaging system 'Generic CT' is not consistent with the station name 'ctstrcvk01' specified in the DICOM files for image set 'Planning CT'.
- The following image sets have original patient ID different from patient:
  CT Image Planning CT: 27 Feb 2020, 13:25:15 (hr:min:sec) was 'zSTOPBM02'

Patient name	Stopstorm benchmark case 2 zzz_Test2_ACH	Report creation time	05 Dec 2023, 16:31:24 (hr:min:sec)
Patient ID	zzz_Test2_ACH	Plan last save time	06 Nov 2023, 13:51:48 (hr:min:sec)
Treatment plan name	case2_copy	Plan approved by	-
Plan and structure set approved	No	Plan approval time	-

Beam set report

Beam set data

Beam set name	case2_copy
Modality	Protons
Treatment technique	Pencil Beam Scanning
Treatment unit	G_IR3_p_11A
Commission time	12 Jul 2021, 09:55:32 (hr:min:sec)
Number of beams	3
DICOM plan UID	1.2.752.243.1.1.20231106135148267.1500.51000
Planning image set	
Name	Planning CT
Image modality	CT
Imaging system	Generic CT 20 Jul 2011, 15:25:00 (hr:min:sec)
Patient scanning position	HFS
Series date and time	27 Feb 2020, 13:25:50 (hr:min:sec)
Acquisition date and time	27 Feb 2020, 13:25:15 (hr:min:sec)
Is a converted image set	No
Patient treatment position	HFS : Head First Supine
Dose calculation algorithm	Monte Carlo, Version 5.3 Tot. ions: 61931520
RBE model	Constant 1.1, Constant factor
Density calculation algorithm version	2.1
Number of fractions	1
ROI(s) with material override	
Beam set approval data	
Approved	No
Approved by	-
Approval time	-
Structure set UID	1.2.752.243.1.1.20231020124740863.5500.77631
Structure set approval data	
Approved	No
Approved by	-
Approval time	-

Beam data overview [Isocenter: case2_copy 3_moved 1, **R-L:** -14.64 cm, **I-S:** -30.91 cm, **P-A:** 5.54 cm**]**

#	Beam name	Gantry angle [deg]	Couch rotation angle [deg]	Snout ID / position [cm]	Air gap Min / CAX [cm]	Range shifter	Beam meterset [10^6 NP/fx]
2	b2g40c0	40.0	0.0	HBL_Nozzle / 64.80	18.00 / 19.34	No	150137.3304

Beam data overview [Isocenter: case2_copy 4_moved 1, **R-L:** -14.05 cm, **I-S:** -26.97 cm, **P-A:** 24.59 cm**]**

#	Beam name	Gantry angle [deg]	Couch rotation angle [deg]	Snout ID / position [cm]	Air gap Min / CAX [cm]	Range shifter	Beam meterset [10^6 NP/fx]
3	b3g70c10	70.0	10.0	HBL_Nozzle / 64.80	18.00 / 29.90	No	130711.5911

Beam data overview [Isocenter: case2_copy 2_moved 1, **R-L:** 8.27 cm, **I-S:** -51.47 cm, **P-A:** 3.47 cm**]**

#	Beam name	Gantry angle [deg]	Couch rotation angle [deg]	Snout ID / position [cm]	Air gap Min / CAX [cm]	Range shifter	Beam meterset [10^6 NP/fx]
4	b1g35c270	35.0	270.0	HBL_Nozzle / 64.80	18.00 / 19.17	No	185477.1869

MedAustron

Patient name	Stopstorm benchmark case 2 zzz_Test2_ACH	Report creation time	05 Dec 2023, 16:31:24 (hr:min:sec)
Patient ID	zzz_Test2_ACH	Plan last save time	06 Nov 2023, 13:51:48 (hr:min:sec)
Treatment plan name	case2_copy	Plan approved by	-
Plan and structure set approved	No	Plan approval time	-

Objectives

Dose	Function	ROI	Description	Robust	Weight	Value
	Physical composite objective					
Plan (RBE)	Max dose	A_LAD	Max dose 24.00 Gy (RBE)	No	100.00	4.7052E-5
Beam set (RBE)	Min DVH	PTV-arteries	Min DVH 25.00 Gy (RBE) to 60.00% volume, All beams	No	100.00	
Beam set (RBE)	Max dose	PTV-cITV	Max dose 40.00 Gy (RBE), All beams	No	100.00	
Plan (RBE)	Max dose	Stomach	Max dose 0.10 Gy (RBE)	No	40.00	0.0000
Plan (RBE)	Max DVH	tentative_skin	Max DVH 5.70 Gy (RBE) to 0.05% volume	No	10.00	6.2963E-4
Plan (RBE)	Max dose	PTV-cITV	Max dose 27.00 Gy (RBE)	No	90.00	0.0058
Plan (RBE)	Max dose	A_Aorta	Max dose 24.00 Gy (RBE)	No	65.00	0.0000
Plan (RBE)	Max DVH	A_Aorta	Max DVH 24.00 Gy (RBE) to 0.01% volume	No	80.00	0.0000
Plan (RBE)	Max dose	A_LCX	Max dose 24.00 Gy (RBE)	No	90.00	0.0000
Plan (RBE)	Max DVH	A_LM	Max DVH 18.00 Gy (RBE) to 1.00% volume	No	5.00	0.0000
Plan (RBE)	Max DVH	A_Pulmonary	Max DVH 24.00 Gy (RBE) to 0.01% volume	No	60.00	0.0000
Plan (RBE)	Min DVH	PTV-arteries	Min DVH 25.00 Gy (RBE) to 90.00% volume	No	100.00	0.0011
Plan (RBE)	Max dose	ring	Max dose 23.00 Gy (RBE)	No	12.00	1.4082E-4
Plan (RBE)	Max EUD	ring	Max EUD 9.00 Gy (RBE), Parameter A 1	No	6.00	0.0000
Plan (RBE)	Dose fall-off	ring	Dose fall-off [H]25.00 Gy (RBE) [L]14.00 Gy (RBE), Low dose distance 1.00 cm	No	10.00	0.0012
Beam set (RBE)	Max dose	ring	Max dose 13.00 Gy (RBE), Beam 'b3g70c10'	No	10.00	3.8564E-7
Beam set (RBE)	Max dose	ring	Max dose 13.00 Gy (RBE), Beam 'b2g40c0'	No	10.00	0.0000
Plan (RBE)	Max dose	TV_expanded	Max dose 32.00 Gy (RBE)	No	90.00	0.0035
Beam set (RBE)	Max dose	TV_expanded	Max dose 46.00 Gy (RBE), All beams	No	60.00	
Plan (RBE)	Min DVH	TV_expanded	Min DVH 32.00 Gy (RBE) to 98.00% volume	No	100.00	0.0069
Beam set (RBE)	Max dose	ring	Max dose 13.00 Gy (RBE), Beam 'b1g35c270'	No	10.00	1.0503E-7

Constraints

No constraints defined

Patient name	Stopstorm benchmark case 2 zzz_Test2_ACH	Report creation time	05 Dec 2023, 16:31:24 (hr:min:sec)
Patient ID	zzz_Test2_ACH	Plan last save time	06 Nov 2023, 13:51:48 (hr:min:sec)
Treatment plan name	case2_copy	Plan approved by	-
Plan and structure set approved	No	Plan approval time	-

Prescription

Primary prescription

Treatment site	TV
Prescription type	Median dose (D50%)
Prescribed dose	32.00 Gy (RBE) x 1 fx = 32.00 Gy (RBE)
Dose type	Relates to beam set dose
Fulfillment	Fulfilled (32.05 Gy (RBE) x 1 fx = 32.05 Gy (RBE))

Treatment site	PTV
Prescription type	Median dose (D50%)
Prescribed dose	25.00 Gy (RBE) x 1 fx = 25.00 Gy (RBE)
Dose type	Relates to beam set dose
Fulfillment	Not fulfilled (28.55 Gy (RBE))

Nominal contributions

	Treatment site: **TV** **Prescription type:** **Median dose (D50%)**		**PTV** **Median dose (D50%)**
Beam no.	Beam name	Nominal contribution/fx [Gy (RBE)]	Nominal contribution/fx [Gy (RBE)]
2	b2g40c0	10.30	8.05
3	b3g70c10	8.97	7.01
4	b1g35c270	12.73	9.94
-	Total:	32.00	25.00

Nominal contribution can be used to track nominal progress towards a prescription during treatment delivery.
The table presents nominal contribution per beam and prescription.
Nominal contribution is defined as prescribed fraction dose weighted with each beam's relative weight (based on beam meterset).

Note: Nominal contribution is unrelated to the calculated beam set dose in RayStation, and is based solely on the prescribed fraction dose. It is not affected by whether the prescription is fulfilled or not.

Note: Nominal contributions will only be DICOM exported if corresponding setting is made in the machine.

Beam collision status

Beam #	Beam name	Collision status	
		Nominal	Within setup margins
2	b2g40c0	Unknown	Unknown
3	b3g70c10	Unknown	Unknown
4	b1g35c270	Unknown	Unknown

Setup margins

Lateral [cm]		Longitudinal [cm]		Vertical [cm]		Yaw [deg]		Pitch [deg]		Roll [deg]	
Lower	Upper	Lower	Upper	Lower	Upper	Lower	Upper	Lower	Upper	Lower	Upper
-2.00	2.00	-2.00	2.00	-2.00	2.00	-3.00	3.00	-3.00	3.00	-3.00	3.00

Patient setup

Localization point
No localization point defined.
Patient setup
No localization point defined.
Patient setup
No localization point defined.
Patient setup
No localization point defined.

BeamsetDoseData

Isocenter name	case2_copy 3_moved 1
Isocenter [cm]	Right-Left: -14.64 Inf-Sup: -30.91 Post-Ant: 5.54
Dose type	RBE
Dose grid resolution [cm]	Right-Left: 0.20 Inf-Sup: 0.20 Post-Ant: 0.20

BeamsetDoseData

Isocenter name	case2_copy 4_moved 1
Isocenter [cm]	Right-Left: -14.05 Inf-Sup: -26.97 Post-Ant: 24.59
Dose type	RBE
Dose grid resolution [cm]	Right-Left: 0.20 Inf-Sup: 0.20 Post-Ant: 0.20

	Patient name	Stopstorm benchmark case 2 zzz_Test2_ACH		Report creation time	05 Dec 2023, 16:31:24 (hr:min:sec)
MedAustron	Patient ID	zzz_Test2_ACH		Plan last save time	06 Nov 2023, 13:51:48 (hr:min:sec)
	Treatment plan name	case2_copy		Plan approved by	-
	Plan and structure set approved	No		Plan approval time	-

BeamsetDoseData

Isocenter name	case2_copy 2_moved 1
Isocenter [cm]	Right-Left: 8.27 Inf-Sup: -51.47 Post-Ant: 3.47
Dose type	RBE
Dose grid resolution [cm]	Right-Left: 0.20 Inf-Sup: 0.20 Post-Ant: 0.20

Points of Interest

No POI geometries found

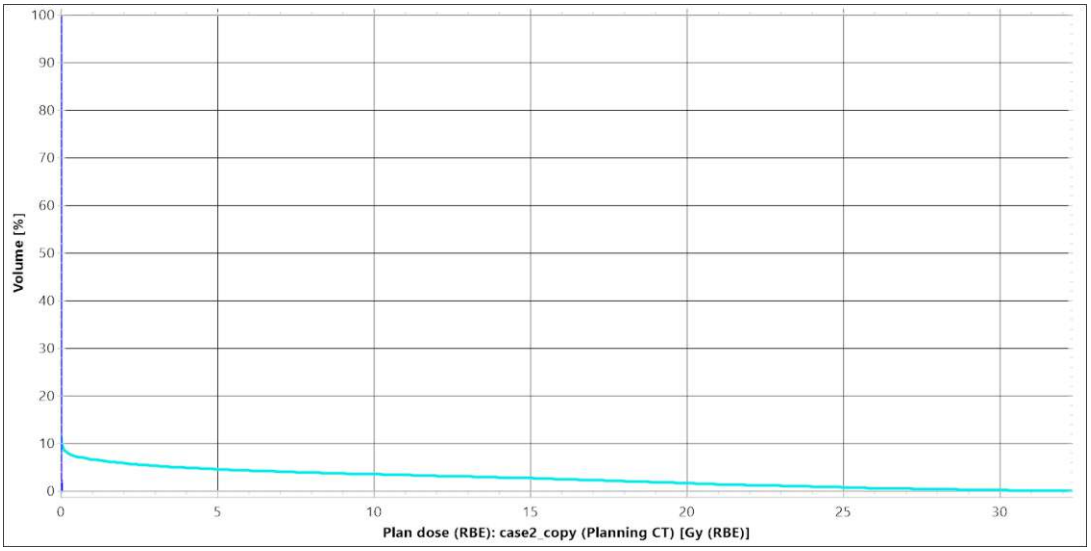

POI dose statistics

No POI dose statistics

ROI dose statistics [beam set dose]

Name	Volume [cm³]	D99 [Gy (RBE)]	D98 [Gy (RBE)]	D95 [Gy (RBE)]	Average [Gy (RBE)]	D50 [Gy (RBE)]	D2 [Gy (RBE)]	D1 [Gy (RBE)]	% outside grid
A_Aorta	237.51	0.00	0.00	0.00	0.00	0.00	0.00	0.00	0
A_LAD	2.19	0.00	0.00	0.00	3.93	0.25	21.19	22.82	0
A_LCX	0.25	0.00	0.00	0.00	0.00	0.00	0.00	0.00	0
A_LM	0.46	0.00	0.00	0.00	0.00	0.00	0.00	0.00	0
A_Pulmonary	79.93	0.00	0.00	0.00	0.00	0.00	0.00	0.01	0
A_RCA	2.23	0.00	0.00	0.00	0.00	0.00	0.00	0.00	0
Artifact	286.24	0.00	0.00	0.00	5.89	0.41	31.77	32.09	0
Atrium_L	242.76	0.00	0.00	0.00	0.00	0.00	0.00	0.01	0
Atrium_R	355.18	0.00	0.00	0.00	0.00	0.00	0.00	0.00	0
AVN	3.57	0.00	0.00	0.00	0.00	0.00	0.00	0.00	0
Bronchus_Main	19.22	0.00	0.00	0.00	0.00	0.00	0.00	0.00	0
cITV	28.58	27.54	28.09	28.82	31.21	31.72	32.50	32.58	0
Colon	4357.83	0.00	0.00	0.00	0.00	0.00	0.00	0.00	0
Esophagus	58.24	0.00	0.00	0.00	0.00	0.00	0.00	0.00	0
External	51659.36	0.00	0.00	0.00	0.18	0.00	1.63	6.65	0

MedAustron

Patient name	Stopstorm benchmark case 2 zzz_Test2_ACH					Report creation time	05 Dec 2023, 16:31:24 (hr:min:sec)		
Patient ID	zzz_Test2_ACH					Plan last save time	06 Nov 2023, 13:51:48 (hr:min:sec)		
Treatment plan name	case2_copy					Plan approved by	-		
Plan and structure set approved	No					Plan approval time	-		

Heart	1763.29	0.00	0.00	0.00	1.98	0.00	27.20	31.31	0
ICD	57.89	0.00	0.00	0.00	0.00	0.00	0.00	0.00	0
implant	115.49	0.00	0.00	0.00	0.82	0.00	18.14	23.21	0
Liver	2029.39	0.00	0.00	0.00	0.00	0.00	0.00	0.00	0
Lung_L	1692.12	0.00	0.00	0.00	0.30	0.00	6.26	11.16	0
Lung_R	1962.00	0.00	0.00	0.00	0.00	0.00	0.00	0.00	0
LVAT	189.45	0.00	0.00	0.00	0.00	0.00	0.01	0.01	0
PTV	61.99	20.14	21.82	23.33	28.36	28.55	32.40	32.49	0
PTV-arteries	61.93	20.16	21.84	23.36	28.37	28.57	32.40	32.49	0
PTV-clTV	22.39	17.02	19.41	21.73	25.00	25.25	27.88	28.16	0
PTV-LAD	61.93	20.16	21.84	23.36	28.37	28.57	32.40	32.49	0
ring	356.34	0.02	0.07	0.21	8.93	8.74	22.32	23.00	0
SAN	2.35	0.00	0.00	0.00	0.00	0.00	0.00	0.00	0
SpinalCanal	99.02	0.00	0.00	0.00	0.00	0.00	0.00	0.00	0
Stomach	197.60	0.00	0.00	0.00	0.00	0.00	0.00	0.00	0
tentative_skin	1517.93	0.00	0.00	0.00	0.07	0.00	0.12	3.25	0
Trachea	16.04	0.00	0.00	0.00	0.00	0.00	0.00	0.00	0
TV	13.97	31.01	31.21	31.48	32.02	32.05	32.57	32.68	0
TV_expanded	16.58	30.47	30.78	31.18	31.95	32.01	32.56	32.63	0
V_Venacava_I	35.31	0.00	0.00	0.00	0.00	0.00	0.00	0.00	0
V_Venacava_S	45.71	0.00	0.00	0.00	0.00	0.00	0.00	0.00	0
Valve_Aortic	22.48	0.00	0.00	0.00	0.00	0.00	0.00	0.00	0
Valve_Mitral	6.17	0.00	0.00	0.00	0.00	0.00	0.00	0.00	0
Valve_Pulmonic	11.48	0.00	0.00	0.00	0.00	0.00	0.01	0.01	0
Valve_Tricuspid	5.55	0.00	0.00	0.00	0.00	0.00	0.00	0.00	0
Ventricle_L	232.00	0.00	0.00	0.00	6.41	0.06	32.17	32.30	0
Ventricle_L_A	33.99	0.00	0.00	0.00	16.29	18.70	32.42	32.50	0
Ventricle_L_I	19.78	0.00	0.00	0.00	1.73	0.01	23.90	27.64	0
Ventricle_L_L	28.36	0.00	0.00	0.00	1.00	0.01	13.61	16.38	0
Ventricle_L_S	12.83	0.00	0.00	0.00	16.52	20.13	32.45	32.55	0
Ventricle_R	497.49	0.00	0.00	0.00	2.74	0.02	24.65	27.57	0

External — This ROI is set as the external ROI that defines the outer border of the patient

MedAustron	Patient name	Stopstorm benchmark case 2 zzz_Test2_ACH	Report creation time	05 Dec 2023, 16:31:24 (hr:min:sec)
	Patient ID	zzz_Test2_ACH	Plan last save time	06 Nov 2023, 13:51:48 (hr:min:sec)
	Treatment plan name	case2_copy	Plan approved by	-
	Plan and structure set approved	No	Plan approval time	-

Beam data

Beam number	2
Beam name	b2g40c0
Beam description	
Gantry angle [deg]	40.0
Couch rotation angle [deg]	0.0
Isocenter [cm]	case2_copy 3_moved 1 - Right-Left: -14.64 Inf-Sup: -30.91 Post-Ant: 5.54
Treatment technique	Pencil Beam Scanning
Number of fractions	1
Beam weight [%]	32.20
Dose calculation algorithm	Monte Carlo, Version 5.3 Uncert: 0.49% Tot. ions: 18579456
Treatment unit	G_IR3_p_11A
Commission time	12 Jul 2021, 09:55:32 (hr:min:sec)
SnoutID	HBL_Nozzle
Snout position [cm]	64.80
Spot tune ID	4.0
Range shifter	No
Range modulator	No
NumberOfEnergyLayers	32
Number of spots	3649
Beam meterset [10⁶ NP/fx]	150137.3304
Min spot meterset [10⁶ NP/fx]	0.9587
Max spot meterset [10⁶ NP/fx]	308.7820

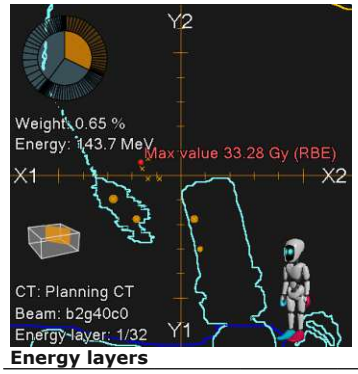

Energy layers

No	Energy [MeV]	Rel. weight [%]	[10⁶ NP/fx]	No. of spots	Spot spacing [cm]	Min spot meterset [10⁶ NP/fx]	Max spot meterset [10⁶ NP/fx]	No. of paintings	NP/spill [10⁶ NP]	Spill [sec]	Deg
1	143.70	0.65	974.2255	8	0.47	3.3819	253.8096	1	20000	10	0.00
2	142.00	1.31	1959.6597	28	0.47	1.9277	284.7663	1	20000	10	0.00
3	140.30	3.98	5969.6657	44	0.47	1.8587	284.7413	1	20000	10	0.00
4	138.50	4.63	6956.7987	55	0.47	1.8165	308.7820	1	20000	10	0.00
5	136.80	4.04	6066.1449	69	0.46	1.4398	272.7210	1	20000	10	0.00
6	135.00	4.69	7038.6024	75	0.46	0.9937	277.0157	1	20000	10	0.00
7	133.20	4.48	6724.2620	85	0.46	1.0278	283.9717	1	20000	10	0.00
8	131.40	3.54	5310.1265	93	0.46	1.0132	283.4357	1	20000	10	0.00
9	129.60	4.50	6763.6392	106	0.46	1.0141	298.8645	1	20000	10	0.00
10	127.80	4.51	6773.2772	127	0.46	0.9587	240.4000	1	20000	10	0.00
11	125.90	5.66	8505.1272	145	0.46	0.9765	256.4121	1	20000	10	0.00
12	124.00	5.62	8442.5083	164	0.46	1.0198	289.9916	1	20000	10	0.00
13	122.10	6.17	9262.1615	170	0.46	0.9952	268.5115	1	20000	10	0.00
14	120.90	4.88	7320.9525	170	0.46	1.0241	265.5775	1	20000	10	0.00
15	119.60	4.23	6343.4860	178	0.46	1.0485	196.9845	1	20000	10	0.00
16	118.30	3.79	5692.1459	185	0.46	1.0193	240.7122	1	20000	10	0.00

17	117.00	4.22	6333.5980	190	0.46	0.9881	251.1897	1	20000	10	0.00
18	115.70	4.08	6131.2242	195	0.46	0.9981	244.2113	1	20000	10	0.00
19	114.30	4.13	6201.6651	197	0.46	0.9645	233.3262	1	20000	10	0.00
20	113.00	4.19	6291.3881	194	0.46	0.9650	242.7291	1	20000	10	0.00
21	111.60	3.56	5344.2779	186	0.46	0.9726	219.3684	1	20000	10	0.00
22	110.30	3.73	5606.5651	179	0.47	0.9880	246.6377	1	20000	10	0.00
23	108.90	2.91	4369.3323	164	0.47	0.9868	221.9738	1	20000	10	0.00
24	107.50	1.97	2963.4891	138	0.47	1.0174	208.1238	1	20000	10	0.00
25	106.10	1.62	2427.5087	124	0.47	0.9730	140.2735	1	20000	10	0.00
26	104.70	1.09	1642.9143	110	0.47	0.9704	227.3376	1	20000	10	0.00
27	103.30	0.90	1356.8430	85	0.47	0.9745	147.2711	1	20000	10	0.00
28	101.80	0.37	560.9244	57	0.47	0.9681	68.2533	1	20000	10	0.00
29	100.40	0.19	289.7107	44	0.47	0.9992	49.8110	1	20000	10	0.00
30	98.90	0.11	165.9193	38	0.47	1.0161	28.0341	1	20000	10	0.00
31	97.40	0.20	305.4038	28	0.47	0.9868	141.7983	1	20000	10	0.00
32	95.90	0.03	43.7828	18	0.47	0.9844	8.0626	1	20000	10	0.00

Beam data

Beam number	3
Beam name	b3g70c10
Beam description	
Gantry angle [deg]	70.0
Couch rotation angle [deg]	10.0
Isocenter [cm]	case2_copy 4_moved 1 - Right-Left: -14.05 Inf-Sup: -26.97 Post-Ant: 24.59
Treatment technique	Pencil Beam Scanning
Number of fractions	1
Beam weight [%]	28.03
Dose calculation algorithm	Monte Carlo, Version 5.3 Uncert: 0.48% Tot. ions: 18579456
Treatment unit	G_IR3_p_11A
Commission time	12 Jul 2021, 09:55:32 (hr:min:sec)
SnoutID	HBL_Nozzle
Snout position [cm]	64.80
Spot tune ID	4.0
Range shifter	No
Range modulator	No
NumberOfEnergyLayers	40
Number of spots	1941
Beam meterset [10^6 NP/fx]	130711.5911
Min spot meterset [10^6 NP/fx]	0.9530
Max spot meterset [10^6 NP/fx]	379.9836

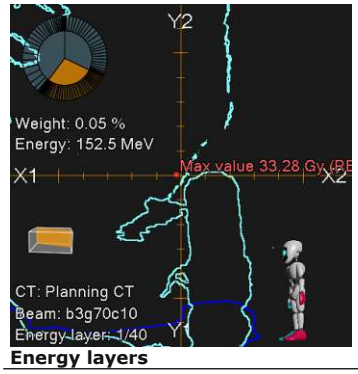

Energy layers

No	Energy [MeV]	Rel. weight [%]	[10^6 NP/fx]	No. of spots	Spot spacing [cm]	Min spot meterset [10^6 NP/fx]	Max spot meterset [10^6 NP/fx]	No. of paintings	NP/spill [10^6 NP]	Spill [sec]	Deg
1	152.50	0.05	61.6245	1	0.51	61.6245	61.6245	1	20000	10	0.00
2	150.40	0.54	710.0141	9	0.51	1.1986	378.2291	1	20000	10	0.00
3	148.20	2.64	3444.6088	14	0.51	3.0103	379.8705	1	20000	10	0.00
4	146.50	2.34	3052.7483	15	0.51	4.7290	377.2670	1	20000	10	0.00
5	144.80	2.66	3475.9400	23	0.50	1.3677	379.9836	1	20000	10	0.00
6	143.10	2.30	3012.5649	24	0.50	0.9974	354.3628	1	20000	10	0.00
7	141.40	2.35	3068.5793	31	0.50	1.0334	379.5781	1	20000	10	0.00
8	139.70	2.15	2810.0334	32	0.50	1.8415	374.8458	1	20000	10	0.00
9	137.90	2.48	3241.5361	36	0.50	1.2730	355.6287	1	20000	10	0.00
10	136.20	2.45	3206.9710	42	0.49	1.2654	330.9120	1	20000	10	0.00
11	134.40	3.80	4968.0361	46	0.49	0.9886	366.3003	1	20000	10	0.00
12	132.60	3.31	4326.5814	52	0.49	1.0551	353.4108	1	20000	10	0.00
13	130.80	3.68	4804.5192	61	0.49	1.0312	369.0704	1	20000	10	0.00
14	129.00	4.28	5595.9958	68	0.50	1.0311	376.9012	1	20000	10	0.00
15	127.20	3.25	4248.1999	72	0.50	0.9713	364.7510	1	20000	10	0.00
16	125.30	4.64	6065.1877	83	0.50	0.9867	379.6584	1	20000	10	0.00

17	123.40	4.39	5739.0743	83	0.50	0.9941	379.3535	1	20000	10	0.00
18	122.10	4.34	5668.4666	80	0.50	0.9981	376.2556	1	20000	10	0.00
19	120.90	3.58	4674.2026	83	0.50	1.0105	376.3007	1	20000	10	0.00
20	119.60	4.21	5505.4456	87	0.50	1.0048	373.7556	1	20000	10	0.00
21	118.30	3.87	5059.9912	92	0.50	1.0331	378.3542	1	20000	10	0.00
22	117.00	4.08	5329.7404	83	0.50	1.0385	372.2445	1	20000	10	0.00
23	115.70	3.83	5006.4458	91	0.50	0.9636	318.1067	1	20000	10	0.00
24	114.30	3.29	4298.9029	87	0.50	0.9752	359.2122	1	20000	10	0.00
25	113.00	2.60	3402.1392	86	0.50	0.9753	288.6669	1	20000	10	0.00
26	111.60	4.62	6034.3300	89	0.50	0.9692	377.7670	1	20000	10	0.00
27	110.30	3.84	5024.0969	82	0.51	0.9530	377.1878	1	20000	10	0.00
28	108.90	2.53	3308.0595	72	0.51	0.9748	254.8688	1	20000	10	0.00
29	107.50	2.16	2821.0825	73	0.51	0.9853	378.6242	1	20000	10	0.00
30	106.10	1.75	2286.8816	59	0.51	1.0002	336.6002	1	20000	10	0.00
31	104.70	1.68	2198.0128	44	0.51	0.9746	352.1991	1	20000	10	0.00
32	103.30	1.15	1500.7913	30	0.51	1.0341	309.8031	1	20000	10	0.00
33	101.80	1.27	1655.7931	24	0.51	0.9951	379.7967	1	20000	10	0.00
34	100.40	1.46	1903.3824	23	0.51	0.9983	353.6363	1	20000	10	0.00
35	98.90	1.16	1509.9860	21	0.51	1.0092	374.5322	1	20000	10	0.00
36	97.40	0.87	1131.1362	20	0.51	0.9993	316.3806	1	20000	10	0.00
37	95.90	0.27	348.1356	11	0.52	1.1322	177.2883	1	20000	10	0.00
38	94.30	0.12	159.9338	7	0.52	1.1628	123.5587	1	20000	10	0.00
39	92.80	0.03	33.0695	3	0.53	1.1022	30.6600	1	20000	10	0.00
40	91.20	0.01	19.3511	2	0.53	1.1071	18.2440	1	20000	10	0.00

Beam data

Beam number	4
Beam name	b1g35c270
Beam description	
Gantry angle [deg]	35.0
Couch rotation angle [deg]	270.0
Isocenter [cm]	case2_copy 2_moved 1 - Right-Left: 8.27 Inf-Sup: -51.47 Post-Ant: 3.47
Treatment technique	Pencil Beam Scanning
Number of fractions	1
Beam weight [%]	39.77
Dose calculation algorithm	Monte Carlo, Version 5.3 Uncert: 0.49% Tot. ions: 24772608
Treatment unit	G_IR3_p_11A
Commission time	12 Jul 2021, 09:55:32 (hr:min:sec)
SnoutID	HBL_Nozzle
Snout position [cm]	64.80
Spot tune ID	4.0
Range shifter	No
Range modulator	No
NumberOfEnergyLayers	33
Number of spots	3702
Beam meterset [10^6 NP/fx]	185477.1869
Min spot meterset [10^6 NP/fx]	0.9593
Max spot meterset [10^6 NP/fx]	329.1799

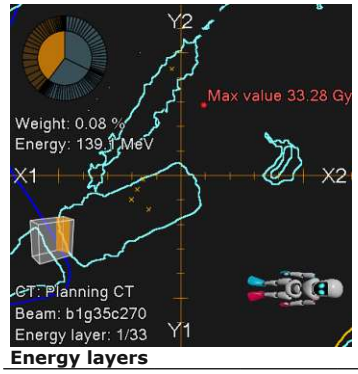

Energy layers

No	Energy [MeV]	Rel. weight [%]	[10^6 NP/fx]	No. of spots	Spot spacing [cm]	Min spot meterset [10^6 NP/fx]	Max spot meterset [10^6 NP/fx]	No. of paintings	NP/spill [10^6 NP]	Spill [sec]	Deg
1	139.10	0.08	145.0186	5	0.47	2.3171	50.4734	1	20000	10	0.00
2	137.40	0.60	1117.9639	11	0.47	1.2988	231.3230	1	20000	10	0.00
3	135.60	1.33	2458.2664	32	0.47	1.8256	252.1365	1	20000	10	0.00
4	133.80	3.94	7300.9793	61	0.47	1.2530	329.1799	1	20000	10	0.00
5	132.00	6.39	11844.8836	90	0.47	1.2157	292.8885	1	20000	10	0.00
6	130.20	7.52	13952.3425	113	0.47	1.5450	298.9848	1	20000	10	0.00
7	128.40	7.83	14525.0765	134	0.47	1.6872	293.1497	1	20000	10	0.00
8	126.50	7.57	14041.9632	150	0.47	2.3141	267.4708	1	20000	10	0.00
9	124.70	7.05	13068.0291	168	0.46	1.1466	228.6401	1	20000	10	0.00
10	122.80	6.87	12748.8004	178	0.46	1.0577	307.7674	1	20000	10	0.00

11	121.50	4.97	9223.7967	185	0.46	0.9594	249.1073	1	20000	10	0.00
12	120.20	4.55	8434.9628	201	0.46	1.0026	213.6984	1	20000	10	0.00
13	118.90	4.67	8665.9285	200	0.46	0.9782	238.4551	1	20000	10	0.00
14	117.60	4.23	7851.7960	203	0.46	0.9932	226.2933	1	20000	10	0.00
15	116.30	3.66	6792.4140	201	0.46	0.9658	229.4445	1	20000	10	0.00
16	115.00	3.62	6710.6173	192	0.46	0.9685	210.8414	1	20000	10	0.00
17	113.70	3.15	5849.9924	185	0.46	0.9732	241.8705	1	20000	10	0.00
18	112.30	2.00	3706.3483	157	0.46	0.9947	149.8419	1	20000	10	0.00
19	111.60	2.41	4465.9373	150	0.46	0.9593	224.3334	1	20000	10	0.00
20	110.30	3.28	6079.7759	151	0.47	0.9668	225.8997	1	20000	10	0.00
21	108.90	2.38	4416.2654	138	0.47	0.9660	185.0286	1	20000	10	0.00
22	107.50	1.95	3624.2418	129	0.47	0.9699	128.3245	1	20000	10	0.00
23	106.10	1.55	2874.1906	120	0.47	0.9872	144.9145	1	20000	10	0.00
24	104.70	1.69	3128.7948	100	0.47	0.9838	250.8549	1	20000	10	0.00
25	103.30	1.59	2956.6460	92	0.47	0.9809	219.3343	1	20000	10	0.00
26	101.80	1.38	2568.4784	78	0.47	1.0351	236.6386	1	20000	10	0.00
27	100.40	0.97	1795.4654	69	0.47	0.9671	177.3177	1	20000	10	0.00
28	98.90	0.46	858.8226	50	0.48	1.0098	114.3441	1	20000	10	0.00
29	97.40	0.50	921.0633	34	0.48	0.9817	255.3799	1	20000	10	0.00
30	95.90	0.51	951.0344	34	0.48	0.9971	166.0371	1	20000	10	0.00
31	94.30	0.70	1299.6223	37	0.48	1.2869	112.4883	1	20000	10	0.00
32	92.80	0.45	837.1455	32	0.49	1.3896	229.8694	1	20000	10	0.00
33	91.20	0.14	260.5240	22	0.49	1.0566	123.5333	1	20000	10	0.00

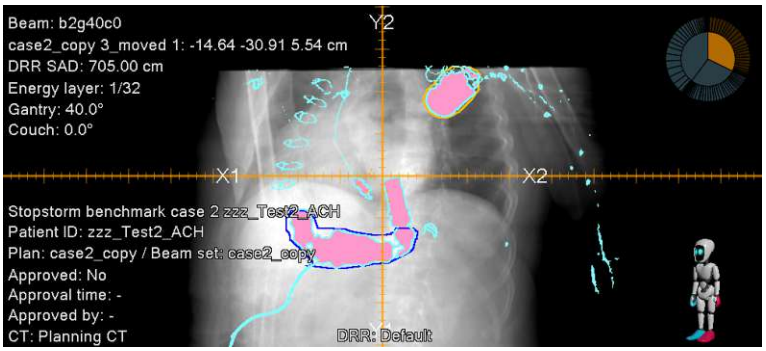

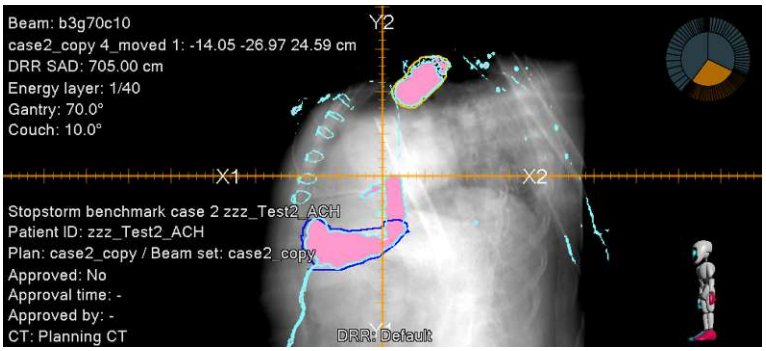

Patient name	Stopstorm benchmark case 2 zzz_Test2_ACH	Report creation time	05 Dec 2023, 16:31:24 (hr:min:sec)
Patient ID	zzz_Test2_ACH	Plan last save time	06 Nov 2023, 13:51:48 (hr:min:sec)
Treatment plan name	case2_copy	Plan approved by	-
Plan and structure set approved	No	Plan approval time	-

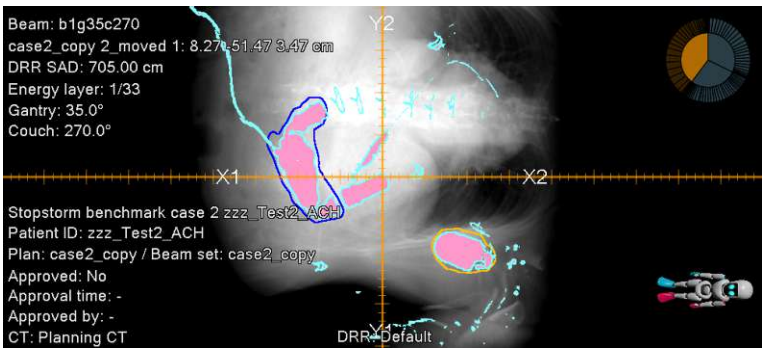

Patient name	Stopstorm benchmark case 3 zzz_Test3_ACH	Report creation time	05 Dec 2023, 16:33:24 (hr:min:sec)
Patient ID	zzz_Test3_ACH	Plan last save time	24 Oct 2023, 16:46:52 (hr:min:sec)
Treatment plan name	VT_STOPSTORM_CASE3_Test01_05102023	Plan approved by	-
Plan and structure set approved	No	Plan approval time	-

Plan Report

Patient data

Patient ID	zzz_Test3_ACH
Patient name	Stopstorm benchmark case 3 zzz_Test3_ACH
Patient gender	Male
Patient birth date	
Case data	
Case name	Case 1
Physician	-
Body site	-

Treatment plan data

Treatment plan name	VT_STOPSTORM_CASE3_Test01_05102023
Plan last save time	24 Oct 2023, 16:46:52 (hr:min:sec)
Planned by	
Number of beam sets	1
Treatment plan approval data	
Approved	No
Approved by	-
Approval time	-
Plan comment	STOPSTORM - RAVENTA CASE 3
Total dose image set	CT Planning
External ROI	External

General data

Treatment planning system	RayStation 11B (12.1.0.1221)
Report creation time	05 Dec 2023, 16:33:24 (hr:min:sec)
Template name	2022-04-25_PlanReportTemplate_11BSP1
Patient coordinate system	IEC 61217

ROI properties

No material override

Beam set overview

Beam set name	VT_STOPSTORM_CAS
Treatment technique	Pencil Beam Scanning
Treatment unit	G_IR3_p_11A
Planning image set	CT Planning
Patient treatment position	HFS : Head First Supine
Number of beams	3
RBE model	Constant 1.1, Constant factor

Warnings [VT_STOPSTORM_CAS]

Warnings confirmed at report creation by: MEDAUSTRON\AC1.

- There are spots with meterset values above the machine default for beams: b1g40c230, b2g25c0, b3g70c10
- The primary prescription is not fulfilled.
  Prescription: 32.00 Gy (RBE) x 1 fx = 32.00 Gy (RBE)
  Median dose (D50%)
  ROI: TV
  Computed dose: 32.17 Gy (RBE) x 1 fx = 32.17 Gy (RBE)
  Relates to beam set dose
- The following prescription is not fulfilled.
  Prescription: 25.00 Gy (RBE) x 1 fx = 25.00 Gy (RBE)
  Median dose (D50%)
  ROI: PTV
  Computed dose: 27.39 Gy (RBE) x 1 fx = 27.39 Gy (RBE)
  Relates to beam set dose
- The following image sets have original patient ID different from patient:
  CT Image CT Planning: 15 Apr 2019, 11:30:15 (hr:min:sec) was 'zSTOPBM03'

Beam set report

Beam set data

Beam set name	VT_STOPSTORM_CAS
Modality	Protons
Treatment technique	Pencil Beam Scanning
Treatment unit	G_IR3_p_11A
Commission time	12 Jul 2021, 09:55:32 (hr:min:sec)
Number of beams	3
DICOM plan UID	1.2.752.243.1.1.20231024164652852.3500.35021
Planning image set	
Name	CT Planning
Image modality	CT
Imaging system	Generic CT 20 Jul 2011, 15:25:00 (hr:min:sec)
Patient scanning position	HFS
Series date and time	15 Apr 2019, 11:31:17 (hr:min:sec)
Acquisition date and time	15 Apr 2019, 11:30:15 (hr:min:sec)
Is a converted image set	No
Patient treatment position	HFS : Head First Supine
Dose calculation algorithm	Monte Carlo, Version 5.3 Tot. ions: 72253440
RBE model	Constant 1.1, Constant factor
Density calculation algorithm version	2.1
Number of fractions	1
ROI(s) with material override	
Beam set approval data	
Approved	No
Approved by	-
Approval time	-
Structure set UID	1.2.752.243.1.1.20231012161450022.1200.76870
Structure set approval data	
Approved	No
Approved by	-
Approval time	-

Beam data overview [Isocenter: VT_STOPSTORM_CAS 1_moved 6, **R-L:** 11.52 cm, **I-S:** -6.30 cm, **P-A:** 3.16 cm**]**

#	Beam name	Gantry angle [deg]	Couch rotation angle [deg]	Snout ID / position [cm]	Air gap Min / CAX [cm]	Range shifter	Beam meterset [10^6 NP/fx]
1	b1g40c230	40.0	230.0	HBL_Nozzle / 64.80	16.00 / 23.61	No	213203.7833

Beam data overview [Isocenter: VT_STOPSTORM_CAS 1_moved 5, **R-L:** -15.47 cm, **I-S:** 9.13 cm, **P-A:** -5.10 cm**]**

#	Beam name	Gantry angle [deg]	Couch rotation angle [deg]	Snout ID / position [cm]	Air gap Min / CAX [cm]	Range shifter	Beam meterset [10^6 NP/fx]
2	b2g25c0	25.0	0.0	HBL_Nozzle / 64.80	16.42 / 19.13	No	198850.5821

Beam data overview [Isocenter: VT_STOPSTORM_CAS 1_moved 4, **R-L:** -22.52 cm, **I-S:** 12.85 cm, **P-A:** 19.37 cm**]**

#	Beam name	Gantry angle [deg]	Couch rotation angle [deg]	Snout ID / position [cm]	Air gap Min / CAX [cm]	Range shifter	Beam meterset [10^6 NP/fx]
3	b3g70c10	70.0	10.0	HBL_Nozzle / 64.80	20.00 / 28.90	No	210038.7713

Objectives

Dose	Function	ROI	Description	Robust	Weight	Value
	Physical composite objective					0.1503
Plan (RBE)	Max dose	A_LAD	Max dose 24.00 Gy (RBE)	No	100.00	0.0044
Plan (RBE)	Uniform dose	PTV-clTV-arteries	Uniform dose 25.00 Gy (RBE)	No	50.00	0.0609
Beam set (RBE)	Min DVH	PTV-arteries	Min DVH 25.00 Gy (RBE) to 60.00% volume, All beams	No	100.00	0.0000
Beam set (RBE)	Max dose	PTV-clTV	Max dose 40.00 Gy (RBE), All beams	No	100.00	5.3051E-5
Plan (RBE)	Max dose	ring	Max dose 23.80 Gy (RBE)	No	12.00	4.1134E-4
Plan (RBE)	Max EUD	ring	Max EUD 10.80 Gy (RBE), Parameter A 1	No	6.00	2.6893E-4
Plan (RBE)	Dose fall-off	ring	Dose fall-off [H]30.00 Gy (RBE) [L]19.00 Gy (RBE), Low dose distance 1.00 cm	No	5.00	0.0048
Beam set (RBE)	Max dose	ring	Max dose 13.00 Gy (RBE), Beam 'b1g40c230'	No	10.00	3.9060E-5
Beam set (RBE)	Max dose	ring	Max dose 13.00 Gy (RBE), Beam 'b3g70c10'	No	10.00	2.2874E-6
Beam set (RBE)	Max dose	ring	Max dose 13.00 Gy (RBE), Beam 'b2g25c0'	No	10.00	1.3860E-6
Plan (RBE)	Max dose	Stomach	Max dose 0.10 Gy (RBE)	No	40.00	0.0000
Plan (RBE)	Max DVH	TENTATIVE_SKIN	Max DVH 6.00 Gy (RBE) to 0.05% volume	No	12.00	0.0010
Plan (RBE)	Min DVH	TV_exp-LAD	Min DVH 32.00 Gy (RBE) to 96.00% volume	No	110.00	0.0188
Plan (RBE)	Max dose	TV_expanded	Max dose 32.00 Gy (RBE)	No	90.00	0.0073
Plan (RBE)	Uniform dose	TV_exp-LAD	Uniform dose 32.00 Gy (RBE)	No	80.00	0.0385
Beam set (RBE)	Min DVH	TV_exp-LAD	Min DVH 32.00 Gy (RBE) to 70.00% volume, All beams	No	50.00	0.0020
Beam set (RBE)	Max dose	TV_expanded	Max dose 46.00 Gy (RBE), All beams	No	60.00	2.2349E-6
Plan (RBE)	Max dose	PTV-clTV	Max dose 27.00 Gy (RBE)	No	90.00	0.0017
Plan (RBE)	Max DVH	skin_to_spare	Max DVH 7.20 Gy (RBE) to 1.00% volume	No	18.00	1.2378E-4
Plan (RBE)	Min DVH	PTV-arteries	Min DVH 25.00 Gy (RBE) to 96.00% volume	No	100.00	0.0022
Plan (RBE)	Max DVH	A_LM	Max DVH 18.00 Gy (RBE) to 1.00% volume	No	5.00	8.2290E-9
Plan (RBE)	Max dose	A_LCX	Max dose 24.00 Gy (RBE)	No	90.00	0.0067
Plan (RBE)	Max dose	A_Aorta	Max dose 24.40 Gy (RBE)	No	65.00	9.5331E-6
Plan (RBE)	Max DVH	A_Pulmonary	Max DVH 24.00 Gy (RBE) to 0.01% volume	No	60.00	2.0966E-4
Plan (RBE)	Max DVH	A_Aorta	Max DVH 24.00 Gy (RBE) to 0.01% volume	No	80.00	6.0313E-7
Plan (RBE)	Max DVH	hs_arteris	Max DVH 24.80 Gy (RBE) to 1.00% volume	No	15.00	7.7427E-4

Constraints

No constraints defined

Patient name	Stopstorm benchmark case 3 zzz_Test3_ACH	Report creation time	05 Dec 2023, 16:33:24 (hr:min:sec)
Patient ID	zzz_Test3_ACH	Plan last save time	24 Oct 2023, 16:46:52 (hr:min:sec)
Treatment plan name	VT_STOPSTORM_CASE3_Test01_05122023	Plan approved by	-
Plan and structure set approved	No	Plan approval time	-

Prescription

Primary prescription

Treatment site	TV
Prescription type	Median dose (D50%)
Prescribed dose	32.00 Gy (RBE) x 1 fx = 32.00 Gy (RBE)
Dose type	Relates to beam set dose
Fulfillment	Not fulfilled (32.17 Gy (RBE))

Treatment site	PTV
Prescription type	Median dose (D50%)
Prescribed dose	25.00 Gy (RBE) x 1 fx = 25.00 Gy (RBE)
Dose type	Relates to beam set dose
Fulfillment	Not fulfilled (27.39 Gy (RBE))

Nominal contributions

	Treatment site: TV **Prescription type:** **Median dose (D50%)**		**PTV** **Median dose (D50%)**
Beam no.	Beam name	Nominal contribution/fx [Gy (RBE)]	Nominal contribution/fx [Gy (RBE)]
1	b1g40c230	10.97	8.57
2	b2g25c0	10.23	7.99
3	b3g70c10	10.80	8.44
-	Total:	32.00	25.00

Nominal contribution can be used to track nominal progress towards a prescription during treatment delivery.
The table presents nominal contribution per beam and prescription.
Nominal contribution is defined as prescribed fraction dose weighted with each beam's relative weight (based on beam meterset).

Note: Nominal contribution is unrelated to the calculated beam set dose in RayStation, and is based solely on the prescribed fraction dose. It is not affected by whether the prescription is fulfilled or not.

Note: Nominal contributions will only be DICOM exported if corresponding setting is made in the machine.

Beam collision status

Beam #	Beam name	Collision status	
		Nominal	Within setup margins
1	b1g40c230	Unknown	Unknown
2	b2g25c0	Unknown	Unknown
3	b3g70c10	Unknown	Unknown

Setup margins

Lateral [cm]		Longitudinal [cm]		Vertical [cm]		Yaw [deg]		Pitch [deg]		Roll [deg]	
Lower	Upper	Lower	Upper	Lower	Upper	Lower	Upper	Lower	Upper	Lower	Upper
-2.00	2.00	-2.00	2.00	-2.00	2.00	-3.00	3.00	-3.00	3.00	-3.00	3.00

Patient setup

Localization point
No localization point defined.
Patient setup
No localization point defined.
Patient setup
No localization point defined.
Patient setup
No localization point defined.

BeamsetDoseData

Isocenter name	VT_STOPSTORM_CAS 1_moved 6
Isocenter [cm]	Right-Left: 11.52 Inf-Sup: -6.30 Post-Ant: 3.16
Dose type	RBE
Dose grid resolution [cm]	Right-Left: 0.20 Inf-Sup: 0.20 Post-Ant: 0.20

BeamsetDoseData

Isocenter name	VT_STOPSTORM_CAS 1_moved 5
Isocenter [cm]	Right-Left: -15.47 Inf-Sup: 9.13 Post-Ant: -5.10
Dose type	RBE
Dose grid resolution [cm]	Right-Left: 0.20 Inf-Sup: 0.20 Post-Ant: 0.20

Patient name	Stopstorm benchmark case 3 zzz_Test3_ACH	Report creation time	05 Dec 2023, 16:33:24 (hr:min:sec)
Patient ID	zzz_Test3_ACH	Plan last save time	24 Oct 2023, 16:46:52 (hr:min:sec)
Treatment plan name	VT_STOPSTORM_CASE3_Test01_05102023	Plan approved by	-
Plan and structure set approved	No	Plan approval time	-

BeamsetDoseData

Isocenter name	VT_STOPSTORM_CAS 1_moved 4
Isocenter [cm]	Right-Left: -22.52 Inf-Sup: 12.85 Post-Ant: 19.37
Dose type	RBE
Dose grid resolution [cm]	Right-Left: 0.20 Inf-Sup: 0.20 Post-Ant: 0.20

Points of Interest

No POI geometries found

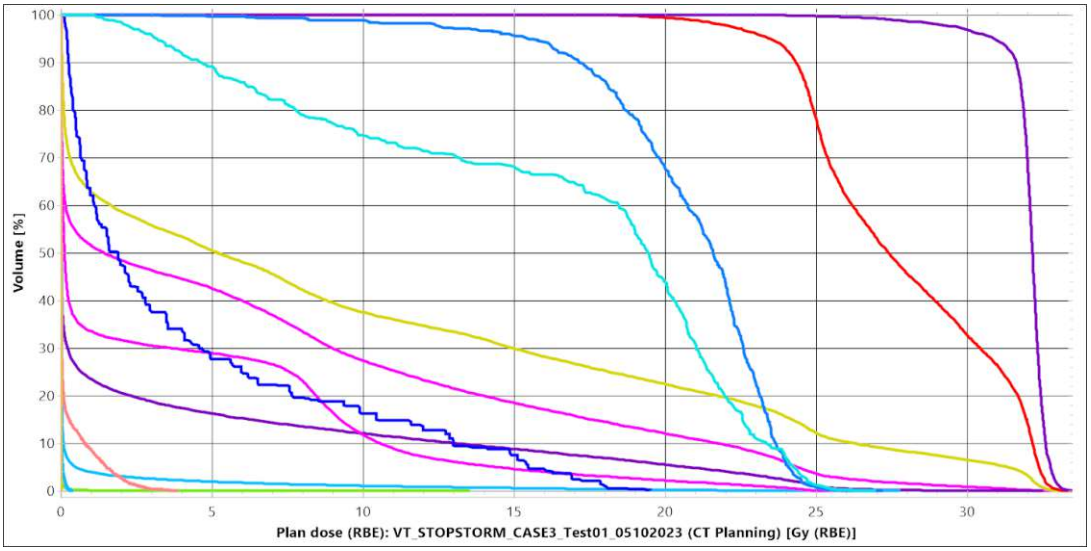

POI dose statistics

No POI dose statistics

ROI dose statistics [beam set dose]

Name	Volume [cm³]	D99 [Gy (RBE)]	D98 [Gy (RBE)]	D95 [Gy (RBE)]	Average [Gy (RBE)]	D50 [Gy (RBE)]	D2 [Gy (RBE)]	D1 [Gy (RBE)]	% outside grid
A_Aorta	361.37	0.00	0.00	0.00	0.31	0.01	4.68	10.32	0
A_LAD	2.62	8.18	12.38	15.44	20.76	21.59	24.52	24.92	0
A_LCX	1.75	1.44	2.07	3.18	16.36	19.43	24.72	25.19	0
A_LM	0.53	0.12	0.15	0.21	4.23	1.90	17.87	18.01	0
A_Pulmonary	144.92	0.00	0.00	0.00	3.35	0.12	20.41	23.10	0
A_RCA	2.35	0.00	0.00	0.00	0.02	0.01	0.14	0.20	0
arm_block	424.52	0.00	0.00	0.00	0.00	0.00	0.00	0.00	0
Atrium_L	211.92	0.00	0.00	0.00	2.81	0.01	24.32	25.11	0
Atrium_R	355.76	0.00	0.00	0.00	0.01	0.00	0.04	0.08	0
AVN	4.43	0.02	0.03	0.03	0.93	0.23	7.05	8.79	0
Bronchus_Main	14.40	0.00	0.00	0.00	0.21	0.00	2.16	2.55	0
clTV	34.71	23.39	24.56	27.19	30.88	31.59	32.78	32.89	0
Colon	511.91	0.00	0.00	0.00	0.00	0.00	0.00	0.00	0
Esophagus	41.21	0.00	0.00	0.00	0.00	0.00	0.02	0.02	0
External	31921.42	0.00	0.00	0.00	0.43	0.00	7.25	11.18	0

Heart	1395.70	0.00	0.00	0.00	4.92	0.05	29.86	31.88	0
hs_arteris	0.65	21.17	22.25	23.32	24.49	24.57	25.56	25.83	0
ICD	49.77	0.00	0.00	0.00	0.00	0.00	0.00	0.00	0
Liver	1785.40	0.00	0.00	0.00	0.00	0.00	0.00	0.00	0
Lung_L	1647.53	0.00	0.00	0.00	1.38	0.06	11.70	14.11	0
Lung_R	1768.05	0.00	0.00	0.00	0.00	0.00	0.01	0.02	0
PTV	82.61	20.70	21.80	23.47	27.86	27.39	32.59	32.75	0
PTV-arteries	74.70	23.77	24.03	24.42	28.31	28.05	32.60	32.76	0
PTV-clTV	30.71	19.40	20.27	22.05	24.84	24.99	27.29	27.64	0
PTV-clTV-arteries	26.41	23.34	23.64	24.01	25.20	25.09	27.34	27.68	0
ring	427.41	0.17	0.23	0.46	10.96	10.57	24.17	24.55	0
SAN	4.28	0.00	0.00	0.00	0.00	0.00	0.00	0.00	0
skin_to_spare	27.10	0.00	0.00	0.00	2.14	0.30	7.20	7.57	0
SpinalCanal	47.91	0.00	0.00	0.00	0.00	0.00	0.00	0.00	0
Stomach	323.75	0.00	0.00	0.00	0.00	0.00	0.01	0.01	0
TENTATIVE_SKIN	1179.79	0.00	0.00	0.00	0.12	0.00	2.69	5.48	0
Trachea	27.16	0.00	0.00	0.00	0.00	0.00	0.01	0.01	0
TV	14.54	27.32	28.99	30.88	32.02	32.17	32.92	33.05	0
TV_expanded	23.52	25.12	27.26	29.44	31.63	32.00	32.85	32.97	0
TV_exp-LAD	22.23	29.41	29.86	30.50	31.87	32.03	32.86	32.99	0
V_Venacava_I	26.42	0.00	0.00	0.00	0.00	0.00	0.00	0.00	0
V_Venacava_S	44.59	0.00	0.00	0.00	0.00	0.00	0.00	0.00	0
Valve_Aortic	14.78	0.02	0.02	0.03	2.91	0.28	19.86	21.32	0
Valve_Mitral	9.92	0.02	0.02	0.03	8.64	2.39	25.65	25.83	0
Valve_Pulmonic	12.48	6.05	6.56	7.51	11.72	9.77	23.57	24.21	0
Valve_Tricuspid	14.62	0.00	0.00	0.00	0.35	0.02	4.09	5.83	0
Ventricle_L	351.60	0.01	0.01	0.02	9.60	5.18	32.21	32.41	0
Ventricle_L_A	34.19	0.07	0.10	0.81	16.64	15.42	32.56	32.66	0
Ventricle_L_I	22.70	0.00	0.00	0.01	0.03	0.03	0.11	0.13	0
Ventricle_L_L	36.46	0.02	0.02	0.03	5.11	0.60	30.24	32.26	0
Ventricle_L_S	37.50	0.02	0.04	0.07	15.96	16.70	32.58	32.75	0
Ventricle_R	264.84	0.00	0.00	0.00	6.60	1.42	26.94	29.64	0

External — This ROI is set as the external ROI that defines the outer border of the patient

Beam data

Beam number	1
Beam name	b1g40c230
Beam description	
Gantry angle [deg]	40.0
Couch rotation angle [deg]	230.0
Isocenter [cm]	VT_STOPSTORM_CAS 1_moved 6 - Right-Left: 11.52 Inf-Sup: -6.30 Post-Ant: 3.16
Treatment technique	Pencil Beam Scanning
Number of fractions	1
Beam weight [%]	34.27
Dose calculation algorithm	Monte Carlo, Version 5.3 Uncert: 0.50% Tot. ions: 24772608
Treatment unit	G_IR3_p_11A
Commission time	12 Jul 2021, 09:55:32 (hr:min:sec)
SnoutID	HBL_Nozzle
Snout position [cm]	64.80
Spot tune ID	4.0
Range shifter	No
Range modulator	No
NumberOfEnergyLayers	50
Number of spots	4141
Beam meterset [10^6 NP/fx]	213203.7833
Min spot meterset [10^6 NP/fx]	0.9627
Max spot meterset [10^6 NP/fx]	379.8295

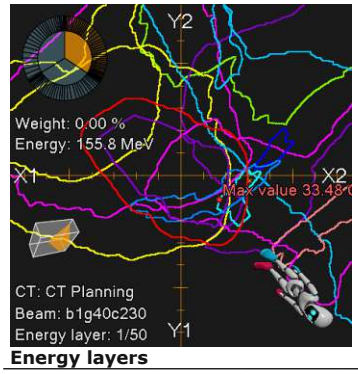

Energy layers

No	Energy [MeV]	Rel. weight [%]	[10^6 NP/fx]	No. of spots	Spot spacing [cm]	Min spot meterset [10^6 NP/fx]	Max spot meterset [10^6 NP/fx]	No. of paintings	NP/spill [10^6 NP]	Spill [sec]	Deg
1	155.80	0.00	2.0278	1	0.54	2.0278	2.0278	1	20000	10	0.00
2	153.60	0.62	1329.5166	11	0.54	1.3469	379.5411	1	20000	10	0.00
3	151.50	1.16	2478.7541	24	0.53	1.1139	379.8016	1	20000	10	0.00
4	149.30	1.85	3952.8442	36	0.53	1.2326	379.5317	1	20000	10	0.00
5	147.60	2.23	4747.8884	40	0.53	1.2082	379.8295	1	20000	10	0.00
6	145.40	3.23	6887.0492	50	0.52	1.0166	379.1524	1	20000	10	0.00
7	143.70	2.49	5302.8736	51	0.52	1.1655	378.9854	1	20000	10	0.00
8	142.00	2.82	6014.9965	57	0.51	1.0552	379.2166	1	20000	10	0.00
9	140.30	2.94	6261.9303	56	0.51	1.1460	379.5268	1	20000	10	0.00
10	138.50	2.37	5048.6465	65	0.51	1.0121	379.0679	1	20000	10	0.00
11	136.80	2.65	5643.4764	67	0.50	1.0225	378.9871	1	20000	10	0.00
12	135.00	2.27	4844.0996	74	0.50	1.0797	379.2692	1	20000	10	0.00
13	133.20	2.52	5380.2351	96	0.50	0.9935	379.2380	1	20000	10	0.00
14	131.40	2.37	5062.5352	107	0.50	1.0097	263.5155	1	20000	10	0.00
15	129.60	3.76	8018.2410	113	0.50	0.9638	379.4435	1	20000	10	0.00
16	127.80	4.22	8987.5185	119	0.49	0.9635	362.9177	1	20000	10	0.00

17	125.90	4.28	9116.7469	125	0.49	1.0180	374.9290	1	20000	10	0.00
18	124.00	4.52	9635.4614	125	0.49	0.9716	364.8470	1	20000	10	0.00
19	122.10	4.09	8729.0463	132	0.49	1.0306	320.5583	1	20000	10	0.00
20	120.90	2.87	6109.6017	130	0.49	1.0423	278.9528	1	20000	10	0.00
21	119.60	3.37	7189.2638	144	0.49	1.0055	248.9883	1	20000	10	0.00
22	118.30	3.00	6393.8826	153	0.49	0.9734	240.3478	1	20000	10	0.00
23	117.00	3.14	6695.8048	154	0.49	0.9627	360.1298	1	20000	10	0.00
24	115.70	3.03	6466.1006	150	0.49	0.9744	379.0390	1	20000	10	0.00
25	114.30	2.56	5466.0636	140	0.49	1.0489	284.1979	1	20000	10	0.00
26	113.00	2.46	5242.5281	137	0.49	1.0102	217.6523	1	20000	10	0.00
27	111.60	2.25	4801.5305	130	0.49	1.0128	289.5206	1	20000	10	0.00
28	110.30	2.44	5194.6521	134	0.49	1.0007	242.2045	1	20000	10	0.00
29	108.90	2.48	5294.1401	124	0.49	0.9977	261.1735	1	20000	10	0.00
30	107.50	2.30	4898.0748	123	0.49	0.9791	230.3380	1	20000	10	0.00
31	106.10	2.05	4380.5475	119	0.49	1.0066	193.9089	1	20000	10	0.00
32	104.70	2.19	4675.4227	118	0.49	1.0144	190.8892	1	20000	10	0.00
33	103.30	1.85	3940.2456	115	0.49	1.0244	244.8034	1	20000	10	0.00
34	101.80	2.39	5103.3463	105	0.49	1.0277	280.2276	1	20000	10	0.00
35	100.40	1.52	3237.9939	101	0.50	0.9736	266.6700	1	20000	10	0.00
36	98.90	1.30	2780.8309	80	0.50	1.0250	215.3871	1	20000	10	0.00
37	97.40	1.21	2585.1509	78	0.50	1.0879	208.6046	1	20000	10	0.00
38	95.90	1.80	3839.5901	89	0.50	1.0639	228.5750	1	20000	10	0.00
39	94.30	1.02	2178.2160	81	0.50	1.0647	228.0019	1	20000	10	0.00
40	92.80	0.36	777.2814	70	0.51	1.0533	182.7615	1	20000	10	0.00
41	91.20	0.46	987.0544	53	0.51	1.1539	206.4180	1	20000	10	0.00
42	89.60	0.90	1921.3334	46	0.51	1.0649	296.0646	1	20000	10	0.00
43	88.00	0.44	936.3537	41	0.52	1.2255	124.1082	1	20000	10	0.00
44	86.40	0.29	613.7605	34	0.52	1.2249	95.3772	1	20000	10	0.00
45	84.70	0.58	1235.2168	34	0.52	1.2529	170.9380	1	20000	10	0.00
46	83.00	0.53	1122.7281	31	0.53	1.3369	154.5853	1	20000	10	0.00
47	81.30	0.36	763.7165	27	0.53	1.2305	158.5957	1	20000	10	0.00
48	79.60	0.35	739.4436	24	0.54	1.3452	170.6797	1	20000	10	0.00
49	77.80	0.08	172.5497	17	0.55	1.4113	50.3005	1	20000	10	0.00
50	76.00	0.01	17.4710	10	0.55	1.3915	2.2636	1	20000	10	0.00

	Patient name	Stopstorm benchmark case 3 zzz_Test3_ACH	Report creation time	05 Dec 2023, 16:33:24 (hr:min:sec)
	Patient ID	zzz_Test3_ACH	Plan last save time	24 Oct 2023, 16:46:52 (hr:min:sec)
	Treatment plan name	VT_STOPSTORM_CASE3_Test01_05122023	Plan approved by	-
	Plan and structure set approved	No	Plan approval time	-

Beam data

Beam number	2
Beam name	b2g25c0
Beam description	
Gantry angle [deg]	25.0
Couch rotation angle [deg]	0.0
Isocenter [cm]	VT_STOPSTORM_CAS 1_moved 5 - Right-Left: -15.47 Inf-Sup: 9.13 Post-Ant: -5.10
Treatment technique	Pencil Beam Scanning
Number of fractions	1
Beam weight [%]	31.96
Dose calculation algorithm	Monte Carlo, Version 5.3 Uncert: 0.49% Tot. ions: 22708224
Treatment unit	G_IR3_p_11A
Commission time	12 Jul 2021, 09:55:32 (hr:min:sec)
SnoutID	HBL_Nozzle
Snout position [cm]	64.80
Spot tune ID	4.0
Range shifter	No
Range modulator	No
NumberOfEnergyLayers	41
Number of spots	4159
Beam meterset [10^6 NP/fx]	198850.5821
Min spot meterset [10^6 NP/fx]	0.9559
Max spot meterset [10^6 NP/fx]	379.5557

Energy layers

No	Energy [MeV]	Rel. weight [%]	[10^6 NP/fx]	No. of spots	Spot spacing [cm]	Min spot meterset [10^6 NP/fx]	Max spot meterset [10^6 NP/fx]	No. of paintings	NP/spill [10^6 NP]	Spill [sec]	Deg
1	145.90	0.37	739.3969	16	0.50	1.1307	375.7072	1	20000	10	0.00
2	143.70	1.34	2664.2469	27	0.49	1.0549	340.7432	1	20000	10	0.00
3	142.00	1.85	3687.8958	37	0.49	1.1898	324.8496	1	20000	10	0.00
4	140.30	2.71	5397.1712	51	0.49	1.0085	379.5557	1	20000	10	0.00
5	138.50	2.82	5600.2910	62	0.49	1.0142	324.8998	1	20000	10	0.00
6	136.80	3.82	7594.1004	75	0.48	1.0214	376.5248	1	20000	10	0.00
7	135.00	2.51	4999.8392	87	0.48	0.9786	379.3646	1	20000	10	0.00
8	133.20	3.84	7633.1901	97	0.48	1.0859	378.7409	1	20000	10	0.00
9	131.40	4.59	9124.8979	103	0.48	0.9577	378.3492	1	20000	10	0.00
10	129.60	3.53	7014.1835	124	0.48	1.0502	278.4047	1	20000	10	0.00
11	127.80	3.59	7135.1849	129	0.48	0.9954	370.4307	1	20000	10	0.00
12	125.90	4.06	8078.4937	146	0.48	1.0043	375.5990	1	20000	10	0.00
13	124.00	5.96	11848.2157	151	0.48	1.0185	378.2169	1	20000	10	0.00
14	122.10	4.67	9290.7233	148	0.48	0.9809	373.9127	1	20000	10	0.00
15	120.90	4.05	8049.9105	155	0.48	0.9713	367.3058	1	20000	10	0.00

16	119.60	3.09	6146.7649	159	0.48	0.9899	361.7674	1	20000	10	0.00
17	118.30	3.09	6134.6370	159	0.48	1.0212	246.4556	1	20000	10	0.00
18	117.00	3.79	7535.1314	161	0.48	0.9797	318.0275	1	20000	10	0.00
19	115.70	3.48	6922.3623	153	0.48	1.0056	291.5900	1	20000	10	0.00
20	114.30	3.19	6341.7559	148	0.48	1.0068	329.7541	1	20000	10	0.00
21	113.00	2.84	5640.1903	149	0.48	1.0046	340.2126	1	20000	10	0.00
22	111.60	3.56	7071.2770	150	0.48	1.0183	352.5030	1	20000	10	0.00
23	110.30	3.34	6639.4822	145	0.48	0.9827	379.1963	1	20000	10	0.00
24	108.90	2.88	5729.2008	146	0.48	1.0023	331.7232	1	20000	10	0.00
25	107.50	2.21	4392.2797	139	0.48	0.9981	366.9906	1	20000	10	0.00
26	106.10	2.94	5852.6774	137	0.48	0.9996	288.2633	1	20000	10	0.00
27	104.70	3.18	6319.0543	127	0.48	1.0012	376.6664	1	20000	10	0.00
28	103.30	2.18	4331.8812	118	0.49	1.0117	229.3051	1	20000	10	0.00
29	101.80	1.88	3741.8191	97	0.49	1.0025	369.0336	1	20000	10	0.00
30	100.40	1.68	3347.9661	96	0.49	1.0156	260.6113	1	20000	10	0.00
31	98.90	2.16	4302.9761	109	0.49	1.0056	271.8331	1	20000	10	0.00
32	97.40	1.69	3359.0021	107	0.49	0.9641	274.4919	1	20000	10	0.00
33	95.90	0.83	1656.8183	93	0.49	1.0193	290.1588	1	20000	10	0.00
34	94.30	0.74	1471.0353	76	0.50	0.9559	202.6140	1	20000	10	0.00
35	92.80	0.49	982.6101	64	0.50	1.0394	139.8921	1	20000	10	0.00
36	91.20	0.34	670.7664	51	0.50	1.0504	130.1406	1	20000	10	0.00
37	89.60	0.13	262.1693	46	0.51	1.0720	81.0495	1	20000	10	0.00
38	88.00	0.18	352.2252	40	0.51	1.0580	107.4034	1	20000	10	0.00
39	86.40	0.21	415.1961	36	0.51	1.0619	135.8214	1	20000	10	0.00
40	84.70	0.17	347.7986	27	0.51	1.0631	117.2581	1	20000	10	0.00
41	83.00	0.01	25.7640	18	0.51	1.0642	1.9031	1	20000	10	0.00

Patient name	Stopstorm benchmark case 3 zzz_Test3_ACH	Report creation time	05 Dec 2023, 16:33:24 (hr:min:sec)
Patient ID	zzz_Test3_ACH	Plan last save time	24 Oct 2023, 16:46:52 (hr:min:sec)
Treatment plan name	VT_STOPSTORM_CASE3_Test01_05122023	Plan approved by	-
Plan and structure set approved	No	Plan approval time	-

Beam data

Beam number	3
Beam name	b3g70c10
Beam description	
Gantry angle [deg]	70.0
Couch rotation angle [deg]	10.0
Isocenter [cm]	VT_STOPSTORM_CAS 1_moved 4 - Right-Left: -22.52 Inf-Sup: 12.85 Post-Ant: 19.37
Treatment technique	Pencil Beam Scanning
Number of fractions	1
Beam weight [%]	33.76
Dose calculation algorithm	Monte Carlo, Version 5.3 Uncert: 0.50% Tot. ions: 24772608
Treatment unit	G_IR3_p_11A
Commission time	12 Jul 2021, 09:55:32 (hr:min:sec)
SnoutID	HBL_Nozzle
Snout position [cm]	64.80
Spot tune ID	4.0
Range shifter	No
Range modulator	No
NumberOfEnergyLayers	29
Number of spots	2970
Beam meterset [10^6 NP/fx]	210038.7713
Min spot meterset [10^6 NP/fx]	0.9746
Max spot meterset [10^6 NP/fx]	379.8251

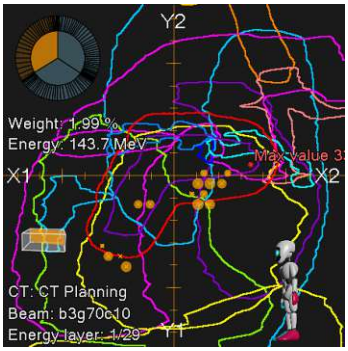

Patient name	Stopstorm benchmark case 3 zzz_Test3_ACH	Report creation time	05 Dec 2023, 16:33:24 (hr:min:sec)
Patient ID	zzz_Test3_ACH	Plan last save time	24 Oct 2023, 16:46:52 (hr:min:sec)
Treatment plan name	VT_STOPSTORM_CASE3_Test01_05102023	Plan approved by	-
Plan and structure set approved	No	Plan approval time	-

Energy layers

No	Energy [MeV]	Rel. weight [%]	[10⁶ NP/fx]	No. of spots	Spot spacing [cm]	Min spot meterset [10⁶ NP/fx]	Max spot meterset [10⁶ NP/fx]	No. of paintings	NP/spill [10⁶ NP]	Spill [sec]	Deg
1	143.70	1.99	4188.0629	15	0.54	80.7286	378.2270	1	20000	10	0.00
2	142.00	5.79	12167.9576	47	0.53	1.8649	379.1537	1	20000	10	0.00
3	140.30	6.04	12690.7441	68	0.53	1.1171	377.6062	1	20000	10	0.00
4	138.50	5.98	12551.5589	90	0.53	1.2820	377.8236	1	20000	10	0.00
5	136.80	6.37	13380.3490	103	0.53	1.2204	378.9093	1	20000	10	0.00
6	135.00	6.55	13762.6710	116	0.53	1.0273	379.8251	1	20000	10	0.00
7	133.20	6.11	12823.0334	130	0.53	1.0551	372.3934	1	20000	10	0.00
8	131.40	5.42	11378.6384	142	0.53	1.1120	316.5866	1	20000	10	0.00
9	129.60	4.93	10364.5102	141	0.53	1.0758	379.5954	1	20000	10	0.00
10	127.80	4.53	9521.2698	141	0.53	0.9912	377.6418	1	20000	10	0.00
11	125.90	4.83	10135.3575	153	0.53	0.9746	298.0231	1	20000	10	0.00
12	124.00	3.97	8335.2483	148	0.53	1.0477	378.2654	1	20000	10	0.00
13	122.10	4.09	8588.1993	156	0.53	1.0243	379.1600	1	20000	10	0.00
14	120.90	3.01	6312.7381	153	0.53	1.0472	379.5865	1	20000	10	0.00
15	119.60	2.82	5923.0574	146	0.53	1.0283	376.7936	1	20000	10	0.00
16	118.30	2.79	5856.8441	126	0.53	1.0258	368.5556	1	20000	10	0.00
17	117.00	2.35	4942.4564	118	0.53	0.9772	379.0928	1	20000	10	0.00
18	115.70	3.07	6445.9644	117	0.53	1.0366	374.5690	1	20000	10	0.00
19	114.30	3.18	6687.5998	128	0.53	1.0134	376.9328	1	20000	10	0.00
20	113.00	3.10	6519.1385	122	0.53	1.0220	369.8311	1	20000	10	0.00
21	111.60	2.32	4867.6601	109	0.54	1.0587	376.5888	1	20000	10	0.00
22	110.30	2.28	4796.9537	87	0.54	1.0248	379.4529	1	20000	10	0.00
23	108.90	1.97	4132.6071	71	0.54	1.0326	369.1661	1	20000	10	0.00
24	107.50	1.37	2886.1844	65	0.54	1.0356	378.5120	1	20000	10	0.00
25	106.10	1.68	3530.6448	68	0.54	1.0575	342.7517	1	20000	10	0.00
26	104.70	1.60	3368.1242	74	0.55	1.2486	338.8762	1	20000	10	0.00
27	103.30	0.77	1612.1302	64	0.55	1.2072	144.9335	1	20000	10	0.00
28	101.80	0.94	1977.8179	41	0.55	1.0521	229.9160	1	20000	10	0.00
29	100.40	0.14	291.2499	31	0.55	1.3760	86.3078	1	20000	10	0.00

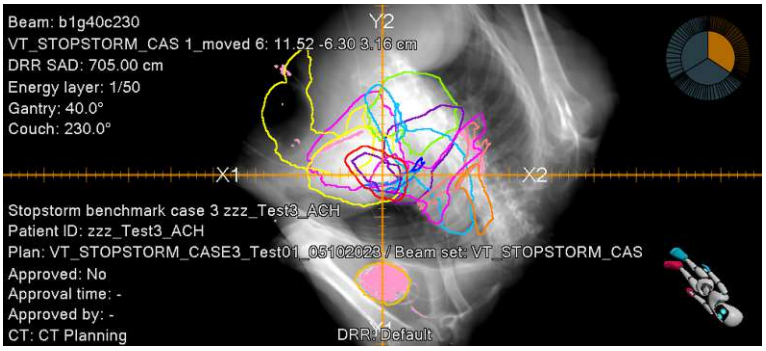

Patient name	Stopstorm benchmark case 3 zzz_Test3_ACH	Report creation time	05 Dec 2023, 16:33:24 (hr:min:sec)
Patient ID	zzz_Test3_ACH	Plan last save time	24 Oct 2023, 16:46:52 (hr:min:sec)
Treatment plan name	VT_STOPSTORM_CASE3_Test01_05102023	Plan approved by	-
Plan and structure set approved	No	Plan approval time	-

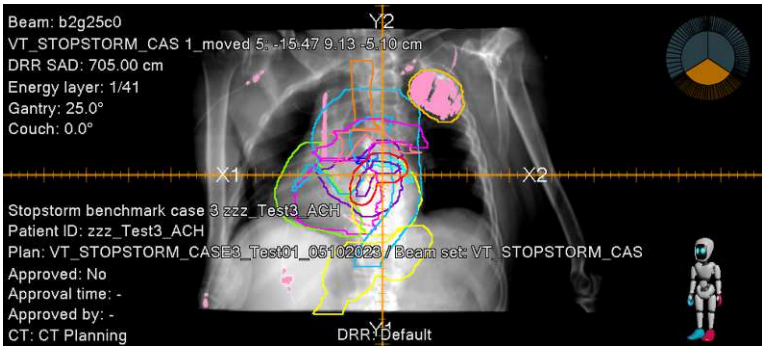

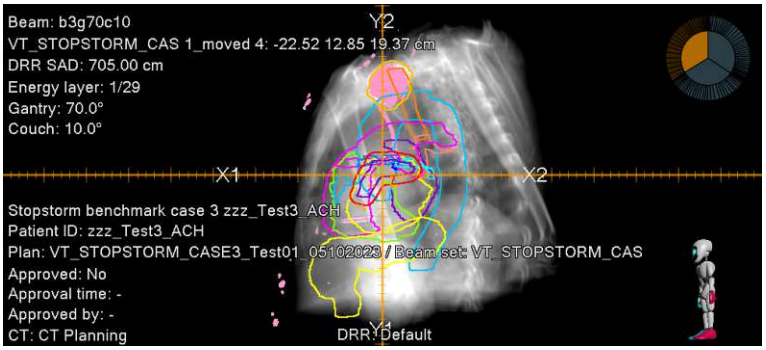

List of Figures

List of Tables

Acronyms

AAPM American Association of Physicists in Medicine. 12

AHA American Heart Association. 51, 52, 131

AI Artificial Intelligence. 12, 46

AP Anteroposterior. 33, 34, 49, 53

APSS Azienda Provinciale per i Servizi Sanitari. 11

AV Atrioventricular Node. 57

AVID Acceleration and Vacuum Technology, Ion Sources and Diagnostics. v, vii, 12

BIS Beam Interlock System. 42

BLM Beam Loss Monitor. 12

CBCT Cone Beam Computed Tomography. 60

CE Conformité Européenne. 47, 48

CERN Conseil Européen pour la Recherche Nucléaire. 29

CHUV Centre Hospitalier Universitaire Vaudois. 61

CITV Cardiac Internal Target Volume. 37, 63, 130

CMR Cardiovascular Magnetic Resonance Imaging. 54

CNAO Centro Nazionale Adroterapia Oncologica. 11, 30, 61, 79

CPAP Continuous Positive Airway Pressure. 26, 56

CT Computed Tomography. v, vii, 7, 12, 27, 33, 34, 36, 37, 44, 47–57, 60, 61, 63, 64, 76–78, 130, 131, 133

CTV Clinical Target Volume. 22–24, 26, 57, 130

DDS Dose Delivery System. 39, 40, 42, 44

DIBH Deep inspiration breath-hold. 56

DICOM Digital Imaging and Communications in Medicine. 33, 43, 47, 48, 53, 55, 78

DIG Dose Delivery System Interlock Gateway. 38–40, 42, 44, 130

DMUX Demultiplexer. 38–40, 42, 130

DNA Deoxyribonucleic Acid. 11

DSB Double-strand DNA Breaks. 18

DTG Delivery System Timing Gateway. 42

DVH Dose Volume Histogram. 65

EAM Electrophysiological Mapping. 6–8, 32–35, 48, 49, 51–57, 61, 69, 78, 79, 130, 131, 133

EBRT External Beam Radiotherapy. 12

ECG Electrocardiogram. 4, 5, 10–12, 26, 34, 36, 45, 52, 54–56, 58, 65, 68, 129–131

EVS Energy Verification System. 42

GID Gating Interface Device. 38–40, 42, 43, 45–47, 78, 130, 131

GSI Gesellschaft für Schwerionenforschung. 10, 25

GTV Gross Tumour Volume. 23, 24, 130

GUI Graphical User Interface. 40, 43, 45, 47

HEBT High Energy Beam Transfer Line. 30

HEPHY High Energy Physics of the Austrian Academy of Science. 30

HIMAC Heavy Ion Medical Accelerator in Chiba. 10, 25

HRS Heart Rhythm Society. 61

HU Hounsfield Units. 27, 53, 55, 65

IAEA International Atomic Energy Agency. v, vii, 23, 25

ICD Implantable Cardioverter Defibrillator. 5–7, 34, 36, 37, 54, 57, 63, 65, 69, 76, 77, 130

ICRU International Commission on Radiation Units and Measurements. 22–25, 57, 130

IH Injector Hall. 30, 130

IM Internal Margin. 23, 26

IMRT Intensity Modulated Radiation Therapy. 24

INF Inferior. 49, 53

IR Irradiation Room. 29, 30, 41, 130

IRSS Irradiation Room Safety System. 42

ITS Independent Termination System. 42

ITV Internal Target Volume. 7, 22–24, 26, 37, 57, 130

LA Left Atria. 36, 130

LEBT Low Energy Beam Transfer Line. 30

LEMI Local Effect Model I. 25

LET Linear Energy Transfer. 18, 19, 25

LINAC Linear Accelerator. 7, 12, 28, 30

LL Left Lateral. 33, 34, 49, 53

LV Left Ventricle. 35, 36, 48, 51–53, 130, 131

LVAD Left Ventricular Assist Device. 68–70, 76, 77, 132

LVEF Left Ventricular Ejection Fraction. 10

MACS MedAustron Control System. 39, 40, 42

MADAM MedAustron Delivery and Allocation Manager. 38, 39, 42

MAPTA MedAustron Particle Therapy Accelerator. 30, 38–41, 43, 45–47, 60, 78, 130, 131

MATEO MedAustron Treatment Environment for Ocular Diseases. 38, 40, 47

MI Miocardial Infraction. 10

MLC Multileaf Collimator. 21, 129

MMKM Modified Microdosimetric Kinetic Model. 25

MP Medical Physicist. 53, 57

MRI Magnetic Resonance Imaging. 7

MTCP MedAustron Particle Therapy Accelerator Treatment Control Panel. 38–40, 42, 44, 130

MUGA Multigated Acquisition Scan. 54, 78

MVT Monomorphic Ventricualr Tachycardia. 4, 5

NCR Non-clinical Research. 30

OAR Organ at Risk. 7, 9, 12, 22–25, 37, 63–66, 68–70, 73, 75–77, 130–132

PA Posteroanterior. 33, 34, 49, 53

PACS Picture Archiving and Communication System. 59

PBS Pencil Beam Scanning. 20, 22, 64

PET Positron Emission Tomography. 7

PET-CT Positron Emission Tomography and Computed Tomography. 54

PIMMS Proton-Ion Medical Machine Study. 29

PRV Planning Organ at Risk Volume. 22–24, 130

PS Passive Scattering. 20

PSQA Patient Specific Quality Assurance. 7, 59, 61

PTV Planning Target Volume. 22–24, 37, 63, 65, 66, 69, 70, 72, 73, 76, 77, 130–132

PVC Premature Ventricular Contraction. 3

PVT Polimorphic Ventricualr Tachycardia. 4, 5

QA Quality Assurance. 48, 53, 59, 133

QOL Quality of Life. 8, 69

RA Right Atria. 36, 130

RAVENTA Radiosurgery for Ventricular Tachycardia. v, vii, 9, 31–34, 37, 48, 51, 61, 63, 64, 69, 75–77, 130, 132, 133

RBE Relative Biological Effectiveness. 11, 24, 25, 57, 64, 130

RF Radio Frequency. 34, 130

RFCA Radiofrequency Catheter Ablation. 1, 6, 8, 33, 34, 48, 53–55, 61

RL Right Lateral. 33, 34, 49, 53

RO Radiation Oncologist. 57

ROI Region of Interest. 65

RT Radiation Therapy. 10, 12, 25, 26, 37, 49, 53, 54, 61, 69, 78, 79, 130

RTT Radiotherapy Technologist. 57

RV Right Ventricle. 36, 130

SA Sinoatrial Node. 3

SH Synchrotron Hall. 30, 130

SI Système International. 18, 19

SOBP Spread of Bragg Peak. 16, 20, 21, 25, 26, 28

SOP Standard Operating Procedures. 12, 53

SSB Single-strand DNA Breaks. 18

STAR Stereotactic Arrhythmia Radioablation. 1, 6–9, 12, 27, 31, 32, 61, 129

STOPSTORM Standardized Treatment and Outcome Platform for Stereotactic Therapy Of Re-entrant tachycardia by a Multidisciplinary. v, vii, 2, 8, 11, 27, 31, 32, 69, 79

SUP Superior. 49, 53

TCS Treatment Control System. 38, 59

THIR Targeted Heavy Ion Irradiation. 10

TOF Time-of-flight. 29

TP Treatment Plan. 33, 42, 47, 63, 64, 66, 67, 71–74, 76, 77, 79, 131, 132

TPS Treatment Planning System. 7, 24, 33, 47, 55, 57, 58, 64, 78, 133

TRS Technical Reports Series. 25

TTL Transistor Transistor Logic. 40, 43, 45, 47

TV Treatment Volume. 23, 24, 37, 57, 63, 65, 66, 69, 70, 73, 76, 77, 130–132

US Ultrasoud. 44–47, 56, 58, 60, 78, 131

USA United States of America. 25, 61, 79

VF Ventricualar Fibrilation. 10

VT Ventricular Tachycardia. 1–14, 27, 31–35, 37, 38, 47–49, 51–58, 61, 69, 78, 79, 129–131

Bibliography

[1] M. Miszczyk et al. „Clinical evidence behind stereotactic radiotherapy for the treatment of ventricular tachycardia (STAR)—A comprehensive review“. In: *Journal of Clinical Medicine* 10 (2021), p. 1238.

[2] L. Wang et al. „Stereotactic arrhythmia radioablation (STAR) of ventricular tachycardia: a treatment planning study“. In: *Cureus* 8 (2016).

[3] B. Kovacs et al. „Stereotactic radioablation of ventricular arrhythmias in patients with structural heart disease–A systematic review“. In: *Radiotherapy and Oncology* 162 (2021), pp. 132–139.

[4] M. Chalkia et al. „Stereotactic arrhythmia radioablation as a novel treatment approach for cardiac arrhythmias: facts and limitations“. In: *Biomedicines* 9 (2021), p. 1461.

[5] L. Widesott et al. „Proton or photon radiosurgery for cardiac ablation of ventricular tachycardia? Breath and ECG gated robust optimization“. In: *Physica Medica* 78 (2020), pp. 15–31.

[6] M. Stock et al. „The technological basis for adaptive ion beam therapy at MedAustron: status and outlook“. In: *Zeitschrift für Medizinische Physik* 28 (2018), pp. 196–210.

[7] C. W. Tsao et al. „Heart disease and stroke statistics—2022 update: a report from the American Heart Association“. In: *Circulation* 145 (2022), e153–e639.

[8] C. Foth, M. K. Gangwani, and H. Alvey. „Ventricular Tachycardia“. In: (2018).

[9] C. De la Pinta and R. Besse. „Stereotactic ablative body radiotherapy for ventricular tachycardia: An alternative therapy for refractory patients“. In: *Anatolian Journal of Cardiology* 25 (2021), p. 858.

[10] M. A. Brodsky et al. „Ventricular tachyarrhythmia associated with psychological stress: the role of the sympathetic nervous system“. In: *Jama* 257 (1987), pp. 2064–2067.

[11] M. E. Josephson et al. „Recurrent sustained ventricular tachycardia. 2. Endocardial mapping.“ In: *Circulation* 57 (1978), pp. 440–447.

[12] J.-J. Goy et al. *Electrocardiography (ECG)*. Vol. 1. Bentham Science Publishers, 2013.

[13] *Cardiac electrophysiology and ECG interpretation – ECG & ECHO — ecgwaves.com*. `https://ecgwaves.com/topic/introduction-electrocardiography-ecg-book/`. [Accessed 06-Jul-2023].

[14] R. Buttner and E. Burns. *Ventricular Tachycardia – Monomorphic VT — litfl.com*. https://litfl.com/ventricular-tachycardia-monomorphic-ecg-library/. [Accessed 03-Jul-2023].

[15] *Monomorphic and Polymorphic Ventricular Tachycardias (Wide QRS Tachycardias) — aclsonline.us*. https://www.aclsonline.us/rhythms/monomorphic-and-polymorphic-ventricular-tachycardias/. [Accessed 05-Jul-2023].

[16] N. K. Movsisyan et al. „Cardiovascular diseases in central and eastern Europe: a call for more surveillance and evidence-based health promotion“. In: *Annals of global health* 86 (2020).

[17] E. J. Kessler and B. P. Knight. „Catheter ablation for ventricular tachycardia: indications and techniques“. In: *Expert review of cardiovascular therapy* 5 (2007), pp. 977–988.

[18] E. WASSERMAN and J. YULES. „Cardiac aneurysm with ventricular tachycardia: case report and brief review of the literature“. In: *Annals of Internal Medicine* 39 (1953), pp. 948–956.

[19] W. Likoff and C. P. Bailey. „Ventriculoplasty: excision of myocardial aneurysm: report of a successful case“. In: *Journal of the American Medical Association* 158 (1955), pp. 915–920.

[20] O. Couch Jr. „Cardiac aneurysm with ventricular tachycardia and subsequent excision of aneurysm: case report“. In: *Circulation* 20 (1959), pp. 251–253.

[21] R. R. ECKER et al. „Control of intractable ventricular tachycardia by coronary revascularization“. In: *Circulation* 44 (1971), pp. 666–670.

[22] A. F. Graham et al. „Surgical treatment of refractory life-threatening ventricular tachycardia“. In: *The American Journal of Cardiology* 32 (1973), pp. 909–912.

[23] G. O. Hartzler. „Electrode catheter ablation of refractory focal ventricular tachycardia“. In: *Journal of the American College of Cardiology* 2 (1983), pp. 1107–1113.

[24] L. S. Klein et al. „Radiofrequency catheter ablation of ventricular tachycardia in patients without structural heart disease.“ In: *Circulation* 85 (1992), pp. 1666–1674.

[25] M. E. Josephson, A. H. Harken, and L. N. Horowitz. „Endocardial excision: a new surgical technique for the treatment of recurrent ventricular tachycardia.“ In: *Circulation* 60 (1979), pp. 1430–1439.

[26] E. Sosa et al. „A new technique to perform epicardial mapping in the electrophysiology laboratory“. In: *Journal of cardiovascular electrophysiology* 7 (1996), pp. 531–536.

[27] F. E. Marchlinski et al. „Linear ablation lesions for control of unmappable ventricular tachycardia in patients with ischemic and nonischemic cardiomyopathy“. In: *Circulation* 101 (2000), pp. 1288–1296.

[28] W. G. Stevenson et al. „Identification of reentry circuit sites during catheter mapping and radiofrequency ablation of ventricular tachycardia late after myocardial infarction.“ In: *Circulation* 88 (1993), pp. 1647–1670.

[29] *Watch: What are beta blockers and what do they do in your body? — bhf.org.uk*. https://www.bhf.org.uk/informationsupport/heart-matters-magazine/medical/drug-cabinet/beta-blockers. [Accessed 05-Jul-2023].

[30] T. A. McDonagh et al. „2021 ESC Guidelines for the diagnosis and treatment of acute and chronic heart failure: Developed by the Task Force for the diagnosis and treatment of acute and chronic heart failure of the European Society of Cardiology (ESC) With the special contribution of the Heart Failure Association (HFA) of the ESC“. In: *European heart journal* 42 (2021), pp. 3599–3726.

[31] R. Tung et al. „Freedom from recurrent ventricular tachycardia after catheter ablation is associated with improved survival in patients with structural heart disease: an International VT Ablation Center Collaborative Group study“. In: *Heart rhythm* 12 (2015), pp. 1997–2007.

[32] J. Fernandez-Armenta et al. „Safety and outcomes of ventricular tachycardia substrate ablation during sinus rhythm: a prospective multicenter registry“. In: *Clinical Electrophysiology* 6 (2020), pp. 1435–1448.

[33] E. Picano et al. „The appropriate and justified use of medical radiation in cardiovascular imaging: a position document of the ESC Associations of Cardiovascular Imaging, Percutaneous Cardiovascular Interventions and Electrophysiology“. In: *European heart journal* 35 (2014), pp. 665–672.

[34] A. Sharma et al. „Noninvasive stereotactic radiosurgery (CyberHeart) for creation of ablation lesions in the atrium“. In: *Heart rhythm* 7 (2010), pp. 802–810.

[35] B. W. Loo Jr et al. „Stereotactic ablative radiotherapy for the treatment of refractory cardiac ventricular arrhythmia“. In: *Circulation: Arrhythmia and Electrophysiology* 8 (2015), pp. 748–750.

[36] J. Cvek et al. „Cardiac radiosurgery for malignant ventricular tachycardia“. In: *Cureus* 6 (2014).

[37] S. Hohmann et al. „Stereotactic radioablation for ventricular tachycardia“. In: *Herzschrittmachertherapie+ Elektrophysiologie* (2021), pp. 1–6.

[38] R. Jumeau et al. „Stereotactic radiotherapy for the management of refractory ventricular tachycardia: promise and future directions“. In: *Frontiers in cardiovascular medicine* 7 (2020), p. 108.

[39] J. Whitaker, R. H. Mak, and P. C. Zei. „Non-invasive ablation of arrhythmias with stereotactic ablative radiotherapy“. In: *Trends in cardiovascular medicine* 32 (2022), pp. 287–296.

[40] A. Suzuki et al. „Catheter-free arrhythmia ablation using scanned proton beams: electrophysiologic outcomes, biophysics, and characterization of lesion formation in a porcine model“. In: *Circulation: Arrhythmia and Electrophysiology* 13 (2020), e008838.

[41] P. S. Cuculich et al. „Noninvasive cardiac radiation for ablation of ventricular tachycardia“. In: *New England Journal of Medicine* 377 (2017), pp. 2325–2336.

[42] R. Neuwirth et al. „Stereotactic radiosurgery for ablation of ventricular tachycardia“. In: *EP Europace* 21 (2019), pp. 1088–1095.

[43] P. Dvorak et al. „Stereotactic ablative radiotherapy of ventricular tachycardia using tracking: optimized target definition workflow“. In: *Frontiers in Cardiovascular Medicine* 9 (2022), p. 870127.

[44] S. Abdel-Kafi et al. „Accuracy of electroanatomical mapping-guided cardiac radiotherapy for ventricular tachycardia: pitfalls and solutions“. In: *EP Europace* 23 (2021), pp. 1989–1997.

[45] J. Boda-Heggemann et al. „Interdisciplinary clinical target volume generation for cardiac radioablation: Multicenter benchmarking for the RAdiosurgery for VENtricular TAchycardia (RAVENTA) trial“. In: *International Journal of Radiation Oncology* Biology* Physics* 110 (2021), pp. 745–756.

[46] P. Suzanne Lydiard et al. „A review of cardiac radioablation (CR) for arrhythmias: procedures, technology, and future opportunities“. In: *International Journal of Radiation Oncology* Biology* Physics* 109 (2021), pp. 783–800.

[47] C. L. Brett et al. „Novel workflow for conversion of catheter-based electroanatomic mapping to DICOM imaging for noninvasive radioablation of ventricular tachycardia“. In: *Practical Radiation Oncology* 11 (2021), pp. 84–88.

[48] G. D. Hugo and M. Rosu. „Advances in 4D radiation therapy for managing respiration: part I–4D imaging“. In: *Zeitschrift für medizinische Physik* 22 (2012), pp. 258–271.

[49] A. Kluge et al. „Treatment planning for cardiac radioablation: multicenter multiplatform benchmarking for the RAdiosurgery for VENtricular TAchycardia (RAVENTA) trial“. In: *International Journal of Radiation Oncology* Biology* Physics* 114 (2022), pp. 360–372.

[50] D. Krug et al. „Radiosurgery for ventricular tachycardia (RAVENTA): interim analysis of a multicenter multiplatform feasibility trial“. In: *Strahlentherapie und Onkologie* (2023), pp. 1–10.

[51] C. Wei et al. „Non-invasive stereotactic radioablation: a new option for the treatment of ventricular arrhythmias“. In: *Arrhythmia & Electrophysiology Review* 8 (2019), p. 285.

[52] D. M. Zhang et al. „Cardiac radiotherapy induces electrical conduction reprogramming in the absence of transmural fibrosis“. In: *Nature communications* 12 (2021), p. 5558.

[53] J. S. Kim et al. „Impact of high-dose irradiation on human iPSC-derived cardiomyocytes using multi-electrode arrays: implications for the antiarrhythmic effects of cardiac radioablation“. In: *International Journal of Molecular Sciences* 23 (2021), p. 351.

[54] J. Kautzner et al. „Radiation-induced changes in ventricular myocardium after stereotactic body radiotherapy for recurrent ventricular tachycardia“. In: *Clinical Electrophysiology* 7 (2021), pp. 1487–1492.

[55] O. Blanck et al. „Cardiac stereotactic radiotherapy induces electrical conduction reprogramming“. In: *Strahlentherapie und Onkologie: Organ der Deutschen Rontgengesellschaft...[et al]* 198 (2021), pp. 209–211.

[56] C. G. Robinson et al. „Phase I/II trial of electrophysiology-guided noninvasive cardiac radioablation for ventricular tachycardia“. In: *Circulation* 139 (2019), pp. 313–321.

[57] M. H. van der Ree et al. „Cardiac radioablation—A systematic review“. In: *Heart rhythm* 17 (2020), pp. 1381–1392.

[58] O. Blanck et al. „Radiosurgery for ventricular tachycardia: preclinical and clinical evidence and study design for a German multi-center multi-platform feasibility trial (RAVENTA)“. In: *Clinical Research in Cardiology* 109 (2020), pp. 1319–1332.

[59] M. Miszczyk et al. „Stereotactic management of arrhythmia–radiosurgery in treatment of ventricular tachycardia (SMART-VT)–clinical trial protocol and study rationale“. In: *OncoReview* 10 (2020).

[60] C. Carbucicchio et al. „STRA-MI-VT (STereotactic RadioAblation by Multimodal Imaging for Ventricular Tachycardia): rationale and design of an Italian experimental prospective study“. In: *Journal of Interventional Cardiac Electrophysiology* 61 (2021), pp. 583–593.

[61] D. Krug et al. „Stereotactic body radiotherapy for ventricular tachycardia (cardiac radiosurgery) First-in-patient treatment in Germany“. In: *Strahlentherapie und Onkologie* 196 (2020), pp. 23–30.

[62] *Project - STOPSTORM — stopstorm.eu*. `https://stopstorm.eu/en/project`. [Accessed 20-Jul-2023].

[63] M. Grehn et al. „Survey results of the STOPSTORM consortium about stereotactic arrhythmia radioablation in Europe“. In: *Europace* 24 (2022), euac053–376.

[64] V. Trojani et al. „Stereotactic Arrhythmia Radioablation in Europe—Treatment Planning Benchmark Results of the STOPSTORM. eu Consortium“. In: *International Journal of Radiation Oncology, Biology, Physics* 114 (2022), e420.

[65] J. Choi and J. O. Kang. „Basics of particle therapy II: relative biological effectiveness“. In: *Radiation oncology journal* 30 (2012), p. 1.

[66] H. Paganetti. *Proton therapy physics*. CRC press, 2018.

[67] J. Franzetti et al. „Stereotactic Radiotherapy Ablation and Atrial Fibrillation: Technical Issues and Clinical Expectations Derived From a Systematic Review“. In: *Frontiers in cardiovascular medicine* 9 (2022).

[68] M. Amino et al. „Heavy ion radiation up-regulates Cx43 and ameliorates arrhythmogenic substrates in hearts after myocardial infarction“. In: *Cardiovascular research* 72 (2006), pp. 412–421.

[69] M. Boerma et al. „Effects of ionizing radiation on the heart“. In: *Mutation Research/Reviews in Mutation Research* 770 (2016), pp. 319–327.

[70] M. Prall et al. „Treatment of arrhythmias by external charged particle beams: a Langendorff feasibility study“. In: *Biomedical Engineering/Biomedizinische Technik* 60 (2015), pp. 147–156.

[71] S. Hohmann et al. „Left ventricular function after noninvasive cardiac ablation using proton beam therapy in a porcine model“. In: *Heart Rhythm* 16 (2019), pp. 1710–1719.

[72] J. Li et al. „Cardiac-specific deletion of BRG1 ameliorates ventricular arrhythmia in mice with myocardial infarction“. In: *Acta Pharmacologica Sinica* (2023), pp. 1–14.

[73] M. Amino et al. „Heavy Ion Irradiation Reduces Vulnerability to Atrial Tachyarrhythmias—Gap Junction and Sympathetic Neural Remodeling—“. In: *Circulation Journal* 87 (2023), pp. 1016–1026.

[74] D. Richter et al. „ECG-based 4D-dose reconstruction of cardiac arrhythmia ablation with carbon ion beams: application in a porcine model“. In: *Physics in Medicine & Biology* 62 (2017), p. 6869.

[75] M. Prall et al. „Immobilization for carbon ion beam ablation of cardiac structures in a porcine model“. In: *Physica Medica* 43 (2017), pp. 134–139.

[76] C. Graeff and C. Bert. „Noninvasive cardiac arrhythmia ablation with particle beams“. In: *Medical Physics* 45 (2018), e1024–e1035.

[77] S. Goddu et al. „Feasibility of noninvasive cardiac ablation utilizing intensity modulated proton therapy to treat ventricular tachycardia“. In: *International Journal of Radiation Oncology, Biology, Physics* 102 (2018), S58.

[78] M. E. Rettmann et al. „Quantitative assessment of the relationship between myocardial lesion formation detected by delayed contrast-enhanced magnetic resonance imaging and proton beam planning dose for treatment of ventricular tachycardia“. In: *Medical Imaging 2019: Image-Guided Procedures, Robotic Interventions, and Modeling*. Vol. 10951. SPIE. 2019, pp. 73–78.

[79] S. Molinelli et al. „Dose prescription in carbon ion radiotherapy: How to compare two different RBE-weighted dose calculation systems“. In: *Radiotherapy and Oncology* 120 (2016), pp. 307–312.

[80] P. Fossati et al. „Dose prescription in carbon ion radiotherapy: a planning study to compare NIRS and LEM approaches with a clinically-oriented strategy“. In: *Physics in Medicine & Biology* 57 (2012), p. 7543.

[81] V. Dusi et al. „First-in-man case of non-invasive proton radiotherapy for the treatment of refractory ventricular tachycardia in advanced heart failure“. In: *European Journal of Heart Failure* 23 (2021), pp. 195–196.

[82] S. Rossi. „Hadron Therapy Achievements and Challenges: The CNAO Experience“. In: *Physics* 4 (2022), pp. 229–257.

[83] *Protons herald new cardiac treatment – CERN Courier — cerncourier.com*. `https://cerncourier.com/a/protons-herald-new-cardiac-treatment/`. [Accessed 20-Jul-2023].

[84] H. Paganetti. „Relative biological effectiveness (RBE) values for proton beam therapy. Variations as a function of biological endpoint, dose, and linear energy transfer“. In: *Physics in Medicine & Biology* 59 (2014), R419.

[85] H. Willers et al. „Toward A variable RBE for proton beam therapy“. In: *Radiotherapy and Oncology* 128 (2018), pp. 68–75.

[86] F. Rapp et al. „Biological cardiac tissue effects of high-energy heavy ions–investigation for myocardial ablation“. In: *Scientific reports* 9 (2019), p. 5000.

[87] H. Li et al. „AAPM Task Group Report 290: Respiratory motion management for particle therapy“. In: *Medical physics* 49 (2022), e50–e81.

[88] R. Jumeau et al. „Rescue procedure for an electrical storm using robotic non-invasive cardiac radio-ablation“. In: *Radiotherapy and Oncology* 128 (2018), pp. 189–191.

[89] N. C. Knutson et al. „Radiation therapy workflow and dosimetric analysis from a phase 1/2 trial of noninvasive cardiac radioablation for ventricular tachycardia“. In: *International Journal of Radiation Oncology* Biology* Physics* 104 (2019), pp. 1114–1123.

[90] EBAMed. *EBAMed | — eba-med.com*. `https://eba-med.com/`. [Accessed 24-11-2023]. 2020.

[91] K. Wittenburg. „Beam loss monitors“. In: (2009).

[92] M. Casula et al. „Feasibility of an automatic ultrasonographic image acquisition system associated with an artificial intelligence algorithm for real-time monitoring of cardiac motion during cardiac radio-ablation“. In: *Frontiers in Cardiovascular Medicine* (2022), p. 950.

[93] R. Perrin et al. „Case Report: Treatment Planning Study to Demonstrate Feasibility of Transthoracic Ultrasound Guidance to Facilitate Ventricular Tachycardia Ablation With Protons“. In: *Frontiers in Cardiovascular Medicine* 9 (2022).

[94] H. Paganetti. „Range uncertainties in proton therapy and the role of Monte Carlo simulations“. In: *Physics in Medicine & Biology* 57 (2012), R99.

[95] B. Larsson and U. Amaldi. *Hadrontherapy in Oncology: Proceedings of the First International Symposium on Hadrontherapy: Como, Italy, 18-21 October 1993*. Elsevier, 1994.

[96] F. Ulrich-Pur et al. „Demonstrator for a Proton CT System at MedAustron“. In: *arXiv: Instrumentation and Detectors* (2020). URL: https://api.semanticscholar.org/CorpusID:211677699.

[97] E. Haettner et al. „Experimental study of nuclear fragmentation of 200 and 400 MeV/u 12C ions in water for applications in particle therapy“. In: *Physics in medicine & biology* 58 (2013), p. 8265.

[98] S. Ruangchan et al. „Dose calculation accuracy in particle therapy: Comparing carbon ions with protons“. In: *Medical Physics* 48 (2021), pp. 7333–7345.

[99] U. Linz. *Ion beam therapy: fundamentals, technology, clinical applications*. Springer Science & Business Media, 2011.

[100] W. D. Newhauser and R. Zhang. „The physics of proton therapy“. In: *Physics in Medicine & Biology* 60 (2015), R155.

[101] A. Lechner. „CERN: Particle interactions with matter“. In: *CERN Yellow Rep. School Proc.* 5 (2018), p. 47.

[102] E. L. Alpen. *Radiation biophysics*. Academic press, 1997.

[103] I. C. on Radiation Units. *Linear energy transfer*. Vol. 16. International commission on radiation units and measurements, 1970.

[104] M. F. L'ANNUNZIATA. „1 - NUCLEAR RADIATION, ITS INTERACTION WITH MATTER AND RADIOISOTOPE DECAY“. In: *Handbook of Radioactivity Analysis (Second Edition)*. Ed. by M. F. L'Annunziata. Second Edition. San Diego: Academic Press, 2003, pp. 1–121. ISBN: 978-0-12-436603-9. DOI: https://doi.org/10.1016/B978-012436603-9/50006-5. URL: https://www.sciencedirect.com/science/article/pii/B9780124366039500065.

[105] A. Kowalska et al. „Production and distribution of chromosome aberrations in human lymphocytes by particle beams with different LET“. In: *Radiation and environmental biophysics* 58 (2019), pp. 99–108.

[106] S. J. McMahon. „The linear quadratic model: usage, interpretation and challenges“. In: *Physics in Medicine & Biology* 64 (2018), 01TR01.

[107] M. F. L'Annunziata. „Nuclear radiation, its interaction with matter and radioisotope decay“. In: *Handbook of Radioactivity Analysis* 1 (2003), p. 122.

[108] N. Tsoulfanidis and S. Landsberger. *Measurement and detection of radiation*. CRC press, 2021.

[109] P. Sigmund and A. Schinner. „The Bloch correction, key to heavy-ion stopping“. In: *Journal of Applied Physics* 128 (2020).

[110] O. Jäkel. „Physical advantages of particles: protons and light ions“. In: *The British journal of radiology* 93 (2020), p. 20190428.

[111] W. R. Leo and W. R. Leo. „Passage of radiation through matter“. In: *Techniques for nuclear and particle physics experiments: a how-to approach* (1994), pp. 17–68.

[112] A. Asadi et al. „Dosimetric Comparison of Passive Scattering and Active Scanning Proton Therapy Techniques Using GATE Simulation“. In: *arXiv preprint arXiv:2107.12185* (2021).

[113] A. S. Mathew and S. Nangia. „Proton Beam Therapy in Gastrointestinal Cancers: A Paradigm Shift in Radiotherapy“. In: *GI Surgery Annual: Volume 26*. Springer, 2022, pp. 163–183.

[114] R. Slopsema. „Beam delivery using passive scattering“. In: *Proton therapy physics* (2012), pp. 125–156.

[115] S. Safai et al. „Improving the precision and performance of proton pencil beam scanning“. In: *Transl Cancer Res* 1 (2012), pp. 196–206.

[116] C. Peucelle. „Spatial fractionation of the dose in charged particle therapy“. PhD thesis. Université Paris Saclay (COmUE), 2016.

[117] L. Santanam et al. „Standardizing naming conventions in radiation oncology“. In: *International Journal of Radiation Oncology* Biology* Physics* 83 (2012), pp. 1344–1349.

[118] D. Jones. *ICRU report 50—prescribing, recording and reporting photon beam therapy*. 1994.

[119] A. Wambersie. „ICRU report 62, prescribing, recording and reporting photon beam therapy (supplement to ICRU Report 50)“. In: *Icru News* (1999).

[120] *11.02 - ICRU Reports 50 and 62 - OzRadOnc — ozradonc.wikidot.com*. `http://ozradonc.wikidot.com/current-icru-recommendations`. [Accessed 30-11-2023].

[121] M. Schlachter et al. „State-of-the-Art Report: Visual Computing in Radiation Therapy Planning“. In: *Computer Graphics Forum*. Vol. 38. Wiley Online Library. 2019, pp. 753–779.

[122] C. Hoeppner et al. *Dose Reporting in Ion Beam Therapy*. Tech. rep. IAEA-TECDOC-1560, 53, 2006.

[123] P. DeLuca et al. „ICRU Report 78. Prescribing, recording, and reporting proton-beam therapy“. In: *J ICRU* 7 (2007), pp. 29–48.

[124] I. A. E. Agency. *Relative biological effectiveness in ion beam therapy*. International Atomic Energy Agency, 2008.

[125] J.-i. Kim, J. M. Park, and H.-G. Wu. „Carbon ion therapy: a review of an advanced technology“. In: *Progress in Medical Physics* 31 (2020), pp. 71–80.

[126] C. P. Karger et al. „The RBE in ion beam radiotherapy: In vivo studies and clinical application“. In: *Zeitschrift für Medizinische Physik* 31 (2021), pp. 105–121.

[127] O. Steinsträter et al. „Mapping of RBE-weighted doses between HIMAC–and LEM–based treatment planning systems for carbon ion therapy“. In: *International Journal of Radiation Oncology* Biology* Physics* 84 (2012), pp. 854–860.

[128] C. Bert and M. Durante. „Motion in radiotherapy: particle therapy“. In: *Physics in Medicine & Biology* 56 (2011), R113.

[129] S. Ceberg et al. „Evaluation of breathing interplay effects during VMAT by using 3D gel measurements“. In: *Journal of Physics: Conference Series*. Vol. 444. IOP Publishing. 2013, p. 012098.

[130] C. Liu et al. „Impact of spot size and spacing on the quality of robustly optimized intensity modulated proton therapy plans for lung cancer“. In: *International Journal of Radiation Oncology* Biology* Physics* 101 (2018), pp. 479–489.

[131] A. K. Berthelsen et al. „What's new in target volume definition for radiologists in ICRU Report 71? How can the ICRU volume definitions be integrated in clinical practice?“ In: *Cancer Imaging* 7 (2007), p. 104.

[132] Y. Zhang et al. „A survey of practice patterns for real-time intrafractional motion-management in particle therapy“. In: *Physics and imaging in radiation oncology* 26 (2023), p. 100439.

[133] M. Lee et al. „Comparing phase-and amplitude-gated volumetric modulated arc therapy for stereotactic body radiation therapy using 3D printed lung phantom“. In: *Journal of applied clinical medical physics* 20 (2019), pp. 107–113.

[134] P. Gut et al. „Combining rescanning and gating for a time-efficient treatment of mobile tumors using pencil beam scanning proton therapy“. In: *Radiotherapy and oncology* 160 (2021), pp. 82–89.

[135] R. P. Johnson. „Review of medical radiography and tomography with proton beams“. In: *Reports on progress in physics* 81 (2017), p. 016701.

[136] G. Poludniowski, N. Allinson, and P. Evans. „Proton radiography and tomography with application to proton therapy“. In: *The British journal of radiology* 88 (2015), p. 20150134.

[137] H. Wiedemann. *Particle accelerator physics*. Springer Nature, 2015.

[138] U. Themes. *Proton Beam Therapy — radiologykey.com*. `https://radiologykey.com/proton-beam-therapy-2/`. [Accessed 29-11-2023]. 2016.

[139] K. Hiramoto et al. „The synchrotron and its related technology for ion beam therapy“. In: *Nuclear Instruments and Methods in Physics Research Section B: Beam Interactions with Materials and Atoms* 261 (2007), pp. 786–790.

[140] A. Hofmann. *The physics of synchrotron radiation*. Vol. 20. Cambridge university press, 2004.

[141] *Bewegte Ladungen in Feldern - Synchrotron*. URL: `https://www.leifiphysik.de/elektrizitaetslehre/bewegte-ladungen-feldern/ausblick/synchrotron`.

[142] N. R. Lobanov, P. Linardakis, and D. Tempra. „Bunching and chopping for tandem accelerators. Part II: Chopping“. In: *Nuclear Instruments and Methods in Physics Research Section B: Beam Interactions with Materials and Atoms* 499 (2021), pp. 142–147.

[143] J. Borburgh et al. *Design and development of kickers and septa for MedAustron*. Tech. rep. 2010.

[144] M. Stock et al. „The technological basis for adaptive ion beam therapy at MedAustron: Status and outlook“. In: *Zeitschrift f Medizinische Physik* 28 (2018), pp. 196–210. ISSN: 09393889. DOI: 10.1016/j.zemedi.2017.09.007.

[145] S. G. Laskar et al. „Access to Radiation Therapy: From Local to Global and Equality to Equity“. In: *JCO Global Oncology* 8 (2022), e2100358.

[146] F. Osmic et al. „Overview of the Beam diagnostics in the MedAustron Accelerator: Design choices and test Beam commissioning“. In: *Conf. Proc.* Vol. 1205201. 2012, MOPPR002.

[147] M. Benedikt and A. Wrulich. „MedAustron—Project overview and status“. In: *The European Physical Journal Plus* 126 (2011), pp. 1–11.

[148] J. Lettry et al. „Ion sources for MedAustron“. In: *Review of Scientific Instruments* 81 (2010).

[149] B. Synch Let. *Accelerator layout > 1000 components (almost 300 magnets and power converters, 153 beam diagnostic devices, about 400m of vacuum pipes, a not neglectable. - ppt download — slideplayer.com*. https://slideplayer.com/slide/13370780/. [Accessed 21-08-2023].

[150] G.-H. Günter. *MedAustron Gating Interface Information Session*. MedAustron Internal Presentation. 2023.

[151] G. I. Danzinger S. Gruber-Hammer G. *Interface Design Description GID*. MedAustron Internal Documentation:DB010_GID_2104191. 2022.

[152] M. S. O. Triebl. *MAPTA System Architecture Overview Diagram*. MedAustron Internal Documentation:$DB010_{M}APTA_{1}405232$. 2022.

[153] D. Systems. *DICOM Modality Worklist — Dicom Systems — dcmsys.com*. https://dcmsys.com/solutions/dicom-modality-worklist/. [Accessed 03-12-2023]. 2022.

[154] A. A. Mohamed, A. A. Arifi, and A. Omran. „The basics of echocardiography“. In: *Journal of the Saudi Heart Association* 22 (2010), pp. 71–76.

[155] J. Lee et al. *Cardiac stereotactic ablative radiotherapy for control of refractory ventricular tachycardia: initial UK multicentre experience. Open Heart 8: e1770*. 2021.

[156] S. Hohmann et al. „A novel open-source software-based high-precision workflow for target definition in cardiac radioablation“. In: *Journal of Cardiovascular Electrophysiology* 31 (2020), pp. 2689–2695.

[157] G. Ho et al. „Computational ECG mapping and respiratory gating to optimize stereotactic ablative radiotherapy workflow for refractory ventricular tachycardia“. In: *Heart rhythm O2* 2 (2021), pp. 511–520.

[158] P. C. Qian et al. „Substrate modification using stereotactic radioablation to treat refractory ventricular tachycardia in patients with ischemic cardiomyopathy“. In: *Clinical Electrophysiology* 8 (2022), pp. 49–58.

[159] M. Mayinger et al. „Quality assurance process within the RAdiosurgery for VENtricular TAchycardia (RAVENTA) trial for the fusion of electroanatomical mapping and radiotherapy planning imaging data in cardiac radioablation“. In: *Physics and imaging in radiation oncology* 25 (2023), p. 100406.

[160] A. H. A. W. G. on Myocardial Segmentation et al. „Standardized myocardial segmentation and nomenclature for tomographic imaging of the heart: a statement for healthcare professionals from the Cardiac Imaging Committee of the Council on Clinical Cardiology of the American Heart Association“. In: *Circulation* 105 (2002), pp. 539–542.

[161] B. S. Selvadurai et al. „Definition of left ventricular segments for cardiac magnetic resonance imaging“. In: (2017).

[162] J. Brownstein et al. „Method and atlas to enable targeting for cardiac radioablation employing the American Heart Association segmented model“. In: *International Journal of Radiation Oncology* Biology* Physics* 111 (2021), pp. 178–185.

[163] M. D. Cerqueira. „American Heart Association Writing Group on Myocardial Segmentation and Registration for Cardiac Imaging: Standardized myocardial segmentation and nomenclature for tomographic imaging of the heart: a statement for healthcare professionals from the Cardiac Imaging Committee of the Council on Clinical Cardiology of the American Heart Association“. In: *Circulation* 105 (2002), pp. 539–542.

[164] V. Prieto-Vargas et al. „PET-Myocardial Perfusion Imaging in the Assessment of Coronary Artery Disease: the basics“. In: *Clin Res Trials* 8 (2022).

[165] R. Martin et al. „Ventricular tachycardia isthmus characteristics: insights from high-density mapping“. In: *Arrhythmia & Electrophysiology Review* 8 (2019), p. 54.

[166] Liryc. *Discover Liryc's major research projects. — ihu-liryc.fr*. https://www.ihu-liryc.fr/en/major-strategic-research-projects/. [Accessed 13-11-2023]. 2023.

[167] J. Z. Lee et al. „Causes of early mortality after ventricular tachycardia ablation in patients with reduced ejection fraction“. In: *Clinical Electrophysiology* 9 (2023), pp. 824–832.

[168] J. Kim. *C ARTO xAE; 3 System - Biosense Webster - PDF Catalogs | Technical Documentation — pdf.medicalexpo.com*. https://pdf.medicalexpo.com/pdf/biosense-webster/c-arto-3-system/71118-152009.html. [Accessed 06-09-2023].

[169] *EnSite Precision Cardiac Mapping System Product Overview | Abbott — cardiovascular.abbott*. https://www.cardiovascular.abbott/us/en/hcp/products/electrophysiology/mapping-systems/ensite.html. [Accessed 29-11-2023].

[170] Medtronic. *Cardioinsight Mapping Vest — medtronic.com*. https://www.medtronic.com/us-en/healthcare-professionals/products/cardiac-rhythm/cardiac-mapping/cardioinsight-mapping-vest.html. [Accessed 06-09-2023].

[171] E. Osorio-Jaramillo et al. *Noninvasive Electrocardiographic Imaging: A Novel Tool for Understanding Atrial Fibrillation in Candidates for Cardiac Surgery?* 2020.

[172] F. Mehrhof et al. „Cardiac radioablation of incessant ventricular tachycardia in patients with terminal heart failure under permanent left ventricular assist device therapy—description of two cases“. In: *Strahlentherapie und Onkologie* 199 (2023), pp. 511–519.

[173] M. H. van der Ree et al. „Stereotactic Arrhythmia Radioablation: a multicenter pre-post intervention safety evaluation of the Implantable Cardioverter-Defibrillator function“. In: *Radiotherapy and Oncology* (2023), p. 109910.

[174] H. Paganetti et al. „Report of the AAPM TG-256 on the relative biological effectiveness of proton beams in radiation therapy“. In: *Medical physics* 46 (2019), e53–e78.

[175] C. S. Tuta et al. „Alanine pellets comparison using EPR dosimetry in the frame of quality assurance for a Gamma Knife system in Romania“. In: *Radiation Physics and Chemistry* 170 (2020), p. 108653.

[176] M. S. A. Carlino P. Roisl. *Dosimetric patient-specific plan verification for IR2 with protons and carbon ions*. MedAustron Internal Documentation:$DC022_{5}0233_{1}806151$. 2021.

[177] K. C. Siontis et al. „CE-452773-1 PROTON CARDIAC RADIOABLATION FOR REFRACTORY VENTRICULAR TACHYCARDIA: DOSE DISTRIBUTION TO TARGET MYOCARDIUM AND ORGANS AT RISK“. In: *Heart Rhythm* 20 (2023), S98–S99.

[178] B. Balgobind et al. „STereotactic Arrhythmia Radioablation: Critical Structure Contouring Benchmark Results of STOPSTORM“. In: *International Journal of Radiation Oncology, Biology, Physics* 114 (2022), e415–e416.

[179] P. A. Iaizzo. *Handbook of cardiac anatomy, physiology, and devices*. Springer Science & Business Media, 2010.

[180] R. Drzymala et al. „Dose-volume histograms“. In: *International Journal of Radiation Oncology* Biology* Physics* 21 (1991), pp. 71–78.

[181] H. Alnsasra et al. „Depression among Patients with an Implanted Left Ventricular Assist Device: Uncovering Pathophysiological Mechanisms and Implications for Patient Care“. In: *International Journal of Molecular Sciences* 24 (2023), p. 11270.

[182] O. Blanck et al. „Dose-escalation study for cardiac radiosurgery in a porcine model“. In: *International Journal of Radiation Oncology* Biology* Physics* 89 (2014), pp. 590–598.